Molecular imaging targets in prostate cancers with neuroendocrine gene signature

by

Martin (Mohamadreza) Khosravi Bakht

A Dissertation
Submitted to the Faculty of Graduate Studies
through the Department of Biological Sciences
in Partial Fulfillment of the Requirements for
the Degree of Doctor of Philosophy
at the University of Windsor

Windsor, Ontario, Canada

2019

Molecular imaging targets in prostate cancers with neuroendocrine gene signature

by

Martin (Mohamadreza) Khosravi Bakht

APPROVED BY:

_____

T. Tsakiridis, External Examiner
McMaster University

_____

L. Rueda
School of Computer Science

_____

J. Hudson
Department of Biomedical Sciences

_____

P. Vacratsis
Department of Chemistry and Biochemistry

_____

L. Porter, Advisor
Department of Biomedical Sciences

4th December 2019

DECLARATION OF CO-AUTHORSHIP / PREVIOUS PUBLICATION

I. Co-Authorship

I hereby declare that this thesis incorporates material that is result of joint research, as follows:

Chapter 2 of the thesis was co-authored with Iulian Derecichei, Yinan Li, Rosa-Maria Ferraiuolo, Mark J Dunning, So Won Oh, Abdulkadir Hussein, Hyewon Youn, Keith F Stringer, Chang Wook Jeong, Gi Jeong Cheon, Cheol Kwak, Keon Wook Kang, Alastair Lamb, Yuzhuo Wang, Xuesen Dong, under the supervision of professor Lisa A. Porter. In all cases, the key ideas, primary contributions, experimental designs, data analysis, interpretation, and writing were performed by the author and corresponding authors, and the detailed contribution of authors are as follow: The conception and design of the study was by MKB, GJC, ADL, KFS, YW, XD and LAP. MKB (most of the experiments), YL (PCR data) and XD and YW (PDX model) did the experiments and obtained the data. MKB (most of data), ID (microscopy data), YL (Beltran cohort data) and ADL (The Cambridge cohort data) analyzed the data. MKB (most of the manuscript), ID (survival curves), RMF (biology review), SWO (clinical review), HY(molecular imaging review) and LAP(final critical review) drafted the manuscript. MK, RMF, HY, KFS, CWJ, GJC, CK, MD, KWK, ADL, XD and LAP provided feedback on refinement of ideas and editing of the manuscript. MKB and AH contributed to the statistical analysis.

Chapter 3 of the thesis was co-authored with Jessica M. Lovnicki, Janice Tubman, Keith F. Stringer, Jonathan Chiaramonte, Michael R. Reynolds, Iulian Derecichei, Rosa-Maria Ferraiuolo, Bre-Anne Fifield, Dorota Lubanska, So Won Oh, Gi Jeong Cheon, Cheol Kwak, Chang Wook Jeong, Keon Wook Kang, John F. Trant, Colm Morrissey, Ilsa Coleman, Yuzhuo Wang, Hojjat Ahmadzadehfar and Xuesen Dong under the supervision of professor Lisa A. Porter. In all cases, the key ideas, primary contributions, experimental designs, data analysis, interpretation, and writing were performed by the author and corresponding authors, and the detailed contribution of authors are as follow: The conception and design of the study were by MKB, GJC, KWK, HA, XD and LAP. MRR and JFT synthesized and optimized (MKB, JC, MRR and JFT) the fluorescent glucose bioprobe, GB2-Cy3, for in vitro and in vivo imaging. MKB, JT, RF and DL conducted zebrafish

husbandry (MKB, JT, RF and DL), transplantation (JT) and microscopy (MKB, JT). MKB, JML, YW and XD contributed in PDX model experiments and data analyzes. CM and IC obtained and analyzed the expression of suppressed patients in FHCRC cohort. MKB, ID, SO, BF, and CWJ contributed to obtaining in vitro data and analysis of gene expression data. MKB, JT, JC, MRR, ID, RMF, SWO and LAP drafted the manuscript. MKB, DL, KFS, CM, IC, GJC, CK, and LAP crucially reviewed and enhanced the intellectual content of the manuscript. GJC, JFT, CK, KWK, CM, HA, XD, and LAP approved the final content of the manuscript.

Chapter 4 of the thesis was co-authored with So W Oh, Do W Hwang, Yun-Sang Lee, Hyewon Youn, ***Lisa A Porter****, Gi J Cheon, Cheol Kwak, Dong S Lee, Keon W Kang. under the supervision of professor Lisa A. Porter. In all cases, the key ideas, primary contributions, review designs, interpretation, and writing were performed by the author and corresponding author, and the detailed contribution of authors are as follow: The conception and design of the review were by MKB, GJC, KWK, and LAP.MKB, SWO, DWH, YSL, HY, GJC, CK, and DSL crucially reviewed and enhanced the intellectual content of the manuscript. GJC and LAP approved the final content of the manuscript.*

I am aware of the University of Windsor Senate Policy on Authorship and I certify that I have properly acknowledged the contribution of other researchers to my thesis, and have obtained written permission from each of the co-author(s) to include the above material(s) in my thesis.

I certify that, with the above qualification, this thesis, and the research to which it refers, is the product of my own work.

II. Previous Publication

This thesis includes 3 original papers that have been previously published/submitted for publication in peer reviewed journals, as follows:

Thesis Chapter	Publication title and full citation	Publication status
Chapter [2,5]	***Martin K Bakht,*** *Iulian Derecichei, Yinan Li, Rosa-Maria Ferraiuolo, Mark J Dunning, So Won Oh, Abdulkadir Hussein, Hyewon Youn, Keith F Stringer, Chang Wook Jeong, Gi Jeong Cheon, Cheol Kwak, Keon Wook Kang, Alastair Lamb, Yuzhuo Wang, Xuesen Dong,* ***Lisa A. Porter.*** *Neuroendocrine differentiation of prostate cancer leads to PSMA suppression.* ***Endocrine Related Cancer****. 2019;26:131-146.*	*Published doi: 10.1530/ERC-18-0226*
Chapter [3,5]	***Martin K. Bakht,*** *Jessica M. Lovnicki, Janice Tubman, Keith F. Stringer, Jonathan Chiaramonte, Michael R. Reynolds, Iulian Derecichei, Rosa-Maria Ferraiuolo, Bre-Anne Fifield, Dorota Lubanska, So Won Oh, Gi Jeong Cheon, Cheol Kwak, Chang Wook Jeong, Keon Wook Kang, John F. Trant, Colm Morrissey, Ilsa Coleman, Yuzhuo Wang, Hojjat Ahmadzadehfar, Xuesen Dong, and* ***Lisa A. Porter.*** *Differential expression of glucose transporters and hexokinases in prostate cancer with a neuroendocrine gene signature: a mechanistic perspective for FDG imaging of PSMA-suppressed tumors.* ***Journal of Nuclear Medicine****. 2019; In press.*	*Published doi: 10.2967/jnumed.119.231068*
Chapters [1,4,5]	***Martin K Bakht****, So W Oh, Do W Hwang, Yun-Sang Lee, Hyewon Youn,* ***Lisa A Porter****, Gi J Cheon, Cheol Kwak, Dong S Lee, Keon W Kang. Differential expression of glucose transporters and hexokinases in prostate cancer with a neuroendocrine gene signature: a mechanistic perspective for FDG imaging of PSMA-suppressed tumors.* ***Current Pharmaceutical Design****. 2017;23: 2976-2990.*	*Published doi: 10.2174/1381612823666170216122412*

I certify that I have obtained a written permission from the copyright owner(s) to include the above published material(s) in my thesis. I certify that the above material describes work completed during my registration as a graduate student at the University of Windsor.

III. General

I declare that, to the best of my knowledge, my thesis does not infringe upon anyone's copyright nor violate any proprietary rights and that any ideas, techniques, quotations, or any other material from the work of other people included in my thesis, published or otherwise, are fully acknowledged in accordance with the standard referencing practices. Furthermore, to the extent that I have included copyrighted material that surpasses the bounds of fair dealing within the meaning of the Canada Copyright Act, I certify that I have obtained a written permission from the copyright owner(s) to include such material(s) in my thesis.

I declare that this is a true copy of my thesis, including any final revisions, as approved by my thesis committee and the Graduate Studies office, and that this thesis has not been submitted for a higher degree to any other University or Institution.

ABSTRACT

The main treatment option for castration-resistant prostate cancer (CRPC) is androgen receptor pathway inhibition (ARPI). Selection pressure and lineage plasticity of ARPI could lead to neuroendocrine (NE) differentiation of prostate cancer (PC), promoting the more prevalent subtype of CRPC which is termed treatment-induced neuroendocrine prostate cancer (NEPC) or t-NEPC. Treatment options for NEPC are limited to platinum- and cisplatin-based combinations and median survival of NEPC patients is much lower than patients with CRPC. Early identification of NEPC and novel targeting options could be valuable. The transmembrane protein prostate-specific membrane antigen (PSMA) is an appealing target for molecular imaging and therapy of PC since it is over-expressed in a majority of PC tumors and metastatic lesions. Targeting PSMA is feasible by a wide variety of radio-ligands. The PSMA ligands can also be labeled with therapeutic radionuclides which can irradiate PSMA-expressing cells. Despite the positive implications of PSMA for many forms of advanced AdPC there are clinical reports supporting that PSMA-targeted imaging is not able to delineate NEPC tumors. Previous clinical reports indicate that PCs with a phenotype related to NE tumors can be more responsive to imaging by ^{18}F-Fluorodeoxyglucose (FDG) rather than PSMA-targeting radioligands.

In this work, we evaluated the association between NE gene signature and FDG uptake-associated genes including glucose transporters (GLUTs) and hexokinases, with the goal of providing a genomic signature to explain the reported FDG-avidity of PSMA-suppressed tumors. We use data mining approaches, cell lines and patient-derived xenograft (PDX) models to study the levels of 14 members of the *SLC2A* family (encoding GLUT proteins), 4 members of the hexokinase family (genes: *HK1* to 3 and *GCK*) and

PSMA (*FOLH1* gene) following AR-inhibition and in correlation with NE hallmarks. Also, we characterize a NE-like PC (NELPC) subset among a cohort of primary and metastatic PC samples with no NE histopathology. We measured glucose uptake in a NE-induced *in vitro* model and a zebrafish model by non-radioactive imaging of glucose uptake using fluorescent glucose bioprobe, GB2-Cy3.

This work demonstrates that a NE gene signature associates with differential expression of genes encoding GLUT and hexokinase proteins. In NELPC, elevated expression of GCK (encoding glucokinase protein) and decreased expression of *SLC2A12* correlated with earlier biochemical recurrence. In tumors treated with AR-inhibitors, enhanced expression of GCK and low expression of SLC2A12 correlated with NE histopathology and PSMA gene suppression. GLUT12-suppression and enhanced expression of glucokinase was observed in NE-induced PC cell lines and PDX models. A higher glucose uptake was confirmed in low-PSMA tumors using a GB2-Cy3 probe in a zebrafish model.

In summary, a NE gene signature in NEPC and NELPC associates with a distinct transcriptional profile of GLUTs and HKs. In transcriptomic level, PSMA-suppression correlates with GLUT12-supression and glucokinase-upregulation. Alteration of FDG uptake-associated genes correlated positively with higher glucose uptake in AR and PSMA-suppressed tumors. Zebrafish xenograft tumor models are an accurate and efficient pre-clinical method for monitoring non-radioactive glucose uptake.

DEDICATION

This work I dedicate to my family, whose loving support has seen given me the strength to succeed in all my endeavours.

To my beloved father, *Majid*, who was an amazing father and chemistry lecturer. When my dear father became ill with brain cancer, he kept his cancer a secret until so close to the end to keep me focused on doing my PhD study.

To my strong and beloved, mother, *Simin*, who has supported me as her only-child through the long years of studying abroad. Thank you for taking care of my father by yourself and sorry for not being with you in his funeral and other difficult days.

To my aunt and uncle, *Phyllida* and *Peter*, who have supported me and given me transformative advice, and been there through my struggles.

ACKNOWLEDGEMENTS

I have no word to express my gratitude to my supervisor *Dr. Lisa A. Porter* for her excellent scientific guidance, encouragement and help in directing my research. I appreciate her for providing me the opportunity of collaboration with many other labs. She fostered a supportive and inclusive environment for me.

I would like to acknowledge *Drs. G.J. Cheon and K.W. Kang* from *Seoul National University* for their help and guidance throughout this project. I would like to extend my sincere thanks and appreciation to *Drs. Y. Wang and X. Dong* for sharing valuable resources such as PDX models with me and hosting me in *Vancouver Prostate Centre* in summer 2018. This study would not have been possible without the valuable contribution and resources of *Dr. John F. Trant* and his highly skilled team at the *Department of Biochemistry*. I sincerely appreciate the time, educational feedback and excellent resources provided by *Dr. Colm Morrissey of University of Washington*. I would also like to thank my committee members *Drs. J. Hudson and L. Rueda and P. Vacratsis* for their valuable advice.

I would like to say a special word of thanks to *Dr. R. Ferraiuolo, Ms. J. Tubman* and *Drs. K. Stringer, Fifield, Fidalgo* and *Lubanska* for mentoring me and teaching me a variety of techniques and methodologies of cancer biology. I would like to say thank you to *Mr. Derecichei, Ms. Fong, Mr. Stover, Mr. Pillon, Ms. Dare-Shih, Ms. Laurie, Ms. Mehri, Ms. Ross* and *Drs. Crozier, Bashiri* and *Qemo, Mr. Labute, Mr. Stokes, Ms. Parasram* and *Ms. Gosselin* for their continued friendship, scientific conversations, language advice, advice for being a good Graduate Assistants , and helps during my PhD and GAship. My sincere thanks also go to *Ms. Barkley* and *Mr. Hodge* for their administrative supports. I would also like to acknowledge all of undergraduates' students and the only high school students of Porter lab (*Mr. Tronchin*) for their helps and I wish them all a bright future.

This study was supported by Canadian Institutes of Health Research (#142189 (LAP) & #PJT156150 (XD)), Natural Sciences and Engineering Research Council of Canada #2018-06338 (JFT) and a grant of the Korea Health Technology R&D Project through the Korea Health Industry Development Institute (KHIDI), funded by the Ministry of Health & Welfare, Republic of Korea (#H18C1916 (GJC&KWK). The financial support of TELUS

Ride for Dad, Prostate Cancer Fight Foundation (LAP) and Ontario Trillium Scholarship Program (MKB) is greatly appreciated. The gene expression analysis was supported in part by a Department of Defense Idea Development Award-Partnering-PI (W81XWH-17-1-0414;W81XWH-17-1-0415 (CM)) and the Pacific Northwest Prostate Cancer SPORE (P50CA97186 (CM)).

TABLE OF CONTENTS

LIST OF TABLES

LIST OF FIGURES

LIST OF ABBREVIATIONS

^{18}F-FCH ……^{18}F-fluorocholine

^{18}F-FDG ……..……^{18}F-fluorodeoxyglucose

^{18}F-FDHT …… ^{18}F-fluoro-5-dihydrotestosterone

5-FU …… 5-fluorouracil

AdPC…….. Adenocarcinoma of prostate cancer

ADT…… Androgen deprivation therapy

AJCC…… American joint committee on cancer

Akt……..……Protein kinase B

AR ……Androgen receptor

ARPI……..……..…Androgen receptor pathway inhibition

BCR …… Biochemical recurrence

BNF ……..…….. Bionized nanoferrite

cAMP……..……..…. cyclic Adenosine monophosphate

CANF ……..……C-atrial natriuretic factor

CCAC ……..….Canadian council on animal care

CHGA……..……Chromogranin A

CNT ……..…… Carbon nanotubes

CRPC ……...……. Castration-resistant prostate cancer

CSS ……...……..… Charcoal- stripped serum

CT …….. Computed tomography

DHT ……...……...……. Dihydrotestosterone

DNPC ……...…….. Double-negative prostate cancer

DOTA ……..…… 1,4,7,10-tetraazacyclododecane-1,4,7,10-tetraacetic acid

E-MEM ……..……Eagle's minimum essential medium

ENZ…….…… Enzalutamide

FBS……..…… Fetal bovine serum

FC ……...…….. 5-fluorocytosine

FDG……..……..…… Fluorodeoxyglucose

FDR …….……...…… False discovery rate

FOLH1…….…… Folate Hydrolase 1

FRET …… Förster resonance energy transfer

GCK …….…… Glucokinase

GLUT…….…… Glucose transporter

GnRH……..…….. Gonadotropin-releasing hormone

GRPR ……..…… Gastrin-releasing peptide receptor

GSEA ……..…….…… Gene set enrichment analysis

GUL ……..……..…… Glu-Ureido-Lys

HK ……..…… Hexokinases

HPA…….. Human Protein Atlas

HPF …… Hours post-fertilization

HPMA ……..…..…….. Hydroxypropyl methacrylamide

HSP……..…….…….. .Heat shock proteins

IHC……..……Immunohistochemistry

IO ……..……...…….. Iron oxide

IONP ……..……Iron oxide nanoparticle

ITI ……..… Initial test of independence

KLK3……..Kallikrein related peptidase 3

LH…….Luteinizing hormone

mCRPC ……..….. metastatic Castration-resistant prostate cancer

MRI ……..…….Magnetic resonance imaging

MSKCC …….Memorial Sloan Kettering Cancer Center

mTOR……Mammalian target of rapamycin

MWCNT …….Multi-walled carbon nanotube

NAAG……..N-acetyl-l-aspartyl-l-glutamate

NE…….. …….Neuroendocrine

NEGS …… Neuroendocrine gene signature

NELPC…….Neuroendocrine-like prostate cancer

NEPC……..Neuroendocrine prostate cancer

NIR …… Near-infrared

NIRF …….. Near-infrared fluorescence

NPCR …….. Natriuretic peptide clearance receptor

NPRA ……Natriuretic peptide receptor A

NSE…… Neuron specific enolase

p53…….. ……..Protein 53

PC /PCa……..……Prostate cancer

PDX …… Patient-derived xenograft

PET …….. Positron emission tomography

PI3K…….. Phosphatidylinositol 3-kinase

PRRT …….Peptide receptor radiotherapy

PSA ……Prostate specific antigen

PSMA …….. Prostate-specific membrane antigen

QD …… Quantum dots

REST…… Repressor element 1-silencing transcription factor

RP …… Recursive partitioning

SEM ..…… Standard error of the mean

shRNA ……... Small hairpin RNA

siRNA …….. Small interfering RNA

SPECT …….. Single photon emission computed tomography

SRRM4…….. Serine/arginine repetitive matrix protein 4

SSTR2…… Somatostatin receptor subtype 2

MWCNT ……... Single-walled carbon nanotubes

SYP …….. Synaptophysin

UBC…….……..University of British Columbia

UW ……..University of Washington

CHAPTER 1 : GENERAL INTRODUCTION

1.1 PROSTATE MOLECULAR BIOLOGY

1.1.1 Androgen Synthesis in Leydig Cells

Hormones that contribute in male traits and reproductive activity are referred as androgens. Testosterone is formed mostly by the testicles and dihydrotestosterone (DHT) as a metabolite of testosterone mainly regulates the prostate *(Wein, Kavoussi et al., 2011)*. Testosterone, as principle androgen, regulates key steps of male reproductive system development and is indispensable for homeostasis of a variety of tissues including prostate gland *(Wang, Chen et al., 2017)*. Figure 1-1A shows gonadotropin-releasing hormone (GnRH) which is produced by the hypothalamus and regulates secretion of luteinizing hormone (LH). The anterior pituitary gland releases gonadotropic hormone LH into the blood. LH binds to its receptors on Leydig cells in testis, stimulating testosterone synthesis by increasing levels of intracellular level of cyclic adenosine monophosphate (cAMP) which stimulates the transport of cholesterol to the mitochondria to be converted to pregnenolone. Pregnenolone is converted into testosterone in the smooth endoplasmic reticulum and then testosterone is released to the blood.

1.1.2 Androgen Signaling in Prostate Gland

The prostate is an exocrine gland of the male reproductive system in most mammals *(Josef Marx & Karenberg, 2009)*. This walnut-sized gland surrounds the urethra under the bladder and can be sensed during a rectal exam as a first method of detecting potential prostate problems *(Fowke, Motley et al., 2007)*. Figure 1-1B illustrates the anatomic location of the prostate and demonstrates that the gland contains epithelial tissues surrounded by a fibromuscular stroma. The function of the prostate is to secrete a slightly alkaline fluid that constitutes about 30% of the volume of semen together with spermatozoa and seminal

vesicle fluid. The alkalinity of semen helps to neutralize the acidity of the vaginal tract thereby extending the lifetime of sperm *(Huggins, Scott et al., 1942)*. At a cellular level AR-positive secretory epithelial cells are situated on a basal lamina (Figure 1-1C). Basal cells and rare neuroendocrine (NE) cells are in the epithelial compartment. The stromal cells surrounding the epithelial layer consists of a variety of cell types such as smooth muscle cells, fibroblasts cells and blood vessels *(Barron & Rowley, 2012)*. NE-like cells have been suggested to comprise another possible subset of prostate cells with partial NE-characters *(Bakht, Derecichei et al., 2019a, Bakht, Lovnicki et al., 2019c, Spratt, Alshalalfa et al., 2019)*.

The AR protein is encoded by *the AR* gene and acts as a nuclear receptor which is activated by binding testosterone and DHT. When AR is unoccupied by androgens it can be associate as a complex with heat shock proteins (HSP) to prevent AR degradation *(Smith & Toft, 2008)*. Figure 1-1C displays binding of DHT to the AR leading to dissociation from HSP and nuclear translocation of the AR. As a DNA-binding transcription factor AR regulates gene expression of a variety of proteins *(Dai, Heemers et al., 2017)*.

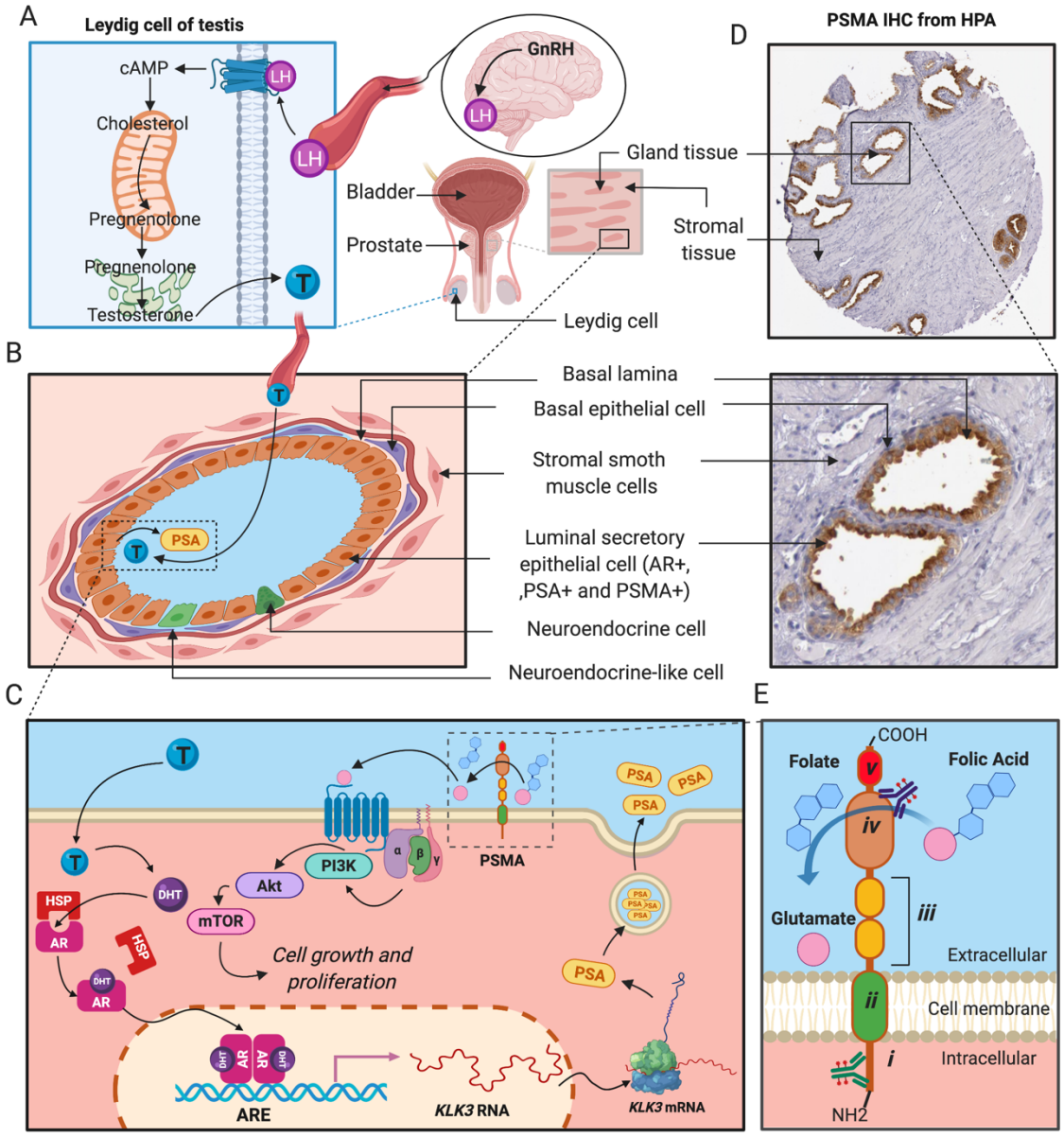

Figure 1-1 Leydig cell steroidogenesis and PSMA expression in prostate gland.

(A) A schematic of the testosterone production in Leydig cell of testis. (B) A schematic of cellular structure of a prostate gland. (C) A summary of androgen activated AR signaling, PSA expression and secretion. (D) A representative PSMA IHC staining of normal prostate tissue. Image available from version 18, Human Protein Atlas (HPA) (https://www.proteinatlas.org/ENSG00000086205-FOLH1). (E) A schematic of the PSMA structure and enzymatic function suggested by *(Kaittanis, Andreou et al., 2018)*. PSMA has intracellular (i), transmembrane (ii) and extracellular (ii-iv) portions. T, testosterone; DHT, dihydrotestosterone; HSP, heat shock protein; ARE, androgen response element.

1.1.3 Prostate Specific Antigen Biology

Kallikreins are a subset of serine proteases and prostate specific antigen (PSA) is a glycoprotein in this subset. *Kallikrein related peptidase 3* (*KLK3)* gene is positively regulated by AR protein and codes PSA protein *(Salman, Schoots et al., 2015)*. Figure 1-1C demonstrates PSA regulation and its secretion. The majority of secreted PSA goes into the seminal fluid to cleave the proteins responsible for seminal clot formation. PSA enzymatic activity leads to declining seminal viscosity and helps motility of spermatozoa *(Salman et al., 2015)*. Figure 1-1B illustrates PSA should be restricted to the prostate gland due to well-fitting and arranged prostate gland architecture in a normal prostate tissue. However, a very low level of the secreted PSA in a gland could be transported in the circulation *(Salman et al., 2015)*.

1.1.4 PSMA biology

PSMA is transmembrane glycoprotein with folate hydrolase and carboxypeptidase capabilities that is encoded by *Folate Hydrolase 1 (FOLH1)* gene located on short arm of chromosome 11. PSMA has a 19-amino-acid intracellular portion (Figure 1-1E-i), a 24-amino-acid transmembrane portion (Figure 1-1E-ii) and a 707-amino-acid extracellular portion (Figure 1-1E-ii,iii and iv) *(Maurer, Eiber et al., 2016, Rahn, Watkins et al., 2012b)*. PSMA is expressed in the renal tissue and duodenum and contributes to the required enzymatic processing of dietary folates *(Rahn, Slusher et al., 2012a)*. Also, a lower level of PSMA in the brain tissue activates metabotropic glutamate receptor (mGluR) pathway activity by facilities N-acetyl-l-aspartyl-l-glutamate (NAAG) cleavage *(Rahn et al., 2012b)*. In prostate tissue, PSMA can activate signaling phosphatidylinositol 3-kinase (PI3K) /Akt (Protein Kinase B)/mammalian target of rapamycin (mTOR) pathway by

release of glutamate *(Kaittanis et al., 2018)*. Figure 1-1C&E illustrates the enzyme actions of PSMA. The catalytic domain of PSMA (Figure 1-1E-iv) facilitates glutamate release from the cleavage of vitamin B9 or folic acid. Free glutamate induces mGluR I activation and activates PI3K through phosphorylation of p110β. Finally, activated PI3K leads to activation of Akt-mTOR and it elevates protein synthesis and growth *(Palamiuc & Emerling, 2018)*.

A representative PSMA immunohistochemistry (IHC) staining of normal prostate tissue from Human Protein Atlas (HPA) on Figure 1-1D displays PSMA expression is highest in AR-positive epithelial cells of the prostate. This work, and previously published papers, show AR-positive cell lines are PSMA-positive as well. On the contrary, AR-negative cell lines are PSMA-negative. However, PSMA is not positively regulated by androgen *(Bakht et al., 2019a, Bakht, Oh et al., 2016, Miyahira, Pienta et al., 2018)*.

1.1.5 Prostate cancer (PC)

The prostate gland is derived from the endoderm germ layer during development and represents a major site for the incidence of malignancy in comparison to its adjacent tissues such as the seminal vesicle with mesoderm origin. PC is defined as a malignant neoplasm of the prostate tissue *(Shen & Rubin, 2019)*. Almost all of PCs originate in the epithelial cells of the prostate gland, a form of cancer classified as a carcinoma. Glandular carcinomas, such as the prostate gland, are commonly referred to as adenocarcinomas. There are rare incidences of prostate sarcomas that originate from cells within the prostate that originate from the surrounding mesenchyme, as well as prostate lymphomas which arise from lymphocytes. Huggins and Hodges *(Huggins & Hodges, 1941)* discovered the androgen-dependent landscape of PC in the 1940s *(Sathianathen, Konety et al., 2018)*. As

a consequence of that seminal study and understanding the key role of androgen signaling in progression of PC, the androgen deprivation therapy (ADT) has become the backbone for treating PC *(Mateo, Fizazi et al., 2018)*.

1.1.6 PC progression

At early stages of PC, cancer cell with a higher AR activity exist among benign prostate gland cells, while higher PSA secretion as an AR-regulated protein is detectible in blood (Figure 1-2A-B). Most men in this level respond to ADT and prostatectomy, but their disease progresses and becomes resistant to further hormonal therapy. Progressively, these cancer cells start to increase and spread to the nearby the stroma leading tumor formation (Figure 1-2C). Ultimately, the cancer cells could metastasis to other organs such as lymph nodes the bones *(Wein et al., 2011)*.

1.1.7 Castration-resistant prostate cancer (CRPC)

Most patients with metastatic disease managed with ADT eventually relapse with CRPC *(Heidenreich, Bastian et al., 2014)*. In CRPC, AR signaling is suggested to be reactivated in several ways, including (*i*) AR overexpression, (*ii*) AR splice variants such as AR-V7 (*iii*) AR gene mutations leading to improvement of the ligand response such as AR^{F876L}, (*iv*) crosstalk with other signaling pathways (*v*) alterations in expression of transcriptional coactivators resulting in improved AR transactivation (vi) prostate cancer stem-like cells *(Bakht, Oh et al., 2017a, Wang et al., 2017)*. Effective and safely administrable AR pathway inhibitor(ARPI), enzalutamide (MDV3100) is a promising treatment option for metastatic CRPC. Also, some recent data suggests the potential of enzalutamide therapy for localized PC *(Caffo, Maines et al., 2014)*. Neuroendocrine prostate cancer (NEPC)

Lineage switching or cellular plasticity is an important developmental process that allows a particular genotype to profoundly alter its phenotype in response to changes in the microenvironment *(Nijhout & development, 2003)*. For cancer cells, cellular plasticity is an opportunistic adaptation to reprogram to a phenotypic version capable of evading cancer treatments to maintain their proliferation *(Davies, Beltran et al., 2018b)*.

The effectiveness of next-generation ARPIs such as abiraterone acetate and enzalutamide, in managing CRPC has been obstructed by the development of cellular plasticity-dependent resistance to ARPIs. In other words, this developed resistance to ARPIs is due to the capability of PC cells to modify their phenotype to adopt AR-independent pathways for proliferation. Around 25% of CRPC tumors treated by ARPI undertaken lineage switching to become AR-independent and to obtain a neuroendocrine (NE) feature. These highly aggressive tumors are named neuroendocrine prostate cancer (NEPC) and show re-activation of developmental or embryonic pathways *(Davies et al., 2018b)*. In this work, patients with lack of NE histopathology or gene signature are referred as adenocarcinoma PC (AdPC).

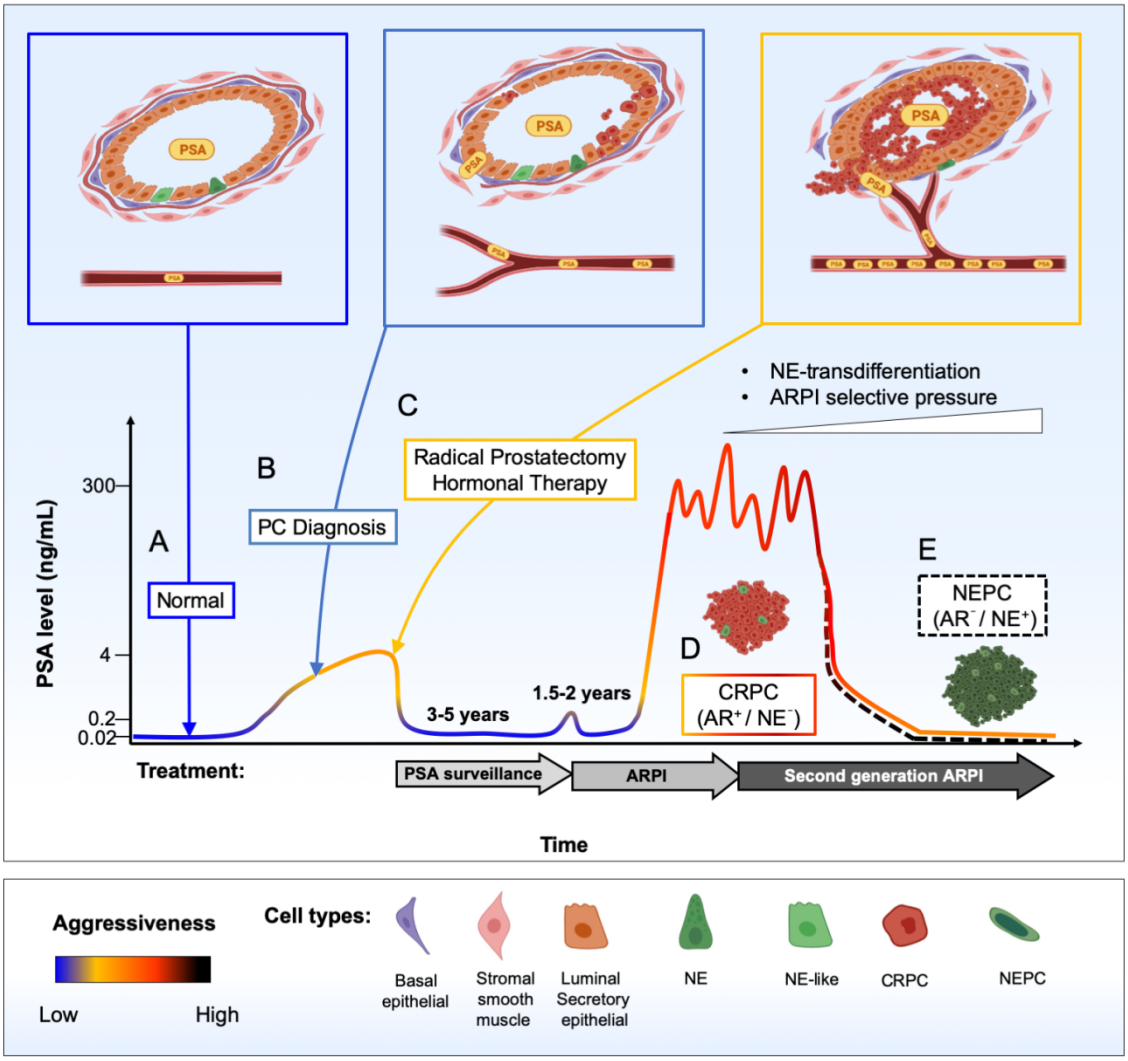

Figure 1-2 A schematic of PC progression and PSA alterations from normal to NEPC.

(A) The normal prostate gland has a well-organized structure and it prevents secretion of PSA in to the blood. (B) Early stage PC is diagnosed after elevation of PSA to above 4 ng/mL increasing angiogenesis. (C) The appropriate ADT approach leads to PSA level decline and ARPI starts as soon as CRPC is formed. (D) CRPC tumor is not responsive to ARPI and PSA is drastically increasing. So, second generation of ARPI is prescribed and PSA level decreases. (E) PSA level surveillance is not effective anymore due to the possibility of NEPC formation.

There are two hypotheses that explain the potential origin of NEPC. First, that normal neuroendocrine cells of the prostate gland undergo oncogenic alteration and form NEPC. Second, AdPC cells undergo transdifferentiation or lineage switching to a NEPC lineage by genetic and epigenetic changes. Recent studies on NEPC profoundly favors the transdifferentiation hypothesis *(Beltran, Prandi et al., 2016b)*. NEPC tumors express common NE markers such as neuron specific enolase (NSE; gene *ENO2*), chromogranin A (CHGA) and synaptophysin (SYP) *(Parimi, Goyal et al., 2014)*. NEPC is associated with the loss of RE1-silencing transcription factor (REST) due to alternate splicing by the RNA splicing factor serine/arginine repetitive matrix 4 (SRRM4). SRRM4 plays a key role in transdifferentiation of AdPC to NEPC under ARPI *(Li, Donmez et al., 2017)*. SRRM4 can induce NEPC in patients treated by ARPI through compromising the function of genes such as REST *(Li et al., 2017)*. The elevation of SRRM4 and the loss of REST are indicators of treatment-induced NEPC.

1.1.8 PC screening

The main aim of PC screening is to identify aggressive PCs as early as possible to prevent progression to a metastatic state, a goal which will ultimately increase survival rates *(Smith, Andrews et al., 2018)*. Screening for PC using a multiparametric protocol by incorporation of transrectal ultrasound (TRUS) data, digital rectal examination (DRE), and PSA level was suggested in the early 1990s *(Cooner, Mosley et al., 1990)*.Multiparametric magnetic resonance imaging (mpMRI) is commonly combined for local staging *(Descotes, 2019)*. PSA screening has considerable shortcomings such as false-positive results that cause redundant biopsies. Recently, US Preventive Services Task Force and Canadian Task Force on Preventive Health Care modified PC screening protocols to decrease chance of over-

diagnosis and overtreatment of PC *(Jin, 2018, Rendon, Mason et al., 2017)*. Currently, the DRE and PSA test followed by a TRUS guided biopsy is still standard of care for PC screening around the world, including Canada *(Rendon et al., 2017)*. Technetium scintigraphy is also the current gold standard for detection of bone metastasis *(Descotes, 2019)*.

1.1.9 Gleason scoring and PC staging

In 1966, Dr. Donald Gleason established his grading scoring system for PC *(Gleason, 1966)*. The Gleason system assigns grades are based on the level of similarity between PC and benign tissues. If the apparent PC tissue is similar to benign prostate tissue, a grade of 1 is apportioned *(Sathianathen et al., 2018)*. If the malignant tissue seems hugely abnormal, a grade of 5 will be assigned. Grades 2 to 4 have characters in between these extremes. Since PC regularly have zones with dissimilar grades, a grade is assigned to the 2 regions that contribute the most of malignancy. Finally, these 2 grades are added to yield the Gleason score. So, the first number given is the grade that is most common in the tissue *(Partin, Kattan et al., 1997)*. To increase agreement between needle biopsy and radical prostatectomy pathology, a Modified Gleason scoring classification was published by Epstein et al.in 2016 and accepted by the WHO *(Epstein, Egevad et al., 2016, Harnden, Shelley et al., 2007)*.

As the most prevalent staging protocol for PC is the American Joint Committee on Cancer (AJCC) proposed tumor nodes metastasized (TNM) system (Table 1-1). The TNM system for prostate cancer is based on five main points: (i) The extent of the main (primary) tumor (T category) (ii) Whether the cancer has spread to nearby lymph nodes (N category) (iii) Whether the cancer has metastasized to other parts of the body (M category) (iv) The PSA

level at the time of diagnosis (v) The Gleason score *(Mottet, Bellmunt et al., 2017)*. The main stages of PC range from I (1) to IV (4) *(Grignon, 2018)*.

1.1.10 PC in Canada

In 2019, it is estimated that 22,900 men will be diagnosed with PC in Canada. Also, 4,100 men will die from PC, which denotes 9% of all cancer deaths in men in 2019. In other words, on average, 63 Canadian men will be diagnosed with PC, and 11 Canadian men will die from PC every day.

In Canada, the five-year net survival for prostate cancer is among the highest of all cancers at 95%. Estimates from the United States (where five-year survival is closer to 97%), indicate that survival for early stage disease is almost 100%. But it is much lower for cancers that presented with distant metastases (stage IV) at diagnosis (29%) (Table 1-1).

Table 1-1 AJCC stating protocol and percent distribution of PC at diagnosis in Canada.

Stages of PC and percent distribution of PC by stage at diagnosis in Canadian men between 2011–2015 *(CCSsACoC, 2014, Grignon, 2018, Mottet et al., 2017)*.

AJCC Stage	Stage grouping	Percent distribution of PC at diagnosis in Canada
I	cT1, N0, M0 Grade Group 1 (Gleason score 6 or less) PSA less than 10	22.5%
	cT2a, N0, M0 Grade Group 1 (Gleason score 6 or less) PSA less than 10	
	pT2, N0, M0 Grade Group 1 (Gleason score 6 or less) PSA less than 10	
IIA	cT1, N0, M0 Grade Group 1 (Gleason score 6 or less) PSA at least 10 but less than 20	51.9%
	cT2a or pT2, N0, M0 Grade Group 1 (Gleason score 6 or less) PSA at least 10 but less than 20	
IIB	cT2b or cT2c, N0, M0 Grade Group 1 (Gleason score 6 or less) PSA less than 20 T1 or T2, N0, M0 Grade Group 2 (Gleason score 3+4=7) PSA less than 20	
IIC	T1 or T2, N0, M0 Grade Group 3 or 4 (Gleason score 4+3=7 or 8) PSA less than 20	
IIIA	T1 or T2, N0, M0 Grade Group 1 to 4 (Gleason score 8 or less) PSA at least 20	13.8%
IIIB	T3 or T4, N0, M0 Grade Group 1 to 4 (Gleason score 8 or less) Any PSA	
IIIC	Any T, N0, M0 Grade Group 5 (Gleason score 9 or 10) Any PSA	
IVA	Any T, N1, M0 Any Grade Group Any PSA	8.6%
IVB	Any T, any N, M1 Any Grade Group Any PSA	

1.2 NUCLEAR MEDICINE AND MOLECULAR IMAGING

Nuclear imaging modalities can be commonly classified into positron emission tomography (PET) and single photon emission computed tomography (SPECT). Unlike CT or MRI, which visualize structure or anatomic of tissue, PET and SPECT generate functional or metabolic images of tissues *(Khan & Gibbons, 2014, Mayles, Nahum et al., 2007)*. The fusion of therapy and diagnostics to optimize the efficacy and safety of therapeutic regimes is named theranostics and is a rapidly growing approach. Currently, PET and SPECT images are regularly fused with other structural imaging modalities, such as CT or MRI, to correlate functional with anatomical information *(Azad & Cook, 2016, Maurer, 2008)*.

1.2.1 PC Molecular Imaging

A variety of radiopharmaceuticals are being used for PC molecular imaging and we can classify them in these categories: (i) bone imaging, (ii) PC metabolic activity, and (iii) PSMA expression.

Table 1-2 summarises these options. Also, the flow-chart on Figure 1-3 represents the significance of molecular imaging in the management of PC *(Evangelista, Briganti et al., 2016)*.

Table 1-2 An overview of the radiopharmaceuticals for PC molecular imaging.

Adopted with permission *(Glumac, 2019)*.

Radiopharmaceutical	Target	Indication	Regulatory Status
FDG	Glucose metabolism	minimal use in PC, only used when other tracers are not available	FDA approved, August 5, 2004
NaF	Osteoblastic activity	Known or suspected osseous lesions	FDA Approved, January 26, 2011
^{11}C-choline	Cell membrane metabolism	High-risk staging, biochemical relapse at high PSA levels	FDA approved, September 12, 2012
^{11}C-acetate	Fatty acid synthesis	Useful for monitoring recurrence after focal therapy, unreliable in biochemical recurrence, not as effective as other agents on the market	Under investigation
Fluciclovine	Amino acid transport	High-risk staging, biochemical relapse at high PSA levels	FDA approved, May 27, 2016
FDHT	AR	Early stage disease detection and prognosis	Under investigation
anti-PSMA ligands	PSMA	Multiple stages including biochemical relapse at low PSA	Under investigation

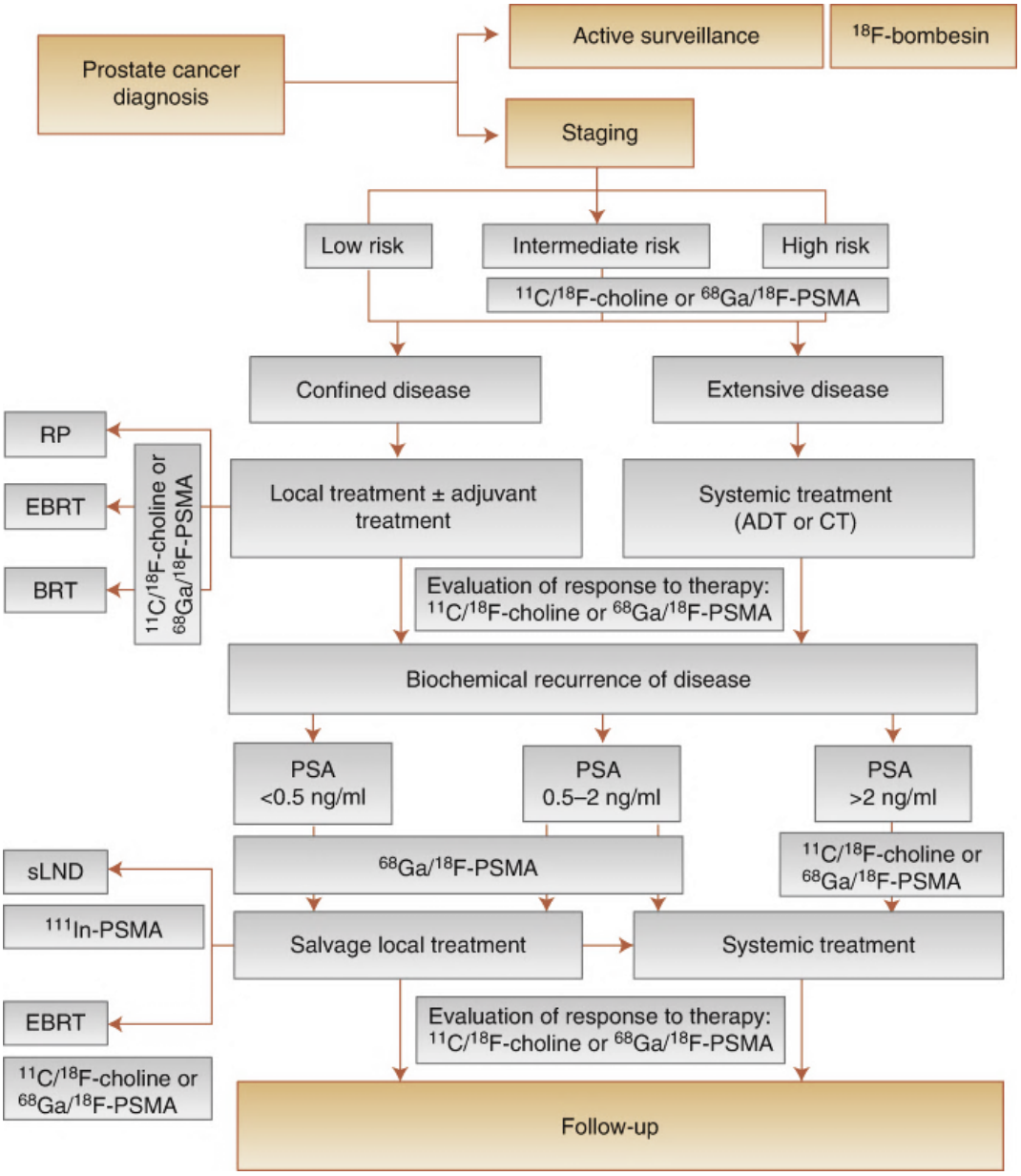

Figure 1-3 Flow-chart depicting the roles of molecular imaging in the diagnostic management of prostate cancer patients.

ADT, Antiandrogen therapy; BRT, brachytherapy; CT, chemotherapy; EBRT, external beam radiotherapy; PSA, prostate-specific antigen; PSMA, prostate-specific membrane antigen; RP, radical prostatectomy; sLND, salvage lymphadenectomy; ^{18}F, fluorine-18; ^{11}C, choline-11; ^{68}Ga, gallium-68; ^{111}In, indium-111. Reprinted with permission *(Evangelista et al., 2016)*

1.2.2 PSMA-targeted molecular imaging

PSMA is an appealing target for molecular imaging and therapy of PC since it is over-expressed in a majority of PC tumors and metastatic lesions *(Rai, Baum et al., 2016)*. Targeting PSMA is feasible by a wide variety of radio-ligands *(Jadvar & Ballas, 2018, Kopka, Benešová et al., 2017, Rowe, Gorin et al., 2017)*. The PSMA ligands can also be labelled with therapeutic radionuclides which can irradiate PSMA-expressing cells *(Boegemann, Schrader et al., 2017)*. In spite of the promissing applications of PSMA for many forms of advanced PC there are clinical reports supporting that PSMA-targeted imaging is not able to define NEPC tumors *(Chakraborty, Tripathi et al., 2015, Parimi et al., 2014, Sheikhbahaei, Afshar-Oromieh et al., 2017, Tosoian, Gorin et al., 2017a, Usmani, Ahmed et al., 2017)*.

1.2.3 Somatostatin receptor-targeted molecular imaging

The somatostatin receptor subtype 2 (SSTR2) is prevalent in the majority NE tumors and DOTATOC and DOTA-TATE radioligands with affinity to SSTR are radiotracers for delineation of NE tumors *(Poeppel, Binse et al., 2011)*. Recently, Gofrit et al. suggested that ^{68}Ga-DOTA-TATE might be a potential option for NEPC imaging *(Gofrit, Frank et al., 2017)*. Interestingly, Usmani et al. compared ^{68}Ga-PSMA versus ^{68}Ga-DOTA in a NEPC patient and reported that the NEPC tumor and metastatic lesions have avid uptake of ^{68}Ga-DOTA while the ^{68}Ga-PSMA uptake was faint and inconclusive *(Usmani et al., 2017)*. These same reports suggest that targeting somatostatin receptor type 2 (SSTR2) could be an alternative diagnostic target for NEPC patients.

1.2.4 FDG metabolic imaging

Similar to glucose, ^{18}F-fluorodeoxyglucose (FDG) is actively transported into the cell by the protein family of glucose transporters (GLUTs), encoded by *SLC2A* genes, followed by phosphorylation by hexokinase *(Haberkorn, Ziegler et al., 1994)*. In some types of tumors a positive correlation has been reported between FDG uptake and the levels of specific GLUTs and hexokinases *(Avril, 2004, Haberkorn et al., 1994, Yang, Zhong et al., 2019)*. FDG-positron emission tomography (PET) is a well-accepted approach for delineation of proliferative and poorly-differentiated/dedifferentiated NE-tumors *(Bozkurt, Virgolini et al., 2017)*. Despite this, FDG-PET has been considered ineffective in assessing metastatic tumor burden and monitoring therapy response *(Jadvar, 2016)*. Previous clinical reports indicate that PCs with a phenotype similar to NE tumors can be more amenable to imaging by FDG rather than PSMA-targeting radioligands.

1.3 NANOMEDICINE

Nanotechnology has been used in most areas of biomedical research *(Bawarski, Chidlowsky et al., 2008, Davis & Shin, 2008, Fontanarosa & Bauchner, 2015, Liu, MacDonald et al., 2013, Morris, Molina et al., 2015, Sitharaman, 2016)*, with many applications in cancer therapy *(Chen, Gu et al., 2015, Currell & Bellringer, 2016, Ferrari, 2005, Mirkin, Meade et al., 2015, Wang, Yang et al., 2008)*, it is expected that nanomedicine could play important diagnostic and therapeutic roles in oncology *(Bregoli, Movia et al., 2016)*. Nanomedicine may improve screening and therapeutic options for different cancers by exploiting the unique characteristics of each tumor *(Hammond, 2016, Kuncic, 2015, Tong & Kohane, 2016, Wicki, Witzigmann et al., 2015, Xu, Ho et al., 2015)*. Thereby, nanomedicine may represent a vehicle for the delivery of important aspects of

personalized cancer management *(Collins & Varmus, 2015, Hammond, 2016, Herrmann & Rösslein, 2016)*.

1.4 HYPOTHESES AND OBJECTIVES

In Chapter 2, the correlation between expression of *FOLH1*, NEPC marker genes and *SSTR2* is investigated. We evaluated the transcript abundance for *FOLH1* and *SSTR2* genes as well as NE markers in a variety of models. This study scrutinizes the reliability of using PMSA as a target for molecular imaging of NEPC. The observed elevation of *SSTR2* in NEPC supports the possible ability of SSTR2-targeted imaging for follow-up imaging of low-PSMA patients and monitoring for NEPC development. Specifically, the following topics will be investigated:

- The possible inconsistency of PSMA gene expression in high grade CRPC.
- The correlation between the expression of PSMA and common NE biomarker genes.
- The apparent suppression of PSMA in treatment-induced NEPC.
- The possible inverse correlation between the expression of *FOLH1* and *SSTR2*.
- The survival rates of patients with enhanced expressions of NE-makers.

In Chapter 3, the association between NE gene signature and FDG uptake-associated genes including glucose transporters (GLUTs) and hexokinases is evaluated, with the goal of providing a genomic signature to explain the reported FDG-avidity of PSMA-suppressed tumors. We measured glucose uptake in a NE-induced *in vitro* model and a zebrafish model by non-radioactive imaging of glucose uptake using fluorescent glucose bioprobe, GB2-Cy3. Spesifically, the following topics will be investigated:

- The identification of a NE-like PC (NELPC) subset among a cohort of primary and metastatic PC samples.
- The assumable differential expression of SLC2A and HK in NEPC and NELPC.
- The possible association of SLC2A and HK expression with Gleason score and biochemical recurrence in NELPC.
- The possible used of zebrafish model for in vivo imaging of glucose uptake.

In Chapter 4 as a review chapter, a wide variety of nanostructure-based prostate cancer research using radiation technology and nuclear medicine is discussed. Radionanomedicine is a recently coined term for the simultaneous application of either radiation technology or nuclear medicine with nanomedicine. Radioexosomics is our suggested term for the study of exosomes functions, cytotoxicity, cancerogenicity, and biodistribution using radiation technology and nuclear medicine tracing technology. In addition, we will present what is currently known about the function of exosomes in PC. The review concludes by summarizing the current status and future perspectives of radionanomedicine and radioexosomic for understanding PC biology and the perspectives in targeting strategies, drug delivery, molecular imaging and therapy.

1.5 REFERENCES

Avril N (2004) GLUT1 Expression in Tissue and 18F-FDG Uptake. *J Nucl Med* 45: 930-932

Azad GK, Cook GJ (2016) Multi-technique imaging of bone metastases: spotlight on PET-CT. *Clinical radiology* 71: 620-631

Bakht MK, Derecichei I, Li Y, Ferraiuolo R-M, Dunning M, Oh SW, Hussein A, Youn H, Stringer KF, Jeong CW, Cheon GJ, Kwak C, Kang KW, Lamb AD, Wang Y, Dong X, Porter LA (2019a) Neuroendocrine differentiation of prostate cancer leads to PSMA suppression. *Endocrine-Related Cancer* 26: 131

Bakht MK, Lovnicki JM, Tubman J, Stringer KF, Chiaramonte J, Reynolds MR, al e (2019c) Differential expression of glucose transporters and hexokinases in prostate cancer with a neuroendocrine gene signature: a mechanistic perspective for FDG imaging of PSMA-suppressed tumors. *Journal of Nuclear Medicine*

Bakht MK, Oh SW, Hwang DW, Lee YS, Youn H, Porter LA, Cheon GJ, Kwak C, Lee DS, Kang KW (2017a) The Potential Roles of Radionanomedicine and Radioexosomics in Prostate Cancer Research and Treatment. *Curr Pharm Des* 23: 2976-2990
Bakht MK, Oh SW, Youn H, Cheon GJ, Kwak C, Kang KW (2016) Influence of Androgen Deprivation Therapy on the Uptake of PSMA-Targeted Agents: Emerging Opportunities and Challenges. *Nuclear medicine and molecular imaging*: 1-10
Barron DA, Rowley DR (2012) The reactive stroma microenvironment and prostate cancer progression. 19: R187
Bawarski WE, Chidlowsky E, Bharali DJ, Mousa SA (2008) Emerging nanopharmaceuticals. *Nanomedicine: Nanotechnology, Biology and Medicine* 4: 273-282
Beltran H, Prandi D, Mosquera JM, Benelli M, Puca L, Cyrta J, Marotz C, Giannopoulou E, Chakravarthi BV, Varambally SJNm (2016b) Divergent clonal evolution of castration-resistant neuroendocrine prostate cancer. 22: 298
Boegemann M, Schrader AJ, Rahbar K (2017) [177Lu-PSMA therapy : Current evidence for use in the treatment of patients with metastatic prostate cancer]. *Urologe A*
Bozkurt MF, Virgolini I, Balogova S, Beheshti M, Rubello D, Decristoforo C, Ambrosini V, Kjaer A, Delgado-Bolton R, Kunikowska J, Oyen WJG, Chiti A, Giammarile F, Fanti S (2017) Guideline for PET/CT imaging of neuroendocrine neoplasms with 68Ga-DOTA-conjugated somatostatin receptor targeting peptides and 18F–DOPA. *European journal of nuclear medicine and molecular imaging* 44: 1588-1601
Bregoli L, Movia D, Gavigan-Imedio JD, Lysaght J, Reynolds J, Prina-Mello A (2016) Nanomedicine applied to translational oncology: a future perspective on cancer treatment. *Nanomedicine: Nanotechnology, Biology and Medicine* 12: 81-103
Caffo O, Maines F, Donner D, Veccia A, Chierichetti F, Galligioni E (2014) Impact of enzalutamide administration on primary prostate cancer volume: a metabolic evaluation by choline positron emission tomography in castration-resistant prostate cancer patients. *Clinical genitourinary cancer* 12: 312-6
CCSsACoC S (2014) Canadian cancer statistics 2014. *Toronto, ON: Canadian Cancer Society* 2014
Chakraborty PS, Tripathi M, Agarwal KK, Kumar R, Vijay MK, Bal C (2015) Metastatic poorly differentiated prostatic carcinoma with neuroendocrine differentiation: negative on 68Ga-PSMA PET/CT. *Clinical nuclear medicine* 40: e163-166
Chen J, Gu W, Yang L, Chen C, Shao R, Xu K, Xu ZP (2015) Nanotechnology in the management of cervical cancer. *Reviews in medical virology* 25: 72-83
Collins FS, Varmus H (2015) A new initiative on precision medicine. *New England Journal of Medicine* 372: 793-795
Cooner WH, Mosley BR, Rutherford CL, Jr., Beard JH, Pond HS, Terry WJ, Igel TC, Kidd DD (1990) Prostate cancer detection in a clinical urological practice by ultrasonography, digital rectal examination and prostate specific antigen. *J Urol* 143: 1146-52; discussion 1152-4
Currell F, Bellringer M (2016) Cancer Nanotechnology Startup Challenge: a new way to realize the fruits of innovation. *Cancer nanotechnology* 7: 1-2
Dai C, Heemers H, Sharifi N (2017) Androgen Signaling in Prostate Cancer. *Cold Spring Harb Perspect Med* 7
Davies AH, Beltran H, Zoubeidi A (2018b) Cellular plasticity and the neuroendocrine phenotype in prostate cancer. *Nature reviews Urology* 15: 271-286
Davis ME, Shin DM (2008) Nanoparticle therapeutics: an emerging treatment modality for cancer. *Nature reviews Drug discovery* 7: 771-782
Descotes J-L (2019) Diagnosis of prostate cancer. *Asian J Urol* 6: 129-136
Epstein JI, Egevad L, Amin MB, Delahunt B, Srigley JR, Humphrey PA (2016) The 2014 International Society of Urological Pathology (ISUP) Consensus Conference on Gleason Grading

of Prostatic Carcinoma: Definition of Grading Patterns and Proposal for a New Grading System. *Am J Surg Pathol* 40: 244-52
Evangelista L, Briganti A, Fanti S, Joniau S, Reske S, Schiavina R, Stief C, Thalmann GN, Picchio M (2016) New Clinical Indications for (18)F/(11)C-choline, New Tracers for Positron Emission Tomography and a Promising Hybrid Device for Prostate Cancer Staging: A Systematic Review of the Literature. *Eur Urol* 70: 161-175
Ferrari M (2005) Cancer nanotechnology: opportunities and challenges. *Nature Reviews Cancer* 5: 161-171
Fontanarosa PB, Bauchner H (2015) Scientific discovery and the future of medicine. *JAMA* 313: 145-146
Fowke J, Motley S, Cookson M, Concepcion R, Chang S, Wills M, Smith Jr J (2007) The association between body size, prostate volume and prostate-specific antigen. *Prostate Cancer Prostatic Dis* 10: 137
Gleason DF (1966) Classification of prostatic carcinomas. *Cancer Chemother Rep* 50: 125-8
Glumac PM (2019) Targeting CD133 In Androgen Receptor Indifferent, Neuroendocrine Differentiated Aggressive Variant Prostate Cancer.
Gofrit ON, Frank S, Meirovitz A, Nechushtan H, Orevi M (2017) PET/CT With 68Ga-DOTA-TATE for Diagnosis of Neuroendocrine: Differentiation in Patients With Castrate-Resistant Prostate Cancer. *Clinical nuclear medicine* 42: 1-6
Grignon DJ (2018) Prostate cancer reporting and staging: needle biopsy and radical prostatectomy specimens. *Mod Pathol* 31: S96
Haberkorn U, Ziegler SI, Oberdorfer F, Trojan H, Haag D, Peschke P, Berger MR, Altmann A, Van Kaick G (1994) FDG uptake, tumor proliferation and expression of glycolysis associated genes in animal tumor models. *Nucl Med Biol* 21: 827-834
Hammond PT (2016) Shooting for the Moon: Nanoscale Approaches to Cancer. *ACS nano* 10: 1711-1713
Harnden P, Shelley MD, Coles B, Staffurth J, Mason MD (2007) Should the Gleason grading system for prostate cancer be modified to account for high-grade tertiary components? A systematic review and meta-analysis. *The Lancet Oncology* 8: 411-419
Heidenreich A, Bastian PJ, Bellmunt J, Bolla M, Joniau S, van der Kwast T, Mason M, Matveev V, Wiegel T, Zattoni F, Mottet N (2014) EAU guidelines on prostate cancer. Part II: Treatment of advanced, relapsing, and castration-resistant prostate cancer. *European urology* 65: 467-79
Herrmann IK, Rösslein M (2016) Personalized medicine: the enabling role of nanotechnology. *Nanomedicine* 11: 1-3
Huggins C, Hodges CV (1941) Studies on prostatic cancer. *Cancer Res* 1: 297
Huggins C, Scott WW, Heinen JH (1942) Chemical composition of human semen and of the secretions of the prostate and seminal vesicles. *American Journal of Physiology-Legacy Content* 136: 467-473
Jadvar H (2016) PET of glucose metabolism and cellular proliferation in prostate cancer. *J Nucl Med* 57: 25S-29S
Jadvar H, Ballas LK (2018) PSMA PET: Transformational change in prostate cancer management? *Journal of Nuclear Medicine* 59: 228-229
Jin J (2018) Screening for Prostate Cancer. *JAMA* 319: 1946-1946
Josef Marx F, Karenberg A (2009) History of the term prostate. *The Prostate* 69: 208-213
Kaittanis C, Andreou C, Hieronymus H, Mao N, Foss CA, Eiber M, Weirich G, Panchal P, Gopalan A, Zurita J, Achilefu S, Chiosis G, Ponomarev V, Schwaiger M, Carver BS, Pomper MG, Grimm J (2018) Prostate-specific membrane antigen cleavage of vitamin B9 stimulates oncogenic signaling through metabotropic glutamate receptors. *J Exp Med* 215: 159-175
Khan FM, Gibbons JP (2014) *Khan's the physics of radiation therapy*. Lippincott Williams & Wilkins,

Kopka K, Benešová M, Bařinka C, Haberkorn U, Babich J (2017) Glu-Ureido–Based Inhibitors of Prostate-Specific Membrane Antigen: Lessons Learned During the Development of a Novel Class of Low-Molecular-Weight Theranostic Radiotracers. *Journal of Nuclear Medicine* 58: 17S-26S

Kuncic Z (2015) Cancer nanomedicine: challenges and opportunities. *The Medical journal of Australia* 203: 204-205

Li Y, Donmez N, Sahinalp C, Xie N, Wang Y, Xue H, Mo F, Beltran H, Gleave M, Wang Y, Collins C, Dong X (2017) SRRM4 Drives Neuroendocrine Transdifferentiation of Prostate Adenocarcinoma Under Androgen Receptor Pathway Inhibition. *Eur Urol* 71: 68-78

Liu TW, MacDonald TD, Jin CS, Gold JM, Bristow RG, Wilson BC, Zheng G (2013) Inherently Multimodal Nanoparticle-Driven Tracking and Real-Time Delineation of Orthotopic Prostate Tumors and Micrometastases. *ACS Nano* 7: 4221-4232

Mateo J, Fizazi K, Gillessen S, Heidenreich A, Perez-Lopez R, Oyen WJG, Shore N, Smith M, Sweeney C, Tombal B, Tomlins SA, de Bono JS (2018) Managing Nonmetastatic Castration-resistant Prostate Cancer. *Eur Urol*

Maurer AH (2008) COMBINED IMAGING MODALITIES: PET/CT AND SPECT/CT. *Health physics* 95: 571-576

Maurer T, Eiber M, Schwaiger M, Gschwend JE (2016) Current use of PSMA-PET in prostate cancer management. *Nat Rev Urol* 13: 226-35

Mayles P, Nahum A, Rosenwald J-C (2007) *Handbook of radiotherapy physics: theory and practice*. CRC Press,

Mirkin CA, Meade TJ, Petrosko SH, Stegh AH (2015) *Nanotechnology-Based Precision Tools for the Detection and Treatment of Cancer*. Springer,

Miyahira AK, Pienta KJ, Morris MJ, Bander NH, Baum RP, Fendler WP, Goeckeler W, Gorin MA, Hennekes H, Pomper MG (2018) Meeting report from the Prostate Cancer Foundation PSMA-directed radionuclide scientific working group. *The Prostate* 78: 775-789

Morris MJ, Molina A, Small EJ, de Bono JS, Logothetis CJ, Fizazi K, de Souza P, Kantoff PW, Higano CS, Li J (2015) Radiographic progression-free survival as a response biomarker in metastatic castration-resistant prostate cancer: COU-AA-302 results. *Journal of Clinical Oncology* 33: 1356-1363

Mottet N, Bellmunt J, Bolla M, Briers E, Cumberbatch MG, De Santis M, Fossati N, Gross T, Henry AM, Joniau S, Lam TB, Mason MD, Matveev VB, Moldovan PC, van den Bergh RCN, Van den Broeck T, van der Poel HG, van der Kwast TH, Rouvière O, Schoots IG et al. (2017) EAU-ESTRO-SIOG Guidelines on Prostate Cancer. Part 1: Screening, Diagnosis, and Local Treatment with Curative Intent. *Eur Urol* 71: 618-629

Nijhout HFJE, development (2003) Development and evolution of adaptive polyphenisms. 5: 9-18

Palamiuc L, Emerling BM (2018) PSMA brings new flavors to PI3K signaling: A role for glutamate in prostate cancer. *The Journal of Experimental Medicine* 215: 17-19

Parimi V, Goyal R, Poropatich K, Yang XJ (2014) Neuroendocrine differentiation of prostate cancer: a review. *American Journal of Clinical and Experimental Urology* 2: 273-285

Partin AW, Kattan MW, Subong EN, Walsh PC, Wojno KJ, Oesterling JE, Scardino PT, Pearson J (1997) Combination of prostate-specific antigen, clinical stage, and Gleason score to predict pathological stage of localized prostate cancer: a multi-institutional update. *JAMA* 277: 1445-1451

Poeppel TD, Binse I, Petersenn S, Lahner H, Schott M, Antoch G, Brandau W, Bockisch A, Boy C (2011) 68Ga-DOTATOC versus 68Ga-DOTATATE PET/CT in functional imaging of neuroendocrine tumors. *J Nucl Med* 52: 1864-70

Rahn KA, Slusher BS, Kaplin AI (2012a) Glutamate in CNS neurodegeneration and cognition and its regulation by GCPII inhibition. *Curr Med Chem* 19: 1335-45

Rahn KA, Watkins CC, Alt J, Rais R, Stathis M, Grishkan I, Crainiceau CM, Pomper MG, Rojas C, Pletnikov MV, Calabresi PA, Brandt J, Barker PB, Slusher BS, Kaplin AI (2012b) Inhibition of Glutamate Carboxypeptidase II (GCPII) activity as a treatment for cognitive impairment in multiple sclerosis. *Proceedings of the National Academy of Sciences* 109: 20101-20106

Rai BP, Baum R, Patel A, Hughes R, Alonzi R, Lane T, Adshead J, Vasdev N (2016) The Role PET with 68 Gallium (Ga)-Labelled Prostate-Specific Membrane Antigen (PSMA) in the Management of Patient with Organ Confined and Locally Advanced Prostate Cancer Prior to Radical Treatment and after Radical Prostatectomy. *Urology*

Rendon RA, Mason RJ, Marzouk K, Finelli A, Saad F, So A, Violette P, Breau RH (2017) Recommandations de l'Association des urologues du Canada sur le dépistage et le diagnostic précoce du cancer de la prostate. *Canadian Urological Association journal* 11: 298-309

Rowe SP, Gorin MA, Pomper MG (2017) Imaging of Prostate-Specific Membrane Antigen Using [18F] DCFPyL. *PET clinics* 12: 289-296

Salman JW, Schoots IG, Carlsson SV, Jenster G, Roobol MJ (2015) Prostate Specific Antigen as a Tumor Marker in Prostate Cancer: Biochemical and Clinical Aspects. *Adv Exp Med Biol* 867: 93-114

Sathianathen NJ, Konety BR, Crook J, Saad F, Lawrentschuk N (2018) Landmarks in prostate cancer. *Nature reviews Urology* 15: 627-642

Sheikhbahaei S, Afshar-Oromieh A, Eiber M, Solnes LB, Javadi MS, Ross AE, Pienta KJ, Allaf ME, Haberkorn U, Pomper MG, Gorin MA, Rowe SP (2017) Pearls and pitfalls in clinical interpretation of prostate-specific membrane antigen (PSMA)-targeted PET imaging. *European journal of nuclear medicine and molecular imaging* 44: 2117-2136

Shen MM, Rubin MA (2019) Prostate Cancer Research at the Crossroads. *Cold Spring Harb Perspect Med* 9

Sitharaman B (2016) *Nanobiomaterials handbook*. CRC Press,

Smith DF, Toft DO (2008) Minireview: the intersection of steroid receptors with molecular chaperones: observations and questions. *Mol Endocrinol* 22: 2229-40

Smith RA, Andrews KS, Brooks D, Fedewa SA, Manassaram-Baptiste D, Saslow D, Brawley OW, Wender RC (2018) Cancer screening in the United States, 2018: A review of current American Cancer Society guidelines and current issues in cancer screening. *CA: A Cancer Journal for Clinicians* 68: 297-316

Spratt DE, Alshalalfa M, Fishbane N, Weiner AB, Mehra R, Mahal BA, Lehrer J, Liu Y, Zhao SG, Speers C, Morgan TM, Dicker AP, Freedland SJ, Karnes RJ, Weinmann S, Davicioni E, Ross AE, Den RB, Nguyen PL, Feng FY et al. (2019) Transcriptomic heterogeneity of androgen receptor (AR) activity defines a de novo low AR-active subclass in treatment naïve primary prostate cancer. *Clinical Cancer Research*: clincanres.1587.2019

Tong R, Kohane DS (2016) New strategies in cancer nanomedicine. *Annual review of pharmacology and toxicology* 56: 41-57

Tosoian JJ, Gorin MA, Rowe SP, Andreas D, Szabo Z, Pienta KJ, Pomper MG, Lotan TL, Ross AE (2017a) Correlation of PSMA-Targeted (18)F-DCFPyL PET/CT Findings With Immunohistochemical and Genomic Data in a Patient With Metastatic Neuroendocrine Prostate Cancer. *Clinical genitourinary cancer* 15: e65-e68

Usmani S, Ahmed N, Marafi F, Rasheed R, Amanguno HG, Al Kandari F (2017) Molecular Imaging in Neuroendocrine Differentiation of Prostate Cancer: 68Ga-PSMA Versus 68Ga-DOTA NOC PET-CT. *Clinical nuclear medicine* 42: 410-413

Wang X, Yang L, Chen ZG, Shin DM (2008) Application of nanotechnology in cancer therapy and imaging. *CA: a cancer journal for clinicians* 58: 97-110

Wang Y, Chen F, Ye L, Zirkin B, Chen H (2017) Steroidogenesis in Leydig cells: effects of aging and environmental factors. *Reproduction* 154: R111-r122

Wein AJ, Kavoussi LR, Novick AC, Partin AW, Peters CA (2011) *Campbell-Walsh urology: expert consult premium edition: enhanced online features and print, 4-volume set*. Elsevier Health Sciences,
Wicki A, Witzigmann D, Balasubramanian V, Huwyler J (2015) Nanomedicine in cancer therapy: challenges, opportunities, and clinical applications. *Journal of Controlled Release* 200: 138-157
Xu X, Ho W, Zhang X, Bertrand N, Farokhzad O (2015) Cancer nanomedicine: from targeted delivery to combination therapy. *Trends in molecular medicine* 21: 223-232
Yang H, Zhong JT, Zhou SH, Han HM (2019) Roles of GLUT-1 and HK-II expression in the biological behavior of head and neck cancer. *Oncotarget* 10: 3066-3083

CHAPTER 2 : NEUROENDOCRINE DIFFERENTIATION OF PROSTATE CANCER LEADS TO PSMA SUPPRESSION

2.1 INTRODUCTION

The main treatment protocol for patients suffering from castration-resistant prostate cancer (CRPC) is androgen receptor pathway inhibition (ARPI). Selection pressure and lineage plasticity of ARPI can lead to neuroendocrine (NE) differentiation of prostate adenocarcinoma (AdPC), promoting the more prevalent subtype of CRPC which is termed treatment-induced neuroendocrine prostate cancer (NEPC) *(Davies, Beltran et al., 2018a)*. It has been speculated that mutations in lineage regulators such as retinoblastoma 1 (Rb1) and tumor protein 53 (p53) could also pave the way of ARPI to confer AdPC lineage plasticity and development of NEPC *(Chen, Dong et al., 2018)*.

Due to the presumed androgen receptor (AR)-negativity of NEPC tumors, treatment options are restricted to platinum- and cisplatin-based combinations and median survival of NEPC patients is much lower than patients with AdPC *(Vlachostergios & Papandreou, 2015)*. Early identification of NEPC and novel targeting options could be beneficial. Despite the positive implications of PSMA for many forms of advanced AdPC there are clinical reports supporting that PSMA-targeted imaging is not able to delineate NEPC tumors *(Chakraborty et al., 2015, Parimi et al., 2014, Sheikhbahaei et al., 2017, Tosoian et al., 2017a, Usmani et al., 2017)*. In four specific cases NEPC patients did not show substantial PSMA-radioligand uptake, in one case this was described due to a down-regulation of PSMA *(Chakraborty et al., 2015, Parida, Tripathy et al., 2018, Tosoian et al., 2017a, Usmani et al., 2017)*. To date the relevance of these clinical reports have not been investigated.

In this study we use bioinformatic datasets, cell lines and patient-derived xenograft (PDX) models to study the correlation between expression of the PSMA gene, *FOLH1*, NE

biomarkers and SSTR2. This work supports that NEPC tumors have a distinct PSMA-suppressed signature and demonstrate the possibility that SSTR2-targeted imaging could be an alternative diagnostic target for this aggressive form of prostate cancer.

2.2 MATERIAL AND METHODS

2.2.1 Cell lines and Cell Culture

The LNCaP and DU-145 cell lines were purchased from ATCC (Manassas, VA, USA). The high passage LNCaP cell line (LNCaP-HP) was a generous gift from Dr. Dora Cavallo-Medved of University of Windsor. LNCaP and LNCaP-HP cells were grown in RPMI 1640 in the presence of 10% fetal bovine serum (FBS). DU-145 cells were grown in Eagle's minimum essential medium (E-MEM) supplemented with 10% FBS. For induction of NE-transdifferentiation, LNCaP cells were cultured in RPMI1640 medium with 10% charcoal-stripped serum (CSS) over 10 passages during 4 weeks. LNCaP cells were cultured in RPMI medium supplemented with 10% CSS when treated with 10 μM enzalutamide (ENZ) from Selleckchem (Houston, TX, USA).

2.2.2 Plasmids and Infection

Small hairpin RNA (shRNA)-based p53 knockdown was attained by transducing LNCaP cells with p53 shRNA lentiviral particles and transduction control cells were produced by using control shRNA lentiviral Particles. pLKO1 shp53-targeting shRNA (Addgene, #19119) (MOI=8) and pLKO1-control (Addgene, #8453) as an empty backbone were gifts from Dr. Bob Weinberg of Massachusetts Institute of Technology. The lentiviral production was previously described *(Al Sorkhy, Ferraiuolo et al., 2012)*. 10,000 cells were seeded in fully supplemented growth media in 24-well plates for 24 hours. Cells were starved by removing serum from the media, followed by the use of 1 mg/ml polybrene

(Santa Cruz, sc-134220) and MOI 3 of the specific vector used. Infected media was changed to fully supplemented media 24 hours after infection. Cells were incubated with 1mg/ml puromycin (Sigma, P8833) 48 hours after infection for 72 hours to allow for puromycin selection. Media is thereafter changed every 48 hours with puromycin included. The isolated single cell clones were cultured in RPMI medium supplemented with 10% CSS.

2.2.3 Immunoblotting and Immunocytochemistry

Immunoblotting and immunocytochemistry techniques were described previously *(da Silva, Botsford et al., 2016, Li et al., 2017)*. In brief: Cells were lysed in TNE buffer (50mM Tris, 150mM NaCl, 5mM EDTA) with protease inhibitors (leupeptin 2μg/mL, aprotinin 5μg/mL, PMSF 100μg/mL). Protein concentrations were assessed using the Bradford assay and equal amounts of protein were analyzed using SDS-PAGE and transferred to PVDF membranes. Membranes were blocked for 1 hour at room temperature in 1% BSA and incubated in primary antibody overnight at 4°C, followed by secondary at a concentration of 1:10,000 for 1 hour at room temperature. Visualization was conducted using chemiluminescent peroxidase substrate (Pierce) as per manufacturer's instructions. Images were captured on Alpha Innotech HD 2 using AlphaEase FC software.

For immunocytochemistry primary antibodies were diluted in 3% BSA-0.1% Tween-20 in 1x PBS and used at a concentration of 1:200. Secondary antibodies were used at a concentration of 1:750. Slides were imaged using the LEICA DMI6000 inverted microscope with LAS 3.6 software.

Actin antibody was purchased from Chemicon-Millipore (MAB150 1R). PSMA (D4S1F) was purchased from Cell Signaling (12702). The secondary rabbit and mouse antibodies were purchased from Sigma. SSTR2 (sc-365502), AR (sc-815), NSE (sc-271384) and p53 (sc-53394) were purchased from Santa Cruz Biotechnology.

2.2.4 Cell Proliferation Assay

Cell proliferation assay was conducted by plating 20,000 LNCaP cells per well of a 24-well cell culture plate in 500 μL of RPMI medium supplemented with 10% CSS and treated with vehicle control (DMSO) or enzalutamide (10 μM) for 6 days. Cell numbers were counted using trypan blue exclusion and using a haemocytometer; counts were also verified using a TC10 automated cell counter (Biorad).

2.2.5 Colony Formation Assay

To evaluate the anchorage-independent ability of LNCaP cells with different levels of PSMA, the colony formation assay was used. LNCaP cells were seeded in 6-well plates at a concentration of 2500 cells per well. They were then cultured for 1 week in RPMI supplemented with CSS, followed by treatment for 1 more week with vehicle control (DMSO) or enzalutamide (10 μM). The cell colonies were fixed with 4% paraformaldehyde and stained with crystal violet (Sigma-Aldrich). Colonies were photographed and scored via NIH ImageJ software.

2.2.6 Neurite length measurement and statistical analysis

Neurite length for each separate cell was measured by manual tracing and determined using NIH ImageJ software as previously described *(Ding, Li et al., 2015)*. The neurites were defined as a process with lengths equivalent to one diameters of a cell body. The percentage

of neurite-bearing cells was calculated from the total number of counted cells (n = 3, ~1000 cells measured).

2.2.7 Quantitative Real-Time PCR Analysis

RNA was isolated using Qiagen RNeasy Plus Mini Kit as per manufacturer's instructions. cDNA was synthesized using Superscript II (Invitrogen) as per manufacturer's instructions. SYBR Green detection (Applied Biosystems) was used for real-time PCR and was performed and analyzed using Viia7 Real Time PCR System (Life Technologies) and software. The primers used are listed on Table 2-1.

Table 2-1 Sequence of primers used for RT-PCR studies.

Gene	**Forward primer (5'-3')**	**Reverse primer (5'-3')**
FOLH1	GGAGAGGAAGTCTCAAAGTGCC	TGGTTCCACTGCTCCTCTGAGA
GAPDH	GGAGTCAACGGATTTGGT	GTGATGGGATTTCCATTGAT

2.2.8 In Silico Dataset

Using Human Protein Atlas (www.proteinatlas.org) *(Thul, Åkesson et al., 2017, Uhlen, Zhang et al., 2017)*, cBioPortal webportal (http://cbioportal.org) *(Gao, Aksoy et al., 2013)* and the web-portal UALCAN *(Chandrashekar, Bashel et al., 2017)* we evaluated the transcript abundance for PSMA gene (*FOLH1*), prostate specific antigen (PSA) gene (*KLK3*), four well-known NE biomarker genes including neuron specific enolase (NSE) gene (*ENO2*), CD56 gene (*NCAM1*), synaptophysin gene (*SYP*), chromogranin A gene (*CHGA*).

An multiple AdPC genomic datasets named Cambridge Carcinoma of the Prostate App (http://bioinformatics.cruk.cam.ac.uk/apps/camcAPP) was used in this study

(Dunning, Vowler et al., 2017). The web-portal UALCAN *(Chandrashekar et al., 2017)* was also used which focuses on TCGA level 3 RNA-seq and clinical data from 31 cancer types. We analyzed relative expression of genes across AdPC tumors and normal samples, based on Gleason grading system using this resource. In addition, we used the Beltran dataset *(Beltran, Prandi et al., 2016a)* including 34 AdPC samples from 33 patients and 15 NEPC samples from 10 patients. Table 1 provides an overview of the datasets used in analysis.

The expression of PSMA protein was examined in a variety of organs using the Human Protein Atlas (www.proteinatlas.org). Two anti-PSMA antibodies including HPA010593 (Sigma-Aldrich) and CAB001451 (Novocastra) were used for visualization and measurement of PSMA in all major tissues and organs (n = 45) in the human body, supplemented with RNA-sequencing data for 31 of the tissues. The same antibodies used for immunohistochemistry images of AdPC tissues in different stages and each annotated by pathologists *(Thul et al., 2017, Uhlen et al., 2017)*.

2.2.9 The Survival Data and Pairwise-Correlations of Gene Expression

The specialized web interface, Cambridge Carcinoma of the Prostate App (http://bioinformatics.cruk.cam.ac.uk/apps/camcAPP/) as a source for multiple AdPC genomic datasets was used in this study *(Dunning et al., 2017)*. Table 1 provides an overview of the datasets used in this analysis *(Ross-Adams, Lamb et al., 2015, Taylor, Schultz et al., 2010)*. The Cambridge *(Ross-Adams et al., 2015)* cohort involved 358 fresh frozen samples from 156 patients comprising; 125 primary prostate cancer from radical prostatectomy with matched benign tissue, 64 matched germline genomic DNA (gDNA), 19 CRPC from channel transurethral resection of the prostate, 13 with matched germline

gDNA, and 12 independent benign samples from holmium laser enucleation of the prostate. The camcAPP was used for recursive partitioning-based survival analysis and Kaplan-Meier plots, pairwise-correlations of gene expression and heatmaps of gene expression data.

Survival data and heatmaps were generated using camcAPP, which is implemented in R code as a Shiny application *(Dunning et al., 2017)*. Kaplan-Meier biochemical relapse-free survival plots were generated using a recursive partitioning (RP) analysis named unbiased recursive partitioning *(Hothorn, Hornik et al., 2006)*. This conditional inference framework was used to determine if the samples could be split into groups based on the expression data from each of the genes of interest. The algorithm tailored for our case can be described as follows: a statistical test of independence was run between gene expression levels and the survival times. When the p-value of initial test of independence (ITI) was found to be less than 0.05, an optimal cutoff point was determined in the expression data such that a weighted log-rank statistic (a loss function based on log-rank) comparing the two groups resulting from dividing the sample of patients by the cutoff point would be maximized. Afterwards, the samples were split at the optimal cutoff point on the expression scale and represented as a log-rank comparing those two groups. When the algorithm did not confirm dependence between survival times and gene expression, we split samples into two groups based on median expression level of the gene. In the cases with ITI p-values more than 0.05 we are unable to state a definitive relationship between the expression of the gene and survival. The value quoted on the Kaplan-Meier plots of this manuscript indicate where the recursive partitioning algorithm has found two distinct groups of samples as high and low expression levels and the log-rank test was employed to identify

statistical difference between the high and low expressing groups. Pearson correlation was used for pairwise-correlations of the studied gene expression analysis.

2.2.10 Animals and PDX models

Fresh AdPC or NEPC tissues from patients were grafted under the kidney capsules of non-obese diabetic/severe combined immunodeficient (NOD/SCID) mice. This study followed the ethical guidelines stated in the Declaration of Helsinki, specimens were obtained from patients with their informed written consent approved by the Institutional Review Board of the University of British Columbia (UBC). Animal care and experimental procedures were carried out in accordance with the guidelines of the Canadian Council on Animal Care (CCAC) under the approval of the Animal Care Committee of the UBC.

The expression of the PSMA gene in 5 AdPC PDX models (LTL-313-B, LTL-313-B-R, LTL-418, LTL-418-R and LTL-331-7) and 2 NEPC PDX models (LTL-331-7-R and LTL-352) was studied by real time PCR analysis. Transcription of *FOLH1* and *SSTR2* genes in 18 PDX models including 3 NEPC models were analyzed. Transcriptomic analysis for all PDX models, with the exception of the LTL331-331R castration time-series samples, was achieved by GE 8×60K microarray and transcriptomic analysis of the LTL331-331R time-series performed using RNA-sequencing data *(Akamatsu, Wyatt et al., 2015b, Ci, Hao et al., 2018)*. We previously characterized and validated these models as having AdPC and NEPC mRNA and protein signatures *(Li et al., Lin, Wyatt et al., 2014a, Nabavi, Saidy et al., 2017)*.

2.2.11 Statistical Analysis

All of the *in vitro* experiments were performed in triplicates and repeated three times. All *in vitro* and *in vivo* results are expressed as the mean ± standard error of the mean (SEM). In the box whisker plots, the line inside each box is the median, upper box border represents the 75th quartile, lower box border represents the 25th quartile and whiskers represent the range. Statistical analysis was done using the GraphPad Prism 5.01 software (GraphPad Software, CA, USA). Differences between the two groups were compared by unpaired Student's t-test. One-way ANOVA followed by a Benjamini-Hochberg, Tukey, or Newman-Keuls multiple comparison test was used to compare differences among multiple groups. The false discovery rate (FDR) less than 0.05 considered as significant in Benjamini–Hochberg adjustment. The levels of significance were set at $p < 0.05$ as *, $p < 0.01$ as ** and $p < 0.001$ as ***

For quantification of *FOLH1* heatmaps, -0.5<Z-score and +0.5>Z-score are considered as suppression and upregulationthresholds for gene expression. The percent of patients with suppression (Z-score≤ -0.5), no alteration (-0.5 <Z-score< +0.5) and upregulation (Z-score≥ +0.5) of *FOLH1* in each group of samples were calculated. Total number of patients with enhanced expression of gene of interests were counted and set as the maximum value. Of the maximum value patients, those who were co-upregulated with *FOLH1* were categorized as "Upregulation", while those whose *FOLH1* status did not change or was down-regulated were categorized as "No Alteration" and "Suppressed" respectively. The values for all three categories were then divided by the maximum value and graphed under their respective categories.

2.3 RESULTS

2.3.1 High Grade CRPC Has Inconsistent Expression of The PSMA Gene (FOLH1)

FOLH1 expression was highly up-regulated in prostate tissue and relatively upregulated in both the hippocampus and salivary gland (Figure 2-1A). Similarly, protein level of PSMA was higher in prostate tissue than all other organs and tissues. Only the kidney, small intestine and duodenum reached medium levels of protein expression (Figure 2-1B).

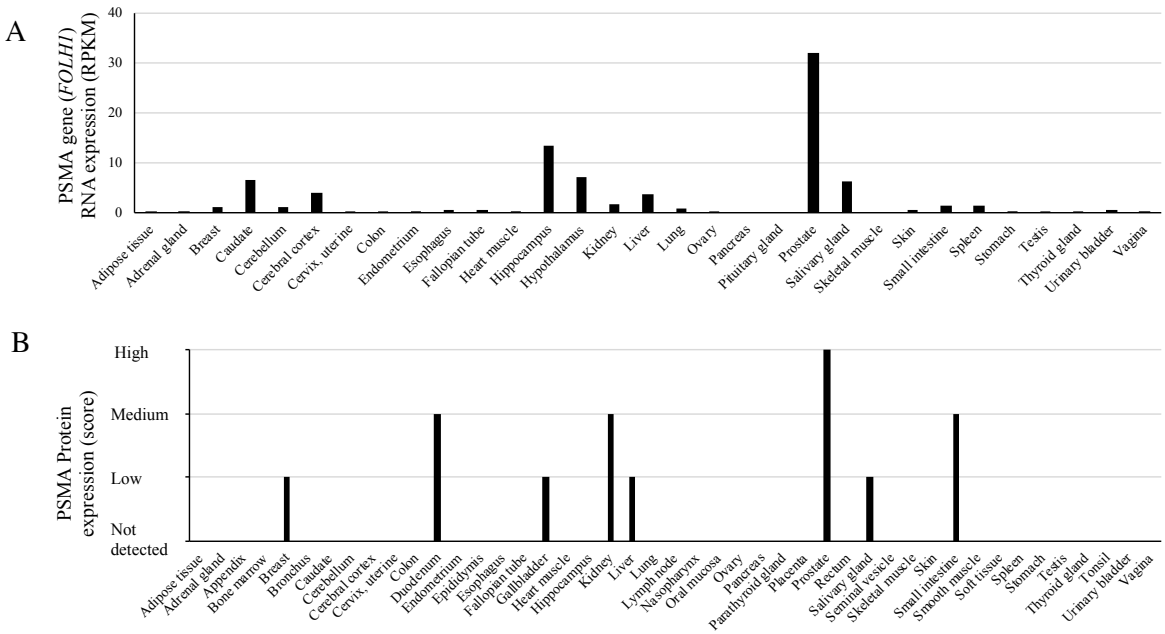

Figure 2-1 The evaluation of PSMA levels in different human organs.

The level of PSMA in a variety of human organs in (A) mRNA and (B) protein level from version 18, Human Protein Atlas (HPA) (https://www.proteinatlas.org/ENSG00000086205-FOLH1/tissue).

As compared to a spectrum of other cancer types *(Gao et al., 2013)*, *FOLH1* expression is highly enhanced in AdPC (Figure 2-2A). AdPC patients with enhanced expression of *FOLH1* gene have a significant poorer survival rate in MSKCC (Taylor et al. 2010) dataset (Figure 2-2B). Similarly, the Cambridge (Ross-Adams et al. 2015) dataset displayed

differential outcomes for men with low versus high *FOLH1* expression (log-rank p=0.047) however the initial test of independence shows no significance and hence conclusions cannot be drawn from this dataset (ITI p=0.31).

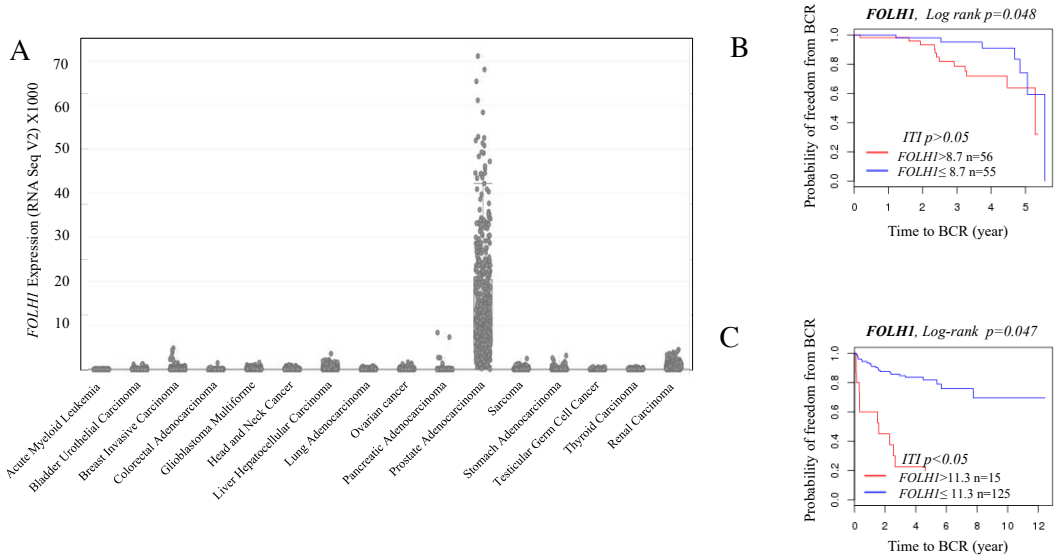

Figure 2-2 The levels of *FOLH1* in a variety of cancers and its correlation with survival.

(A) Alteration of *FOLH1* in a variety of cancers from cBioPortal dataset *(Gao et al., 2013)* (B, C) Survival rate of patients with low vs high PSMA gene expression among patients of (b) Cambridge *(Ross-Adams et al., 2015)* and (C) MSKCC *(Taylor et al., 2010)* datasets.

With the aim of exploring PSMA gene levels during progression of AdPC to clinically relevant CRPC, the Michigan and Cambridge datasets were used and gene expression levels studied (Figure 2-3 A, B). The Michigan dataset *(Grasso, Wu et al., 2012)* showed that there is an expected rise from normal to AdPC tissue in expression of *FOLH1* but there was no statistically significant difference between hormone-responsive AdPC and CRPC tumors (Figure 2-3 A). A cluster of samples with very low expression of the PSMA gene is observable in CRPC samples. Similarly, Figure 2-3B illustrates an increase from benign

to hormone-responsive tumor in the expression of *FOLH1* in the Cambridge dataset and, interestingly, there was a significant drop in expression when transitioning to CRPC. To further explore this inconsistency, we evaluated the expression of *FOLH1* by Gleason grading score (Figure 2-3C) in TCGA dataset *(Chandrashekar et al., 2017)*.

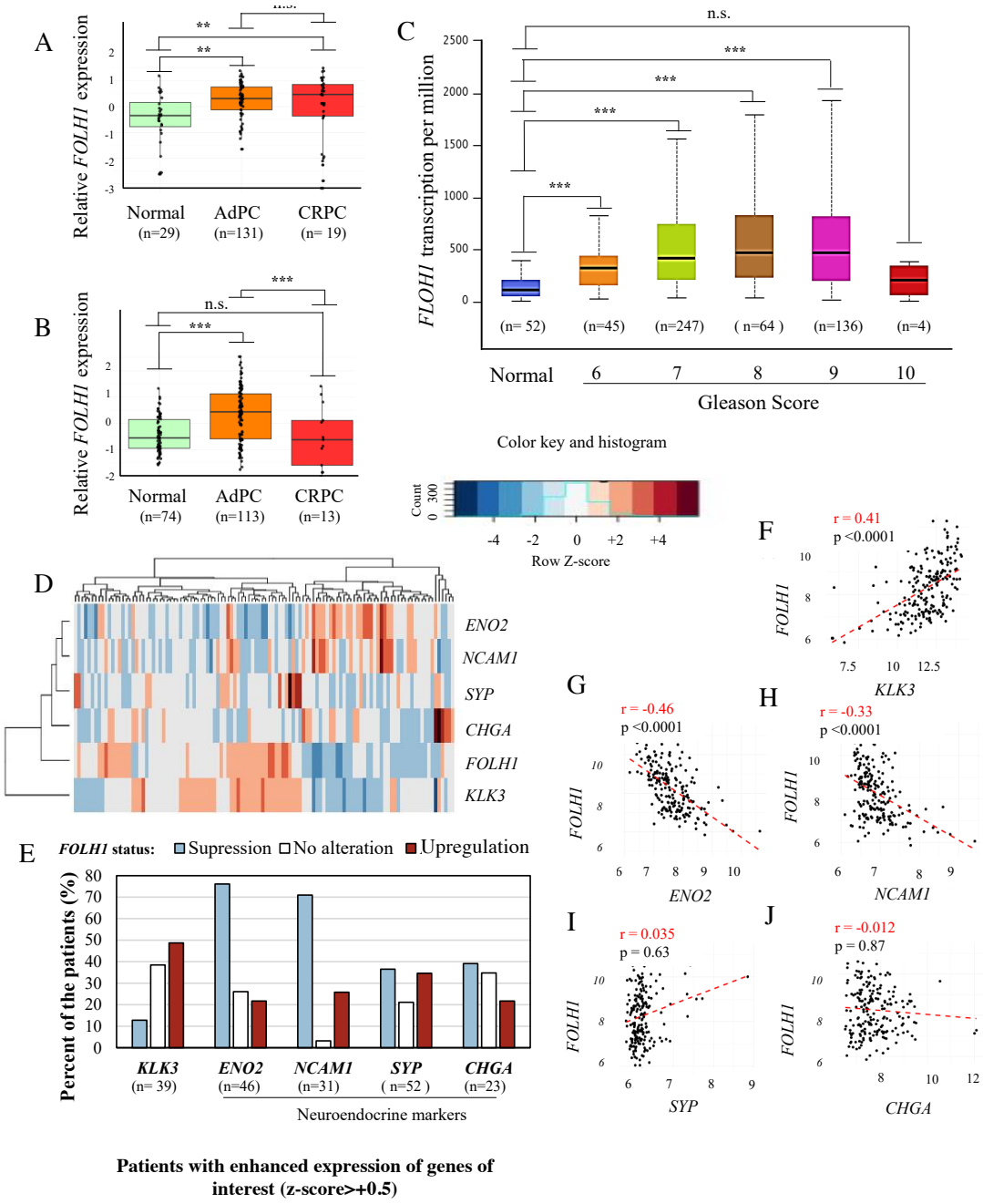

Figure 2-3 Expression of PSMA at varying grades of CRPC.

(A, B) Box-whisker plots showing the expression of *FOLH1* gene in three different classes of samples from (A) Michigan (Grasso, et al. 2012) and (B) Cambridge *(Ross-Adams et al., 2015)* datasets (C) The expression of *FOLH1* during progression of AdPC based on Gleason score from TCGA dataset generated by web-portal UALCAN *(Chandrashekar et al., 2017)*. One-way ANOVA followed by unpaired t-tests were performed with Benjamini–Hochberg adjustment for multiple test correction; **$p < 0.01$ and***$p < 0.001$, n.s.: no significant. (D) Heatmap plot of the mean expression levels of *FOLH1*, PSA gene *(KLK3)* and four major clinically significant NE marker genes including among patients of Cambridge *(Ross-Adams et al., 2015)* datasets. (E) Percent of patients with suppression (Z-score≤+0.5), no alteration (-0.5<Z-score<+0.5) and upregulation in gene expression (Z-score≥+0.5) of *FOLH1* in each group of samples. (F-J) pairwise-correlations of the studied gene expression and Pearson correlation analysis from Cambridge *(Ross-Adams et al., 2015)* datasets.

From benign tissue (normal) to Gleason score (GS) 8 *FOLH1* levels steadily increase and then they remain unchanged between the transition from 8 to 9. Samples with GS of 10 showed no significant elevation in comparison with the normal samples. While the sample size (n=4) prevents definitive conclusions for GS 10, the observed fall in *FOLH1* expression supports the possibility of a suppression in high-grad AdPC. Collectively, this led us to conclude that expression of *FOLH1* in high grade CRPC is variable and that there is a need to question whether *FOLH1* expression and PSMA protein levels are effective in determining progression to the highest grades of AdPC.

2.3.2 An Inverse Correlation Between The Expression of FOLH1 And Common NE Biomarker Genes

Figure 2-3D shows the mean expression levels of *FOLH1*, PSA gene (*KLK3*) and NE marker genes over 144 patients. As we expected, *KLK3* and *FOLH1* expression had a direct correlation where 49% of patients with an enhanced expression of *KLK3* also showed an enhanced expression of *FOLH1* gene (Figure 2-3E). In contrast, an inverse correlation between *FOLH1* and NE biomarker gene expression was identified. Particularly, suppression of *FOLH1* was observed in 65% and 53% of patients who were overexpressing

the NE genes *ENO2* and *NCAM1*, respectively. The numbers of patients with enhanced expression of genes of interest based on level of *FOLH1* gene expression are presented on Table 2-2.

In Figure 2-3F-J, this relationship was further characterized through the use of a Pearson correlation. On Figure 2-3G&H, a strong inverse correlation between *FOLH1* and *ENO2* and *NCAM1*, is prevalent (r= -0.46 and -0.33), while correlation between *FOLH1* and the other NE-markers was not significant. Figure 3f shows there was a significant direct correlation between *FOLH1* and *KLK3* genes (r=0.41). Table 2-3 provides confidence interval (CI) parameters of these gene correlations. Fig. 4 shows the mean expression levels of *FOLH1*, NE genes, AR and AR target genes. Similar to the PSA gene (*KLK3*), *AR* and some other *AR* target genes such as *KLK2, FKBP5, CAMKK2 and NKX3-1* are also inversely correlated with *FOLH1* expression. The overall regression analysis led us to conclude that PSMA and NE biomarkers are inversely correlated.

Table 2-2 The numbers of patients with enhanced expression of genes of interests based on level of *FOLH1* gene expression.

Gene name	Total number of patients with z-score >+0.5	Patients with Suppression of *FOLH1*	Patients with no alteration of *FOLH1*	Patients with upregulation of *FOLH1* expression
KLK3	39	5	15	19
ENO2	46	35	12	10
NCAM1	31	22	1	8
SYP	52	19	11	18
CHGA	23	9	8	5

Table 2-3 An overview of Pearson correlations between *FOLH1* and other studied genes and calculated confidence interval parameters.

Dataset	Gene	Pearson Correlation		t-statistic	p-value	95% CI of Correlation	
		Correlation (r)	Coefficient of determination (r^2)			LCL*	UCL**
MSKCC (Taylor et al. 2010)	*CHGA*	-0.012	0.0001	-0.15668	0.87	-0.156	0.133
	ENO2	-0.460	0.2114	-7.00394	<0.0001	-0.566	-0.338
	KLK3	0.413	0.1704	6.132873	<0.0001	0.286	0.526
	NCAM1	-0.329	0.1085	-4.72098	<0.0001	-0.452	-0.194
	SYP	-0.035	0.0012	-0.47877	0.63	-0.179	0.109
	SSTR2	-0.182	0.0034	-2.514	0.01	-0.318	-0.395
Cambridge (Ross-Adams et al. 2015)	*CHGA*	-0.069	0.0048	-0.9804	0.32	-0.206	0.070
	ENO2	-0.567	0.3215	-9.66179	<0.0001	-0.654	-0.464
	KLK3	0.505	0.2551	8.214723	<0.0001	0.393	0.601
	NCAM1	-0.417	0.1746	-6.45597	<0.0001	-0.5263	-0.296
	SYP	0.202	0.0409	2.900693	0.004	0.065	0.332
	SSTR2	-0.502	0.2525	-8.159	<0.0001	-0.599	-0.390

* Lower confidence level

** Upper confidence level

2.3.3 Treatment-induced NEPC correlates with PSMA suppression

Previously we showed *SRRM4* can induce NEPC in patients treated by ARPI through compromising the function of genes such as *REST (Li et al., 2017)*. The elevation of *SRRM4* and the loss of *REST* are indicators of treatment-induced NEPC.

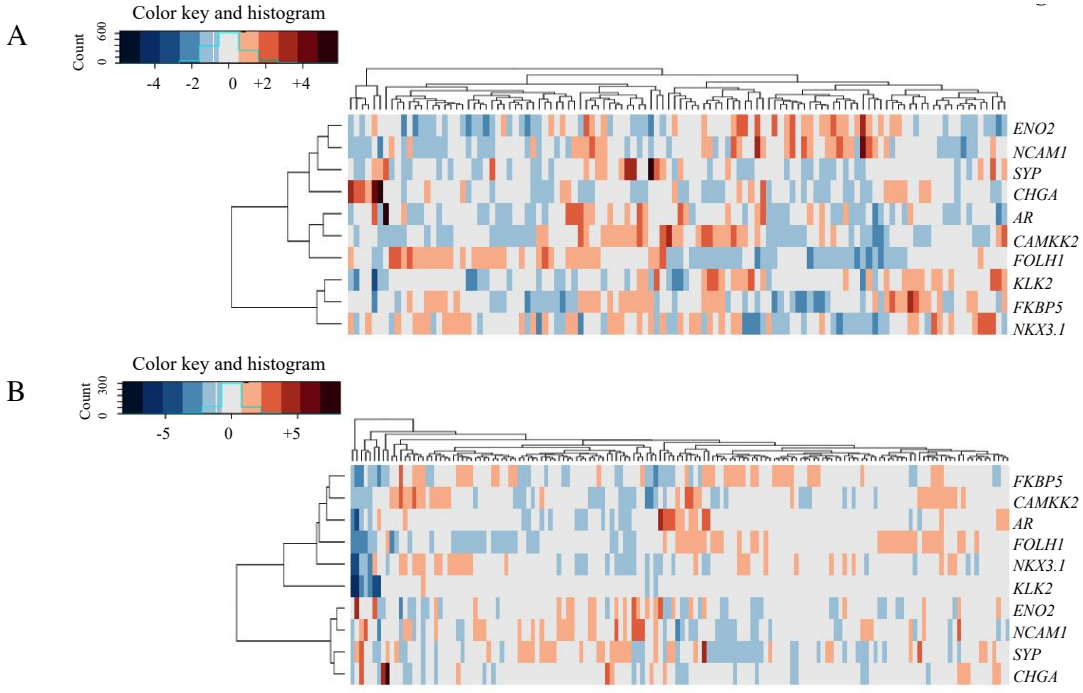

Figure 2-4 Correlative analysis of *FOLH1* with *SSRT2* and NE genes.

(A) The heatmap plot of the mean expression levels of *FOLH1*, NE genes and somatostatin receptor-2 gene (*SSTR2*) expression among patients of Cambridge dataset *(Ross-Adams et al., 2015)* (Method to calculate distances is euclidean). (B) The percent of patients with suppression (Z-score≤+0.5), no alteration (-0.5<Z-score<+0.5) and upregulation (Z-score≥+0.5) of *FOLH1* in each group of samples. (C) Pairwise-correlation of treatment-induced gene expressions and Pearson correlation analysis from Cambridge dataset *(Ross-Adams et al., 2015)* (27). (D) The expression of *SSTR2* during progression of AdPC based on Gleason score from TCGA dataset generated by web-portal UALCAN *(Chandrashekar et al., 2017)*. One-way ANOVA followed by a t-test was performed with Benjamini–Hochberg adjustment for multiple test correction; **p < 0.01 and***p < 0.001, n.s.: no significant. (E) The comparison of *SSTR2* expressions between AdPC and NEPC samples of Beltran dataset *(Beltran et al., 2016a)* Error bars reflect SEM and Student's t-test was performed.

Figure 2-5A-B show that when *SRRM4* is upregulated *FOLH1* is highly suppressed and, conversely, when *REST* is upregulated *FOLH1* expression is enhanced. Specifically, the suppression of *FOLH1* was observed in 57% of patients who were overexpressing *SRRM4,* while only 15% of patients who were overexpressing *REST* had suppression of *FOLH1*.

As summarized on Table 2-4, Beltran dataset *(Beltran et al., 2016a)* patient samples are histologically characterized as AdPC and NEPC. Figure 2-5C shows NEPC has significantly lower expression of *FOLH1* ($p<0.001$) as compared to AdPC. Following this we analyzed the association between *FOLH1* and *SRRM4* expression in NEPC samples and found that a significant ($p=0.011$) inverse correlation was present between the two biomarkers ($r=-0.358$) (Figure 2-2D). Also, Figure 2-5E shows *FOLH1* directly correlated to *REST* expression ($r=0.561$). The relationship of *SRRM4* and *REST* to *FOLH1* collectively supports that treatment-induced NE transdifferentiation correlates with suppressed PSMA gene expression.

Table 2-4 An overview of the prostate cancer datasets used in this study.

Dataset name	**Source**	**Platform: gene expression**	**Platform: copy number**	**Sample size and tumor type**
Cambridge 2015	Ross-Adams et al. *(Ross-Adams, Lamb et al.)*	Illumina HT12	Illumina Omni 2.5	125 Primary 19 Advanced
MSKCC 2010	Taylor et al. *(Taylor, Schultz et al.)*	Affymetrix Human 1.0 ST	Agilent 244k	109 Primary 19 Advanced
Michigan 2012	Grasso et al. *(Grasso et al., 2012)*	Agilent Whole Human 44k	Agilent 105k/244k	59 Primary 32 Advanced
TCGA for prostate cancer	UALCAN *(Chandrashekar et al., 2017)*	Illumina	Illumina HiSeq 2000N	497 Primary
Beltran 2016	Beltran et al. *(Beltran et al., 2016a)*	Agilent 2100	Illumina HiSeq	34 AdPC 15 NEPC

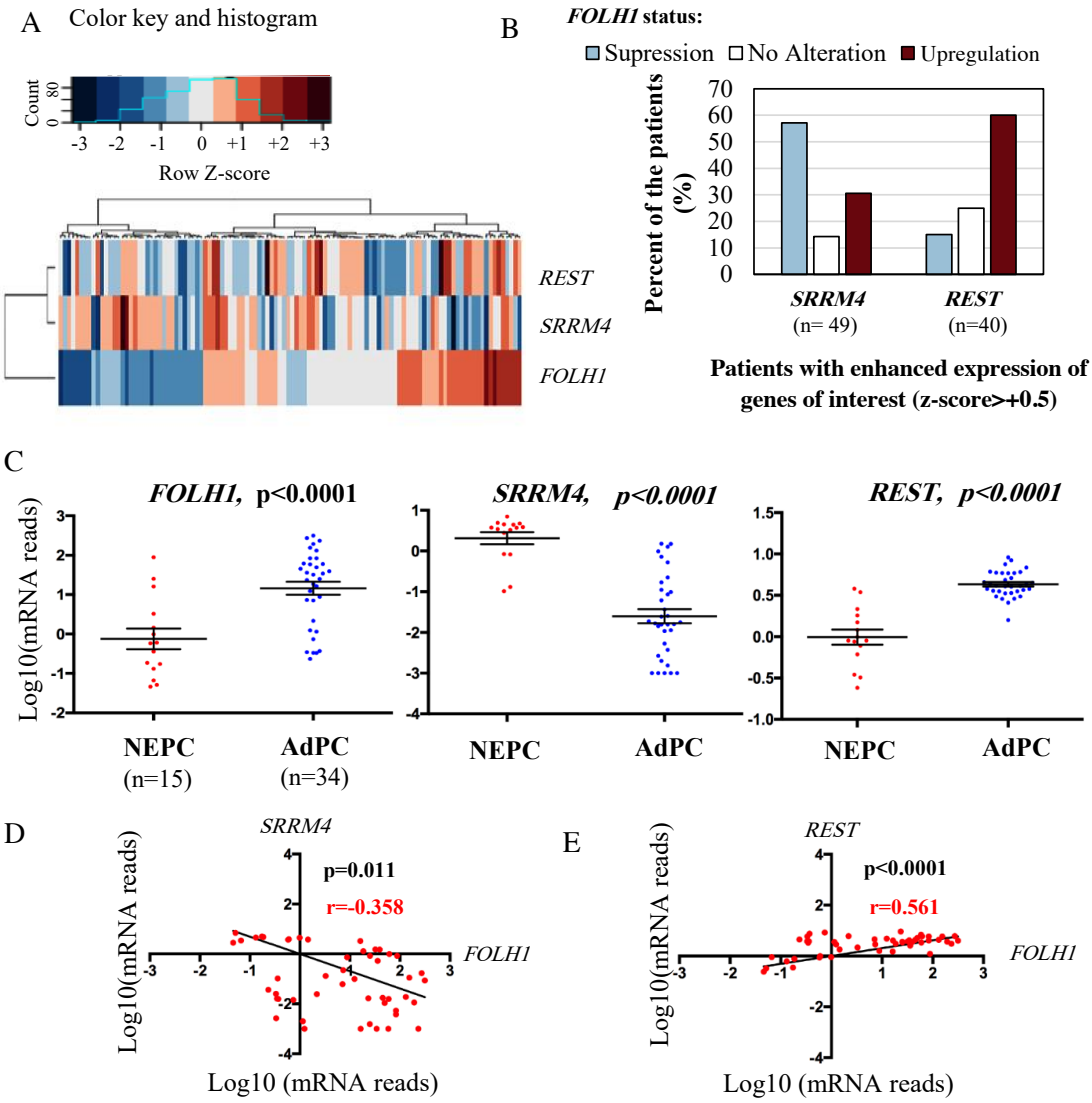

Figure 2-5 Analysis of *FOLH1*, *SRRM4* and *REST* in tumor datasets.

(A) The heatmap plot of the mean expression levels of *FOLH1*, *SRRM4* and *REST* genes among patients of Cambridge dataset *(Ross-Adams et al., 2015)*. (B) The percent of patients with suppression (Z-score≤+0.5), no alteration (-0.5<Z-score<+0.5) and upregulation(Z-score≥+0.5) of *FOLH1* in each group of samples. (C) The comparison of *FOLH1*, *SRRM4* and *REST* expressions between AdPC and NEPC samples of Beltran dataset *(Beltran et al., 2016a)*. Error bars reflect SEM and Student's t-test was performed (D, E) The relationship between *FOLH1* and *SRRM4* levels in NEPC samples in Beltran dataset *(Beltran et al., 2016a)* by Pearson correlation analysis.

2.3.4 An inverse correlation between the expression of FOLH1 and SSTR2

The heatmap plot in Figure 2-6A displays NE marker genes clustered together at the top which showed less difference while *SSTR2* and *FOLH1* represented the largest difference; consequently, Figure 2-6B demonstrates that more than 61% of patients with elevation of *SSTR2* are *FOLH1*-suppressed. Figure 2-6C and Table 3 show a modest inverse correlation between SSRT2 and *FOLH1* ($r = -0.50$). Figure 2-6D shows that from benign tissue (normal) to (GS) 9, *FOLH1* is suppressed while there is an evidence of a 2-fold increase in the expression of *SSTR2* at GS of 10 ($p<0.05$). SSRT2 level in NEPC sample showed no suppression (Figure 2-6E). This led us to conclude that the observed suppression of *FOLH1* could be accompanied by *SSTR2* gene overexpression at high grade CRPC.

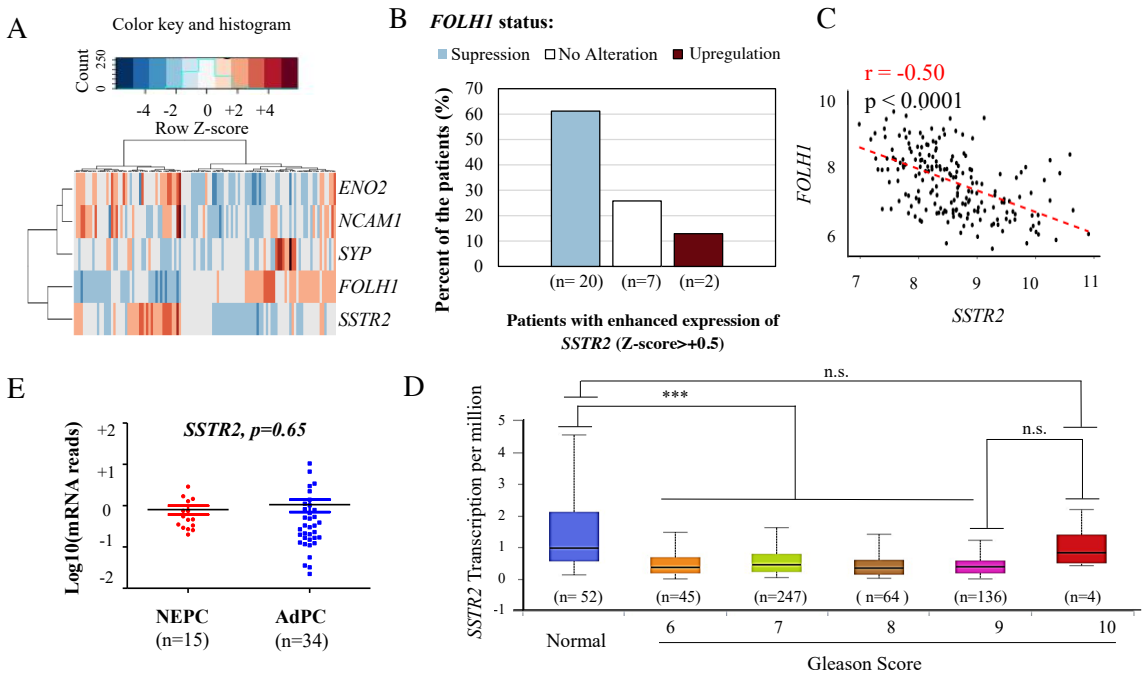

Figure 2-6 Correlative analysis of *FOLH1* with *SSRT2* and NE genes.

(A) The heatmap plot of the mean expression levels of *FOLH1*, NE genes and somatostatin receptor-2 gene (*SSTR2*) expression among patients of Cambridge dataset *(Ross-Adams et al., 2015)* (Method to calculate distances is euclidean). (B) The percent of patients with suppression (Z-score≤+0.5), no alteration (-0.5<Z-score<+0.5) and upregulation(Z-score≥+0.5) of *FOLH1* in each group of samples. (C) Pairwise-correlation of treatment-induced gene expressions and Pearson correlation analysis from Cambridge dataset *(Ross-Adams et al., 2015)* (27). (D) The expression of *SSTR2* during progression of AdPC based on Gleason score from TCGA dataset generated by web-portal UALCAN *(Chandrashekar et al., 2017)*. One-way ANOVA followed by a t-test was performed with Benjamini–Hochberg adjustment for multiple test correction; **p < 0.01 and***p < 0.001, n.s.: no significant. (D) The comparison of *SSTR2* expressions between AdPC and NEPC samples of Beltran dataset *(Beltran et al., 2016a)* Error bars reflect SEM and Student's t-test was performed.

2.3.5 *NEPC-Like Patients Have Significantly Worse Survival Rates Than Non-NEPC-Like Patients.*

Kaplan Meier survival curves studying high and low expression levels of the PSA gene, *KLK3*, fail to reveal any consistent correlation with patient survival over two different datasets (Figure 2-7A& Figure 2-8A).

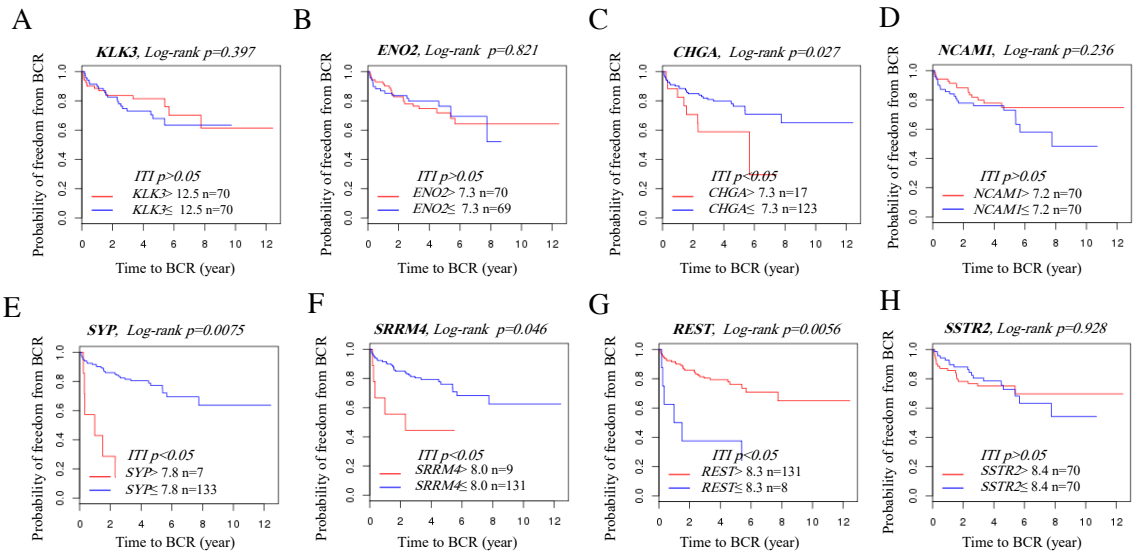

Figure 2-7 The probability of freedom from biochemical recurrence (BCR) of prostate cancer patients grouped according to the gene expression levels.

Kaplan Meyer survival curves for high and low expression levels of (A) *KLK3* (B) *ENO2* (C) *CHGA* (D) *NCAM1* (E) *SYP* (F) *SRRM4* (G) *REST* (H) *SSTR2* genes generated by MSKCC *(Taylor et al., 2010)*.

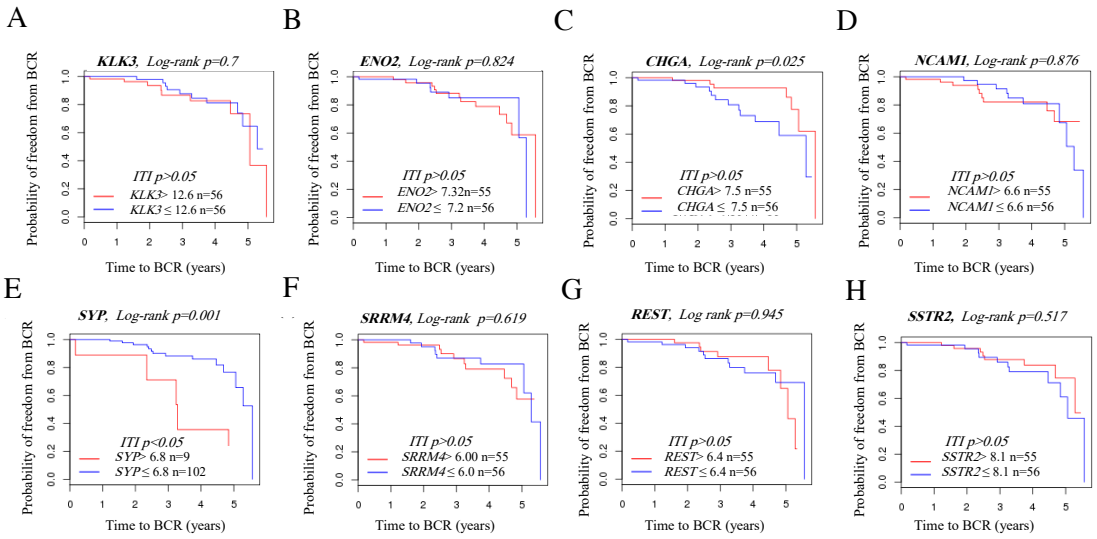

Figure 2-8 The probability of freedom from biochemical recurrence of prostate cancer patients grouped according to the gene expression levels.

Kaplan Meier survival curves for high and low expression levels of (A) *KLK3* (B) *ENO2* (C) *CHGA* (D) *NCAM1* (E) *SYP* (F) *SRRM4* (G) *REST* (H) *SSTR2* genes generated by Cambridge dataset *(Ross-Adams et al., 2015)*.

SSTR2 and NE genes including *ENO2* and *NCAM1* did not correlate with a difference in BCR (Figure 2-7B, D, H and Figure 2-8 B, D, H). Figure 2-7E& Figure 2-8E show that enhanced expression of *SYP* was associated with decreased relapse-free survival (poor outcome) in both of studied datasets (log-rank $p<0.05$). Enhanced expression of *CHGA* was also correlated with poor outcome in MSKCC (Taylor et al. 2010) dataset (Figure 2-7C). Similarly, Kaplan–Meier analysis of *CHGA* in Cambridge *(Ross-Adams et al., 2015)* dataset showed clear partitioning for men with low versus high *CHGA* expression (log-rank $p=0.025$) however the initial test of independence was not significant and hence no conclusion can be drawn from this dataset (ITI $p=0.28$).

The evaluation of treatment-induced NEPC, *SRRM4*, showed the *SRRM4* high group had a significantly (log rank $p=0.046$) poorer prognosis than *SRRM4* low group (Figure 2-7F).

This trend continued with its down-stream target, *REST*; where *REST* high group had a significantly (log rank p=0.0056) better prognosis than *REST* low group (Figure 2-7G).

The relationships observed in MSKCC *(Taylor et al., 2010)* dataset were not consistently observed in the Cambridge *(Ross-Adams et al., 2015)* dataset. Results found non-significant in the Cambridge dataset do not prove that there is no relationship with survival for those genes, but this inconsistency provides evidence that the effects of several genes on survival are not clear-cut.

In all, the trends in Kaplan Meier survival curves in Figure 2-7and Figure 2-2B, C imply that NE markers, especially treatment-induced NEPC, could be clinically significant in determining survival rates and correlate with poorer prognosis. Further examination into *FOLH1* and *KLK3* is required before a definitive correlation can be made for these genes.

2.3.6 PSMA Suppression And SSTR2 Overexpression in NE-Induced AdPC Cell Line

The levels of PSMA, SSTR2, AR and NSE were measured in three different cell line models representing androgen-sensitive AdPC, CRPC and NEPC (Figure 2-9A,B) LNCaP cell line as an AR-positive cell line has wild-type p53 and it is considered a typical model for androgen-sensitive AdPC *(Chen et al., 2018)*. In addition, LNCaP-HP as a high passage LNCaP cell line could be a model of CRPC due to its androgen insensitivity while it has positivity for AR *(Unni, Sun et al., 2004)*. AR-negative DU145 cells, suggested to be used as a NEPC model, contain two different point mutations in the *TP53* gene (Phe223Leu and Val274Phe), one on either allele, producing nonfunctional protein product *(Chappell, Lehmann et al., 2012, Li, Cohen et al., 2016b)*.

Figure 2-9B shows the level of NSE as a NE marker has continuous elevation from AdPC to NEPC. AdPC and CRPC *in vitro* models are AR and PSMA positive while NEPC models are PSMA and AR negative. SSTR2 has significantly higher level in DU145 model.

To examine the impact of NE transdifferentiation of AdPC on PSMA levels we used the LNCaP cell line which mimics the phenotype of NEPC cells when maintained overtime in steroid-reduced conditions *(Zelivianski, Verni et al., 2001)*. LNCaP cells maintained in 10% CSS for one month have an altered phenotype compared to control cells maintained in 10% FBS (Figure 2-9C). Almost 75% of the CSS-FBS treated LNCaP cells (LNCaP) extended neurites, whereas less than 10% of control or LNCaP-FBS cells bore neurites (Figure 2-9D). Additionally, both the mean length of the longest neurite and the total neurite length were significantly increased in LNCaP-CSS cells compared with the LNCaP-FBS (Figure 2-9E,F). These observations indicate that LNCaP growth conditions can play the role of *in vitro* models for AdPC and NEPC. The western blot assay (Figure 2-9G,H) demonstrated that SSTR2 and NSE as a NE marker protein are expressed at a higher level in the LNCaP-CSS cell line. In contrast, PSMA, AR and p53 proteins have a significant decline. Immunofluorescence microscopy of LNCaP cell lines support western blot data (Figure 2-9I,L). Collectively, these data demonstrate that LNCaP-CSS are differentiating toward a NE phenotype and that this occurs coincidentally with a decrease in PSMA and AR levels.

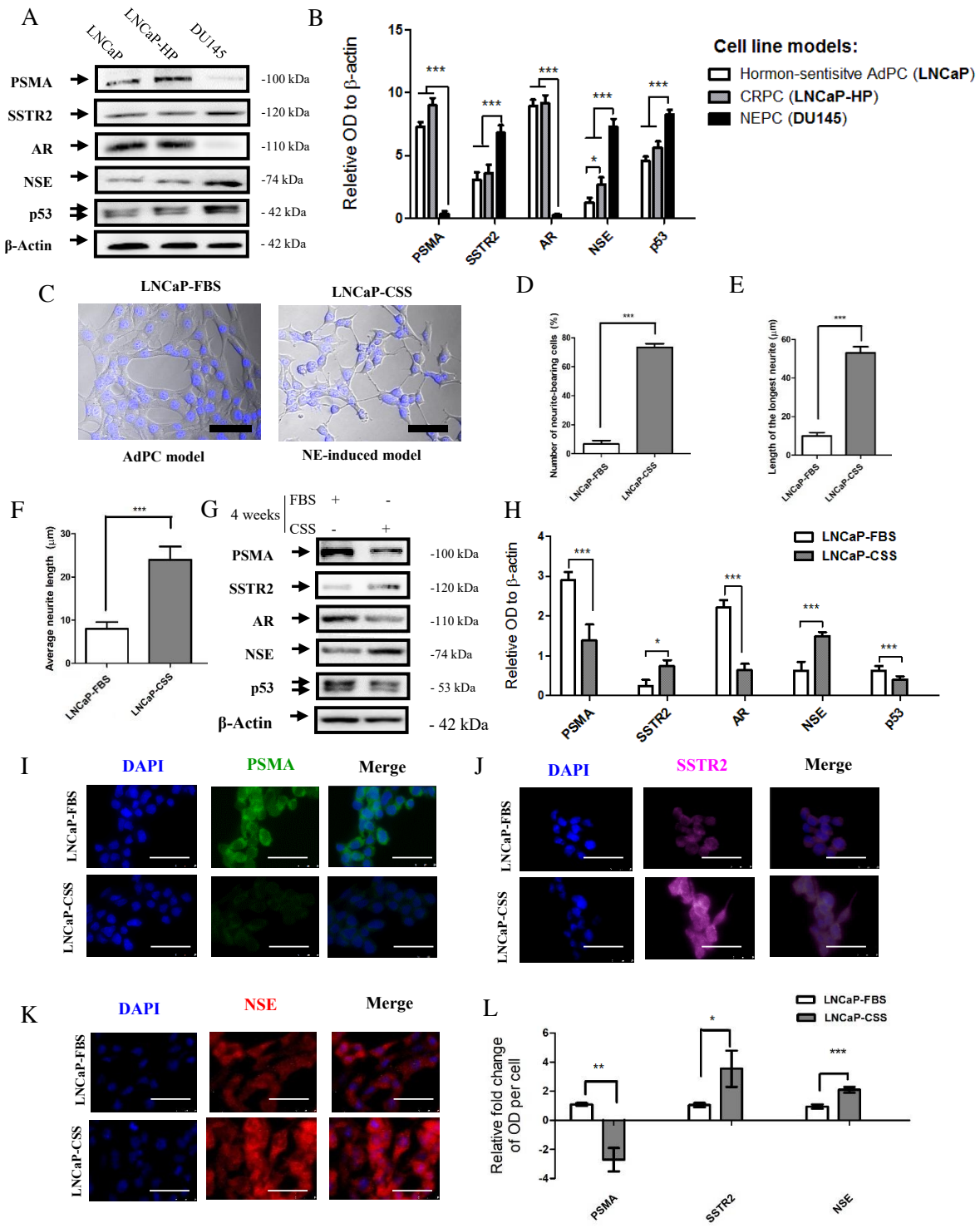
A
LNCaP
LNCaP-HP
DU145
PSMA
SSTR2
AR
NSE
p53
β-Actin
-100 kDa
-120 kDa
-110 kDa
-74 kDa
- 42 kDa
- 42 kDa
B
Releative OD to β-actin
Cell line models:
Hormon-sentisitve AdPC (LNCaP)
CRPC (LNCaP-HP)
NEPC (DU145)
C
LNCaP-FBS
LNCaP-CSS
AdPC model
NE-induced model
D
Number of neurite-bearing cells (%)
E
Length of the longest neurite (μm)
F
Average neurite length (μm)
G
4 weeks
FBS
CSS
-100 kDa
-120 kDa
-110 kDa
-74 kDa
- 53 kDa
- 42 kDa
H
Releative OD to β-actin
I
DAPI
PSMA
Merge
J
DAPI
SSTR2
Merge
K
DAPI
NSE
Merge
L
Relative fold change of OD per cell

Figure 2-9 Analysis of PSMA and SSTR2 in a NEPC induced cell line.

(A-B) Western blot analyses of protein level of PSMA, SSTR2, AR, NSE and p53 in 3 different prostate cancer cell line models. (A) immunoblotting (B) diagram showing the relative density of protein levels (C) Representative photos of control (left) and CSS-treated (right) LNCaP cells stained with Hoechst. Scale bar: 50 μm. (D-F) Neurites were studied under an inverted microscope: (D) % of cells with neurites counted over 3 fields of view over 3 separate experiments. (E) Neurites were measured using ImageJ software and longest neurite calculated. (F) Average neurite. (G-L) LNCaP cells are treated with either FBS or CSS as indicated and level of PSMA, SSTR2, AR, NSE and p53 were detected by (G-H) immunoblotting and (I-K) immunocytochemistry. (L) Data is quantified using ImageJ software. Stat: Error bars reflect SEM between 3 separate experiments. The data were analyzed by either Student's t-test or one-way ANOVA followed by a Tukey's multiple comparison tests.; **$p < 0.01$ and***$p < 0.001$.

2.3.7 Development of ENZ-Resistance Following a p53-Dependent Suppression of PSMA

Treatment of LNCaP cell line with ENZ (10 μM) resulted in an increase in PSMA protein levels in medium containing either FBS or CSS (Figure 2-10A,B). AR levels show no significant alteration under these conditions. Treatment with ENZ in medium supplemented with CSS had an increase in levels of NSE. This experiment, and previously reported data, supports that short-term exposure of LNCaP cell lines to either ENZ treatment or serum removal cannot be a viable approach to make a clinically relevant PSMA-suppressed *in vitro* model of AdPC with NE features. Recently, it had been reported that p53 knockdown could lead to suppression of luminal markers and overexpression of basal and NE markers *(Li et al., 2017, Mu, Zhang et al., 2017)*. Figure 2-10C,D shows p53 knockdown of LNCaP cells in a medium supplemented in CSS for 6 days causes suppression AR and PSMA. DU145 as an AR and PSMA negative cell line have a significant higher level of NSE ($p<0.01$). Due to overexpression of NSE and suppression of PSMA we used the p53-knockdown cell line as a model of low-PSMA cancer with NE features for the next steps of our experiments. The LNCaP cell line transduced with

shControl is also referred to as high-PSMA cell line. Figure 2-10E shows that LNCaP cells with low level of PSMA have slightly higher proliferation during 6 day treatment with the control vehicle (DMSO) but it was not statistically significant (p=0.65). During ENZ (10 μM) treatment, low-PSMA cells demonstrate a higher growth rate (p=0.0048) and on the sixth day of cell counting low-PSMA cell numbers were 2.8 times higher than high-PSMA cells. It can be inferred that low-PSMA cells are less sensitive to ENZ (10 μM) than high-PSMA cells over this 6 day experiment. In addition, we tested sensitivity of LNCaP cells with different levels of PSMA using colony formation assay (Figure 2-10F) and find that low-PSMA cells have more colonies formed under ENZ (10μM) treatment than treatment of cells with high PSMA. Therefore, low-PSMA cells were less sensitive to ENZ treatment, supporting the hypothesis that suppression of PSMA, as found in NEPC, correlates with more aggressive disease.

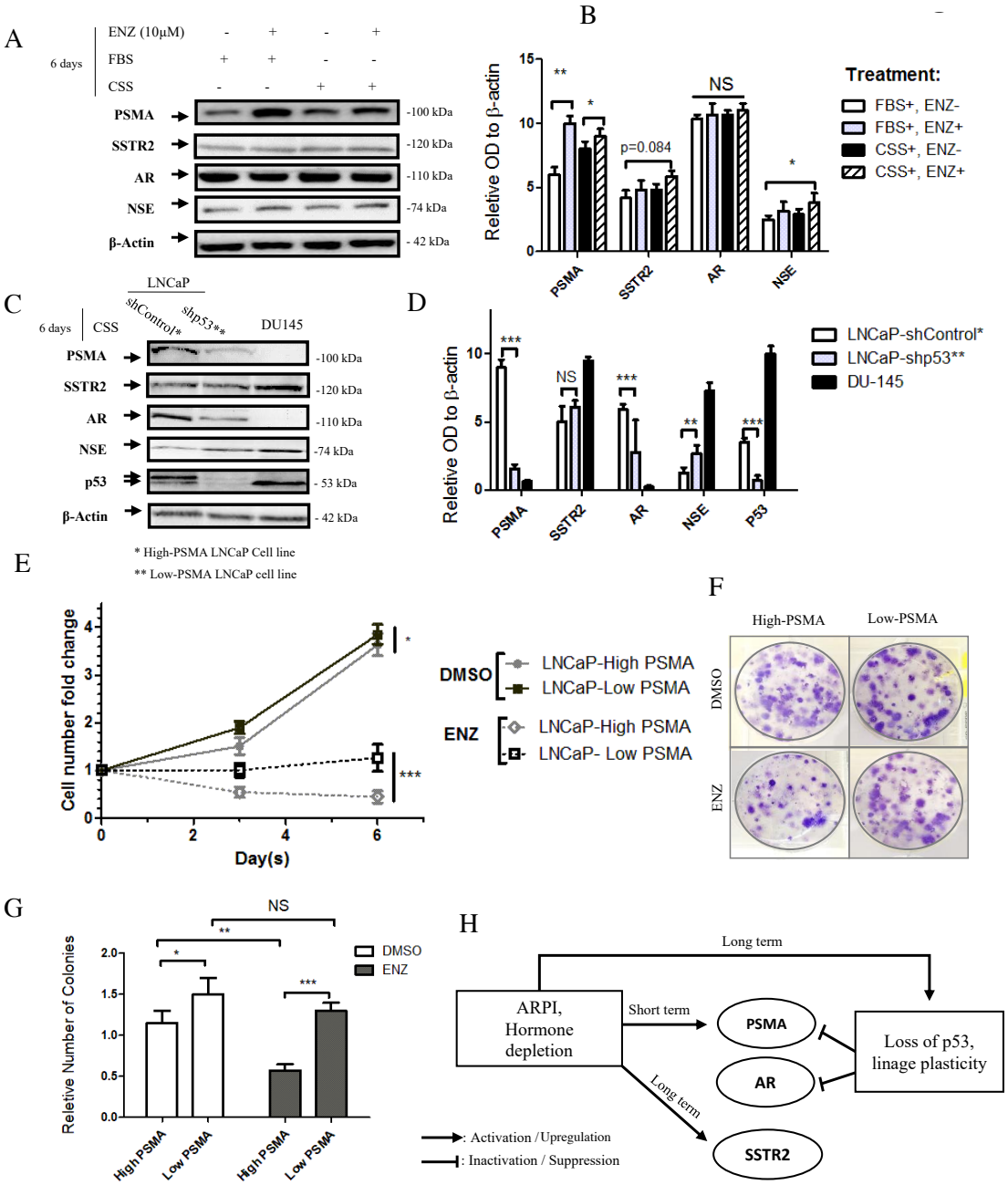

Figure 2-10 Analysis of treatment response to ENZ following a p53-dependent suppression of PSMA.

(An-B) Western blot analyses of protein level of PSMA, SSTR2, AR and NSE in LNCaP cell line treated with vehicle control (DMSO) or ENZ (10 μM) supplemented with either FBS or CSS for 6 days (A) representative immunoblot (B) the relative density of protein levels. (C, D) Western blot analyses of protein level of PSMA, SSTR2, AR, NSE and p53 in LNCaP cell line transduced with annotated shRNA supplemented with CSS for 6 days. (C) representative immunoblot (D) the relative density of protein levels. (E) Growth curve of LNCaP cell lines with different levels of PSMA following treatment with vehicle control (DMSO) or ENZ (10 μM) in supplemented with CSS. (F, G) The colony-forming ability of high-PSMA and

low-PSMA seeded in 10% CSS for 1 week and treated with either ENZ(10 μM) or DMSO for 1 more week. (F) representative wells (G) quantification of the number of the colonies using CellProfiler software. (H) Schematic of the impact of ARPI, hormonal deletion and loss of p53 on PSMA, AR and SSTR2 based on the obtained data in figs. 9 and 10. Error bars reflect SEM between 3 separate experiments. The data were analyzed by either Student's t-test or one-way ANOVA followed by a Tukey's multiple comparison tests.; **$p < 0.01$ and***$p < 0.001$.

Figure 2-10H shows a schematic of the associations in changing gene expression found using *in vitro* models. Hormone depletion, which is modeled by serum deprivation, suppresses PSMA, AR and p53 levels and elevates levels of SSTR2. ARPI which is modeled by treating cells with ENZ, showed no alteration of AR or SSTR2 but increased levels of PSMA. A p53 knockdown *in vitro* model, supports that suppression of PSMA and AR are associated with p53-dependent cellular plasticity and that this is independent of SSTR2 levels.

2.3.8 NEPC Has a Distinct FOLH1-Suppressed Signature in PDX Models

Following pathological investigation, patient tumours were stratified into either AdPC or NEPC phenotypes put into PDX mouse models and studied before or after castration (schema Figure 2-11A-C). Significant suppression of *FOLH1* was observed in the LTL-331R-G7 and LTL-352 mice which were found to progress to NEPC, as compared to those mice lacking NE marker expression ($p<0.05$) (Figure 2-11D). There was a wide spectrum of *FOLH1* expression in different AdPC models. In the LTL-313-B model, after castration of mice which can mimic treatment-induced relapse in the form of CRPC, we observed a 2.4 folds elevation in *FOLH1*. However, in the LTL-418 model there was no significant alteration in *FOLH1* expression. For simulation of treatment-induced NEPC, after inducing NE to LTL-331-7 model as a CRPC model, a 2.1 times suppression of *FOLH1* was observed. Similarly, the PDX model obtained by direct engraftment of tissue from a NEPC

metastases sample had significantly lower *FOLH1* expression in comparison with all AdPC models.

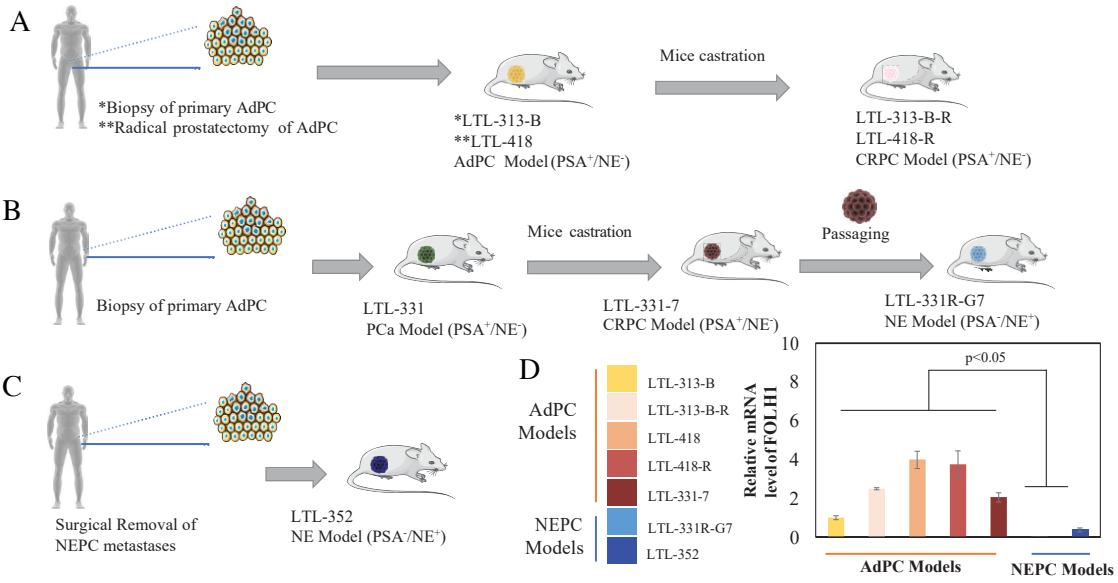

Figure 2-11 Establishment and analysis of AdPC and NEPC PDX mouse models.

(A-D) Schematic of the established PDX mice models of AdPC and NEPC (adopted with permission *(Lin et al., 2014a)*). (D) The levels of *FOLH1* in different PDX models. One-way ANOVA followed by a Newman-Keuls multiple comparison test was used (n=3). Some elements of this figure were produced using Servier Medical Art image bank (www.servier.com).

The transcription of *FOLH1* and *SSTR2* in 18 PDX models including 3 NEPC were investigated (Figure 2-12A,B). Among these PDX models, LTL331 and LTL331R are the first-in-field PDX model of AdPC-to-NEPC transdifferentiation. Figure 2-12C illustrates upon LTL331 model castration, the primary AdPC initially regresses but relapses within 24 to 32 months as typical CRPC and the whole transdifferentiation process is predictive of disease progression and is fully recapitulated in the donor patient *(Akamatsu et al., 2015b, Ci et al., 2018)*. Figure 2-12C shows a 5 fold suppression of *FOLH1* gene expression in NEPC models subsequent with a 2 fold increase in the expression of *SSTR2*. Figure

2-12D shows of the expression levels of *FOLH1* and *SSTR2* through the progression to NEPC. In the AdPC model *FOLH1* is found at a maximum level and SSTR2 at a minimum level. Following castration up to 8 weeks there is low fluctuations in the transcription of both of the genes. However, on 8th week, a sharp decline in *FOLH1* and a profound elevation of *SSTR2* starts. The terminally differentiated NEPC model has a minimal transcriptional level of *FOLH1* and maximal transcription of *SSTR2*.

2.3.9 PSMA Levels Fail to Adequately Predict NE Transdifferentiation of High Grade AdPC

Similar to its RNA, PSMA protein level could have a variable series of staining levels of low grade (Figure 2-13A, D), medium grade (Figure 2-13B, E) and high grade (Figure 2-13C, F) AdPC. These staining patterns imply a series of possible progression paths for AdPC progression and eventual NEPC. On Figure 2-12E, we proposed five possible models for alteration of PSMA during progression of AdPC. Model 1 is the classical model of PSMA expression in which the level of PSMA correlates positively with the stage of AdPC, our data supports that this model is not entirely represented in the data. Model 5 is a representation of a de novo occurrence of NEPC, which shows poor onset PSMA staining. However, models 2 and 3 are relevant as AdPC progression pathways that lead to NE transdifferentiation and subsequent loss of PSMA. In addition, model 4 is representation of a constant poor PSMA staining which against its low abundance is still capable of detecting metastatic sites. The HPA dataset PSMA antibody staining patterns for AdPC progression led us to conclude that model 2 is the most likely progression pattern for the treatment-induced NEPC.

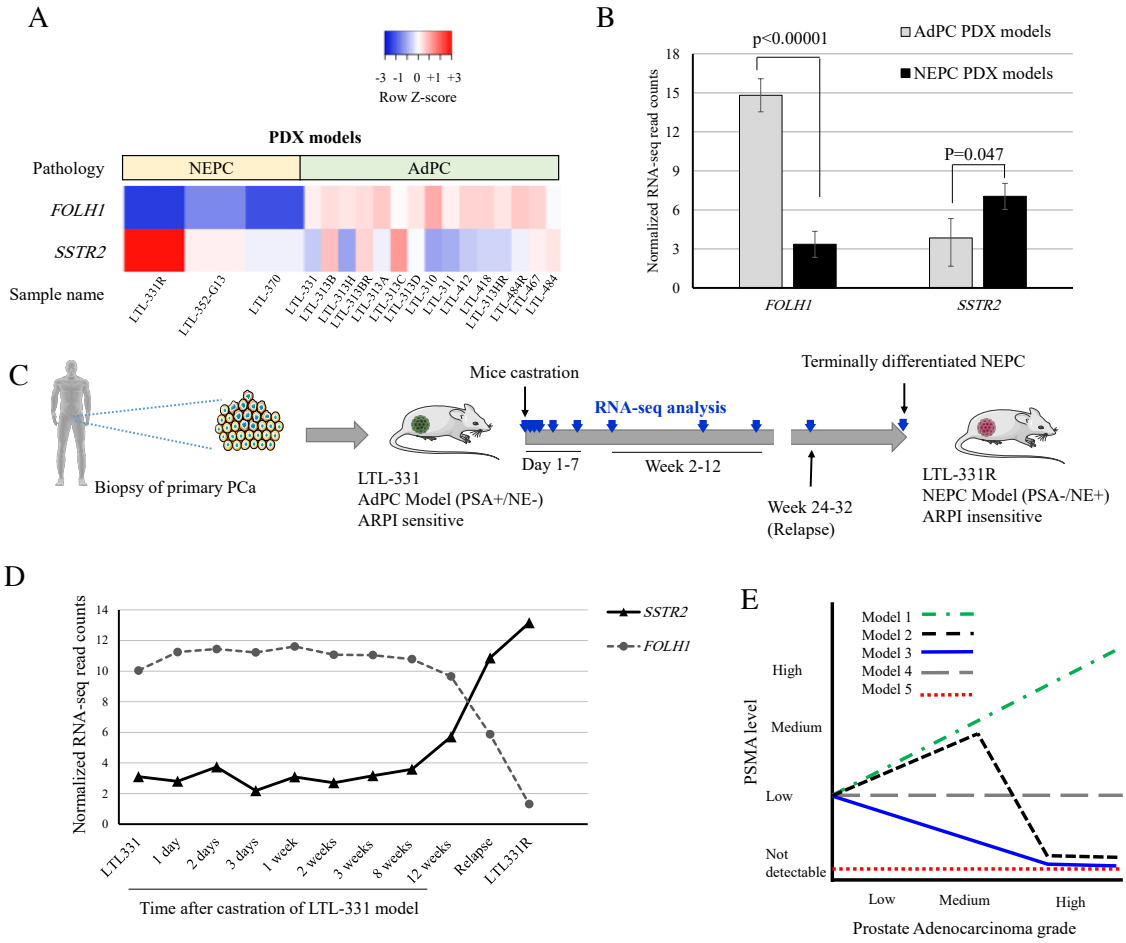

Figure 2-12 NEPC represents a distinctive *FOLH1*-supressed signature in a series of PDX model.

(A-B) Transcriptomic profiles from the PDX models (15 adenocarcinomas vs. 3 NEPCs), (A) heatmap showing the clustering among all PDX samples (B) the average level of *FOLH1* and *SSTR2* suggests a unique down-regulation of *FOLH1* in NEPC PDX tumors while *SSTR2* levels are slightly increased. The data were analyzed by Student's t-test (C) Schematic of development of LTL-331R as terminally differentiated NEPC PDX model following castration of hormone-sensitive LTL-331 PDX model. The time points at which tumors were collected along progression to NEPC are illustrated by blue color arrows. Some elements of this figure were produced using Servier Medical Art image bank (www.servier.com). (D) Transcription of *FOLH1* and *SSTR2* during NE transdifferentiation in the LTL331 system highlighting the suppression of *FOLH1* and enhanced expression of *SSTR2* during development of NEPC as a result of hormone depletion. (E) Possible models of alteration of PSMA level during progression of AdPC. Schema shows possible kinetic changes in PSMA level (Y axis) during progression from low, medium and high grade AdPC.

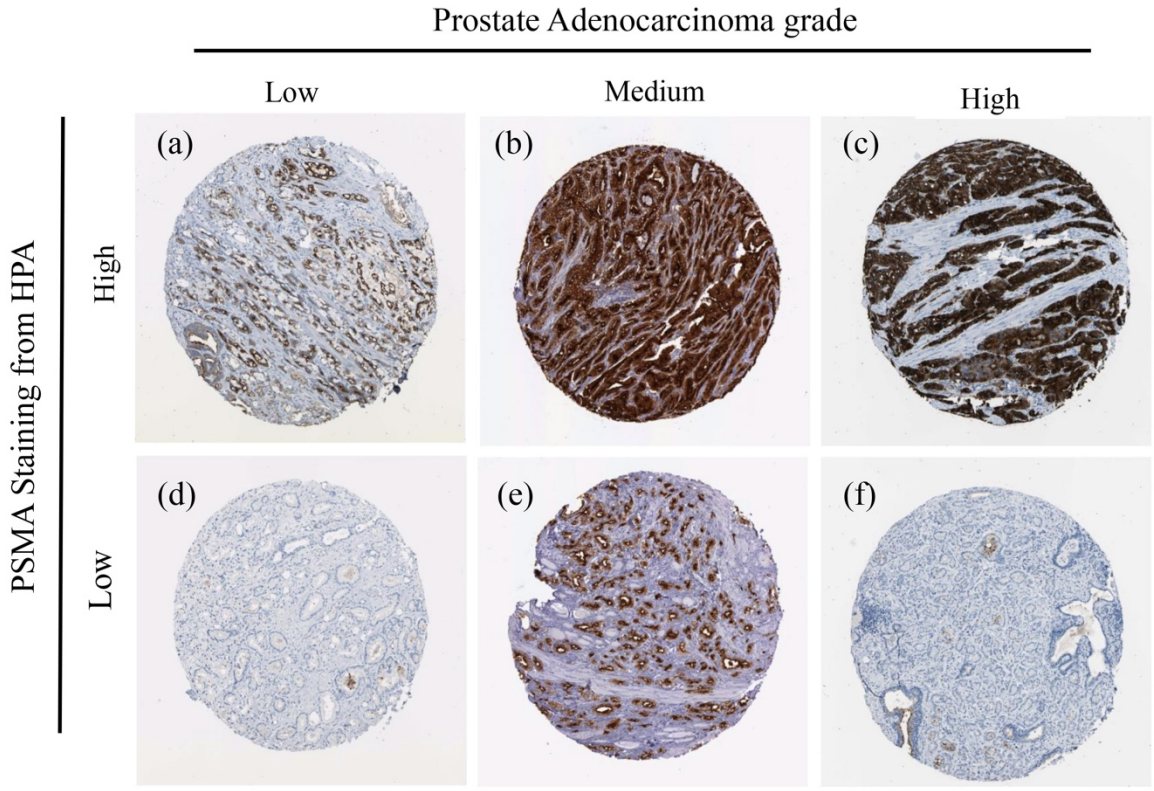

Figure 2-13 The evaluation of PSMA levels.

IHC images of PSMA protein expression staining in different stages of AdPC. Image available from version 18, Human Protein Atlas (HPA) (https://www.proteinatlas.org/ENSG00000086205-FOLH1/pathology).

2.4 DISCUSSION

The development of NE phenotype following hormone depletion in LNCaP cell line is a well-studied observation *(Shen, Dorai et al., 1997, Yuan, Veeramani et al., 2006b)*. Liu et al. *(Liu, Wu et al., 2012)* reported that hormone depletion suppresses AR and PSMA levels in LNCaP cells, however they did not evaluate the expression of NE makers. Suppression

of AR and overexpression of NE makers in LNCaP following p53 knock-down in LNCaP cell has also been described recently *(Li et al., 2017, Mu et al., 2017)*. In this manuscript, we report the suppression of PSMA and overexpression of NSE and SSTR2 in LNCaP cell line following hormone depletion and loss of p53.

2.5 CONCLUSION

The use of potent antiandrogens and lineage plasticity may contribute to the increasing prevalence of NEPC, an aggressive and hormone resistant form of AdPC. While PSMA targeting is a promising approach for the nuclear imaging and therapy of many forms of aggressive AdPC, our data based on transcriptome analysis of tumor samples, cell line models and PDX mice models supports that PSMA (*FOLH1* gene) levels are not consistent with all forms of high grade CRPC. Our *in vitro* data showed a significant suppression of PSMA as a result of both of hormone depletion, loss of p53 and lineage plasticity. A PSMA-suppressed NEPC cell line model showed higher colony formation and resistance to ARPI by ENZ. Our data further shows that induced NE transdifferentiation correlates with an elevated level of the protein SSTR2. SSTR2 levels appear to elevate due to hormone depletion but are not affected by altered cellular plasticity. PDX data support these conclusions, showing an inverse correlation between the expression of the PSMA gene and SSTR2 gene. Specifically we find declining *PSMA* and increasing *SSTR2* gene expression occurring during the development of CRPC and becoming more pronounced in terminally differentiated NEPC. Collectively, this study cautions on the reliability of using PMSA levels as a diagnostic target for molecular imaging in advanced treatment-induced NEPC. Our work supports the recommendation that SSTR2-targeted imaging approaches

may permit more accurate monitoring of PSMA-suppressed patients due to SSTR2-positivity of NEPC tumors.

Declaration of interest

The authors declare that there is no conflict of interest regarding the publication of this article.

Funding

This research was supported by a grant of the Korea Health Technology R&D Project through the Korea Health Industry Development Institute (KHIDI), funded by the Ministry of Health & Welfare, Republic of Korea (grant number : HI14C1072). The financial support of Prostate Cancer Fight Foundation (Motorcycle Ride for Dad Charity, ON, Canada) and Ontario Trillium Scholarship program (Government of Ontario, ON, Canada) is greatly appreciated.

2.6 REFERENCES

Akamatsu S, Wyatt AW, Lin D, Lysakowski S, Zhang F, Kim S, Tse C, Wang K, Mo F, Haegert A (2015b) The placental gene PEG10 promotes progression of neuroendocrine prostate cancer. *Cell reports* 12: 922-936

Al Sorkhy M, Ferraiuolo R-M, Jalili E, Malysa A, Fratiloiu AR, Sloane BF, Porter LA (2012) The cyclin-like protein Spy1/RINGO promotes mammary transformation and is elevated in human breast cancer. *BMC Cancer* 12: 45

Beltran H, Prandi D, Mosquera JM, Benelli M, Puca L, Cyrta J, Marotz C, Giannopoulou E, Chakravarthi BV, Varambally S (2016a) Divergent clonal evolution of castration-resistant neuroendocrine prostate cancer. *Nature medicine* 22: 298-305

Chakraborty PS, Tripathi M, Agarwal KK, Kumar R, Vijay MK, Bal C (2015) Metastatic poorly differentiated prostatic carcinoma with neuroendocrine differentiation: negative on 68Ga-PSMA PET/CT. *Clinical nuclear medicine* 40: e163-166

Chandrashekar DS, Bashel B, Balasubramanya SAH, Creighton CJ, Ponce-Rodriguez I, Chakravarthi BVSK, Varambally S (2017) UALCAN: A Portal for Facilitating Tumor Subgroup Gene Expression and Survival Analyses(). *Neoplasia (New York, NY)* 19: 649-658

Chappell WH, Lehmann BD, Terrian DM, Abrams SL, Steelman LS, McCubrey JA (2012) p53 expression controls prostate cancer sensitivity to chemotherapy and the MDM2 inhibitor Nutlin-3. *Cell Cycle* 11: 4579-4588
Chen R, Dong X, Gleave M (2018) Molecular model for neuroendocrine prostate cancer progression. *BJU Int*
Ci X, Hao J, Dong X, Choi SY, Xue H, Wu R, Qu S, Gout PW, Zhang F, Haegert AM, Fazli L, Crea F, Ong CJ, Zoubeidi A, He HH, Gleave ME, Collins CC, Lin D, Wang Y (2018) Heterochromatin Protein 1alpha Mediates Development and Aggressiveness of Neuroendocrine Prostate Cancer. *Cancer Res* 78: 2691-2704
da Silva EF, Botsford S, Porter LA (2016) Derivation of a novel G2 reporter system. *Cytotechnology* 68: 19-24
Davies AH, Beltran H, Zoubeidi A (2018a) Cellular plasticity and the neuroendocrine phenotype in prostate cancer. *Nature Reviews Urology*
Ding Y, Li Y, Lu L, Zhang R, Zeng L, Wang L, Zhang X (2015) Inhibition of nischarin expression promotes Neurite outgrowth through regulation of PAK activity. *PLOS ONE* 10: e0144948
Dunning MJ, Vowler SL, Lalonde E, Ross-Adams H, Boutros P, Mills IG, Lynch AG, Lamb AD (2017) Mining human prostate cancer datasets: The "camcAPP" Shiny App. *EBioMedicine* 17: 5-6
Gao J, Aksoy BA, Dogrusoz U, Dresdner G, Gross B, Sumer SO, Sun Y, Jacobsen A, Sinha R, Larsson E (2013) Integrative analysis of complex cancer genomics and clinical profiles using the cBioPortal. *Science signaling* 6: pl1
Grasso CS, Wu Y-M, Robinson DR, Cao X, Dhanasekaran SM, Khan AP, Quist MJ, Jing X, Lonigro RJ, Brenner JC, Asangani IA, Ateeq B, Chun SY, Siddiqui J, Sam L, Anstett M, Mehra R, Prensner JR, Palanisamy N, Ryslik GA et al. (2012) The mutational landscape of lethal castration-resistant prostate cancer. *Nature* 487: 239-243
Hothorn T, Hornik K, Zeileis A (2006) Unbiased recursive partitioning: A conditional inference framework. *Journal of Computational and Graphical statistics* 15: 651-674
Li W, Cohen A, Sun Y, Squires J, Braas D, Graeber TG, Du L, Li G, Li Z, Xu X, Chen X, Huang J (2016b) The Role of CD44 in Glucose Metabolism in Prostatic Small Cell Neuroendocrine Carcinoma. *Mol Cancer Res* 14: 344-353
Li Y, Donmez N, Sahinalp C, Xie N, Wang Y, Xue H, Mo F, Beltran H, Gleave M, Wang Y, Collins C, Dong X (2017) SRRM4 Drives Neuroendocrine Transdifferentiation of Prostate Adenocarcinoma Under Androgen Receptor Pathway Inhibition. *Eur Urol* 71: 68-78
Lin D, Wyatt AW, Xue H, Wang Y, Dong X, Haegert A, Wu R, Brahmbhatt S, Mo F, Jong L (2014a) High fidelity patient-derived xenografts for accelerating prostate cancer discovery and drug development. *Cancer research* 74: 1272-1283
Liu T, Wu LY, Fulton MD, Johnson JM, Berkman CE (2012) Prolonged androgen deprivation leads to downregulation of androgen receptor and prostate-specific membrane antigen in prostate cancer cells. *Int J Oncol* 41: 2087-2092
Mu P, Zhang Z, Benelli M, Karthaus WR, Hoover E, Chen CC, Wongvipat J, Ku SY, Gao D, Cao Z, Shah N, Adams EJ, Abida W, Watson PA, Prandi D, Huang CH, de Stanchina E, Lowe SW, Ellis L, Beltran H et al. (2017) SOX2 promotes lineage plasticity and antiandrogen resistance in TP53- and RB1-deficient prostate cancer. *Science* 355: 84-88
Nabavi N, Saidy NRN, Venalainen E, Haegert A, Parolia A, Xue H, Wang Y, Wu R, Dong X, Collins C (2017) miR-100-5p inhibition induces apoptosis in dormant prostate cancer cells and prevents the emergence of castration-resistant prostate cancer. *Sci Rep* 7: 4079
Parida GK, Tripathy S, Datta Gupta S, Singhal A, Kumar R, Bal C, Shamim SA (2018) Adenocarcinoma Prostate With Neuroendocrine Differentiation: Potential Utility of 18F-FDG PET/CT and 68Ga-DOTANOC PET/CT Over 68Ga-PSMA PET/CT. *Clinical nuclear medicine* 43: 248-249

Parimi V, Goyal R, Poropatich K, Yang XJ (2014) Neuroendocrine differentiation of prostate cancer: a review. *American Journal of Clinical and Experimental Urology* 2: 273-285
Ross-Adams H, Lamb AD, Dunning MJ, Halim S, Lindberg J, Massie CM, Egevad LA, Russell R, Ramos-Montoya A, Vowler SL, Sharma NL, Kay J, Whitaker H, Clark J, Hurst R, Gnanapragasam VJ, Shah NC, Warren AY, Cooper CS, Lynch AG et al. Integration of copy number and transcriptomics provides risk stratification in prostate cancer: A discovery and validation cohort study. *EBioMedicine* 2: 1133-1144
Ross-Adams H, Lamb AD, Dunning MJ, Halim S, Lindberg J, Massie CM, Egevad LA, Russell R, Ramos-Montoya A, Vowler SL, Sharma NL, Kay J, Whitaker H, Clark J, Hurst R, Gnanapragasam VJ, Shah NC, Warren AY, Cooper CS, Lynch AG et al. (2015) Integration of copy number and transcriptomics provides risk stratification in prostate cancer: A discovery and validation cohort study. *EBioMedicine* 2: 1133-1144
Sheikhbahaei S, Afshar-Oromieh A, Eiber M, Solnes LB, Javadi MS, Ross AE, Pienta KJ, Allaf ME, Haberkorn U, Pomper MG, Gorin MA, Rowe SP (2017) Pearls and pitfalls in clinical interpretation of prostate-specific membrane antigen (PSMA)-targeted PET imaging. *European journal of nuclear medicine and molecular imaging* 44: 2117-2136
Shen R, Dorai T, Szaboles M, Katz AE, Olsson CA, Buttyan R (1997) Transdifferentiation of cultured human prostate cancer cells to a neuroendocrine cell phenotype in a hormone-depleted medium. *Urologic Oncology: Seminars and Original Investigations* 3: 67-75
Taylor BS, Schultz N, Hieronymus H, Gopalan A, Xiao Y, Carver BS, Arora VK, Kaushik P, Cerami E, Reva B, Antipin Y, Mitsiades N, Landers T, Dolgalev I, Major JE, Wilson M, Socci ND, Lash AE, Heguy A, Eastham JA et al. Integrative Genomic Profiling of Human Prostate Cancer. *Cancer cell* 18: 11-22
Taylor BS, Schultz N, Hieronymus H, Gopalan A, Xiao Y, Carver BS, Arora VK, Kaushik P, Cerami E, Reva B, Antipin Y, Mitsiades N, Landers T, Dolgalev I, Major JE, Wilson M, Socci ND, Lash AE, Heguy A, Eastham JA et al. (2010) Integrative genomic profiling of human prostate cancer. *Cancer Cell* 18: 11-22
Thul PJ, Åkesson L, Wiking M, Mahdessian D, Geladaki A, Ait Blal H, Alm T, Asplund A, Björk L, Breckels LM, Bäckström A, Danielsson F, Fagerberg L, Fall J, Gatto L, Gnann C, Hober S, Hjelmare M, Johansson F, Lee S et al. (2017) A subcellular map of the human proteome. *Science* 356
Tosoian JJ, Gorin MA, Rowe SP, Andreas D, Szabo Z, Pienta KJ, Pomper MG, Lotan TL, Ross AE (2017a) Correlation of PSMA-Targeted (18)F-DCFPyL PET/CT Findings With Immunohistochemical and Genomic Data in a Patient With Metastatic Neuroendocrine Prostate Cancer. *Clinical genitourinary cancer* 15: e65-e68
Uhlen M, Zhang C, Lee S, Sjöstedt E, Fagerberg L, Bidkhori G, Benfeitas R, Arif M, Liu Z, Edfors F, Sanli K, von Feilitzen K, Oksvold P, Lundberg E, Hober S, Nilsson P, Mattsson J, Schwenk JM, Brunnström H, Glimelius B et al. (2017) A pathology atlas of the human cancer transcriptome. *Science* 357
Unni E, Sun S, Nan B, McPhaul MJ, Cheskis B, Mancini MA, Marcelli M (2004) Changes in Androgen Receptor Nongenotropic Signaling Correlate with Transition of LNCaP Cells to Androgen Independence. *Cancer Research* 64: 7156-7168
Usmani S, Ahmed N, Marafi F, Rasheed R, Amanguno HG, Al Kandari F (2017) Molecular Imaging in Neuroendocrine Differentiation of Prostate Cancer: 68Ga-PSMA Versus 68Ga-DOTA NOC PET-CT. *Clinical nuclear medicine* 42: 410-413
Vlachostergios PJ, Papandreou CN (2015) Targeting Neuroendocrine Prostate Cancer: Molecular and Clinical Perspectives. *Front Oncol* 5: 6
Yuan TC, Veeramani S, Lin FF, Kondrikou D, Zelivianski S, Igawa T, Karan D, Batra SK, Lin MF (2006b) Androgen deprivation induces human prostate epithelial neuroendocrine differentiation of androgen-sensitive LNCaP cells. *Endocr Relat Cancer* 13: 151-67

Zelivianski S, Verni M, Moore C, Kondrikov D, Taylor R, Lin M-F (2001) Multipathways for transdifferentiation of human prostate cancer cells into neuroendocrine-like phenotype. *Biochimica et Biophysica Acta (BBA) - Molecular Cell Research* 1539: 28-43

CHAPTER 3 : DIFFERENTIAL EXPRESSION OF GLUCOSE TRANSPORTERS AND HEXOKINASES IN PROSTATE CANCER WITH A NEUROENDOCRINE GENE SIGNATURE: A MECHANISTIC PERSPECTIVE FOR FDG IMAGING OF PSMA-SUPPRESSED TUMORS

3.1 INTRODUCTION

The androgen receptor (AR) plays a central role in regulating the transcriptional events driving prostate cancer (PC) progression and development of metastatic castration-resistant prostate cancer (mCRPC) *(Stelloo, Bergman et al., 2019)*. AR-inhibition is an effective therapeutic approach for most patients at different stages of PC. Although the incidence of *de novo* neuroendocrine (NE) PC (NEPC) is considered rare, several emerging forms of PC with low-levels of AR are identified. The suppression and low activity of AR in these patients is largely associated with a NE gene signature (NEGS) and resistance to AR-inhibition *(Bluemn, Coleman et al., 2017, Stelloo, Nevedomskaya et al., 2018)*.

AR-directed therapy of mCRPC could promote cellular plasticity and development of an AR-suppressed phenotype similar to NEPC which manifests the histopathology of NE disease *(Beltran, Prandi et al., 2016c)*. Another emerging phenotype of mCRPC is AR-null and NE-null, classified as double-negative PC (DNPC) *(Bluemn et al., 2017)*. A recent molecular subtyping of PC patients with no history of AR-directed therapies identified a NE-positive subtype with low chromatin binding and activity of AR. These patients have been referred to as NE-like PC (NELPC) since they do not represent the NE-histopathology *(Alshalalfa, Liu et al., 2019, Stelloo et al., 2018)*.

AR regulates the expression of *FOLH1* gene encoding the transmembrane protein, prostate-specific membrane antigen (PSMA). PSMA-targeted molecular imaging and therapy are transforming the landscape of PC management *(Hope, Goodman et al., 2019, Sheikhbahaei et al., 2017)*. Despite the impactful implications of PSMA, there are clinical reports that suggest that PSMA-targeted imaging does not effectively visualize NEPC tumors *(Chakraborty et al., 2015, Sheikhbahaei et al., 2017, Tosoian, Gorin et al., 2017b)*.

Pre-clinical studies confirmed that the induction of lineage plasticity by AR-inhibition leads to NE-transdifferention and suppression of PSMA *(Bakht, Derecichei et al., 2019b)*.

Recent case reports illustrate NEPC delineation may be more feasible by FDG than PSMA-radioligands *(Parida et al., 2018, Perez, Hope et al., 2019)* and Spratt *et al*. *(Spratt, Gavane et al., 2014)* demonstrated the utility of FDG-PET for NEPC imaging. Interestingly, Thang *et al*. *(Thang, Violet et al., 2018)* screened patients with ^{68}Ga-PSMA-11 and FDG-PET and they identified a subset of patients with low PSMA-radioligand uptake and high FDG uptake.

Development of non-radioactive glucose analogs enabling the delineation of the glucose uptake of tumors have been studied using a variety of optical approaches mostly in mouse models *(Cheng, Levi et al., 2006)*. PC xenograft studies in zebrafish are coming to the forefront as a cost-effective and time-efficient model for drug screening, and the fluorescent glucose bioprobe GB2-Cy3 has been used to monitor glucose uptake in a zebrafish model *(Lee, Lee et al., 2011, Melong, Steele et al., 2017)*. However, the feasibility of monitoring of glucose uptake in PC in a zebrafish model has not been evaluated.

In this work we used data mining approaches, cell lines and patient-derived xenograft (PDX) models to study expression levels of glucose uptake-associated genes including GLUTs and hexokinases in NEPC and NELPC to provide a genomic rationalization for the previously reported FDG-avidity of PSMA-suppressed PC tumors. We also present the feasibility of non-radioactive *in vivo* imaging of glucose uptake using a zebrafish model.

3.2 MATERIAL AND METHODS

3.2.1 Cell Culture

The LNCaP cell line was purchased from ATCC and grown in RPMI-1640 in the presence of 10% fetal bovine serum. Progression to NEPC was achieved by culturing LNCaP cells in RPMI1640 medium with 10% charcoal-stripped serum for 4 months. Under these conditions, cell morphology gradually changed into a mixture of a NE-like phenotype and a non-NE-phenotype. After 4 months, a subclone with a NE-like phenotype was isolated (LNCaP-NEPC). LNCaP cells, maintained in RPMI-1640 + fetal bovine serum, were used as a control and are referred to as LNCaP-AdPC.

3.2.2 Antibodies

The immunoblotting technique used was previously described *(Bakht et al., 2019b)*. Antibodies are as follows: actin (Chemicon-Millipoure; MAB150-1R), PSMA (Cell Signaling; D4S1F), AR (Santa Cruz Biotechnology (SCB); sc-816), NSE (SCB; sc-271384) and GCK (SCB; sc-17819) and GLUT12 (Abcam; ab100993).

3.2.3 Data Mining Analysis

Using 268 PC samples from 3 different cohorts we assessed the transcript abundance for all of the *SLC2A* family (*SLC2A1-14*) and the HK family (*HK1-4, HK4* referred to as *GCK*). In addition, we monitored the PSMA gene (*FOLH1*), the NE marker synaptophysin gene (*SYP*), *SRRM4* as a positive marker of treatment-induced NEPC and *REST* as negative marker of NEPC. Patients with lack of NEGS or NE histopathology are referred as adenocarcinoma PC (AdPC).

To assess the lineage plasticity of mCRPC, samples from a tissue acquisition necropsy platform established at the University of Washington (UW) were used *(Bluemn et al., 2017)*. All rapid autopsy tissues were collected from patients who signed written informed consent under the aegis of the Prostate Cancer Donor Program at the UW and the Institutional Review Board of the UW approved this study. We classified our mCRPC subtypes as AdPC (AR^{+}/NE^{-}), AR-suppressed AdPC (AR^{low}/NE^{-}), NEPC (AR^{-}/NE^{+}), and DNPC (AR^{-}/NE^{-}). In addition, we used the Beltran cohort *(Beltran et al., 2016c)* with histologically confirmed mCRPC-AdPC and mCRPC-NEPC samples. We identify a NELPC subset among AdPC tumors from the Memorial Sloan Kettering Cancer Center (MSKCC) cohort *(Taylor et al., 2010)* using the meta-signature of prototypical high-grade NEPC *(Tsai, Lehrer et al., 2017)*. Gene set enrichment analysis (GSEA) was performed on the identified subsets using gene sets downloaded from the Molecular Signatures Database *(Subramanian, Tamayo et al., 2005)*.

3.2.4 Mice PDX Models

Fresh PC tissues from patients were grafted under the kidney capsules of non-obese diabetic/severe combined immunodeficient mice. Institutional Review Board and Animal Care Committee of the University of British Columbia approved this study and all subjects signed a written informed consent. We previously characterized and validated these models *(Akamatsu, Wyatt et al., 2015a)*.

3.2.5 GB2-Cy3 Synthesis

Synthesis of a glucose bioprobe GB2-Cy3 was previously reported with some modifications *(Korbel, Lalic et al., 2001, Lee et al., 2011, Park, Lee et al., 2007)*. Full experimental details are provided in the Appendix A.

3.2.6 In Vitro Glucose Uptake Imaging

For *in vitro* imaging for glucose uptake by GB2-Cy3 we adopted published protocols *(Lee et al., 2011)*. Briefly, 50,000 LNCaP cells were seeded in 12 well glass-bottom dishes (Corning) overnight at 37°C. Cells were washed 2 times with PBS and incubated for 1 hour at 37°C in glucose-deficient DMEM medium. Cells were treated with 7 μg/mL GB2-Cy3 and 100 ng/mL Hoechst 33342 (Thermo Scientific) in glucose-deficient DMEM at 37 °C for 5, 10 and 30 minutes, respectively. Cells were washed twice with PBS and prepared for live imaging by adding 1 mL of PBS. Fluorescence images were obtained on a LeicaDM IL microscope (Wetzlar, Germany). Cy3 signal was quantified using ImageJ and the mean fluorescent signal measurement from 30–40 cells.

3.2.7 In Vivo Glucose Uptake Imaging

Wild-type zebrafish (*Danio rerio*) were maintained following the Canadian Council on Animal Care Guidelines. *In vivo* uptake of GB2-Cy3 in was visualized in a zebrafish model by modifications of previous protocols *(Melong et al., 2017, Park, Um et al., 2014)*. Full experimental details are provided in the Supplemental Material. This study was approved by the University of Windsor Animal Care Committee. Eggs were collected after fertilization and kept at 33°C for 48 hours post-fertilization (hpf). Three hours before implantation, attached LNCaP cells were incubated with 100 ng/mL Hoechst 33342 for 40 minutes at 37°C. After staining, cells were rinsed twice with PBS and RPMI-10% CSS medium was added.

At 48 hpf embryos were anesthetised with 0.168 mg/mL of Tricaine (Sigma, MS222). 100-150 labelled cells/ 9 nL were loaded into glass capillary needles and injected into the yolk sac of each embryo using a Nanoject II (Fisher Scientific). After injection, embryos were kept in water at 33°C. At 72 hpf the xenograft was examined using a Leica fluorescent stereoscope. 84 hpf embryos were treated with 250 μg/mL GB2-Cy3 at 33°C for 2 hours, followed by a water wash and a 15 minutes incubation. Embryos were then anesthetized, and imaged. Fold change in tumour foci and glucose uptake were quantified by total DAPI and Cy3 fluorescence respectively. The image for each embryo was imported into ImageJ, converted to a 32-bit greyscale, and the threshold was adjusted to eliminate background pixels.

3.2.8 Statistical Analysis

Statistical analysis was done using GraphPad Prism (CA, USA). The results are expressed as the mean ± standard error of the mean (SEM). The box-whisker plots show the median (horizontal line), the interquartile range (margins of box) and the absolute range (vertical line). Differences between two groups were compared by unpaired Student's t-test. One-way ANOVA followed by a Benjamini-Hochberg or Tukey adjustment. Neurite length was measured by manual tracing and determined using NIH ImageJ software as previously described *(Bakht et al., 2019b, Ding et al., 2015)*. Pearson correlation was used for nearest neighbor analysis and pairwise-correlation of the studied genes. Kaplan-Meier plots and heatmaps were generated using camcAPP *(Dunning et al., 2017)* and Broad Institute Morpheus software (MA, USA).

3.3 RESULTS

3.3.1 Differential Expression of FOLH1, SLC2A and HK in mCRPC

Figure 3-1A shows that expression of *SLC2A12* and *FOLH1* are the nearest neighbors to *AR* ($r > 0.6$, $P < 0.01$) and *GCK* is the furthest neighbour ($r = -0.6$, $P < 0.01$) in the UW cohort *(Bluemn et al., 2017)*. We observed a significant suppression of *FOLH1* in low-AR mCRPC phenotypes including NEPC and DNPC samples (Figure 3-1B). Figure 1C shows NEPC tumors have a 5-fold elevation of *GCK* ($P < 0.0001$) when compared to AR-positive samples. Alternatively, Figure 3-1D demonstrates that NEPC and DNPC samples suppress expression of *SLC2A12*. Figure 3-2 verifies that in the Beltran cohort *(Beltran et al., 2016c)* *FOLH1*-suppressed NEPC samples have similar profiles of glucose transporter gene expression. In summary, *GCK* gene expression is elevated and the *SLC2A12* gene is suppressed in NEPC.

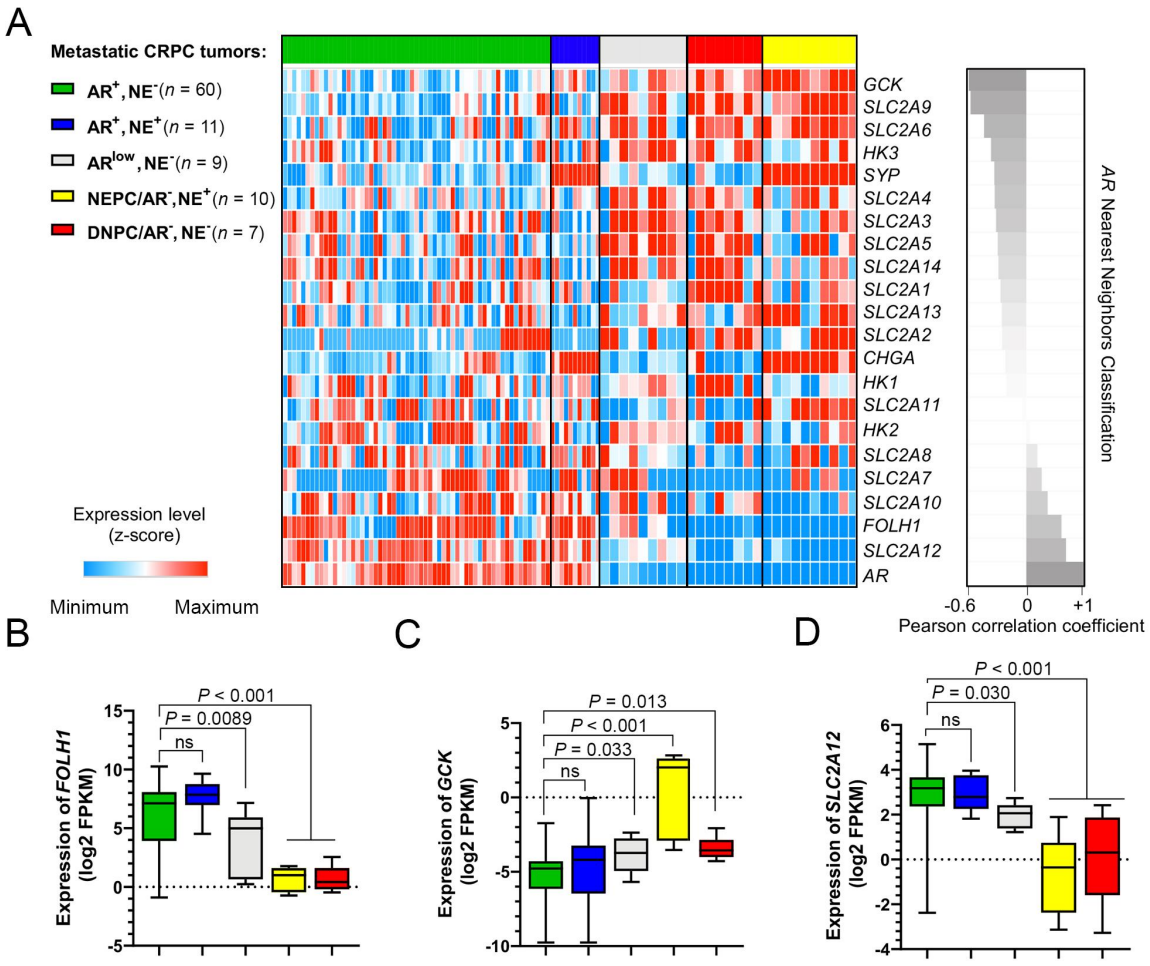

Figure 3-1 AR-negative subsets of mCRPC in UW cohort have suppressed expression of FOLH1 and differential expression of SLC2A and HKs genes.

(A) The heatmap plot of the expression levels of *SLC2A* family members, *HK* genes, *AR*, *FOLH1* and NE-markers sorted based on nearest neighbors clustering to *AR*. (B-D) The box-whisker plots show the expression of *FOLH1*, *SLC2A12* and *GCK*.

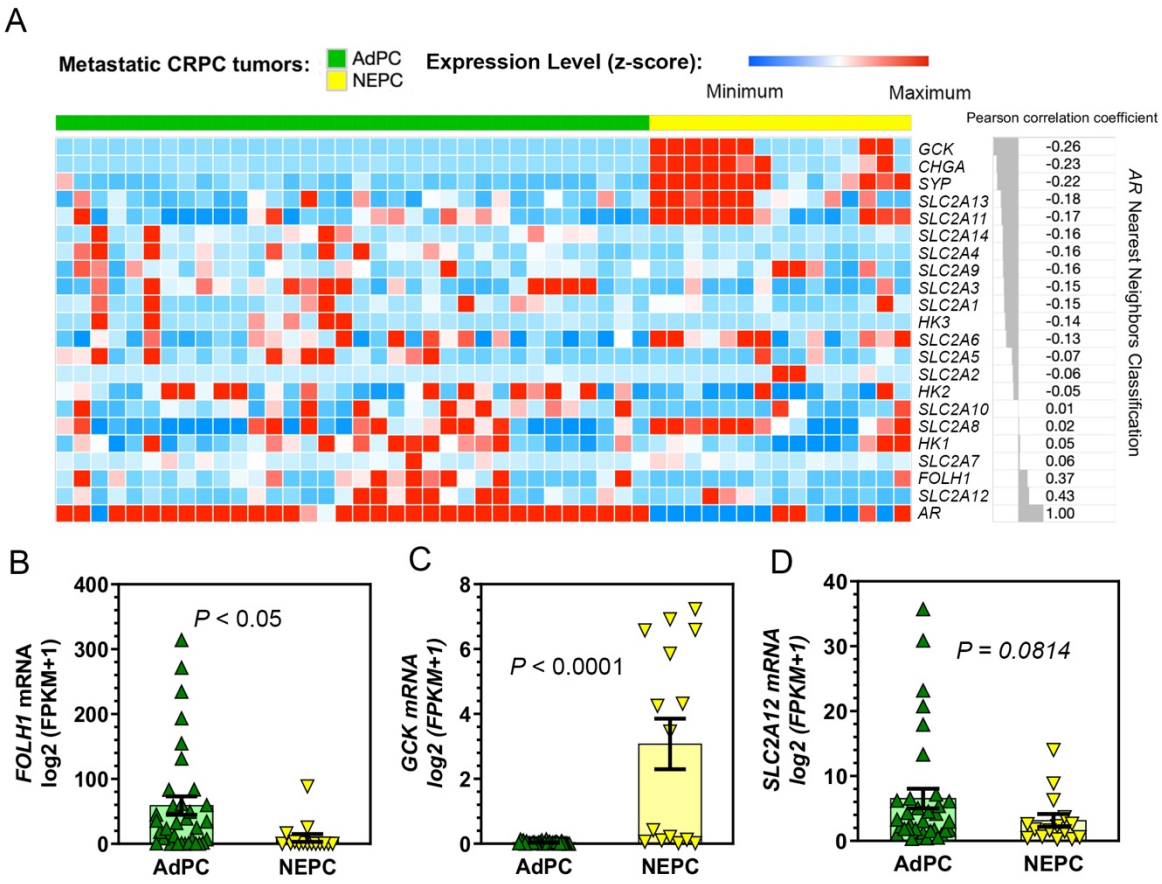

Figure 3-2 NEPC samples of the Beltran cohort have suppressed *FOLH1* and differential *SLC2A12* and *GCK* expression.

(A) Heatmap plot of the expression levels of *SLC2A* family members, *HK* genes, *AR*, *FOLH1*and NE-markers sorted based on nearest neighbors clustering to AR. (B-D) The mean expression of *FOLH1*, *GCK* and *SLC2A12* in metastatic CRPC samples. Error bars reflect SEM and Student's t-test was performed.

3.3.2 Differential Expression of SLC2A and HK in NELPC

The meta-signature of prototypical high-grade NEPC *(Tsai et al., 2017)* was employed to isolate a potential NELPC group among a population of metastatic and primary AdPC samples lacking NEPC histopathology (Figure 3-3 and Figure 3-4). Figure 3-5A shows the transcriptionally identified NELPC subset have shorter time to biochemical recurrence in NELPC (log-rank *P*-value = 0.02). Figure 3-5B displays that a NELPC hallmark can be observed in both primary and metastatic samples, with the more prevalent signature seen in metastatic and high Gleason score samples. Figure 3-5C shows a lack of hallmarks of AR response in NELPC. Figure 3-6 shows that *SLC2A1, 3-5, 9, 10, 12-14* and *HK1, 2* genes cluster with *REST*; herein referred to as *REST*-clustered genes. On the other hand, *SLC2A2, 6-8, 11, HK3* and *CGK* cluster with *SRRM4* and other NE-markers; herein referred to as *SRRM4*-clustered genes. Pairwise-correlation with *SRRM4* expression is presented in Figure 3-7, Figure 3-8 and Figure 3-9. Similar to NEPC, *SLC2A12* and *FOLH1* expression are decreased in NELPC relative to AdPC (Figure 3-5D). *GCK* expression is significantly higher in NELPC.

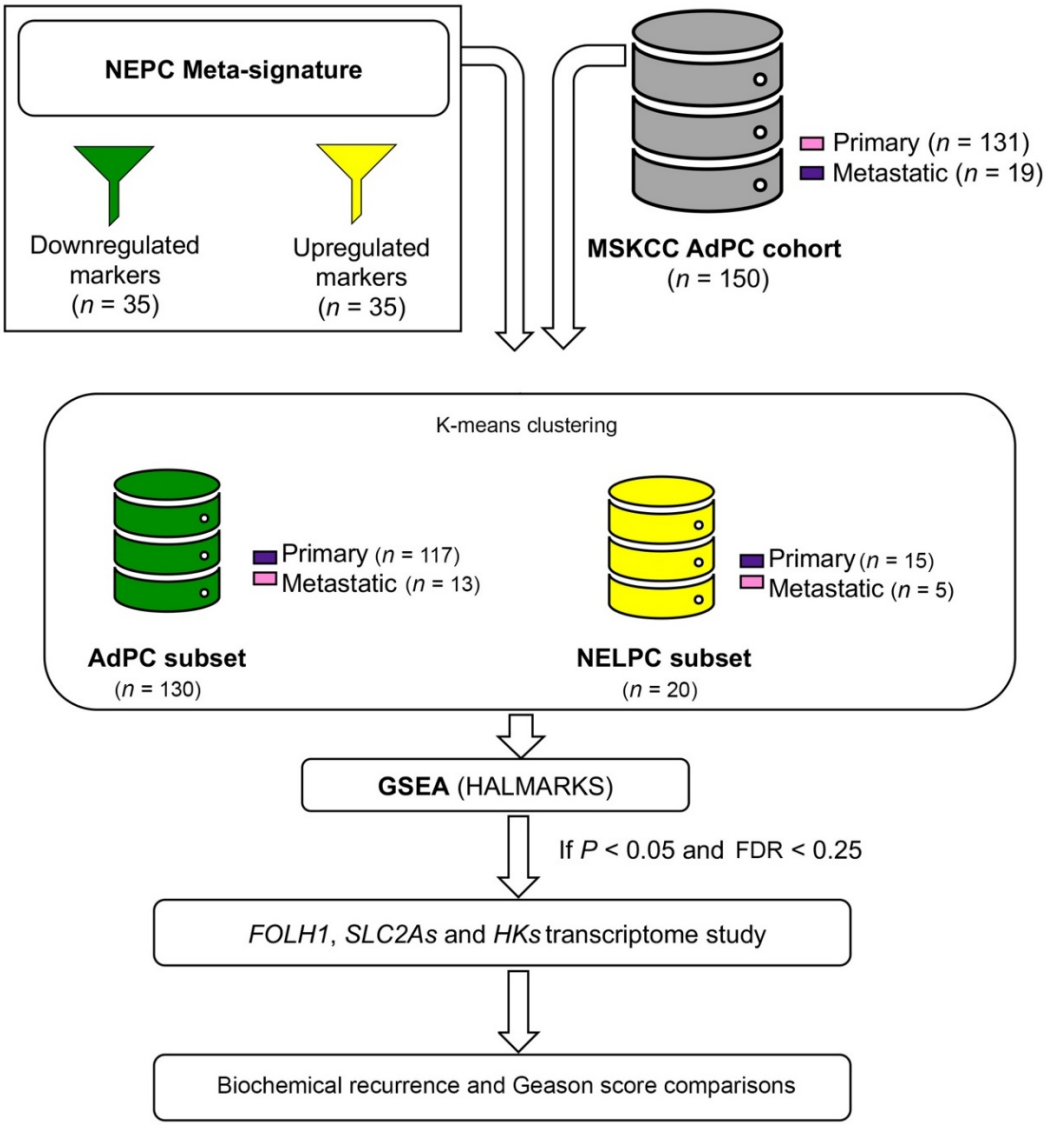

Figure 3-3 A schematic of the process used to identify a NELPC subset among a population of metastatic and primary AdPC samples.

The meta-signature of prototypical high-grade NEPC *(Tsai et al., 2017)* was used to identify a potential NELPC subset among the AdPC MSKCC cohort *(Taylor et al., 2010)*. This meta-signature consists of two sets of markers for classification of AdPC and NEPC. GSEA was used to confirm that the identified subset is characteristic of a low-AR hallmark. FDR = False discovery rate.

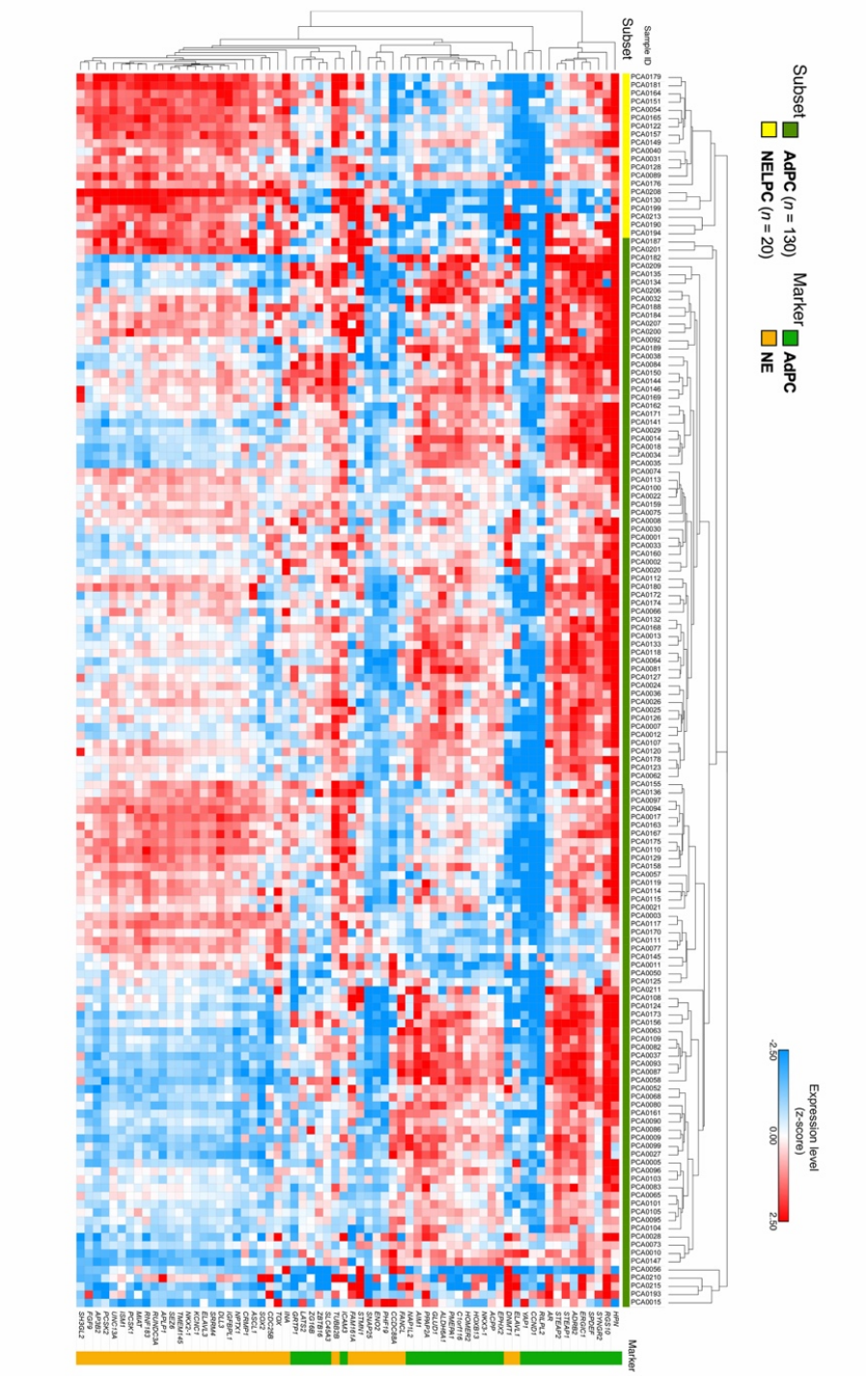

Figure 3-4 Heatmap showing the expression of NEPC markers in the NELPC subset identified from MSKCC cohort.

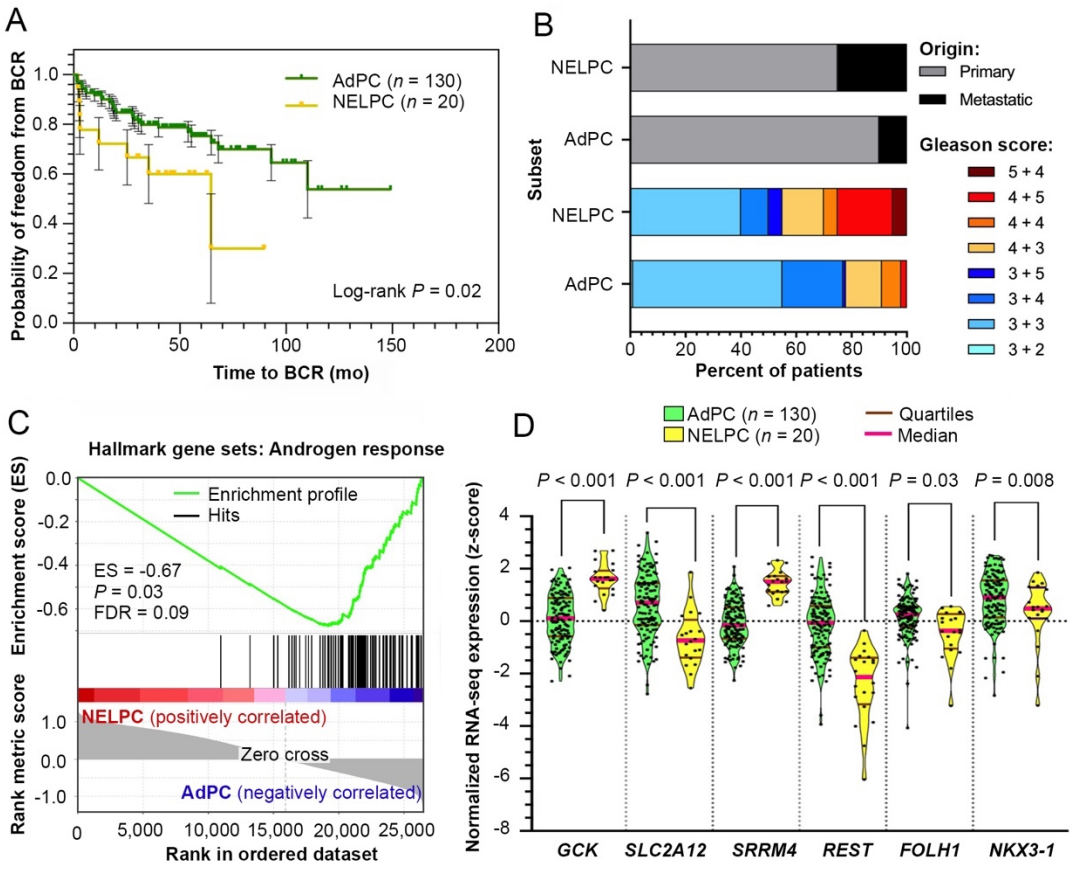

Figure 3-5 The features of NELPC subset identified from MSKCC cohort.

The NELPC subset of MSKCC cohort displays (A) shorter time to BCR, (B) more prevalence of metastatic and high Gleason score specimens and (C) lack of AR response. Violin plots compare the distribution of *SLC2A12*, *GCK* and *FOLH1*expressions in NELPC and AdPC subsets. BCR = biochemical recurrence.

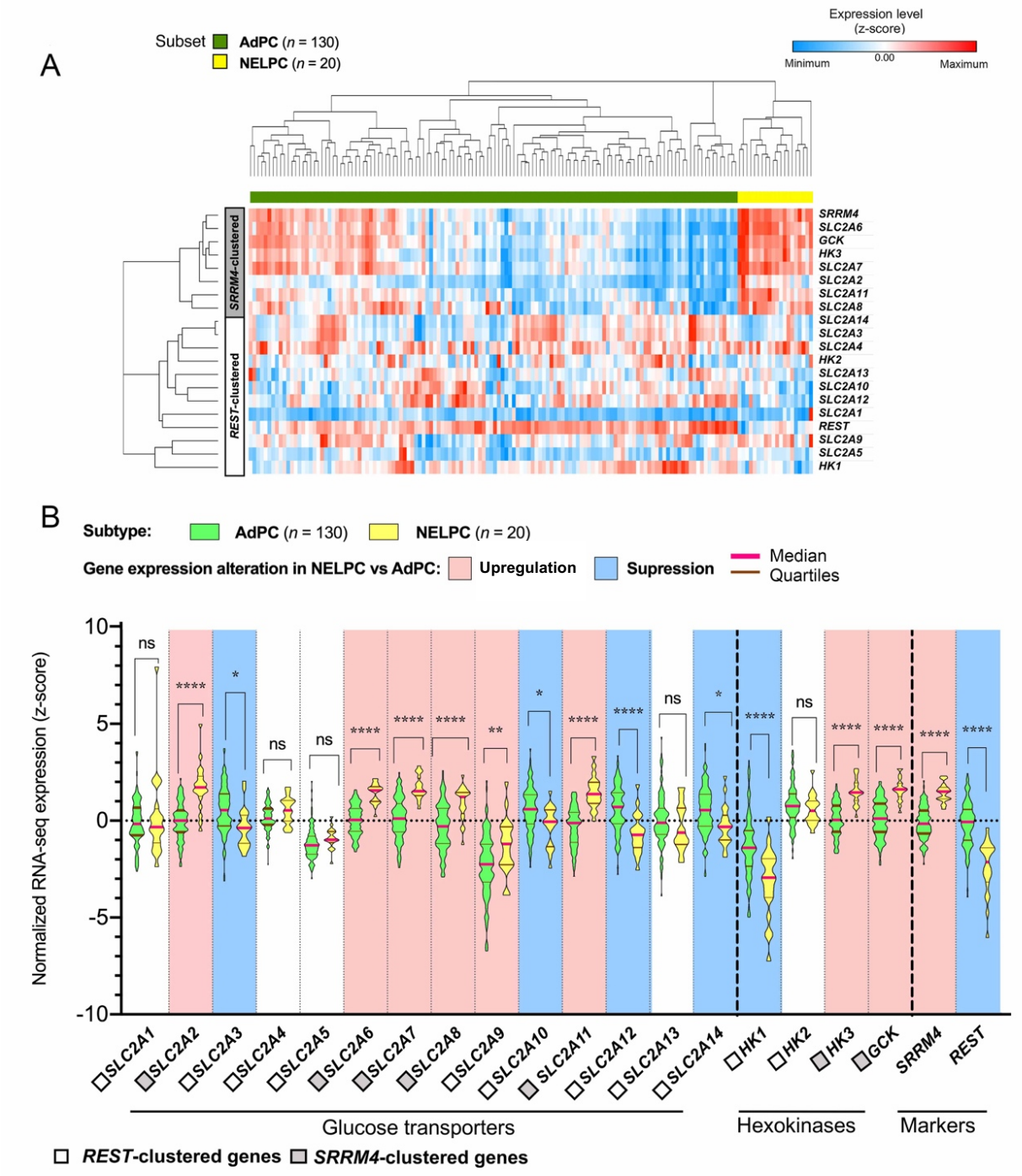

Figure 3-6 Enhanced expression in the expression of *SRRM4*-clustered *SLC2A* and *HK* genes in NELPC subset of patients in MSKCC cohort.

(A) Heatmap plot of the mean expression levels of *SLC2A* family members, *HK* genes, *REST* as AdPC marker and *SRRM4* as NE marker. (B) Violin plots compare the distribution of *SLC2As* and *HK*s expressions in NELPC and AdPC subsets.

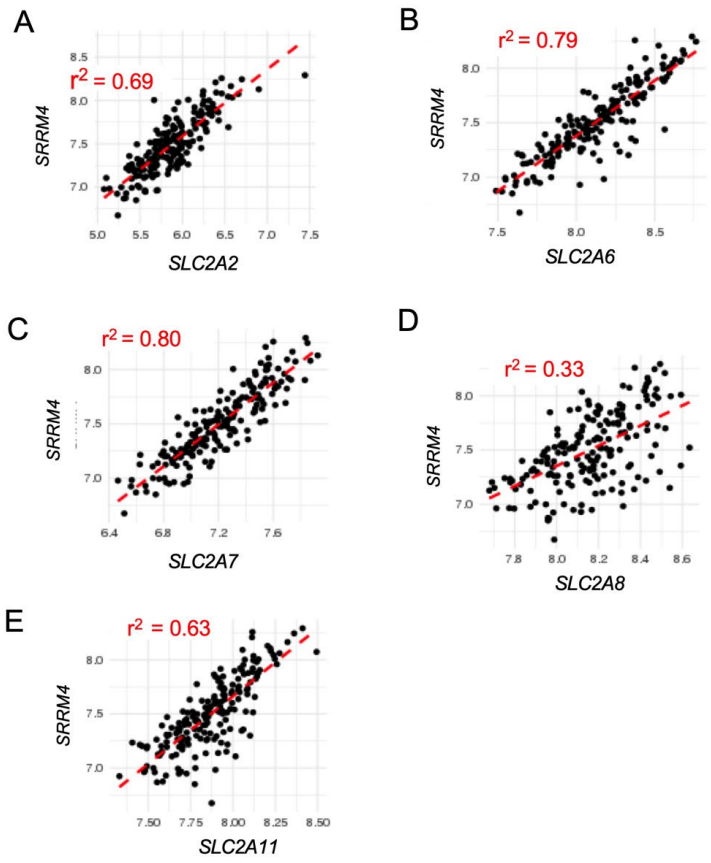

Figure 3-7 *SLC2A2, 6-8, 11* genes are co-expressed with *SRRM4* as a treatment induced NEPC marker.

(A-E) Pairwise-correlation of *SRRM4* and the introduced *SRRM4*-clustered *SLC2A* gene expression followed by Pearson correlation analysis generated using MSKCC PC cohort data *(Taylor et al., 2010)*.

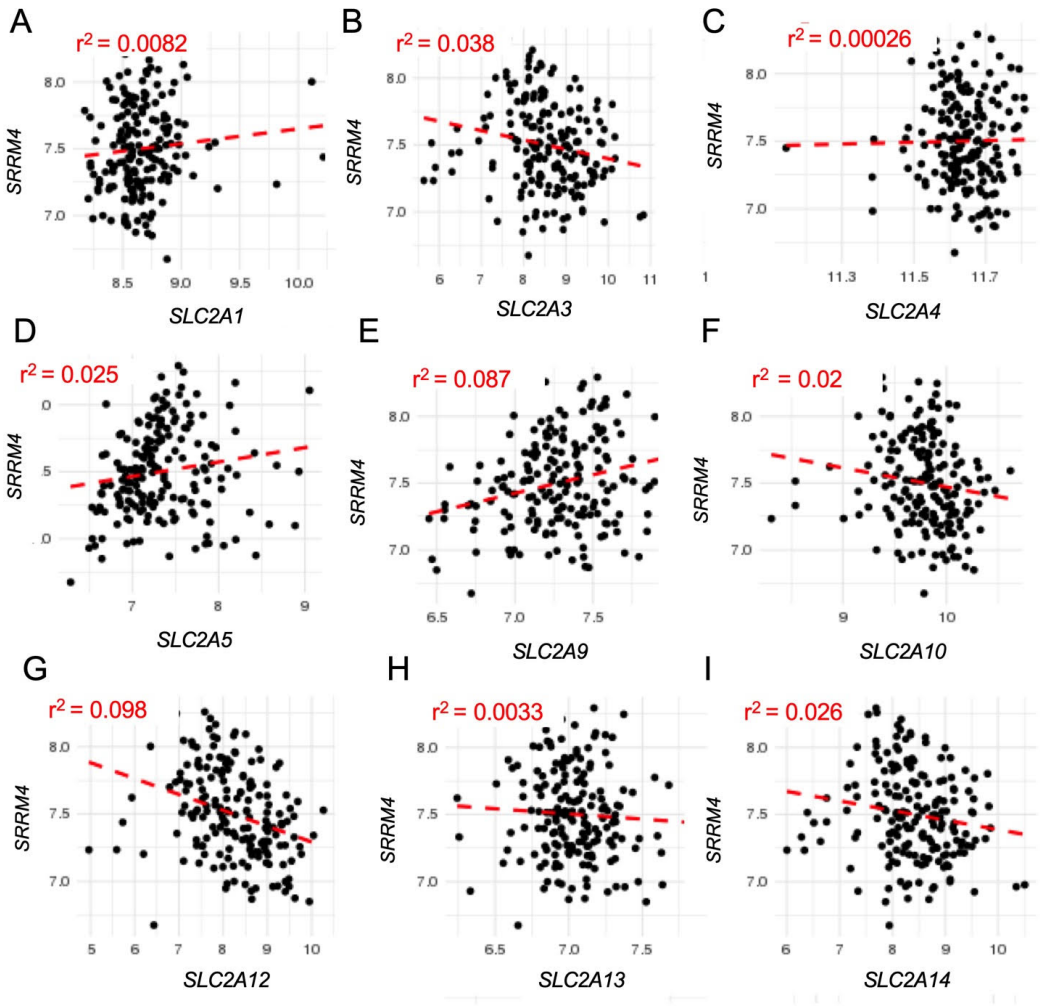

Figure 3-8 *SLC2A1, 3-5, 9-12* genes *as REST*-clustered genes are not co-expressed with *SRRM4* as a treatment induced NEPC marker.

(A-I) Pairwise-correlation of *SRRM4* and the introduced *REST*-clustered *SLC2A* gene expression followed by Pearson correlation analysis generated using MSKCC PC cohort data *(Taylor et al., 2010)*.

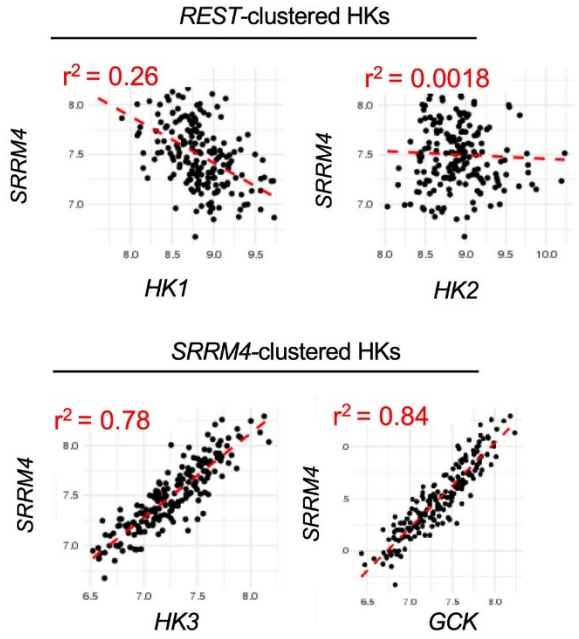

Figure 3-9 Pairwise-correlation of SRRM4 and HK gene expression followed by Pearson correlation analysis generated using MSKCC PC cohort data.

3.3.3 The Association of SLC2A and HK with Gleason Score (GS) and Biochemical Recurrence in NELPC

Figure 3-10, Figure 3-11 and Figure 3-12 depict expression levels of the studied genes during progression of AdPC based on GS. The majority of *REST*-clustered *SLC2A* genes and *HKs* are either unchanged or suppressed at high GS while *SRRM4*-clustered genes are significantly increased in samples with high GS. Kaplan-Meier survival curves studying high and low expression levels of the studied genes are represented in Figure 3-13, Figure 3-14 and Figure 3-15. The enhanced expression of *SRRM4*-clustered genes such as *GCK* and *REST*-clustered gene *SLC2A1* (as an exception) are significantly associated with decreased biochemical recurrence (log-rank *P*-value for *GCK*: 0.015). Interestingly, high levels of *REST*-clustered genes including *SLC2A12* are associated with shorter time to

biochemical recurrence (log-rank *P*-value for *SLC2A12*: 0.012). Table 3-1 summarises the performed analysis on NELPC.

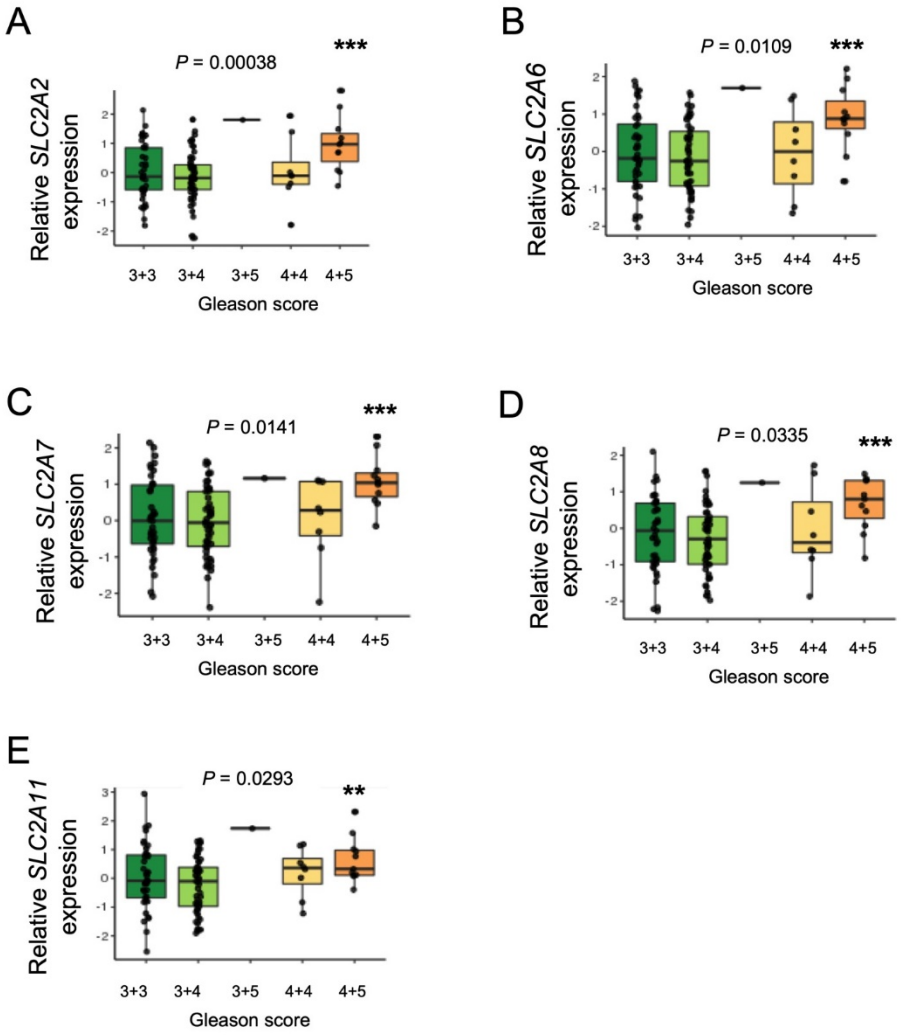

Figure 3-10 Enhanced expression of *SRRM4*-clustered *SLC2A* genes are correlated with higher Gleason scores.

(A-E) Box-whisker plots showing the expression of *SRRM4*-clustered *SLC2A* genes during progression of AdPC based on Gleason score using MSKCC PC cohort data *(Taylor et al., 2010)*. One-way ANOVA followed by unpaired t-tests were performed with Benjamini–Hochberg adjustment for multiple test correction; **: $P < 0.01$ and ***: $P < 0.001$.

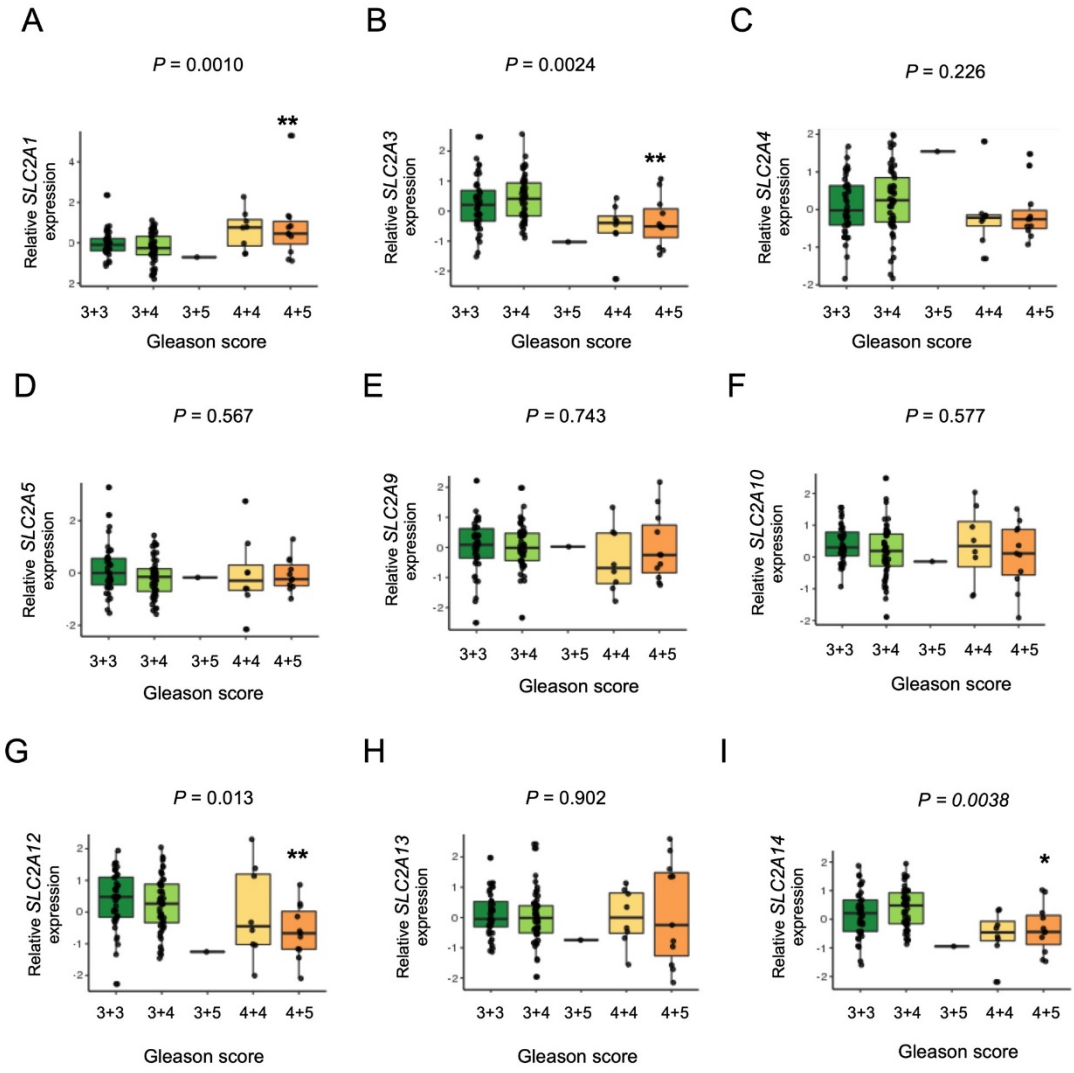

Figure 3-11 Except *SLC2A1* gene, the enhanced expression of *REST*-clustered *SLC2A* gene do not correlate with higher Gleason scores.

(A-I) Box-whisker plots showing the expression of *REST*-clustered *SLC2A* genes during progression of AdPC based on Gleason score using MSKCC PC cohort data *(Taylor et al., 2010)*. One-way ANOVA followed by unpaired t-tests were performed with Benjamini–Hochberg adjustment for multiple test correction; *: $P < 0.05$ **: $P < 0.01$.

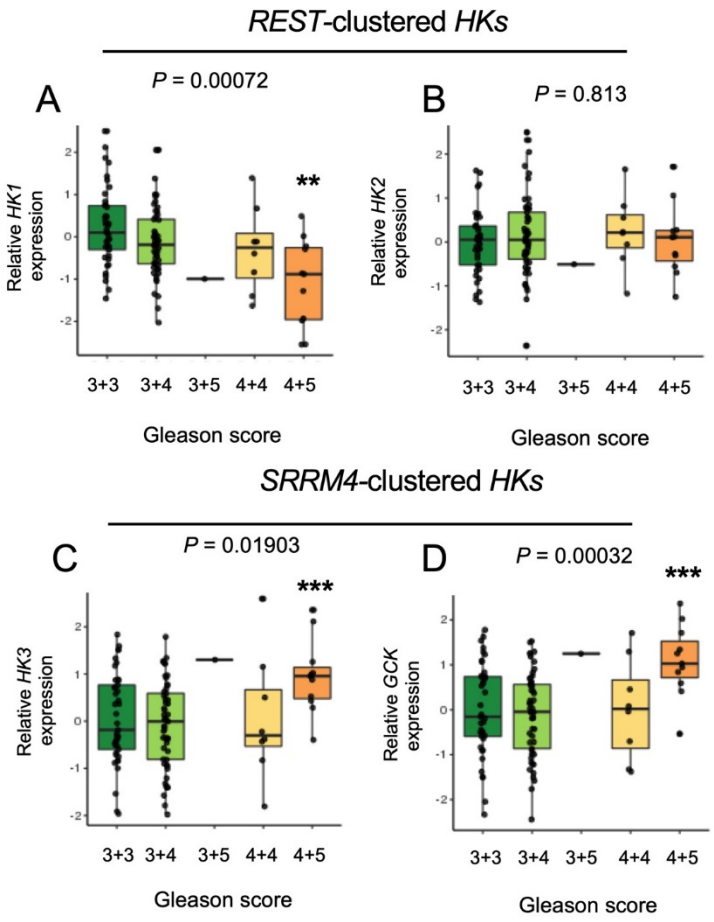

Figure 3-12 Enhanced expression of *SRRM4*-clustered *HK* genes is associated with higher Gleason scores.

(A-D) Box-whisker plots showing the expression of *HK* genes during progression of AdPC based on Gleason score using MSKCC PC cohort data *(Taylor et al., 2010)*. One-way ANOVA followed by unpaired t-tests were performed with Benjamini–Hochberg adjustment for multiple test correction; $^{**}P < 0.01$; $^{***}P < 0.001$.

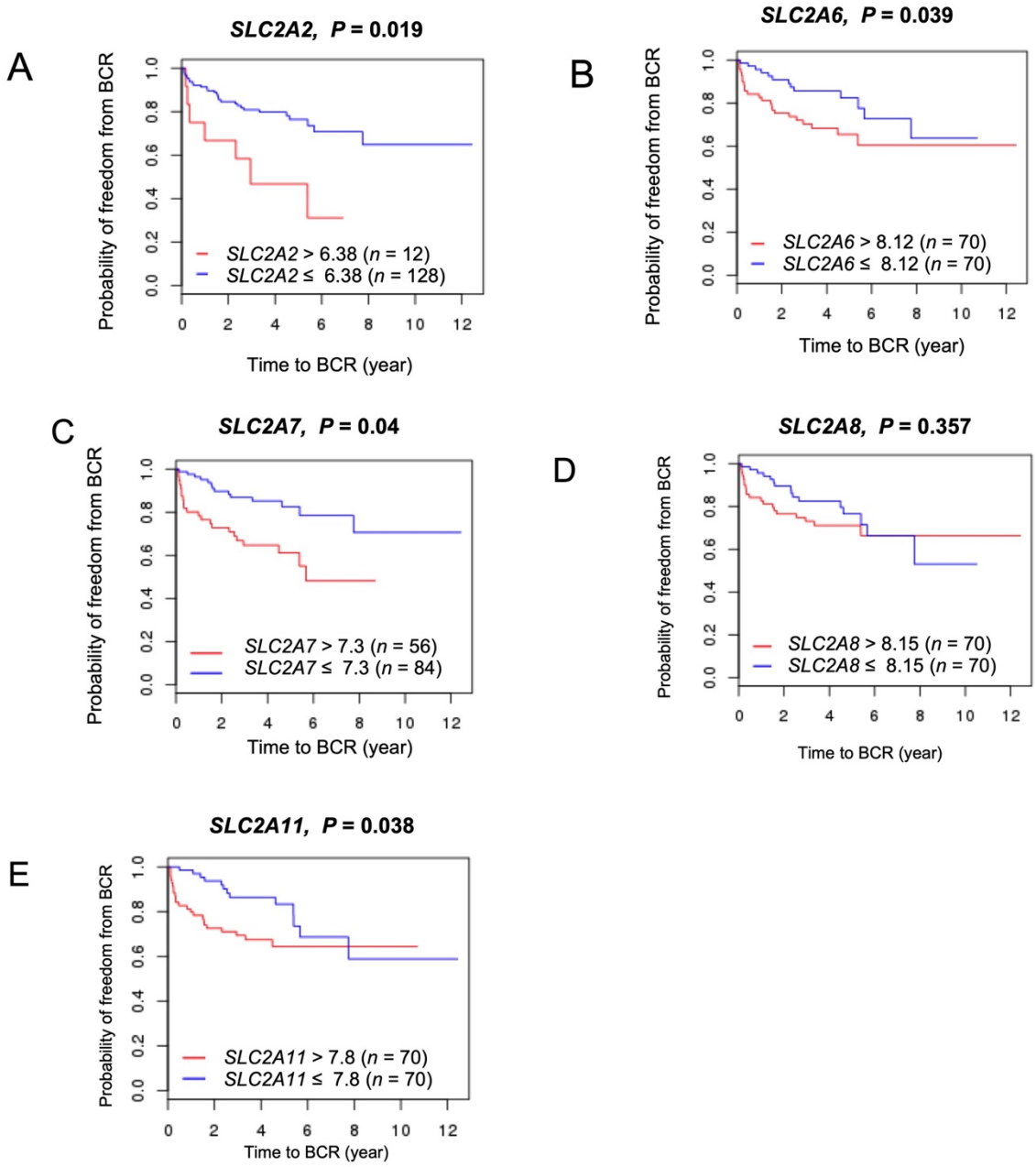

Figure 3-13 Enhanced expression of *SRRM4*-clustered *SLC2A* genes including of *SLC2A2*, *SLC2A6*, *SLC2A7* and *SLC2A11* is associated with shorter time to BCR.

(A-E) Kaplan-Meyer survival curves for high and low expression levels of *SRRM4*-clustered *SLC2A* genes generated using MSKCC PC cohort data *(Taylor et al., 2010)*. The log-rank test was employed to identify statistical difference between the high and low expressing groups. BCR = biochemical recurrence.

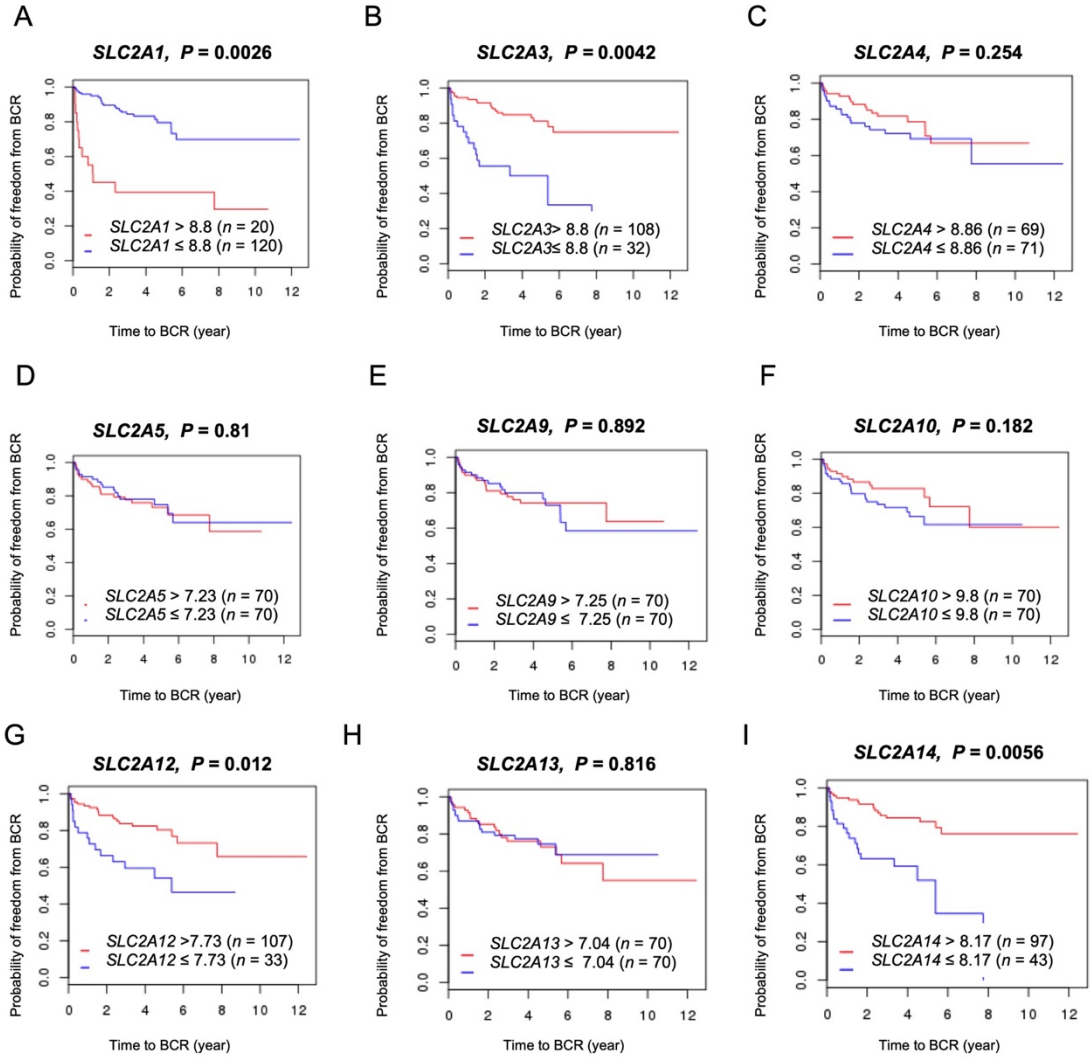

Figure 3-14 Low levels of *REST*-clustered *SLC2A* genes including *SLC2A3, SLC2A12* and *SLC2A14* expression are associated with shorter time to BCR.

(A-I) Kaplan-Meyer survival curves for high and low expression levels of *REST*-clustered *SLC2A* genes generated using MSKCC PC cohort data *(Taylor et al., 2010)*. The log-rank test was employed to identify statistical difference between the high and low expressing groups. BCR = Biochemical recurrence.

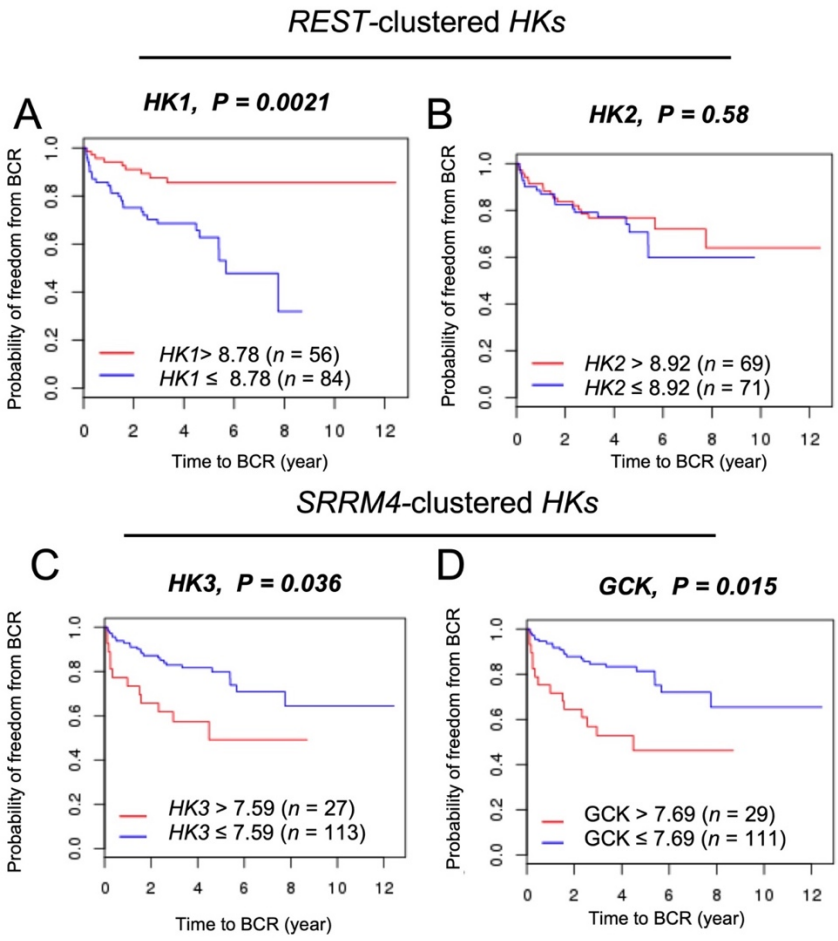

Figure 3-15 Enhanced expression of *SRRM4*-clustered *HK* genes is associated with shorter time to BCR.

(A-E) Kaplan Meyer survival curves for high and low expression levels of *HK* genes generated using MSKCC PC cohort data *(Taylor et al., 2010)*. The log-rank test was employed to identify statistical difference between the high and low expressing groups. BCR = biochemical recurrence.

Table 3-1 An overview of the studied genes in MSKCC cohort.

Gene name	Protein name	Assigned cluster	Type of alteration in NELPC	Pearson correlation coefficient with *SRRM4*	Probability of freedom from BCR (*P*-value)	Gleason Score progression (*P*-value)
SLC2A1	GLUT1	*REST*	No alteration	0.0082	0.0026	0.001
SLC2A2	GLUT2	*SRRM4*	↑↑↑	0.69	0.019	0.003
SLC2A3	GLUT3	*REST*	↓↓	0.036	0.0042	0.0024
SLC2A4	GLUT4	*REST*	No alteration	0.0002	0.254	0.22
SLC2A5	GLUT5	*REST*	↓	0.025	0.81	0.56
SLC2A6	GLUT6	*SRRM4*	↑↑↑	0.79	0.039	0.01
SLC2A7	GLUT7	*SRRM4*	↑↑↑	0.8	0.04	0.01
SLC2A8	GLUT8	*SRRM4*	↑↑	0.33	0.357	0.03
SLC2A9	GLUT9	*REST*	↑	0.06	0.892	0.74
SLC2A10	GLUT10	*REST*	↓	0.02	0.182	0.57
SLC2A11	GLUT11	*SRRM4*	↑↑↑	0.63	0.038	0.029
SLC2A12	GLUT12	*REST*	↓↓	0.098	0.012	0.013
SLC2A13	GLUT13 (HMIT)	*REST*	No alteration	0.003	0.816	0.90
SLC2A14	GLUT14	*REST*	↓↓	0.02	0.0056	0.003
HK1	Hexokinase-I	*REST*	↓↓↓	0.26	0.0021	0.00072
HK2	Hexokinase-II	*REST*	No alteration	0018	0.58	0.81
HK3	Hexokinase-III	*SRRM4*	↑↑↑	0.78	0.036	0.019
GCK	Hexokinase-IV (glucokinase)	*SRRM4*	↑↑↑	0.84	0.015	0.00032

3.3.4 SLC2A12 Suppression and GCK Overexpression are Shared Among NEPC and NELPC

RNA-seq data from 268 PC samples from the MSKCC *(Taylor et al., 2010)*, Beltran *(Beltran et al., 2016c)* and UW *(Bluemn et al., 2017)* cohorts were used to stratify *SLC2A1-14* and *HK1-4* genes into NE-clustered and AdPC-clustered groups (Figure 3-16). The intersection between the clustered genes in different cohorts and inclusion of the most differentially expressed genes showed that *GCK* is the most highly expressed gene and *SLC2A12* is the most suppressed gene in samples with a NEGS.

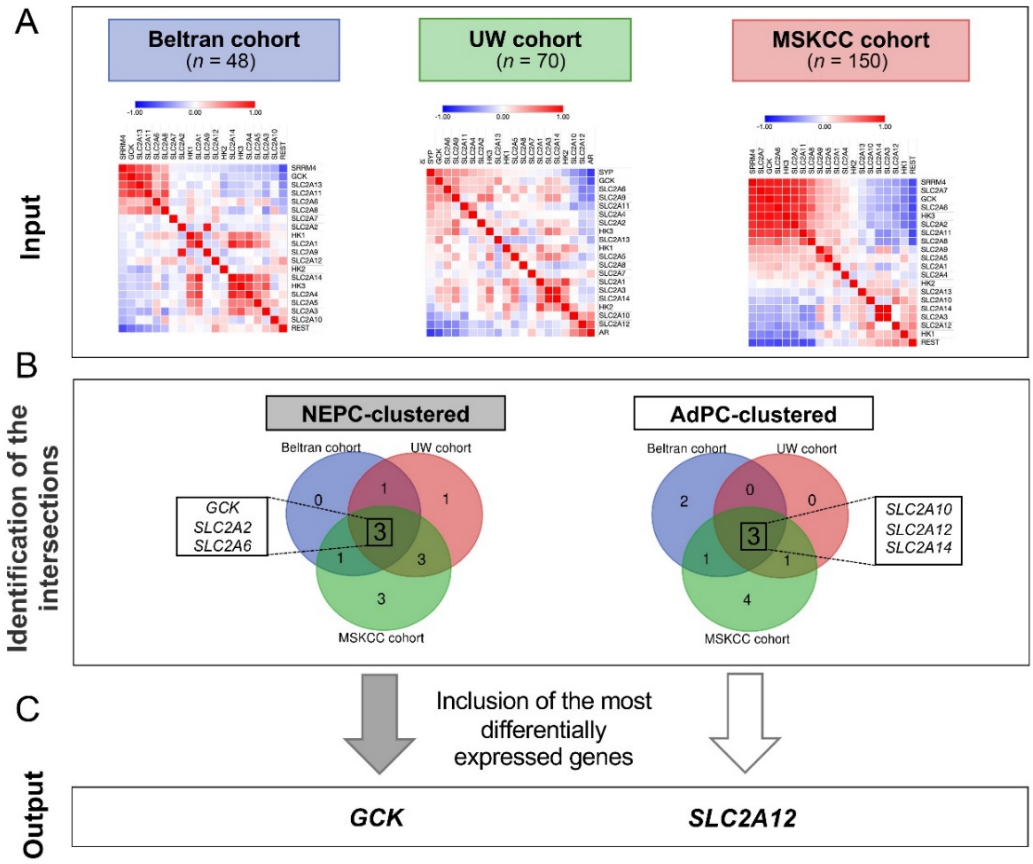

Figure 3-16 Among *SLC2A* family members and *HK* genes, *GCK* is the most highly expressed gene and *SLC2A12* is the most highly suppressed gene in samples with NE gene signature in comparison with samples with an AdPC signature.

(A-C) The schematic showing the process of selecting the most differentially expressed genes. (A) The RNA-seq data from 268 prostate cancer samples from MSKCC *(Taylor et al., 2010)*, Beltran *(Beltran et al., 2016c)* and UW *(Bluemn et al., 2017)* cohorts are used to stratify *SLC2A1-14* and *HK1-4* genes into NEPC-clustered and AdPC-clustered groups. (B) Venn diagram illustrating the intersections between the clustered genes in different cohorts. (C) The most highly differentially expressed genes in the intersections are selected to be studied in cell lines and PDX models.

3.3.5 NEPC Has a Distinct GCK-Upregulated and SLC2A12-Suppressed Signature in PDX Models

The LTL331 PDX is a model of PC progression from AdPC-to-NEPC. LTL331 tumors regress following castration, but relapse within 24 to 32 months with tumors harbouring NEPC phenotypes *(Akamatsu et al., 2015a)*. Figure 3-17A demonstrates that *GCK* expression is minimal before progression to CRPC but reaches maximum levels following cellular plasticity to CRPC and NEPC. Conversely, *SLC2A12* expression is at its maximum level in hormone sensitive AdPC and, with a slight fluctuation, gradually levels decrease following castration. The expression of *SLC2A12* and *FOLH1* are the nearest neighbors to *AR* ($r > 0.6$, $P < 0.01$) and *GCK* is the furthest neighbour ($r = -0.87$, $P < 0.01$) in the UW cohort *(Bluemn et al., 2017)*. Figure 3-17B shows in our other well characterized PDX models consisting of 20 AdPC and 3 NEPC models that we observe significant elevation of *GCK* and suppression of *SLC2A12* gene expression in the NEPC models. Overall, NEPC models have a *SLC2A12*-low and *GCK*-high signature.

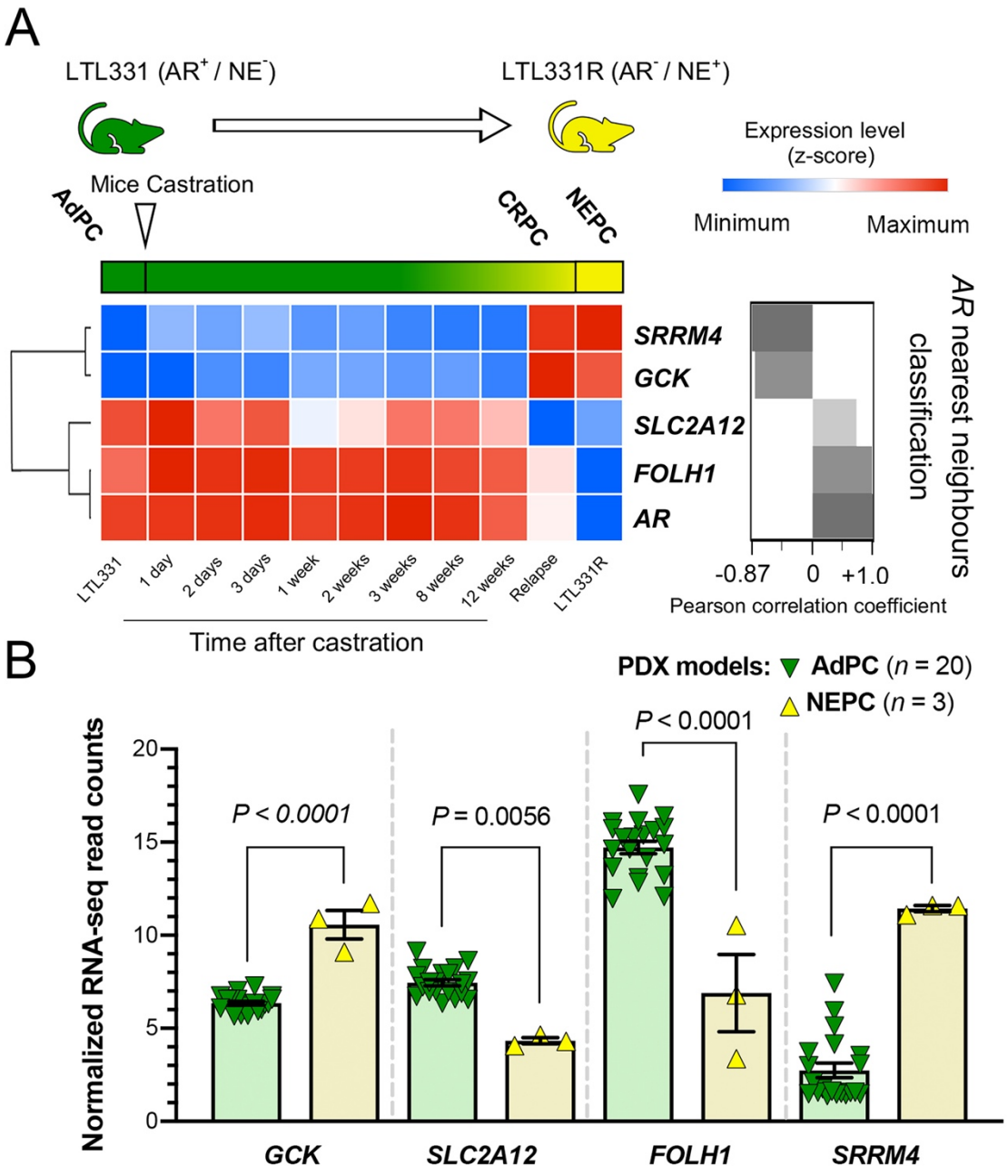

Figure 3-17 NEPC PDX models have suppressed expression of *FOLH1* and differential expressions of *SLC2A12* and *GCK*.

(A) Transcription of the studied genes during progression to NEPC and correlation with *AR*. (B) The expression of the studied genes in PDX models.

3.3.6 Higher In Vitro Glucose Uptake in NE-induced Cell Lines

To investigate the role of progression to a NE phenotype on glucose uptake we used the well-characterized NE subclone cell line (LNCaP-NEPC) in which NEPC cells are derived from LNCaP cells (LNCaP-AdPC) by culturing in an androgen-depleted environment to mimic clinical androgen-deprivation therapy *(Yuan, Veeramani et al., 2006a)* (cartoon of process: Figure 3-18A; characterization of lines in Figure 3-18B-D). Figure 3-19A shows that protein levels of the NE-marker NSE are increased in the LNCaP-NEPC, while PSMA and AR levels are significantly decreased. The LNCaP-NEPC cell line has a significantly higher level of glucokinase (GCK) protein and a significantly lower level of GLUT12 (Figure 3-19B).

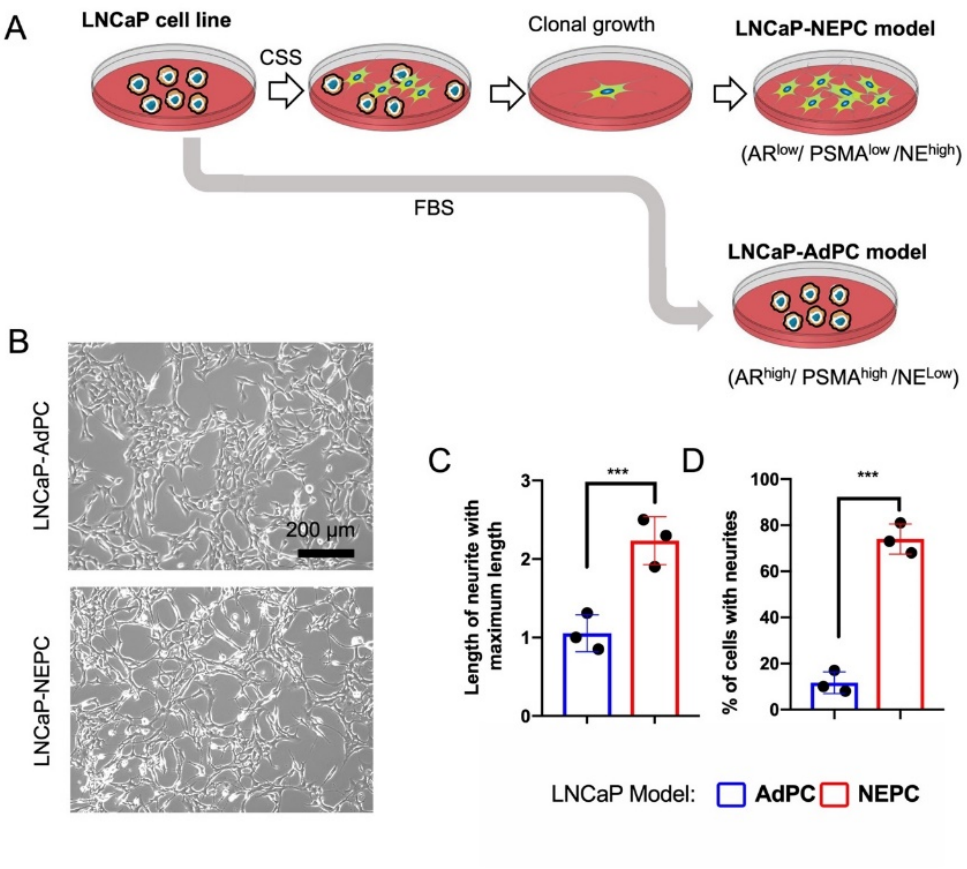

Figure 3-18 Development of a NE-induced LNCaP cell line.

(A) The Schematic showing the steps for progression of the LNCaP cell line to NEPC. (B) Representative photos of control (top) and CSS-treated (bottom) LNCaP cells. (C) Neurites were measured using ImageJ software and longest neurite calculated. (D) % of cells with neurites counted over 3 fields of view. The results are expressed as the mean ± SEM. Differences between two groups were compared by unpaired Student's t-test. ***: $P < 0.001$. Some elements of this figure were produced using Servier Medical Art image bank (www.servier.com). FBS = Fetal bovine serum; CSS = Charcoal- stripped serum.

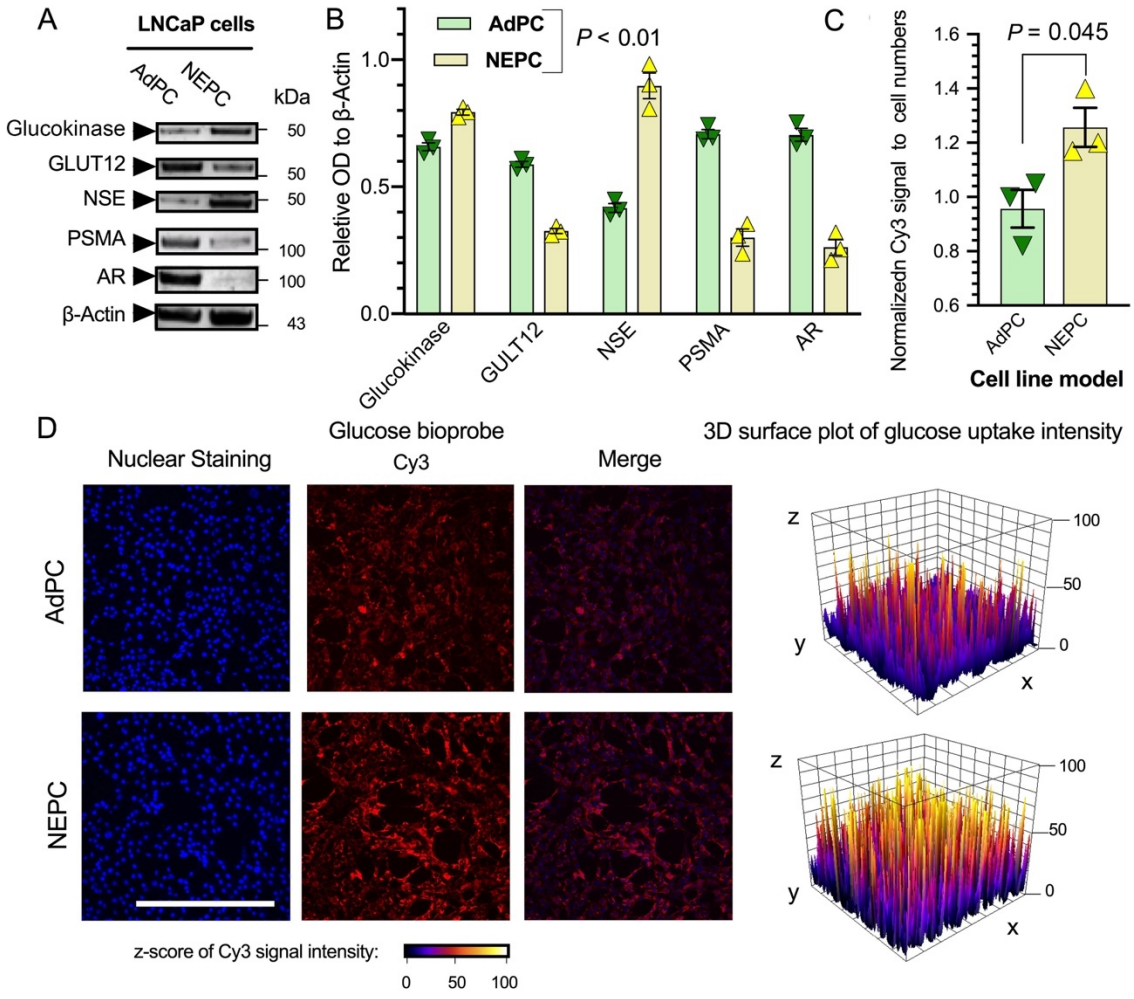

Figure 3-19 The NE-induced LNCaP cell line represents higher glucose uptake and differential protein levels of glucokinase and GLUT12.

(A-B) Western blot analyses of protein levels. (C-D) Quantification of GB2-Cy3 uptake and representative images of LNCaP cells. Scale bar = 200 microns. (n = 3)

Appendix Figure 1-8 demonstrate chemical characterization of the GB2-Cy3. Figure 3-20 illustrates GB2-Cy3 uptake and its localization in LNCaP cells. Figure 3-19C shows the LNCaP-NEPC cell line has a higher *in vitro* uptake of GB2-Cy3.

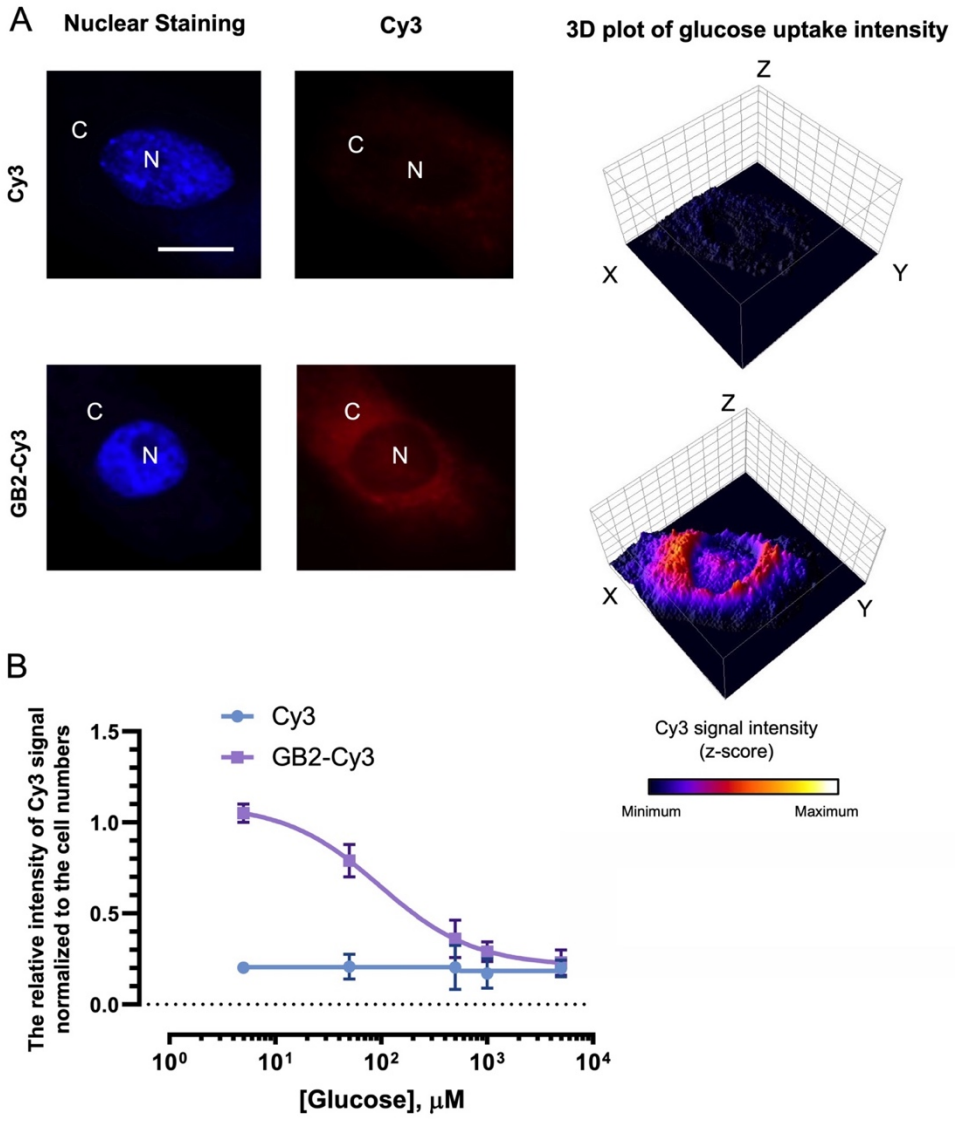

Figure 3-20 GB2-Cy3 uptake and localization in LNCaP cell line.

(A) Free-Cy3 dye showed no specific uptake in LNCaP cells while GB2-Cy3 had high uptake in cytoplasm (showed by C letter) and a minimal intensity in nuclear region (shown by N letter). (B) Glucose competition assay using Cy3 and GB2-Cy3 shows the uptake of GB2-Cy3 by LNCaP cell line could be inhibited as a result of increasing the concentration of glucose.

3.3.7 Higher In Vivo Glucose Uptake in NE-induced Cell Lines

A zebrafish model was used for non-radioactive *in vivo* imaging of glucose uptake and displayed higher GB2-Cy3 in engrafted LNCaP-NEPC cells (Figure 3-21). These observations indicate that suppression of PSMA, AR and elevation of NE-markers in LNCaP cell lines are associated with a differential level of glucose uptake, suppression of GLUT12 and elevation of glucokinase proteins.

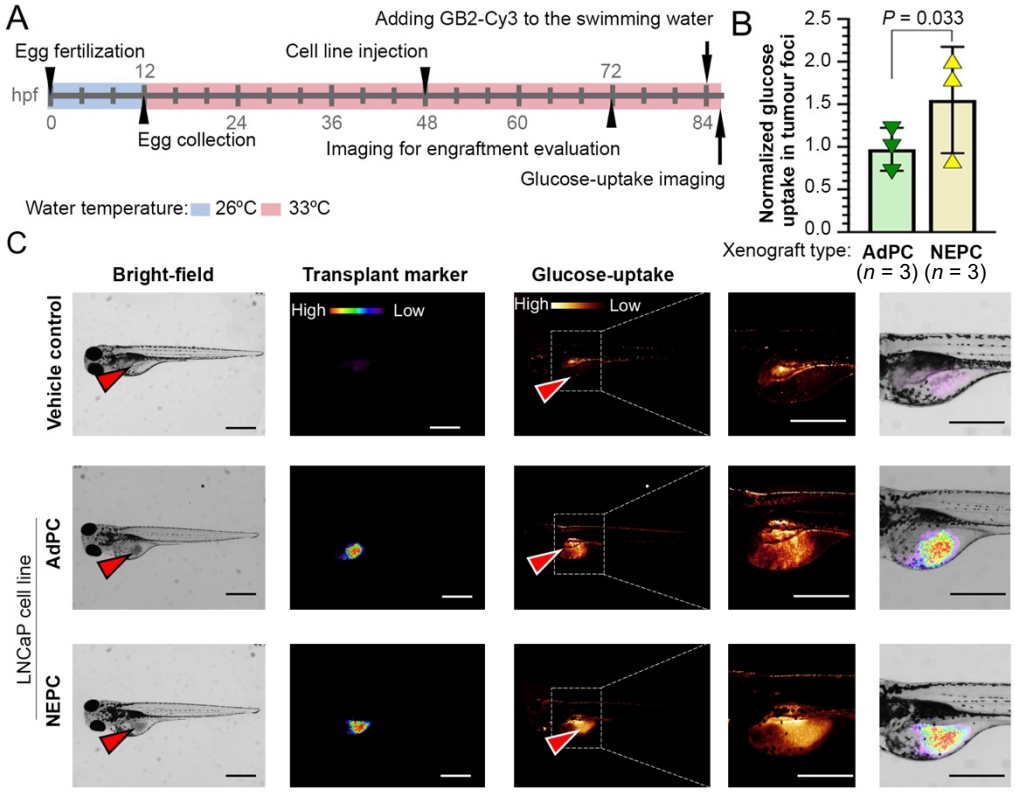

Figure 3-21 The NE-induced LNCaP cell line xenografts represent higher glucose uptake in a zebrafish model.

(A) Schematic of the experiment. (B-C) Quantification of GB2-Cy3 uptake and representative images of embryos injected with different LNCaP cells. Red arrows show the injection sites. Scale bar = 200 microns.

3.4 DISCUSSION

The development of AR-indifferent and NE-positive tumor phenotypes through divergent clonal evolution as a mechanism of resistance to AR-inhibition in mCRPC is a well characterized concept *(Beltran et al., 2016c, Bluemn et al., 2017)*. However, Stelloo *et al. (Stelloo et al., 2018)* identified a NELPC in a treatment naïve and primary cohort. Our work identified a NELPC subset among primary and metastatic samples with no history of exposure to next generation AR-inhibitors. Our data also shows that the incidence of NELPC is more prevalent in metastatic specimens. These data support that either AR-indifferent subsets of cells can exist among AdPC that possess a greater susceptibility for NE-transdifferentiation, or AR-indifferent, NE-like cells exist from an early time point and are gradually selected for during treatment pressures.

3.5 CONCLUSION

NEPC, DNPC and NELPC have distinct differential expression of GLUT and HK genes. In accordance with this, the loss of PSMA in NEPC is associated with elevated glucose uptake.

3.6 REFERENCES

Akamatsu S, Wyatt AW, Lin D, Lysakowski S, Zhang F, Kim S, Tse C, Wang K, Mo F, Haegert A (2015a) The placental gene PEG10 promotes progression of neuroendocrine prostate cancer. *Cell Rep* 12: 922-936

Alshalalfa M, Liu Y, Wyatt AW, Gibb EA, Tsai HK, Erho N, Lehrer J, Takhar M, Ramnarine VR, Collins CC, Den RB, Schaeffer EM, Davicioni E, Lotan TL, Bismar TA (2019) Characterization of transcriptomic signature of primary prostate cancer analogous to prostatic small cell neuroendocrine carcinoma. *International journal of cancer* in press

Bakht MK, Derecichei I, Li Y, Ferraiuolo RM, Dunning M, Oh SW, Hussein A, Youn H, Stringer KF, Jeong CW, Cheon GJ, Kwak C, Kang KW, Lamb AD, Wang Y, Dong X, Porter LA (2019b) Neuroendocrine differentiation of prostate cancer leads to PSMA suppression. *Endocr Relat Cancer* 26: 131-146

Beltran H, Prandi D, Mosquera JM, Benelli M, Puca L, Cyrta J, Marotz C, Giannopoulou E, Chakravarthi BVSK, Varambally S, Tomlins SA, Nanus DM, Tagawa ST, Van Allen EM,

Elemento O, Sboner A, Garraway LA, Rubin MA, Demichelis F (2016c) Divergent clonal evolution of castration resistant neuroendocrine prostate cancer. *Nat Med* 22: 298-305

Bluemn EG, Coleman IM, Lucas JM, Coleman RT, Hernandez-Lopez S, Tharakan R, Bianchi-Frias D, Dumpit RF, Kaipainen A, Corella AN, Yang YC, Nyquist MD, Mostaghel E, Hsieh AC, Zhang X, Corey E, Brown LG, Nguyen HM, Pienta K, Ittmann M et al. (2017) Androgen receptor pathway-independent prostate cancer is sustained through FGF Signaling. *Cancer Cell* 32: 474-489.e6

Chakraborty PS, Tripathi M, Agarwal KK, Kumar R, Vijay MK, Bal C (2015) Metastatic poorly differentiated prostatic carcinoma with neuroendocrine differentiation: negative on 68Ga-PSMA PET/CT. *Clinical nuclear medicine* 40: e163-166

Cheng Z, Levi J, Xiong Z, Gheysens O, Keren S, Chen X, Gambhir SS (2006) Near-infrared fluorescent deoxyglucose analogue for tumor optical imaging in cell culture and living mice. *Bioconjugate chemistry* 17: 662-669

Ding Y, Li Y, Lu L, Zhang R, Zeng L, Wang L, Zhang X (2015) Inhibition of nischarin expression promotes Neurite outgrowth through regulation of PAK activity. *PLOS ONE* 10: e0144948

Dunning MJ, Vowler SL, Lalonde E, Ross-Adams H, Boutros P, Mills IG, Lynch AG, Lamb AD (2017) Mining human prostate cancer datasets: The "camcAPP" Shiny App. *EBioMedicine* 17: 5-6

Hope TA, Goodman JZ, Allen IE, Calais J, Fendler WP, Carroll PR (2019) Meta-analysis of 68Ga-PSMA-11 PET accuracy for the detection of prostate cancer validated by histopathology. *J Nucl Med* 60: 786-793

Korbel GA, Lalic G, Shair MD (2001) Reaction microarrays: a method for rapidly determining the enantiomeric excess of thousands of samples. *Journal of the American Chemical Society* 123: 361-362

Lee HY, Lee JJ, Park J, Park SB (2011) Development of fluorescent glucose bioprobes and their application on real-time and quantitative monitoring of glucose uptake in living cells. *Chemistry* 17: 143-150

Melong N, Steele S, MacDonald M, Holly A, Collins CC, Zoubeidi A, Berman JN, Dellaire G (2017) Enzalutamide inhibits testosterone-induced growth of human prostate cancer xenografts in zebrafish and can induce bradycardia. *Sci Rep* 7: 14698

Parida GK, Tripathy S, Datta Gupta S, Singhal A, Kumar R, Bal C, Shamim SA (2018) Adenocarcinoma Prostate With Neuroendocrine Differentiation: Potential Utility of 18F-FDG PET/CT and 68Ga-DOTANOC PET/CT Over 68Ga-PSMA PET/CT. *Clinical nuclear medicine* 43: 248-249

Park J, Lee HY, Cho MH, Park SB (2007) Development of a cy3-labeled glucose bioprobe and its application in bioimaging and screening for anticancer agents. *Angewandte Chemie (International ed in English)* 46: 2018-22

Park J, Um JI, Jo A, Lee J, Jung D-W, Williams DR, Park SB (2014) Impact of molecular charge on GLUT-specific cellular uptake of glucose bioprobes and in vivo application of the glucose bioprobe, GB2-Cy3. *Chem Comm* 50: 9251-9254

Perez PM, Hope TA, Behr SC, van Zante A, Small EJ, Flavell RR (2019) Intertumoral Heterogeneity of 18F-FDG and 68Ga-PSMA Uptake in Prostate Cancer Pulmonary Metastases. *Clinical nuclear medicine* 44: e28-e32

Sheikhbahaei S, Afshar-Oromieh A, Eiber M, Solnes LB, Javadi MS, Ross AE, Pienta KJ, Allaf ME, Haberkorn U, Pomper MG, Gorin MA, Rowe SP (2017) Pearls and pitfalls in clinical interpretation of prostate-specific membrane antigen (PSMA)-targeted PET imaging. *European journal of nuclear medicine and molecular imaging* 44: 2117-2136

Spratt DE, Gavane S, Tarlinton L, Fareedy SB, Doran MG, Zelefsky MJ, Osborne JR (2014) Utility of FDG-PET in clinical neuroendocrine prostate cancer. *Prostate* 74: 1153-1159

Stelloo S, Bergman AM, Zwart W (2019) Androgen receptor enhancer usage and the chromatin regulatory landscape in human prostate cancers. *Endocrine-related cancer* 26
Stelloo S, Nevedomskaya E, Kim Y, Schuurman K, Valle-Encinas E, Lobo J, Krijgsman O, Peeper DS, Chang SL, Feng FY-C, Wessels LFA, Henrique R, Jerónimo C, Bergman AM, Zwart W (2018) Integrative epigenetic taxonomy of primary prostate cancer. *Nat Commun* 9: 4900
Subramanian A, Tamayo P, Mootha VK, Mukherjee S, Ebert BL, Gillette MA, Paulovich A, Pomeroy SL, Golub TR, Lander ES (2005) Gene set enrichment analysis: a knowledge-based approach for interpreting genome-wide expression profiles. *Proc Natl Acad Sci U S A* 102: 15545-15550
Taylor BS, Schultz N, Hieronymus H, Gopalan A, Xiao Y, Carver BS, Arora VK, Kaushik P, Cerami E, Reva B, Antipin Y, Mitsiades N, Landers T, Dolgalev I, Major JE, Wilson M, Socci ND, Lash AE, Heguy A, Eastham JA et al. (2010) Integrative genomic profiling of human prostate cancer. *Cancer Cell* 18: 11-22
Thang SP, Violet J, Sandhu S, Iravani A, Akhurst T, Kong G, Ravi Kumar A, Murphy DG, Williams SG, Hicks RJ, Hofman MS (2018) Poor outcomes for patients with metastatic castration-resistant prostate cancer with low prostate-specific membrane antigen (PSMA) expression deemed ineligible for 177Lu-labelled PSMA radioligand therapy. *Eur Urol Oncol* in press
Tosoian JJ, Gorin MA, Rowe SP, Andreas D, Szabo Z, Pienta KJ, Pomper MG, Lotan TL, Ross AE (2017b) Correlation of PSMA-targeted (18)F-DCFPyL PET/CT findings with immunohistochemical and genomic data in a patient with metastatic neuroendocrine prostate cancer. *Clin Genitourin Cancer* 15: e65-e68
Tsai HK, Lehrer J, Alshalalfa M, Erho N, Davicioni E, Lotan TL (2017) Gene expression signatures of neuroendocrine prostate cancer and primary small cell prostatic carcinoma. *BMC Cancer* 17: 759
Yuan T-C, Veeramani S, Lin F-F, Kondrikou D, Zelivianski S, Igawa T, Karan D, Batra SK, Lin M-FJE-rc (2006a) Androgen deprivation induces human prostate epithelial neuroendocrine differentiation of androgen-sensitive LNCaP cells. *Endocr Relat Cancer* 13: 151-167

CHAPTER 4 : THE POTENTIAL ROLES OF RADIONANOMEDICINE AND RADIOEXOSOMIC IN PROSTATE CANCER RESEARCH AND TREATMENT

4.1 INTRODUCTION

Both artificial nanostructures, such as nanoparticles, as well as natural nanostructures, such as nano-sized extracellular vesicles known as exosomes, are potential tools for approaching personalized medicine. Artificial nanoscale particles have attracted a great deal of attention owing to their unique electronic, optical, and magnetic properties *(Salata, 2004, Sanvicens & Marco, 2008, Sitharaman, 2016, Steichen, Caldorera-Moore et al., 2013, Sultana, Khan et al., 2013)*. Natural nanostructures, like exosomes, offer unique biological advantages such as the capacity to transport genetic materials and proteins and hence may be employed as drug carriers *(Azmi, Bao et al., 2013, Bruschi, Ravera et al., 2015, Cai, Cheng et al., 2016, D'Incà & Pucillo, 2015, Ha, Yang et al., 2016, Hall, Prabhakar et al., 2016, Kosaka & Ochiya, 2014, Kosaka, Yoshioka et al., 2014, Roma-Rodrigues, Fernandes et al., 2014, Suchorska & Lach, 2016)*.

Prostate cancer (PC) is the most prevalent cancer in men in the western world and the second most prevalent malignancy in the world *(Center, Jemal et al., 2012, Schröder, Hugosson et al., 2012, Siegel, Miller et al., 2015)*. Patients suffering from advanced PC are usually treated with androgen-deprivation therapy (ADT) *(Bolla, De Reijke et al., 2009, Feldman & Feldman, 2001, Saad & Fizazi, 2015, Sharifi, Gulley et al., 2005, Taylor, Canfield et al., 2009)*. While most patients initially respond to ADT, the disease is highly heterogeneous, driven by different genomic alterations which represent challenges for PC management *(Aryee, Liu et al., 2013, Barbieri & Rubin, 2015, Boyd, Mao et al., 2012, Brocks, Assenov et al., 2014a, Chandrasekar, Yang et al., 2015, Katzenwadel & Wolf, 2015, Merseburger & Hupe, 2016, Mitani, Yamaji et al., 2011, Perner, Cronauer et al., 2015, Saad & Fizazi, 2015, Shah, Mehra et al., 2004, Wadosky & Koochekpour, 2016, Zejnullahu,*

Arevalo et al., 2016). Patients relapsing will present with castration-resistant prostate cancer (CRPC) which lacks effective targeted therapies. There is a need to increase our understanding about PC biology, the driving genetic alterations, as well as the mechanisms leading to CRPC. Expanding our understanding in these areas will improve therapeutic options.

Radiation therapy commonly refers to the application of ionizing radiation in cancer treatment using X-rays, gamma rays, and charged particles. The radiation may be delivered by a radiation source outside the body of patient which refers to external-beam radiation therapy, or it could come from radioactive material implanted in the tumor, referred to as brachytherapy. The main purpose of radiation is to maximize the amount of radiation at the tumor location while minimizing the exposure of normal surrounding tissues *(Bakht, Sadeghi et al., 2012, Khan & Gibbons, 2014, Mayles et al., 2007)*. In radiation therapy, some challenges could be encountered such as nonspecific systemic distribution of antitumor agents, insufficient or inefficient amount of radiation to the tumor, and the incomplete capability to visualize therapeutic responses *(Bergs, Wacker et al., 2015, Schaue & McBride, 2015, Wang et al., 2008, Washington & Leaver, 2015)*.

Radionanomedicine is a recently coined term for the application of either radiation technology or nuclear medicine with nanomedicine *(Choi, Lee et al., 2016, Goel, England et al., 2016, Lee, 2016, Lee, Im et al., 2015, Lim, Cho et al., 2015b, Muthu & Wilson, 2010, Pratt, Shaffer et al., 2016, Satpati, Satpati et al., 2016, Soo Lee, 2016)*. From a nuclear medicine point of view, the concept of radionanomedicine could be an extension of "targeted radionuclide therapy" *(Lee, 2016, Lee et al., 2015, Lim et al., 2015b)*. In addition, *radioexosomics* is our proposed term for the study of functions, cytotoxicity,

cancerogenicity and biodistribution of exosomes using radiation technology and nuclear medicine tracing technology.

This chapter will summarize the utility, advantages and limitations of radionanomedicine approaches in PC research. In addition, we will present what is currently known about the secreted exosome by PC cells and what could be the impact of radioexosomics on the future of PC research. We conclude by highlighting some limitations, current status and future perspectives of radionanomedicine and radioexosomics for understanding PC biology, and application in targeting strategies, drug delivery, molecular imaging and therapy *(Bakht et al., 2017a)*.

4.2 PC RADIONANOMEDICINE

PC radionanomedicine depends on the labeling of radionuclides or probes onto the nanomaterials and the application of trace amounts of radiolabeled nanomaterials for imaging and therapy of PC. The labeling of nanomaterials with radionuclides can be done either extrinsically or intrinsically. In extrinsic method, the chelators bind to the surface of nanomaterials while in intrinsic approach the radionuclides are inside the nano-sized structure *(Lee et al., 2015, Sun, Xu et al., 2007, Sun, Hoffman et al., 2012, Yang, Sundaresan et al., 2013)*.

4.2.1 2.1. Nuclear imaging, therapy and theranostics

The use of radioisotopes is important in biomedical research, particularly in oncology. In recent years, there has been increased uptake of the use of radionuclides for diagnostic and therapeutic purposes *(Abou, Pickett et al., 2015, Chatalic, Kwekkeboom et al., 2015, Shah, Da Silva et al., 2015)*. By labeling the appropriate transport molecule with a therapeutic

radionuclide that emits ionizing radiation such as beta-particle, alpha-particle, and Auger electron emitters, it is possible to obtain internal irradiation at the cellular level following the administration of radiopharmaceuticals. Similarly, by labeling the appropriate transport molecule with a diagnostic radionuclide that emits ionizing radiation such as gamma or positron emitters, it is possible to monitor tumor metabolism and proliferation at the cellular level *(Bailey & Humm, 2014, Saha, 2012, Ting, Chang et al., 2010, Zukotynski, Jadvar et al., 2016)*. Table 1 summarizes the used therapeutic and theranostic radioisotopes in combination with nanoscale particles for PC imaging and cancer therapy.

Table 4-1 Therapeutic and theranostic radioisotopes for PC imaging and cancer therapeutic and theranostic.

Isotope	Half-life	Emission type	E_{max} of α or β (keV)	Therapeutic / Theranostic
^{211}At	7.2 h	α	5870	Therapeutic
^{223}Ra	11.4 d	α	–	Therapeutic
^{224}Ra	3.6 d	α	–	Therapeutic
^{225}Ac	10.0 d	α	5830	Therapeutic
^{186}Re	3.7 d	β^-, γ	1069	Theranostic
^{188}Re	17.0 h	β^-, γ	2120	Theranostic
^{90}Y	2.7 d	β^-	2280	Therapeutic
^{32}P	14.3 d	β^-	1710	Therapeutic
^{131}I	8.0 d	β^-, γ	606	Theranostic
^{166}Ho	26.8 h	β^-, γ	1853	Theranostic
^{67}Cu	2.6 d	β^-, γ	580	Theranostic
^{198}Au	2.7 d	β^-	960	Therapeutic
^{111}In	67 h	Auger, γ	420	Theranostic

Interestingly, radionanomedicine utilizes the advantage of an huge surface to volume ratio of nanomaterials by hydrophilization of nanomaterials, which offers production of multi-functional radiopharmaceuticals for both radionuclide therapy and hybrid imaging such as PET/CT and PET/MRI *(Lee, 2016, Lee et al., 2015)*. For instance, 'Jeong's method' is one of the most promising of producing functionally active multi-specific nanoparticles which can make the most metallic or metal-oxide nanoparticles with hydrophobic surface to hydrophilic and synthesizes an multifunction platform only in one step (Figure 4-1) *(Choi, Jeong et al., 2011, Kim, Kim et al., 2012, Lee, Jeong et al., 2012, Moon, Yang et al., 2016, Yang, Moon et al., 2015)*.

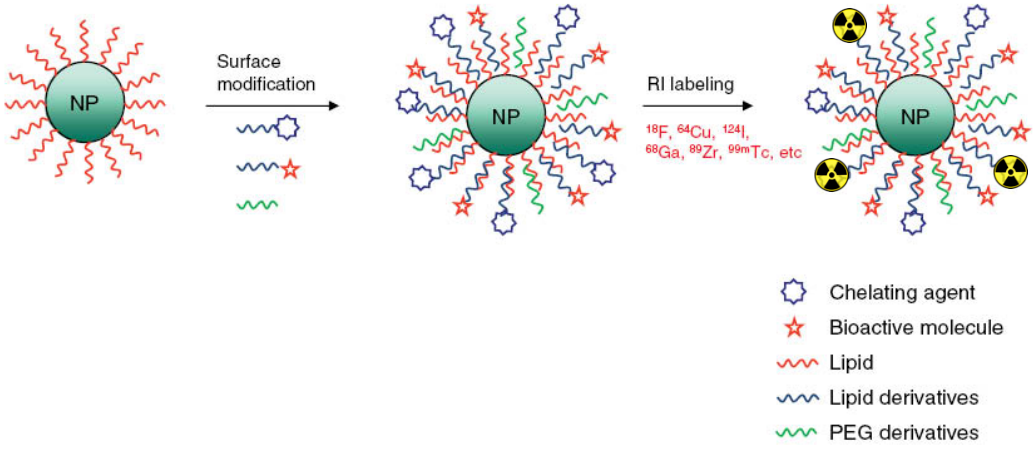

Figure 4-1 The one-step method for multifunctional nanoparticle.

An schematic of Jeong's one step method to generate an metallic or metal-oxide nanoparticles with hydrophobic surface to hydrophilic and synthesizes an multifunction platform. Adopted with permission *(Choi et al., 2011, Kim et al., 2012, Yang et al., 2015)*.

Radiopharmaceuticals including ^{18}F-fluorodeoxyglucose (^{18}F-FDG), ^{18}F-fluoro-5-dihydrotestosterone (^{18}F-FDHT) *(Scher, Beer et al., 2010)*, ^{18}F-fluorocholine (^{18}F-FCH)

(Caffo et al., 2014, De Giorgi, Caroli et al., 2015) and ^{68}Ga-PSMA-11 *(Afshar-Oromieh, Avtzi et al., 2015a, Ebenhan, Vorster et al., 2015, Evans, Smith-Jones et al., 2011, Giesel, Fiedler et al., 2015, Sterzing, Kratochwil et al., 2016)* have been applied in the dose optimization, evaluation of therapeutic pathways and assessment of therapeutic efficacy of PC novel anticancer agents. In the following paragraphs we briefly overview the well-established radiopharmaceuticals for PC imaging and then will review the advantages and challenges of the application of hybridization of nanomedicine technology with radiochemistry.

4.2.2 PC Radiopharmaceuticals

^{18}F-FDHT is a radiolabeled analog of di-hydro-testosterone (DHT) which is the main ligand for androgen receptor (AR) and it can be utilized for delineation and quantification of locations where the AR is overexpressed *(Vargas, Grimm et al., 2015)*. Pioneering efforts by Larson et al. *(Larson, Morris et al., 2004)* and Dehdashti et al. *(Dehdashti, Picus et al., 2005)* led to the establishment of ^{18}F-FDHT as an alternative for the common ^{18}F-FDGPET scan. By virtue of ^{18}F-FDGPET and ^{18}F-FDHT PET scans, Fox et al. *(Fox, Blanc et al., 2009)* categorized phenotypes of CRPC into three categories including AR Predominant (lesions representing preferential accumulation on ^{18}F-FDHT), Glycolysis Predominant (lesions demonstrating preferential accumulation on ^{18}F-FDG), or AR/Glycolysis Concordant (lesions showing preferential accumulation both ^{18}F-FDGand ^{18}F-FDHT in agreement) *(Castellucci & Jadvar, 2012, Vargas et al., 2015)*. Recently, it has been shown that the intensity of ^{18}F-FDHT uptake is meaningfully correlated with overall survival of the patients *(Vargas, Wassberg et al., 2014)*.

Furthermore, higher glucose metabolism in malignant tissue in comparison with normal tissue is known as a hallmark of cancer or as the Warburg effect *(Gillies, Robey et al., 2008)*. Besides, FDG is an analog of glucose which ^{18}F-FDG can track in the glucose metabolism of tissues and PET can visualize preferential accumulation of ^{18}F-FDG in malignant tissue. As a whole, ^{18}F-FDG is the most common radiopharmaceutical in oncology and nuclear medicine procedures *(Jadvar, 2013b)*. However, as Jadvar *(Jadvar, 2013a)* extensively reviewed the utility and limitations of PET ^{18}F-FDG, the helpfulness of FDG PET in prostate cancer is still evolving and FDG PET cannot be favorable in detection of prostate cancer in a relatively large portion of patients since FDG uptake in prostate cancer is associated with the tumor differentiation level. However, the FDG PET scan still could be a valuable method in the assessment of treatment response and in prediction of patient outcome *(Beauregard, Blouin et al., 2015)*.

Moreover, in contrast to the normal prostate cells, fatty acid synthesis plays a crucial role in the rapid proliferation of prostate cancer cells since malignant cells need higher amounts of fatty acid for their new membrane biogenesis *(Suburu & Chen, 2012)*. Particularly, choline is utilized for the biosynthesis of phosphatidylcholine and it is the basis for imaging with ^{18}F-FCH for the visualization of prostate cancer and bone, lymph nodes and visceral metastasis *(Apolo, Pandit-Taskar et al., 2008, Jadvar, 2013b)*. Currently, for staging and monitoring treatment response, choline PET/CT using either ^{11}C or ^{18}F can be performed. It is generally assumed that ADT does not significantly affect choline PET/CT uptake in PC cells considering the biological mechanism of choline-based nuclear imaging procedures *(Choi et al., 2011, Kim et al., 2012, Lee et al., 2012, Moon et al., 2016, Yang et al., 2015)*. However, a tendency of reduction in choline uptake following ADT is

documented, particularly in hormone-naïve patients. Recent *in vitro* and *in vivo* evidence indicates that prostate-specific membrane antigen (PSMA) is regulated by androgens and suggests that ADT could considerably increase PSMA-ligand uptake. This means that for those patients who are undergoing treatment with antiandrogens, evaluation of PSMA targeted scans must account for this upregulation phenomenon. Therefore, the monitoring of ADT response using choline PET/CT might be more reliable than PSMA-based imaging *(Bakht et al., 2016)*.

4.2.3 PSMA targeted radionuclide therapy

PSMA is a transmembrane protein that is over-expressed in more than 85% of primary PC and its metastatic lesions in lymph nodes and bone *(Ananias, van den Heuvel et al., 2009, Minner, Wittmer et al., 2011, Rybalov, Ananias et al., 2014)*, hence representing a promising target for imaging and therapy of PC. From a technical point of view, targeting PSMA either by antibodies or by small molecules is feasible *(Akhtar, Pail et al., 2011, Lutje, Heskamp et al., 2015, Morigi, Stricker et al., 2015, Vargas et al., 2015)*. Particularly, a new class of functional ligands including Glu-NH-CO-NH-Lys-[^{68}Ga-(HBED-CC)] or ^{68}Ga-PSMA-11 *(Afshar-Oromieh et al., 2015a, Ebenhan et al., 2015, Giesel et al., 2015, Sterzing et al., 2016)*, PSMA-DKFZ-617 *(Afshar-Oromieh, Hetzheim et al., 2015b, Delker, Fendler et al., 2016, Kratochwil, Giesel et al., 2015a)*, ^{18}F-DCFPyL *(Szabo, Mena et al., 2015)* and EuK-Subkff-^{68}Ga-DOTAGA *(Herrmann, Bluemel et al., 2015)* have proven affinity to PSMA, and hence made possible the delineation of local PC and the possible metastatic lesions. In addition, radio-metals such as ^{99m}Tc, ^{111}In, ^{64}Cu, ^{86}Y, ^{68}Ga and ^{89}Zr, have been employed for tracking PSMA due to their relative longer physical half-life in comparison with radio-halogens such as ^{18}F, which is required for tracking PSMA

(Banerjee, Pullambhatla et al., 2014). The available PSMA ligands can also be labeled with therapeutic radionuclides such as lutetium-177 *(Lutje et al., 2015)*.

It is expected that this new class of PSMA-binding radioligands can enhance the diagnosis of recurrent PC and radionuclide therapy of PC *(Freitag, Radtke et al., 2016)*. However, the renal uptake of therapeutic PSMA targeted radiopharmaceuticals is a limiting factor *(Weineisen, Schottelius et al., 2015)*. The previously proposed solutions for decreasing off-target radiation to the kidneys includes the application of the small-molecule PSMA inhibitor comedication *(Kratochwil, Giesel et al., 2015b)*, the employment of polyethylene glycol (PEG) polymer chains *(Wilbur, Chyan et al., 2012)* and the use of the nanoparticle-based platforms *(Behnam Azad, Banerjee et al., 2015b, Moon, Yang et al.)*.

Albumin-based platforms

Albumin is the most abundant protein in blood plasma and human serum albumin (HSA) has appeared as a multipurpose carrier in nanomedicine, particularly for treating diabetes and targeting cancer, enhancing the pharmacokinetic profile of delivering therapeutic or diagnostic agents to the malignant tissues *(Elsadek & Kratz, 2012, Loureiro, G Azoia et al., 2016, Zhao, Wang et al., 2016)*. Banerjee et al. *(Banerjee, Wang et al., 2014)* suggested an albumin-based nanoformulation for PSMA by covalent conjugation of fluorescein for PC cell imaging which DTPA used for ^{111}In-labeling for SPECT, Glu-Lys urea used for PSMA targeting and NIR dye 800 CW played the role of in vivo optical imaging probe. In addition, Moon et al. *(Moon et al., 2016)* developed a nanoparticle-based PET/MR dual-modal imaging probe for targeting PSMA with lower kidney uptake. Figure 2B represents the recently proposed PSMA radioligand platforms for targeting PC using Jeong's method *(Choi et al., 2011, Kim et al., 2012, Lee et al., 2012, Moon et al., 2016, Yang et al., 2015)*.

4.2.4 Radioactive gold nanoparticles

Chanda et al. *(Chanda, Kan et al., 2010)* reported on PC therapy using glycoprotein functionalized gold nanoparticles containing radioactive β-emitting Au-198. Intratumoral administration of a single dose of their suggested platform (70 Gy) caused significant tumor regression and effective control in the growth of PC over 30 days. In addition, Shukla et al. *(Shukla, Chanda et al., 2012)* also employed prostate tumor specific epigallocatechin-gallate (EGCg) functionalized radioactive β-emitting Au-198. They reported an 80% reduction of PC-3 xenograft tumor volumes after 28 days intratumoral administration of ^{198}Au-nanoparticle-EGCg.

4.2.5 Nano-sized peptides

Nano-sized peptides are an appealing candidate for peptide receptor radiotherapy (PRRT) of PC. The gastrin-releasing peptide receptor (GRPR) has been revealed to be overexpressed in a wide variety of cancer cells including PC. Bombesin is a nano-sized neuropeptide with high affinity toward GRPR *(de Jong, Breeman et al., 2009, Durkan, Lambrecht et al., 2007, Emonds, Swinnen et al., 2009, Mendoza-Sanchez, Ferro-Flores et al., 2010)*. Therefore, many research groups used radiolabel bombesin for evaluation of its potential for PC therapy and imaging of metastatic areas *(Hoffman, Gali et al., 2003, Liu, Yan et al., 2009, Scopinaro, De Vincentis et al., 2003)*. For instance, Faintuch et al. *(Faintuch, Núñez et al., 2011)* using ^{99m}Tc and nano-sized bombesin showed that a pre-targeting approach with a peptide could be promising for PC therapy. Lim et al. *(Lim, Cho et al., 2015a, Lim et al., 2015b)* studied the feasibility of application of a radiolabeled bombesin compound via ^{177}Lu to prepare radiolabeled candidates for the treatment of GRPR-expressing prostate tumors. Also, a multifunctional system of ^{99m}Tc labelled gold

nanoparticles conjugated to bombesin has been suggested for PC PRRT *(Mendoza-Sanchez et al., 2010)*. The *in vivo* SPECT/CT images in mice presented a considerable uptake in PC3 xenograft. Lastly, Roivainen et al. *(Roivainen, Kahkonen et al., 2013)* reposted the first human study for evaluation of the safety, tolerability, metabolism, pharmacokinetics, biodistribution, and radiation dosimetry of a ^{68}Ga-bombesin compound.

Further, atrial natriuretic peptide has been detected to have anticancer properties by interaction with the cancer cell surface natriuretic peptide receptor A (NPRA) and natriuretic peptide clearance receptor (NPRC). Pressly et al. *(Pressly, Pierce et al., 2013)* designed an amphiphilic comb-like radiolabeled nanoparticle with controlled properties through modular construction containing C-atrial natriuretic factor (CANF). PET imaging with a ^{64}Cu-CANF-Comb in a PC xenograft tumor model presented high blood pool retention, low renal clearance, enhanced tumor uptake, and decreased hepatic burden relative to the non-targeted ^{64}Cu-Comb.

4.2.6 Nano-sized polymers and liposomes

Porphysomes, which were pioneered by Dr. Zheng's group, are formed by the self-assembly of 'porpholipids' into spherical nanostructures (Figure 4-2A) *(Jin & Zheng, 2011, Lovell, Jin et al., 2011, Valic & Zheng, 2016)*. This group validated *in vivo* application of ^{64}Cu-porphysomes in an orthotopic PC and bony metastatic PC animal models. They also displayed a multimodal delineation of orthotopic tumors on both the macro- and the microscopic scales using both PET and fluorescence. Also, the nano-sized Poly(APMA)-DOTA polymer conjugated with a therapeutic β-emitter copper isotope, such as ^{67}Cu has been also suggested for PC therapy *(Yuan, You et al., 2006)*.

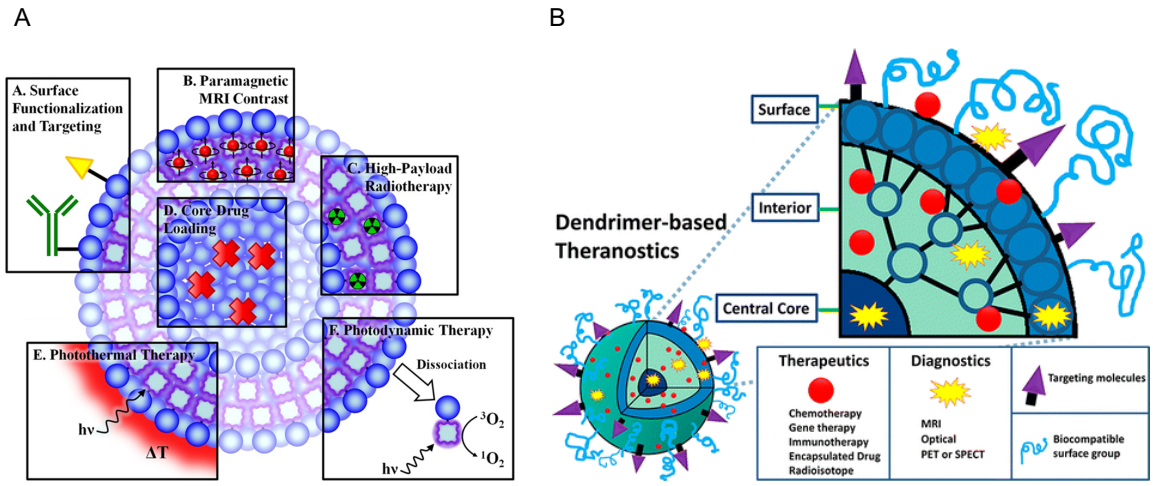

Figure 4-2 Proposed nan-platforms for application in PC radionanomedicine

(A) future potential of porphysomes. Adopted with permission *(Liu et al., 2013)* (B) future potential of dendrimers. Adopted with permission *(Lo, Kumar et al., 2013)* .

4.2.7 X-ray CT imaging

The sensitivity of X-ray CT conventionally can be enhanced by small iodinated compounds as injectable contrast agents. However, the iodinated contrast agents have some limiting factors such as fast renal clearance and short circulation times. Moreover, the X-ray attenuation of iodine is not effective for clinical CT that requires high-energy X-ray. To overcome these challenges, nano-sized iodinated CT contrast agents nanoparticles with heavy atoms including gold, lanthanides, and tantalum might be used as more effective contrast agents *(Lee, Choi et al., 2013)*. In particular, a greater attenuation of gold nanoparticles at both of low and high X-ray energies reported *(Jackson, Rahman et al., 2010, Popovtzer, Agrawal et al., 2008)*. For instance, Kim et al. *(Kim, Jeong et al., 2010)* developed a multifunctional nanoparticle as X-ray CT constant agent and PSMA-targeted delivery of doxorubicin for PC theranostic. The suggested gold nanoplatform displayed up to more than 4-fold greater CT intensity for a LNCaP cell line as a PSMA positive PC cell line than that of a PC-3 cell line as a PSMA negative PC cell. Furthermore, Bacteriolytic

therapy using the anaerobic bacterium *Clostridium novyi-NT* has been proposed as a promising approach for the treatment of solid tumors such as PC *(Diaz, Cheong et al., 2005)*. Recently, Park et al. *(Park, Cho et al., 2016)* labeled *C. novyi-NT* spores with gold nanoparticles for X-ray CT imaging of spore delivery to PC tumor after intratumoral injection to PC-3 cell line xenograft model.

4.2.8 Optical imaging and hyperthermia

While optical imaging and hyperthermia cannot be classified as radiotherapeutic approaches, by the virtue of multifunctionality and surface modification abilities of nanoparticles we can combine them with radiation-based modalities to enhance PC therapy. For example, during development of a nanoplatform for hyperthermia, radiolabeling technology can visualize the biodistribution and the specific organ uptake of nanoparticles *(Cui, Han et al., 2009)*. In addition, the comparison of optical signals with nuclear emissions from multifunctional nanoparticles is a potent approach for confirmation of delineated areas by either optical signals or nuclear emissions *(Hu, Wang et al., 2015)*. Below we briefly summarize the frequently used nanoparticles in optical imaging and hyperthermia in PC considering their potential for combination with radiation technology.

Quantum dots

Quantum dots (QD) can have the dual role of energy donors and acceptors because of their fluorescence resonance energy transfer capability; hence, QD in combination with photosensitizing agents have the potential for application in photodynamic therapy. After exposure to ionizing radiation such as X-rays, heavy nanoscale particles emit scintillation as well as persistent luminescence or Auger electrons. Ionizing radiation (e.g., X-rays and gamma rays) penetrates much more profoundly than non-ionizing radiations such as UV

(Bakht et al., 2012, Kamila, McEwan et al., 2016, Yaghini, Seifalian et al., 2009). The cytotoxicity of QDs is also a crucial issue and in a meta-analyses, Oh et al. *(Oh, Liu et al., 2016)* show that toxicity is closely correlated with QD surface properties (including shell, ligand and surface modifications), diameter, assay type and exposure time.

Moreover, QD-antibody conjugates are developing for immunoassays against prostate specific antigen (PSA). Additionally, the photophysical and nanometric properties of QDs are attractive for their application in Förster resonance energy transfer (FRET) of PSA *(Bhuckory, Lefebvre et al., 2016, Brazhnik, Sokolova et al., 2015, Gao, Zhang et al., 2012, Garcia-Cortes, Encinar et al., 2016, Gokarna, Jin et al., 2008, Hu, Chu et al., 2011, Jin, Li et al., 2012, Kwon, Lee et al., 2013, Leung, 2004a, Leung, 2004b, Li, Li et al., 2014, Lin, Liu et al., 2015, Lin, Ma et al., 2014b, Malic, Sandros et al., 2011, Mitani, Harada et al., 2014, Pei, Zhu et al., 2015, Ruan, Yu et al., 2011, Singh, Singh et al., 2012, Walker, Morgan et al., 2012, Wu, Liu et al., 2016, Yeh, Hsiao et al., 2016, Zhang, Hubbard et al., 2013, Zhang, Dai et al., 2013)*. For instance, Cui et al. *(Cui et al., 2009)* reported conjugation of fluorescent magnetic nanoparticles with a single chain Fv antibody against γ-seminoprotein for PC theranostic. The proposed platform displayed highly specific targeting, fluorescent imaging and MR imaging, and selective anticancer impact on the PC xenografts. Recently, a dual receptor–targeting dual-modality PET/Near-infrared fluorescence (NIRF) probe was proposed by Hu et al. *(Hu et al., 2015)* for assessment of the pharmacokinetics PC using QDs. They demonstrated that their dual-function PET/NIRF imaging is able to evaluate the biodistribution and PC tumor-targeting efficacy of the ^{18}F-labeled functionalized QDs.

Carbon nanotubes

The characteristics of carbon nanotubes (CNTs) can be applied for photodynamic or photothermal irradiation therapy of targeted tumor cells. In addition, CNTs in either single-walled carbon nanotubes (SWCNT) or multi-walled carbon nanotube (MWCNT) formations powerfully absorb Near-infrared (NIR) radiation and convert absorbed energy to released heat *(Hassan, Smyth et al., 2016, Newland, Thomas et al., 2016, Rodrigues, Leite et al., 2016, Wailes & Levi-Polyachenko, 2016)*. It should be noted that the long-term application of CNP may be associated with cancer risk *(Lacerda, Bianco et al., 2006, Marchesan, Kostarelos et al., 2015)*. On the other hand, MWCNT-based field-effect transistors have been widely evaluated due to their applications to electric circuit and bio-sensing chips. Initially, Li et al. *(Li, Curreli et al., 2005)* proposed complementary detection of PSA as a potent PC biomarker using In_2O_3 nanowires and CNTs. In this work, a combination of In_2O_3 nanowires and MWCNTs for the detection of PSA has been used. Consequently, many other research groups have developed more advanced CNT-based sensors for measurement of electrochemical impedance, detection of PSA other PC biomarkers such as osteopontin *(Briman, Artukovic et al., 2007, Chikkaveeraiah, Bhirde et al., 2009, Kim, Lee et al., 2009, Krishnan, Diagaradjane et al., 2010, Lerner, D'Souza et al., 2012, Okuno, Maehashi et al., 2007, Panini, Messina et al., 2008, Patra, Roy et al., 2015, Pei et al., 2015, Salimi, Kavosi et al., 2013, Sharma, Hong et al., 2015, Silva, Lima et al., 2016, Tian, Zhao et al., 2012, Tran, Piro et al., 2013, YeoHeung, Zhongyun et al., 2007)*. Moreover, Tran et al. *(Tran et al., 2013)* suggested a label-free microRNA-141 sensor based on an interpenetrated network of CNTs and electroactive polymer.

Magnetic nanoparticle

Banerjee et al. *(Banerjee, Pullambhatla et al., 2011)* evaluated the feasibility of sequential SPECT and optical imaging of PC. Following this publication, Behnam et al. *(Behnam Azad, Banerjee et al., 2015a)* proposed a PSMA-targeted bionized nanoferrite (BNF) nanoparticle and its biological evaluation in a PC animal model. The BNF fluorescent magnetic nanoparticle formulation displayed proper targeting specificity. They also confirmed the biodistribution of their suggested platform by SPECT imaging. Consequently, Chen et al. *(Chen, Penet et al., 2012)* have developed a theranostic PSMA-targeted nanoplex platform for delivery of small interfering RNA (siRNA) along with a prodrug enzyme to PC xenografts. Down-regulation of the candidate siRNA target, choline kinase, and the conversion of the nontoxic prodrug 5-fluorocytosine (5-FC) to cytotoxic 5-fluorouracil (5-FU) were also visualized with noninvasive imaging. Interestingly, the proposed platform was well-tolerated and a low renal uptake was observed. Huang and Liu *(Huang & Liu, 2015)* have also proposed polymer nanostructures for simultaneous multiphoton imaging and chemo-photothermal therapy of PC.

Wang et al. *(Wang, Sefah et al., 2013)* evaluated aptamers selected against DU145 CRPC cell line and their subpopulation of cancer stem cells were linked to the surfaces of gold nanorods and the resulting conjugates were utilized to target both cancer cells and cancer stem cells by NIR laser irradiation. Lu et al. *(Lu, Singh et al., 2010)* subsequently suggested a multifunctional gold nano-popcorn-based surface-enhanced Raman scattering (SERS) assay for simultaneous imaging and photothermal therapy of PC. They presented that multifunctional popcorn-shaped gold nanoparticles form several hot spots and provide a substantial improvement of the Raman signal intensity.

Buckway et al. *(Buckway, Frazier et al., 2014)* proposed that PC therapy using a therapeutic ^{90}Y labeled N-(2-hydroxypropyl)methacrylamide (HPMA) copolymer can be improved with localized tumor hyperthermia. Additionally, an ^{111}In labeled HPMA copolymer system for SPECT was utilized to monitor the biodistribution and tumor reduction as a result of hyperthermia. They reported considerable shrinkage of tumor size in the hyperthermia treated tumors with ^{90}Y-HPMA copolymer conjugates in comparison with single modality PC treatments.

Dendrimers

Dendrimers have discrete highly compact nano-sized structures with successive branched layers and multivalent functional end groups. These exceptional characteristics have made dendrimers appealing for drug delivery and radionanomedicine applications as nanoscaffold systems *(Glasgow & Chougule, 2015, Sharma & Kakkar, 2015, Sharma, Maheshwari et al., 2015, Sk & Kojima, 2015, Yang, 2016)*. Lo et al. *(Lo et al., 2013)* reviewed and discussed the reported approaches of using dendrimer nanoscaffolds for PC radionanomedicine (Figure 4-2B).

4.2.9 MRI

MRI is a diagnostic modality extensively used in clinics to scrutinize the anatomical structures of the body and also provide some physiological data. The main advantage of MRI is the high level of spatial resolution of tissues, particularly soft tissues such as prostate, as compared to other imaging modalities. Furthermore, in contrast to nuclear medicine modalities including PET and SPECT, MRI does not utilize ionizing radiation for imaging *(Khan & Gibbons, 2014, Mayles et al., 2007)*. The applications of MRI for PC diagnostics are not limited to initial diagnosis, but also have an emerging role in MRI-

guided biopsy and in active surveillance, surgery staging and treatment planning *(Czarniecki, Jakucinski et al., 2016)*.

It should be highlighted that the sensitivity of MRI for molecular imaging is not appealing when relying solely on endogenous contrast of tissues. Magnetic nanoparticles, particularly superparamagnetic iron oxide nanoparticles (SPIONs), have long been considered as MRI contrast agents *(Xie, Liu et al., 2011)*. Many research groups have developed nanoparticle-based contrast agents such as cobalt zinc ferrite nanoparticles *(You, Lee et al., 2015)*, magnetic nanobeads *(Pablico-Lansigan, Hickling et al., 2013)*, paramagnetic gadolinium-based nanoparticle *(Goswami, Ma et al., 2013)*, for improving PC diagnostics by MRI.

The combination of either PET or SPECT with MRI modalities into a single hybrid functional and anatomic modality has been confirmed to synergistically compensate the limitations of each modality. This has the potential to improve diagnostic accuracy and advance the progress of therapeutics. To take advantage of the progress of the fused PET/MRI or SPECT/MRI, nanoparticle-based agents are being developed for multimodal applications *(Garcia, Tang et al., 2015)*. Thoreck et al. *(Thorek, Ulmert et al., 2014)* reported a multimodal nanoparticle, ^{89}Zr-ferumoxytol, for the advanced detection of lymph nodes using fused PET/MRI. As part of their study, they could delineate local and extended lymphatic transport in a transgenic model of PC by their PET/MRI agent. In addition, in a very recent study, Moon et al. *(Moon et al., 2016)* reported the specific PSMA-targeting iron oxide nanoparticle, DOTA-IO-GUL, as a dual-modality probe for complementary PET/MR imaging (Figure 4-3).

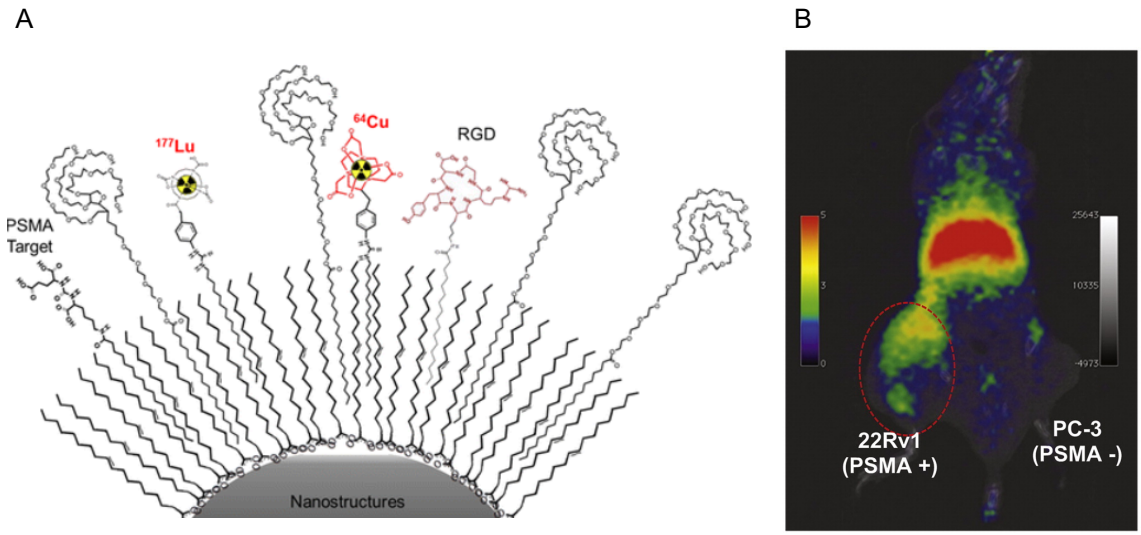

Figure 4-3 An PSMA radionanomedicine platform for targeted PC molecular imaging and therapy.

(A) A diagram of encapsulated multifunctional DOTA-IO-GUL. (B) PSMA-selective uptake result in micro PET imaging. Adopted with permission *(Moon et al., 2016)*.

4.2.10 External beam radiation therapy

A nanoparticle-induced dose enhancement effect has been developed to enhance the therapeutic effectiveness of ionizing radiation in external beam radiotherapy. Application of tumor-specific nanoscale agents in external beam radiation therapy aims to increase the specificity of radiation therapy and decrease toxicity to normal tissues *(Bakht et al., 2012)*. In particular, the application of nanoparticles as radiosensitizers is a fast growing field *(Babaei & Ganjalikhani, 2014, Rahman, Corde et al., 2014, Smith, Ackerly et al., 2015)*. Sensitizers in PC radiotherapy have included gold nanoparticles *(Rahman, Bishara et al., 2009, Zhang, Xing et al., 2008)*, magnetic nanoparticles *(Johannsen, Thiesen et al., 2006)*, yttrium oxide nanoscintillators *(Scaffidi, Gregas et al., 2011)* and superparamagnetic zinc ferrite spinel ($ZnFe_2O_4$) *(Butterworth, McMahon et al., 2013, Coulter, Butterworth et al., 2015, Hidayatullah, Nurhasanah et al., 2016, Meidanchi, Akhavan et al., 2015a)*.

Roa et al. *(Roa, Zhang et al., 2009a)* found that glucose-capped gold nanoparticles improve radiation sensitivity in radiation-resistant human PC cells by altering cell cycle regulation via sensitizing cells to a G1/S cell cycle arrest followed by apoptosis. Yao et al. *(Yao, Qiu et al.)* used two different PC cell lines, PC-3 and 22Rv1 to test the effects of a novel DNA damage repair inhibitor, Dbait nanoparticle, on radiosensitization. Using *in vivo* xenograft models they found that Dbait considerably decreased tumor growth by the accumulation of DNA double strand breaks. In addition, Meidanchi et al. *(Meidanchi, Akhavan et al., 2015b)* used $ZnFe_2O_4$ as a radiosensitizer *in vitro* using xenographs of the LNCaP cell line and gamma irradiation with a ^{60}Co source. In the presence of $ZnFe_2O_4$ nanoparticles, cells were 17 times more sensitive to gamma irradiation.

Among the currently studied nanoparticles, gold and bismuth-based nanostructures are promising candidates for enhancing sensitivity to external beam radiation *(Alqathami, Blencowe et al., 2016)*. Table 4-2 presents a list of PC *in vitro* studies evaluating the radiosensitizing properties of nanoparticles. Bismuth sulfide (Bi_2S_3)-NPs have been examined as a more cost effective radiosensitizer for external beam radiation therapy in PC *(Algethami, Geso et al., 2015)*. The higher enhancement of external beam radiation therapy capability of Bi_2S_3 rather than gold nanoparticles could be due to the fact that bismuth has a higher high atomic number (Z) than gold, causing a higher the photoelectric effect. In addition, bismuth has a higher density of free electrons than gold, which leads to increased probability of Compton scattering. In all, nanoparticle biocompatibility, biodistribution and uptake should be comprehensively investigated to choose the best option among the wide range of possible systems for enhancement of external beam radiation therapy.

Table 4-2 Overview of in vitro experiment using PC representing the radiosensitizing properties of nanostructures.

Reference	Type of radio-sensitizer	Particle size (nm)	Surface coating compound	Concentration	Radiation Source energy	PC Cell line model	Sensitizer enhancement
Butterworth et al. *(Butterworth, Coulter et al., 2010)*	Au NP	1.9	Thiol	2.4 μM and 0.24 μM	160 kVp	DU-145 PC-3	<1 <1.07
Coulter et al. *(Coulter, Jain et al., 2012)*	Au NP	1.9	Thiol	12 μM	160 kVp	DU-145	<1.8
Jain et al. *(Jain, Coulter et al., 2011)*		1.9	Thiol	12 μM	160 kVp 6 MV 15 MV 6 MeV e- 16 MeV e-	DU-145	<1.41 <1.29 1.16 <1.12 1.35
Roa et al. *(Roa, Zhang et al., 2009b)*	Au NP	10.8	thioglucose	15 nM	662 keV	DU-145	>1.5
Zhang et al.*(Zhang et al., 2008)*	Au	30	thioglucose	15 nM	200 kVp	DU-145	>1.3
Wolfe et al. *(Wolfe, Chatterjee et al., 2015)*	Au NP	31 x 9	polyethylene glycol	0.1 µM 40 µM	6 MV	PC-3	1.35
Yao et al. *(Yao et al.)*	Dbait	170	H1 polymer	1 µg/1 mL	9 Gy	PC-3 22Rv1	1.64 1.43
Algethami et al. *(Algethami et al., 2015)*	Au NP	1.9	tetraethylene glycol	0.5 mM 1.0 mM	80KVp	PC-3	1.45 2.65
	Bi_2S_3 NP	3-5	polyvinylpyrrolidone	0.5 mM 1.0 mM	80KVp	PC-3	1.6 3.07

4.2.11 Nanoparticle-based brachytherapy

Brachytherapy is the temporary or permanent implantation of small radioactive sources directly within malignant tissues such as PC. It is one of the highly effective techniques for

the delivery of larger radiation doses in a few number of treatment sections *(Khan & Gibbons, 2014)*. In particular, the radiobiological nature of PC cells represent a low alpha/beta ratio, hence hypofractionation of radiation could lead to the best chance of PC radiation therapy *(Cabrera & Lee, 2013, Sanfilippo & Cooper, 2014)*. Brachytherapy offers considerable benefits to PC treatment including proximity of the radiation source to the PC tissue and the rapid dose fall-off beyond the edge of the prostate which prevent toxicity of surrounding tissue. However, recent clinical evidence indicates that dose conformity and targeting accuracy present challenges for conventional brachytherapy which can lead to adverse side effects for the patients *(Helou, Morton et al., 2014, Morris, Tyldesley et al., 2015, Tselis, Tunn et al., 2013)*. Application of multiparametric MRI to better identify and localize intraprostatic tumors with simultaneous use of nanomolecular radiosensitizers such as gold nanoparticles may enhance doses to PC tissue without the requisite hazard of increased side effects of brachytherapy *(Nicolae, Venugopal et al., 2016)*. Ngwa et al. *(Ngwa, Korideck et al., 2013)* was among the first to present experimental evidence that gold nanoparticles can be used for radiosensitization of brachytherapy. Using γH2AX foci to quantify damaged DNA after brachytherapy with or without gold nanoparticles, this group found that the presence of nanoparticles enhanced DNA damage by 70 to 130%.

Despite the promise of sensitizing brachytherapy with nanoparticles *in vitro*, the delivery of effective concentrations of nanoparticles into a solid tumor such as PC by systematic injection of nanoparticles is a limiting factor in oncology *(Jain & Stylianopoulos, 2010)*. To overcome this technical problem, Sinha et al. *(Sinha, Cifter et al., 2015)* suggested that sustained concentrations of gold nanoparticles could be achieved in PC if they were loaded into routinely used brachytherapy spacers for *in situ* release into the source. Testing this

theory they found that changing the size of gold nanolattices can enhance dose to tumor voxels and subvolumes. Similarly, Kumar et al. *(Kumar, Belz et al., 2015)* produced implantable brachytherapy spacers loaded with silica nanoparticles conjugated to chemotherapy agents and demonstrated a potential to sensitize chemoradiation therapy.

Attempts have been made to replace the source of radiation with compact low-energy X-ray generating devices and to develop different approaches of radiation delivery to tumors. Magnetite nanoparticles for nonradionuclide brachytherapy are also under consideration to construct an X-ray tube small enough to be implanted in or near the tumor *(Liu, Sozontov et al., 2010, Safronov, Sozontov et al., 2015)*. The reported dose enhancements using nanoparticle-based brachytherapy are mainly due to the augmented photoelectron and characteristic X–ray production from the radiosensitizer nanoparticles such as gold nanoparticles. In addition, the Auger electrons escaping from the nanoparticles also can play role in dose enhancement. These radiations from nanoparticles may cause biological damage at cellular and sub–cellular level proportional with the biological distribution of nanoparticles within the PC cells *(Amato, Italiano et al., 2013)*.

4.3 NANOTECHNOLOGY-BASED STUDY OF PC BIOLOGY

Androgen receptor (AR) signaling can be reactivated in several ways to result in more aggressive and difficult to treat CRPC. Known mechanisms of CRPC development include (*i*) AR overexpression, (*ii*) AR splice variants *(Antonarakis, Lu et al., 2014)* (*iii*) mutations arising in the AR such as AR_{F876L} leading to enhanced ligand response *(Korpal, Korn et al., 2013)*, (*iv*) crosstalk with other signaling pathways *(Kaarbø, Klokk et al., 2007, Wong, Ferraldeschi et al., 2014)* and (*v*) altered expression of transcriptional coactivators thereby improving AR transactivation and (vi) the emergence of prostate cancer stem-like cells

(Chesire, Ewing et al., 2000, Debes & Tindall, 2004, Mitani et al., 2014, Mitani et al., 2011, Schaufele, Carbonell et al., 2005). It has been reported that knocking down the expression of the AR gene by a siRNA-based approach can cause cell death via apoptosis. Yang et al. *(Yang, Xie et al., 2012)* utilized a biodegradable nanocarrier to deliver short interfering RNA (siRNA) against the AR in PC cells. Similarly, Wang et al. *(Wang, Zhang et al., 2014)* developed nanobubbles carrying AR siRNA could be possibly used as gene vectors accompanied by ultrasonic irradiation for the treatment of CRPC.

Nanoparticle-facilitated siRNA delivery provides a potential tool for loss-of-function evaluation of genes such as wild type AR, AR splice variants and mutated ARs in the PC models. It is anticipated that radionanomedicine can play crucial role in expanding our knowledge about targeting AR using nanocarrier-based approaches for siRNA delivery due to the importance of visualization of tumor alterations after knocking down the expression of the potential genes.

Such as many other cancers, CRPC is highly heterogeneous *(Brocks, Assenov et al., 2014b, Zhang, Meng et al., 2015)*. Most early-stage tumours are composed of cells positive for PSA and AR, while advanced and metastatic PC evolves to be primarily composed of poorly differentiated cells lacking PSA or AR *(Li, Chen et al., 2008, Patrawala, Calhoun-Davis et al., 2007, Qin, Liu et al., 2012)*. PC stem cells are capable of giving rise to a heterogenous tumour and are highly resistant to known therapies *(Laffin & Tang, 2010)*. PC stem cells are capable of driving relapse, metastasis and therapy resistance and hence identification of this population is an area of high importance. Liu et al. *(Liu, Lau et al., 2010)* used multiplexed QDs and wavelength-resolved spectral imaging for molecular

mapping of tumor heterogeneity on human PC tissue specimens. Hence the use of nanoparticles can aid in the targeting of cells within a heterogeneous environment.

4.3.1 Potential of exosomes in PC theranostic

Exosomes are enriched in bioactive molecules including RNA, miRNAs and proteins *(Liu, Hsieh et al., 2016, Srivastava, Babu et al., 2016, Thind & Wilson, 2016, Wendler, Favicchio et al., 2016, Zhang, Pei et al., 2016)*. It has been confirmed that tumor derived exosomes shuttle RNA, miRNAs and proteins to cells within the tumor environment to suppress the immune response, accelerate tumor proliferation and facilitate metastasis *(Keller, König et al., 2009)*. Exosomal proteins, mRNA and miRNAs can cause alteration in metabolism and function of PC cells. In addition, they can function as potent biomarkers for diagnosis and prognosis.

Tumor-derived exosomes may pave the way for formation of a protumorigenic niche and may direct progenitor cells *(Quail & Joyce, 2013)*. For instance, exosomes derived from metastatic melanoma cells amplified the growth and metastasis of primary tumors *(Peinado, Alečković et al., 2012)*. PC exosomes can drive the malignancy to expand to adjacent normal tissues and sensitize other sites to form a pro-tumorigenic lesion. PC exosomes can be isolated via different sources including serum and urine of PC patients. Rauschenberger et al. *(Rauschenberger, Staar et al., 2016)* demonstrated that exosomes secreted by PC cells can inhibit the viability of adjacent cells via exosome communication to improve the ability of PC cell progression and support the expansion ability. A recent study presented that PTEN carried by exosomes in the tumor microenvironment can compensate for PTEN loss in PC cells, while exosomes found in benign prostate do not carry PTEN *(Gabriel,*

Ingram et al., 2013). Thus, it is speculated the early stage PC could be managed by supplying exosomes containing tumor-suppressor proteins (Figure 4-4).

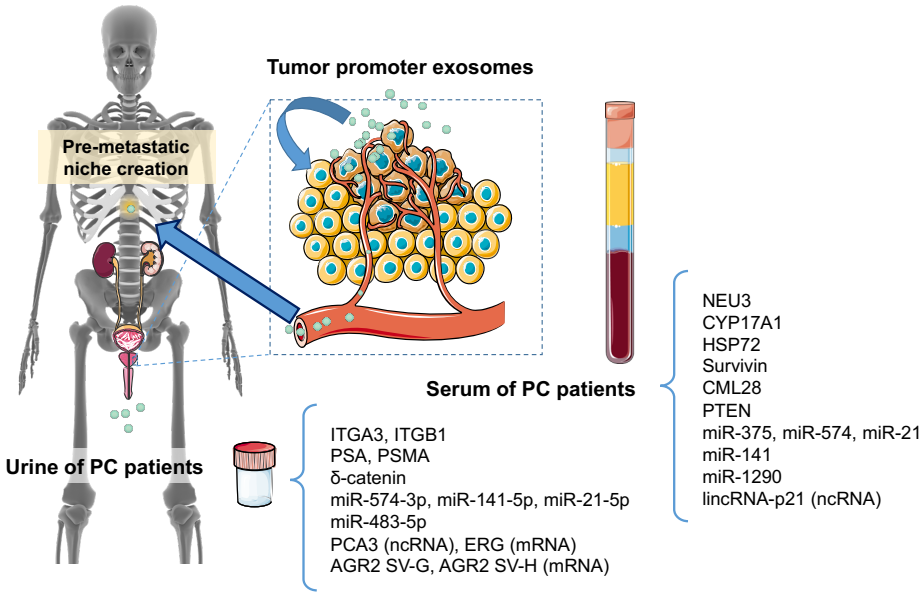

Figure 4-4 A schematic of the tumor promoting impact of PC exosome on prostate benign cells and creation of pre-metastatic niche as a result of circulation of PC exosomes in body. List of exosome specific RNAs and proteins in PC based on isolation source are also presented. Some elements of this figure were produced using Servier Medical Art image bank (www.servier.com).

Radioexosomic is an emerging subcategory of radionanomedicine and many research groups are currently developing radiochemical protocols for the radiolabeling of exosomes. Radiolabeling exosomes will allow researchers and clinicians to visualize exosome distribution *in vivo* and estimate pre-metastatic niches *(Hwang do, Choi et al., 2015, Jung, Youn et al., 2015a, Jung, Kim et al., 2015, Nikolopoulou, Amor-Coarasa et al., 2016)*. Jung et al. *(Jung, Youn et al., 2015b)* isolated exosomes from mouse breast cancer cells and radiolabeled them with ^{64}Cu for PET imaging. Nikolopoulou et al. *(Nikolopoulou et al., 2016)* isolated exosomes from highly metastatic lung-tropic breast cancer cells and radiolabeld them by ^{131}I. Interestingly, ^{131}I-exosomes imaging represented a fast blood and

background tissue clearance with specific uptake in the lungs, one of the primary locations for PC metastasis. It is predicted that the study of PC exosomes, and the resolution of biodistribution using radioexosomic tracing technology, could expand our knowledge about PC biology. Noninvasive imaging of PC exosomes by fluorescence labeling *(Tian, Zhu et al., 2013)*, bioluminescence reporter system *(Lai, Mardini et al., 2014)*, radionuclide-based imaging *(Hwang do et al., 2015, Morishita, Takahashi et al., 2015)* and MRI *(De La Pena, Madrigal et al., 2009, Hu, Wickline et al., 2014)* are feasible and could provide visualization of the biodistribution of PC exosomes. This is reviewed by Choi and Lee *(Choi & Lee, 2016)*and we have provided an illustruation of potential strategies for visualization of exosomes (Fig. 5).

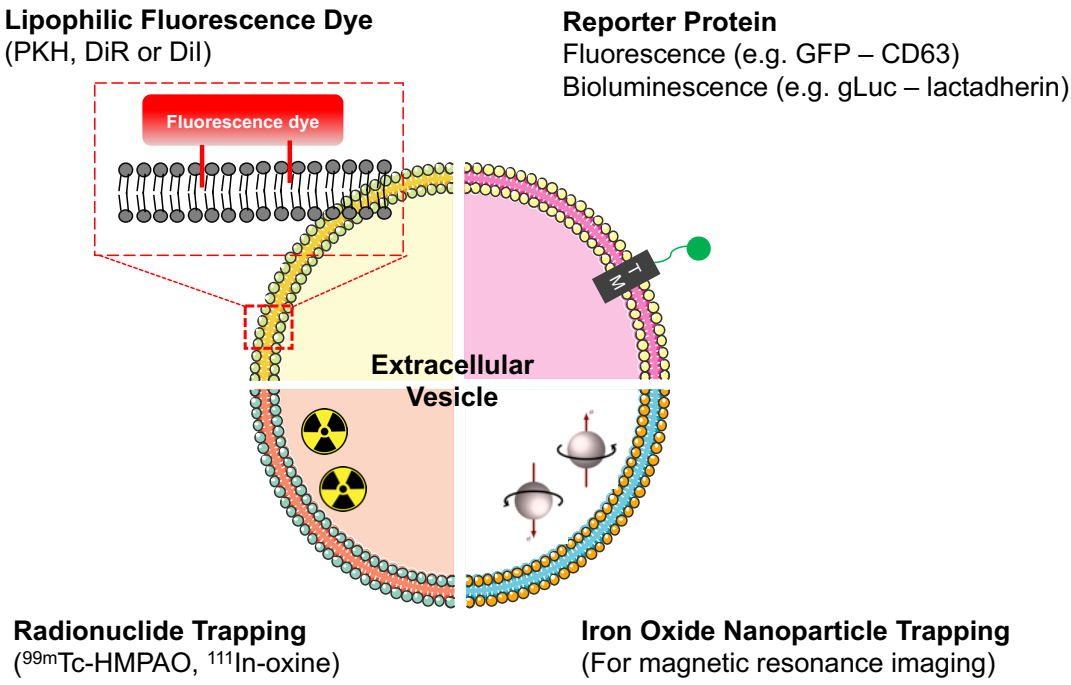

Figure 4-5 Radioesosomic strategies for visualization of exosomes *(Choi & Lee, 2016)*.

4.4 CONCLUSION

Nanoscale particles are constantly evolving for their potential uses as tools in nuclear medicine. This includes artificial nanostructures such as QDs, magnetite nanoparticles, CNTs, dendrimers, gold nanoparticles and nano-sized peptides as well as natural nanostructures such as secreted nano-sized extracellular vesicles (exosomes). Radionanomedicine is a hybrid term for the coincident application of radiation technology and nanomedicine. Radioexosomics use radiation technology and nuclear tracing technology to study exosome functions, cytotoxicity, cancerogenicity, and biodistribution. There are currently many exciting implications for the use of radionanomedicine in the imaging and therapy of PC. Nanomaterials have properties that render them a feasible option in producing multi-functional radiopharmaceuticals used both in radionuclide therapy as well as in hybrid imaging such as PET/CT and PET/MRI. This review summarized some of the cutting edge uses for nanoparticles such as enhancing the sensitivity of MRI and external beam radiation as valuable approaches in the treatment of PC. The ability of nanoparticles to target specific principles of PC biology make them an attractive candidate for personalized medicine.

Conflict of Interest: All of the authors declare that they have no conflict of interest.

Acknowledgements: This work was partly supported by Basic Science Research Program through the National Research Foundation of Korea (NRF) funded by the Ministry of Education (009-0093820)' and National Nuclear R&D Program through the National Research Foundation of Korea(NRF) funded by the Ministry of Education, Science and Technology (NRF-2012M2A2A7014020).

4.5 REFERENCES

Abou DS, Pickett JE, Thorek DL (2015) Nuclear molecular imaging with nanoparticles: radiochemistry, applications and translation. *The British journal of radiology* 88: 20150185

Afshar-Oromieh A, Avtzi E, Giesel FL, Holland-Letz T, Linhart HG, Eder M, Eisenhut M, Boxler S, Hadaschik BA, Kratochwil C, Weichert W, Kopka K, Debus J, Haberkorn U (2015a) The diagnostic value of PET/CT imaging with the (68)Ga-labelled PSMA ligand HBED-CC in the diagnosis of recurrent prostate cancer. *Eur J Nucl Med Mol Imaging* 42: 197-209

Afshar-Oromieh A, Hetzheim H, Kratochwil C, Benesova M, Eder M, Neels OC, Eisenhut M, Kübler W, Holland-Letz T, Giesel FL (2015b) The Theranostic PSMA Ligand PSMA-617 in the Diagnosis of Prostate Cancer by PET/CT: Biodistribution in Humans, Radiation Dosimetry, and First Evaluation of Tumor Lesions. *Journal of Nuclear Medicine* 56: 1697-1705

Akhtar NH, Pail O, Saran A, Tyrell L, Tagawa ST (2011) Prostate-specific membrane antigen-based therapeutics. *Advances in urology* 2012

Algethami M, Geso M, Piva T, Blencowe A, Lu L, Ai K, Harty P, Gan E (2015) Radiation dose enhancement using Bi2S3 nanoparticles in cultured mouse PC3 prostate and B16 melanoma cells. *NanoWorld Journal* 1: 97-102

Alqathami M, Blencowe A, Geso M, Ibbott G (2016) Quantitative 3D determination of radiosensitization by Bismuth-based nanoparticles. *Journal of biomedical nanotechnology* 12: 464-471

Amato E, Italiano A, Pergolizzi S (2013) Gold nanoparticles as a sensitising agent in external beam radiotherapy and brachytherapy: a feasibility study through Monte Carlo simulation. *International Journal of Nanotechnology* 10: 1045-1054

Ananias HJ, van den Heuvel MC, Helfrich W, de Jong IJ (2009) Expression of the gastrin-releasing peptide receptor, the prostate stem cell antigen and the prostate-specific membrane antigen in lymph node and bone metastases of prostate cancer. *The Prostate* 69: 1101-1108

Antonarakis ES, Lu C, Wang H, Luber B, Nakazawa M, Roeser JC, Chen Y, Mohammad TA, Chen Y, Fedor HL (2014) AR-V7 and resistance to enzalutamide and abiraterone in prostate cancer. *New England Journal of Medicine* 371: 1028-1038

Apolo AB, Pandit-Taskar N, Morris MJ (2008) Novel tracers and their development for the imaging of metastatic prostate cancer. *Journal of Nuclear Medicine* 49: 2031-2041

Aryee MJ, Liu W, Engelmann JC, Nuhn P, Gurel M, Haffner MC, Esopi D, Irizarry RA, Getzenberg RH, Nelson WG (2013) DNA methylation alterations exhibit intraindividual stability and interindividual heterogeneity in prostate cancer metastases. *Science translational medicine* 5: 169ra10-169ra10

Azmi AS, Bao B, Sarkar FH (2013) Exosomes in cancer development, metastasis, and drug resistance: a comprehensive review. *Cancer and Metastasis Reviews* 32: 623-642

Babaei M, Ganjalikhani M (2014) The potential effectiveness of nanoparticles as radio sensitizers for radiotherapy. *BioImpacts : BI* 4: 15-20

Bailey D, Humm J (2014) *Nuclear Medicine Physics: A Handbook for Teachers and Students*. IAEA,

Bakht M, Sadeghi M, Pourbaghi-Masouleh M, Tenreiro C (2012) Scope of nanotechnology-based radiation therapy and thermotherapy methods in cancer treatment. *Current cancer drug targets* 12: 998-1015

Bakht MK, Oh SW, Hwang DW, Lee YS, Youn H, Porter LA, Cheon GJ, Kwak C, Lee DS, Kang KW (2017a) The Potential Roles of Radionanomedicine and Radioexosomics in Prostate Cancer Research and Treatment. *Curr Pharm Des* 23: 2976-2990

Bakht MK, Oh SW, Youn H, Cheon GJ, Kwak C, Kang KW (2016) Influence of Androgen Deprivation Therapy on the Uptake of PSMA-Targeted Agents: Emerging Opportunities and Challenges. *Nuclear medicine and molecular imaging*: 1-10

Banerjee SR, Pullambhatla M, Byun Y, Nimmagadda S, Foss CA, Green G, Fox JJ, Lupold SE, Mease RC, Pomper MG (2011) Sequential SPECT and Optical Imaging of Experimental Models of Prostate Cancer with a Dual Modality Inhibitor of the Prostate-Specific Membrane Antigen. *Angewandte Chemie International Edition* 50: 9167-9170

Banerjee SR, Pullambhatla M, Foss CA, Nimmagadda S, Ferdani R, Anderson CJ, Mease RC, Pomper MG (2014) 64Cu-Labeled Inhibitors of Prostate-Specific Membrane Antigen for PET Imaging of Prostate Cancer. *Journal of medicinal chemistry* 57: 2657-2669

Banerjee SR, Wang B, Pullambhatla M, Foss CA, Pomper MG, Morgan RH (2014) Albumin-based nanoformulation for prostate-specific membrane antigen (PSMA). *Nuclear medicine and biology* 41: 641-642

Barbieri CE, Rubin MA (2015) Genomic rearrangements in prostate cancer. *Current opinion in urology* 25: 71-6

Beauregard J-M, Blouin A-C, Fradet V, Caron A, Fradet Y, Lemay C, Lacombe L, Dujardin T, Tiguert R, Rimac G, Bouchard F, Pouliot F (2015) FDG-PET/CT for pre-operative staging and prognostic stratification of patients with high-grade prostate cancer at biopsy. *Cancer Imaging* 15: 2

Behnam Azad B, Banerjee SR, Pullambhatla M, Lacerda S, Foss CA, Wang Y, Ivkov R, Pomper MG (2015a) Evaluation of a PSMA-targeted BNF nanoparticle construct. *Nanoscale* 7: 4432-42

Behnam Azad B, Banerjee SR, Pullambhatla M, Lacerda S, Foss CA, Wang Y, Ivkov R, Pomper MG (2015b) Evaluation of a PSMA-targeted BNF nanoparticle construct. *Nanoscale* 7: 4432-4442

Bergs JW, Wacker MG, Hehlgans S, Piiper A, Multhoff G, Rödel C, Rödel F (2015) The role of recent nanotechnology in enhancing the efficacy of radiation therapy. *Biochimica et Biophysica Acta (BBA)-Reviews on Cancer* 1856: 130-143

Bhuckory S, Lefebvre O, Qiu X, Wegner KD, Hildebrandt N (2016) Evaluating Quantum Dot Performance in Homogeneous FRET Immunoassays for Prostate Specific Antigen. *Sensors (Basel, Switzerland)* 16: 197

Bolla M, De Reijke TM, Van Tienhoven G, Van den Bergh AC, Oddens J, Poortmans PM, Gez E, Kil P, Akdas A, Soete G (2009) Duration of androgen suppression in the treatment of prostate cancer. *New England Journal of Medicine* 360: 2516-2527

Boyd LK, Mao X, Lu Y-J (2012) The complexity of prostate cancer: genomic alterations and heterogeneity. *Nature Reviews Urology* 9: 652-664

Brazhnik K, Sokolova Z, Baryshnikova M, Bilan R, Efimov A, Nabiev I, Sukhanova A (2015) Quantum dot-based lab-on-a-bead system for multiplexed detection of free and total prostate-specific antigens in clinical human serum samples. *Nanomedicine* 11: 1065-75

Briman M, Artukovic E, Zhang L, Chia D, Goodglick L, Gruner G (2007) Direct electronic detection of prostate-specific antigen in serum. *Small* 3: 758-62

Brocks D, Assenov Y, Minner S, Bogatyrova O, Simon R, Koop C, Oakes C, Zucknick M, Lipka DB, Weischenfeldt J (2014a) Intratumor DNA methylation heterogeneity reflects clonal evolution in aggressive prostate cancer. *Cell reports* 8: 798-806

Brocks D, Assenov Y, Minner S, Bogatyrova O, Simon R, Koop C, Oakes C, Zucknick M, Lipka Daniel B, Weischenfeldt J, Feuerbach L, Cowper-Sal·lari R, Lupien M, Brors B, Korbel J, Schlomm T, Tanay A, Sauter G, Gerhäuser C, Plass C (2014b) Intratumor DNA Methylation Heterogeneity Reflects Clonal Evolution in Aggressive Prostate Cancer. *Cell Reports* 8: 798-806

Bruschi M, Ravera S, Santucci L, Candiano G, Bartolucci M, Calzia D, Lavarello C, Inglese E, Petretto A, Ghiggeri G (2015) The human urinary exosome as a potential metabolic effector cargo. *Expert review of proteomics* 12: 425-432

Buckway B, Frazier N, Gormley AJ, Ray A, Ghandehari H (2014) Gold nanorod-mediated hyperthermia enhances the efficacy of HPMA copolymer-90Y conjugates in treatment of prostate tumors. *Nuclear medicine and biology* 41: 282-9
Butterworth KT, Coulter JA, Jain S, Forker J, McMahon SJ, Schettino G, Prise KM, Currell FJ, Hirst DG (2010) Evaluation of cytotoxicity and radiation enhancement using 1.9 nm gold particles: potential application for cancer therapy. *Nanotechnology* 21: 295101
Butterworth KT, McMahon SJ, Taggart LE, Prise KM (2013) Radiosensitization by gold nanoparticles: effective at megavoltage energies and potential role of oxidative stress. *Translational Cancer Research* 2: 269-279
Cabrera AR, Lee WR (2013) Hypofractionation for clinically localized prostate cancer. In Seminars in radiation oncology, pp 191-197. Elsevier
Caffo O, Maines F, Donner D, Veccia A, Chierichetti F, Galligioni E (2014) Impact of enzalutamide administration on primary prostate cancer volume: a metabolic evaluation by choline positron emission tomography in castration-resistant prostate cancer patients. *Clinical genitourinary cancer* 12: 312-6
Cai S, Cheng X, Pan X, Li J (2016) Emerging role of exosomes in liver physiology and pathology. *Hepatology research : the official journal of the Japan Society of Hepatology*
Castellucci P, Jadvar H (2012) PET/CT in prostate cancer: non-choline radiopharmaceuticals. *The quarterly journal of nuclear medicine and molecular imaging : official publication of the Italian Association of Nuclear Medicine (AIMN) [and] the International Association of Radiopharmacology (IAR), [and] Section of the So* 56: 367-74
Center MM, Jemal A, Lortet-Tieulent J, Ward E, Ferlay J, Brawley O, Bray F (2012) International variation in prostate cancer incidence and mortality rates. *European urology* 61: 1079-1092
Chanda N, Kan P, Watkinson LD, Shukla R, Zambre A, Carmack TL, Engelbrecht H, Lever JR, Katti K, Fent GM (2010) Radioactive gold nanoparticles in cancer therapy: therapeutic efficacy studies of GA-198 AuNP nanoconstruct in prostate tumor–bearing mice. *Nanomedicine: Nanotechnology, Biology and Medicine* 6: 201-209
Chandrasekar T, Yang JC, Gao AC, Evans CP (2015) Mechanisms of resistance in castration-resistant prostate cancer (CRPC). *Translational andrology and urology* 4: 365-80
Chatalic KL, Kwekkeboom DJ, de Jong M (2015) Radiopeptides for Imaging and Therapy: A Radiant Future. *Journal of nuclear medicine : official publication, Society of Nuclear Medicine* 56: 1809-12
Chen Z, Penet M-F, Nimmagadda S, Li C, Banerjee SR, Winnard Jr PT, Artemov D, Glunde K, Pomper MG, Bhujwalla ZM (2012) PSMA-targeted theranostic nanoplex for prostate cancer therapy. *ACS nano* 6: 7752-7762
Chesire DR, Ewing CM, Sauvageot J, Bova GS, Isaacs WB (2000) Detection and analysis of β-catenin mutations in prostate cancer. *The Prostate* 45: 323-334
Chikkaveeraiah BV, Bhirde A, Malhotra R, Patel V, Gutkind JS, Rusling JF (2009) Single-wall carbon nanotube forest arrays for immunoelectrochemical measurement of four protein biomarkers for prostate cancer. *Analytical chemistry* 81: 9129-34
Choi H, Lee DS (2016) Illuminating the physiology of extracellular vesicles. *Stem Cell Research & Therapy* 7: 55
Choi H, Lee Y-S, Hwang DW, Lee DS (2016) Translational radionanomedicine: a clinical perspective. *European Journal of Nanomedicine* 8: 71-84
Choi JY, Jeong JM, Yoo BC, Kim K, Kim Y, Yang BY, Lee YS, Lee DS, Chung JK, Lee MC (2011) Development of 68Ga-labeled mannosylated human serum albumin (MSA) as a lymph node imaging agent for positron emission tomography. *Nuclear medicine and biology* 38: 371-9
Coulter J, Butterworth K, Jain S (2015) Prostate cancer radiotherapy: potential applications of metal nanoparticles for imaging and therapy. *The British journal of radiology* 88: 20150256

Coulter JA, Jain S, Butterworth KT, Taggart LE, Dickson GR, McMahon SJ, Hyland WB, Muir MF, Trainor C, Hounsell AR, O'Sullivan JM, Schettino G, Currell FJ, Hirst DG, Prise KM (2012) Cell type-dependent uptake, localization, and cytotoxicity of 1.9 nm gold nanoparticles. *International journal of nanomedicine* 7: 2673-85

Cui D, Han Y, Li Z, Song H, Wang K, He R, Liu B, Liu H, Bao C, Huang P (2009) Fluorescent magnetic nanoprobes for in vivo targeted imaging and hyperthermia therapy of prostate cancer. *Nano Biomed Eng* 1: 94-112

Czarniecki M, Jakucinski M, Krolicki L (2016) Prostate MRI - an update for the referring urologist. *Central European journal of urology* 69: 162-9

D'Incà F, Pucillo CE (2015) Exosomes: Tiny Clues for Mast Cell Communication. *Frontiers in Immunology* 6: 73

De Giorgi U, Caroli P, Scarpi E, Conteduca V, Burgio S, Menna C, Moretti A, Galassi R, Rossi L, Amadori D, Paganelli G, Matteucci F (2015) 18F-Fluorocholine PET/CT for early response assessment in patients with metastatic castration-resistant prostate cancer treated with enzalutamide. *Eur J Nucl Med Mol Imaging* 42: 1276-1283

de Jong M, Breeman WA, Kwekkeboom DJ, Valkema R, Krenning EP (2009) Tumor imaging and therapy using radiolabeled somatostatin analogues. *Accounts of chemical research* 42: 873-80

De La Pena H, Madrigal JA, Rusakiewicz S, Bencsik M, Cave GW, Selman A, Rees RC, Travers PJ, Dodi IA (2009) Artificial exosomes as tools for basic and clinical immunology. *Journal of immunological methods* 344: 121-32

Debes JD, Tindall DJ (2004) Mechanisms of androgen-refractory prostate cancer. *N Engl J Med* 351: 1488-1490

Dehdashti F, Picus J, Michalski JM, Dence CS, Siegel BA, Katzenellenbogen JA, Welch MJ (2005) Positron tomographic assessment of androgen receptors in prostatic carcinoma. *Eur J Nucl Med Mol Imaging* 32: 344-50

Delker A, Fendler WP, Kratochwil C, Brunegraf A, Gosewisch A, Gildehaus FJ, Tritschler S, Stief CG, Kopka K, Haberkorn U (2016) Dosimetry for 177Lu-DKFZ-PSMA-617: a new radiopharmaceutical for the treatment of metastatic prostate cancer. *Eur J Nucl Med Mol Imaging* 43: 42-51

Diaz LA, Jr., Cheong I, Foss CA, Zhang X, Peters BA, Agrawal N, Bettegowda C, Karim B, Liu G, Khan K, Huang X, Kohli M, Dang LH, Hwang P, Vogelstein A, Garrett-Mayer E, Kobrin B, Pomper M, Zhou S, Kinzler KW et al. (2005) Pharmacologic and toxicologic evaluation of C. novyi-NT spores. *Toxicological sciences : an official journal of the Society of Toxicology* 88: 562-75

Durkan K, Lambrecht FY, Unak P (2007) Radiolabeling of bombesin-like peptide with 99mTc: 99mTc-litorin and biodistribution in rats. *Bioconjugate chemistry* 18: 1516-20

Ebenhan T, Vorster M, Marjanovic-Painter B, Wagener J, Suthiram J, Modiselle M, Mokaleng B, Zeevaart JR, Sathekge M (2015) Development of a Single Vial Kit Solution for Radiolabeling of 68Ga-DKFZ-PSMA-11 and Its Performance in Prostate Cancer Patients. *Molecules (Basel, Switzerland)* 20: 14860-78

Elsadek B, Kratz F (2012) Impact of albumin on drug delivery—New applications on the horizon. *Journal of controlled release* 157: 4-28

Emonds KM, Swinnen JV, Mortelmans L, Mottaghy FM (2009) Molecular imaging of prostate cancer. *Methods (San Diego, Calif)* 48: 193-9

Evans MJ, Smith-Jones PM, Wongvipat J, Navarro V, Kim S, Bander NH, Larson SM, Sawyers CL (2011) Noninvasive measurement of androgen receptor signaling with a positron-emitting radiopharmaceutical that targets prostate-specific membrane antigen. *Proceedings of the National Academy of Sciences* 108: 9578-9582

Faintuch BL, Núñez GEF, Teodoro R, Moro AM, Mengatti J (2011) Radiolabeled nano-peptides show specificity for an animal model of human PC3 prostate cancer cells. *Clinics* 66: 327-336

Feldman BJ, Feldman D (2001) The development of androgen-independent prostate cancer. *Nature Reviews Cancer* 1: 34-45
Fox J, Blanc E, Schoder H, Morris M, Scher H, Larson S, Humm JL, Cai S (2009) Diversity of biology in castrate resistant prostate cancer. *J NUCL MED MEETING ABSTRACTS* 50: 523-
Freitag MT, Radtke JP, Hadaschik BA, Kopp-Schneider A, Eder M, Kopka K, Haberkorn U, Roethke M, Schlemmer H-P, Afshar-Oromieh A (2016) Comparison of hybrid 68Ga-PSMA PET/MRI and 68Ga-PSMA PET/CT in the evaluation of lymph node and bone metastases of prostate cancer. *Eur J Nucl Med Mol Imaging* 43: 70-83
Gabriel K, Ingram A, Austin R, Kapoor A, Tang D, Majeed F, Qureshi T, Al-Nedawi K (2013) Regulation of the tumor suppressor PTEN through exosomes: a diagnostic potential for prostate cancer. *PloS one* 8: e70047
Gao X, Zhang H, Li Y, Su X (2012) Mn-doped ZnSe d-dots-based alpha-methylacyl-CoA racemase probe for human prostate cancer cell imaging. *Analytical and bioanalytical chemistry* 402: 1871-7
Garcia J, Tang T, Louie AY (2015) Nanoparticle-based multimodal PET/MRI probes. *Nanomedicine (London, England)* 10: 1343-59
Garcia-Cortes M, Encinar JR, Costa-Fernandez JM, Sanz-Medel A (2016) Highly sensitive nanoparticle-based immunoassays with elemental detection: Application to Prostate-Specific Antigen quantification. *Biosensors & bioelectronics* 85: 128-34
Giesel FL, Fiedler H, Stefanova M, Sterzing F, Rius M, Kopka K, Moltz JH, Afshar-Oromieh A, Choyke PL, Haberkorn U, Kratochwil C (2015) PSMA PET/CT with Glu-urea-Lys-(Ahx)-[(6)(8)Ga(HBED-CC)] versus 3D CT volumetric lymph node assessment in recurrent prostate cancer. *Eur J Nucl Med Mol Imaging* 42: 1794-800
Gillies RJ, Robey I, Gatenby RA (2008) Causes and consequences of increased glucose metabolism of cancers. *Journal of nuclear medicine : official publication, Society of Nuclear Medicine* 49 Suppl 2: 24s-42s
Glasgow MD, Chougule MB (2015) Recent Developments in Active Tumor Targeted Multifunctional Nanoparticles for Combination Chemotherapy in Cancer Treatment and Imaging. *Journal of biomedical nanotechnology* 11: 1859-98
Goel S, England CG, Chen F, Cai W (2016) Positron emission tomography and nanotechnology: A dynamic duo for cancer theranostics. *Advanced drug delivery reviews*
Gokarna A, Jin LH, Hwang JS, Cho YH, Lim YT, Chung BH, Youn SH, Choi DS, Lim JH (2008) Quantum dot-based protein micro- and nanoarrays for detection of prostate cancer biomarkers. *Proteomics* 8: 1809-18
Goswami LN, Ma L, Cai Q, Sarma SJ, Jalisatgi SS, Hawthorne MF (2013) cRGD peptide-conjugated icosahedral closo-B12(2-) core carrying multiple Gd3+-DOTA chelates for alpha(v)beta3 integrin-targeted tumor imaging (MRI). *Inorganic chemistry* 52: 1701-9
Ha D, Yang N, Nadithe V (2016) Exosomes as therapeutic drug carriers and delivery vehicles across biological membranes: current perspectives and future challenges. *Acta pharmaceutica Sinica B* 6: 287-96
Hall J, Prabhakar S, Balaj L, Lai CP, Cerione RA, Breakefield XO (2016) Delivery of Therapeutic Proteins via Extracellular Vesicles: Review and Potential Treatments for Parkinson's Disease, Glioma, and Schwannoma. *Cellular and molecular neurobiology* 36: 417-427
Hassan HA, Smyth L, Rubio N, Ratnasothy K, Wang JT, Bansal SS, Summers HD, Diebold SS, Lombardi G, Al-Jamal KT (2016) Carbon nanotubes' surface chemistry determines their potency as vaccine nanocarriers in vitro and in vivo. *Journal of controlled release : official journal of the Controlled Release Society* 225: 205-16
Helou J, Morton G, Zhang L, Deabreu A, D'Alimonte L, Elias E, Musunuru HB, Mamedov A, Ravi A, Chung H, Cheung P, Loblaw A (2014) A comparative study of quality of life in patients with localized prostate cancer treated at a single institution: stereotactic ablative

radiotherapy or external beam+high dose rate brachytherapy boost. *Radiotherapy and oncology : journal of the European Society for Therapeutic Radiology and Oncology* 113: 404-9
Herrmann K, Bluemel C, Weineisen M, Schottelius M, Wester H-J, Czernin J, Eberlein U, Beykan S, Lapa C, Riedmiller H (2015) Biodistribution and radiation dosimetry for a novel probe targeting prostate specific membrane antigen for Imaging and Therapy (68Ga-PSMA I&T). *Journal of Nuclear Medicine*: jnumed. 115.156133
Hidayatullah M, Nurhasanah I, Budi W (2016) ZnFe2O4 nanoparticles for potential application in radiosensitization. In Journal of Physics: Conference Series, p 012028. IOP Publishing
Hoffman TJ, Gali H, Smith CJ, Sieckman GL, Hayes DL, Owen NK, Volkert WA (2003) Novel series of 111In-labeled bombesin analogs as potential radiopharmaceuticals for specific targeting of gastrin-releasing peptide receptors expressed on human prostate cancer cells. *Journal of nuclear medicine : official publication, Society of Nuclear Medicine* 44: 823-31
Hu K, Wang H, Tang G, Huang T, Tang X, Liang X, Yao S, Nie D (2015) In Vivo Cancer Dual-Targeting and Dual-Modality Imaging with Functionalized Quantum Dots. *Journal of Nuclear Medicine* 56: 1278-1284
Hu L, Wickline SA, Hood JL (2014) Magnetic Resonance Imaging of Melanoma Exosomes in Lymph Nodes. *Magnetic resonance in medicine : official journal of the Society of Magnetic Resonance in Medicine / Society of Magnetic Resonance in Medicine*: 10.1002/mrm.25376
Hu P, Chu GC, Zhu G, Yang H, Luthringer D, Prins G, Habib F, Wang Y, Wang R, Chung LW, Zhau HE (2011) Multiplexed quantum dot labeling of activated c-Met signaling in castration-resistant human prostate cancer. *PloS one* 6: e28670
Huang C-C, Liu T-M (2015) Controlled Au–Polymer Nanostructures for Multiphoton Imaging, Prodrug Delivery, and Chemo–Photothermal Therapy Platforms. *ACS applied materials & interfaces* 7: 25259-25269
Hwang do W, Choi H, Jang SC, Yoo MY, Park JY, Choi NE, Oh HJ, Ha S, Lee YS, Jeong JM, Gho YS, Lee DS (2015) Noninvasive imaging of radiolabeled exosome-mimetic nanovesicle using (99m)Tc-HMPAO. *Scientific reports* 5: 15636
Jackson PA, Rahman WNWA, Wong CJ, Ackerly T, Geso M (2010) Potential dependent superiority of gold nanoparticles in comparison to iodinated contrast agents. *European Journal of Radiology* 75: 104-109
Jadvar H (2013a) Imaging evaluation of prostate cancer with 18F-fluorodeoxyglucose PET/CT: utility and limitations. *Eur J Nucl Med Mol Imaging* 40 Suppl 1: S5-10
Jadvar H (2013b) Molecular imaging of prostate cancer with PET. *Journal of nuclear medicine : official publication, Society of Nuclear Medicine* 54: 1685-8
Jain RK, Stylianopoulos T (2010) Delivering nanomedicine to solid tumors. *Nat Rev Clin Oncol* 7: 653-664
Jain S, Coulter JA, Hounsell AR, Butterworth KT, McMahon SJ, Hyland WB, Muir MF, Dickson GR, Prise KM, Currell FJ, O'Sullivan JM, Hirst DG (2011) Cell-specific radiosensitization by gold nanoparticles at megavoltage radiation energies. *International journal of radiation oncology, biology, physics* 79: 531-9
Jin CS, Zheng G (2011) Liposomal nanostructures for photosensitizer delivery. *Lasers in surgery and medicine* 43: 734-48
Jin LH, Li SM, Cho YH (2012) Enhanced detection sensitivity of pegylated CdSe/ZnS quantum dots-based prostate cancer biomarkers by surface plasmon-coupled emission. *Biosensors & bioelectronics* 33: 284-7
Johannsen M, Thiesen B, Gneveckow U, Taymoorian K, Waldöfner N, Scholz R, Deger S, Jung K, Loening SA, Jordan A (2006) Thermotherapy using magnetic nanoparticles combined with external radiation in an orthotopic rat model of prostate cancer. *The Prostate* 66: 97-104
Jung K, Youn H, Kim M, Kang K, Lee D, Chung J-K (2015a) Cell to cell communication of exosomal miR-210 released by hypoxic breast cancer cell in tumor microenvironment. In

JOURNAL OF NUCLEAR MEDICINE, pp 11-11. SOC NUCLEAR MEDICINE INC 1850 SAMUEL MORSE DR, RESTON, VA 20190-5316 USA
Jung K, Youn H, Kim M, Oh S, Kang K, Lee D, Chung J-K (2015b) In vivo PET imaging of radiolabeled exosomes from breast cancer cells. In JOURNAL OF NUCLEAR MEDICINE, pp 11-11. SOC NUCLEAR MEDICINE INC 1850 SAMUEL MORSE DR, RESTON, VA 20190-5316 USA
Jung KO, Kim Y-H, Chung J-K, Youn H (2015) Abstract B50: Visualizing intercellular transfer of hypoxia-induced exosomal miR-210 between breast cancer cells. *Cancer Research* 75: B50-B50
Kaarbø M, Klokk TI, Saatcioglu F (2007) Androgen signaling and its interactions with other signaling pathways in prostate cancer. *Bioessays* 29: 1227-1238
Kamila S, McEwan C, Costley D, Atchison J, Sheng Y, Hamilton GRC, Fowley C, Callan JF (2016) Diagnostic and Therapeutic Applications of Quantum Dots in Nanomedicine. In *Light-Responsive Nanostructured Systems for Applications in Nanomedicine*, Sortino S (ed) pp 203-224. Cham: Springer International Publishing
Katzenwadel A, Wolf P (2015) Androgen deprivation of prostate cancer: Leading to a therapeutic dead end. *Cancer letters* 367: 12-7
Keller S, König A-K, Marmé F, Runz S, Wolterink S, Koensgen D, Mustea A, Sehouli J, Altevogt P (2009) Systemic presence and tumor-growth promoting effect of ovarian carcinoma released exosomes. *Cancer letters* 278: 73-81
Khan FM, Gibbons JP (2014) *Khan's the physics of radiation therapy*. Lippincott Williams & Wilkins,
Kim D, Jeong YY, Jon S (2010) A drug-loaded aptamer-gold nanoparticle bioconjugate for combined CT imaging and therapy of prostate cancer. *ACS Nano* 4: 3689-96
Kim JP, Lee BY, Lee J, Hong S, Sim SJ (2009) Enhancement of sensitivity and specificity by surface modification of carbon nanotubes in diagnosis of prostate cancer based on carbon nanotube field effect transistors. *Biosensors & bioelectronics* 24: 3372-8
Kim JS, Kim YH, Kim JH, Kang KW, Tae EL, Youn H, Kim D, Kim SK, Kwon JT, Cho MH, Lee YS, Jeong JM, Chung JK, Lee DS (2012) Development and in vivo imaging of a PET/MRI nanoprobe with enhanced NIR fluorescence by dye encapsulation. *Nanomedicine (London, England)* 7: 219-29
Korpal M, Korn JM, Gao X, Rakiec DP, Ruddy DA, Doshi S, Yuan J, Kovats SG, Kim S, Cooke VG (2013) An F876L mutation in androgen receptor confers genetic and phenotypic resistance to MDV3100 (enzalutamide). *Cancer discovery* 3: 1030-1043
Kosaka N, Ochiya T (2014) Functional importance of exosome in cancer development. *Drug Delivery System* 29: 125-133
Kosaka N, Yoshioka Y, Katsuda T, Ono M, Ochiya T (2014) Exosome in disease biology, diagnosis, and therapy. *Inflammation and Regeneration* 34: 233-239
Kratochwil C, Giesel FL, Eder M, Afshar-Oromieh A, Benešová M, Mier W, Kopka K, Haberkorn U (2015a) [177Lu] Lutetium-labelled PSMA ligand-induced remission in a patient with metastatic prostate cancer. *Eur J Nucl Med Mol Imaging* 42: 987-988
Kratochwil C, Giesel FL, Leotta K, Eder M, Hoppe-Tich T, Youssoufian H, Kopka K, Babich JW, Haberkorn U (2015b) PMPA for nephroprotection in PSMA-targeted radionuclide therapy of prostate cancer. *Journal of Nuclear Medicine* 56: 293-298
Krishnan S, Diagaradjane P, Cho SH (2010) Nanoparticle-mediated thermal therapy: evolving strategies for prostate cancer therapy. *International journal of hyperthermia : the official journal of European Society for Hyperthermic Oncology, North American Hyperthermia Group* 26: 775-89
Kumar R, Belz J, Markovic S, Jadhav T, Fowle W, Niedre M, Cormack R, Makrigiorgos MG, Sridhar S (2015) Nanoparticle-Based Brachytherapy Spacers for Delivery of Localized Combined Chemoradiation Therapy. *International Journal of Radiation Oncology*Biology*Physics* 91: 393-400

Kwon H, Lee J, Song R, Hwang SI, Lee J, Kim YH, Lee HJ (2013) In vitro and in vivo imaging of prostate cancer angiogenesis using anti-vascular endothelial growth factor receptor 2 antibody-conjugated quantum dot. *Korean journal of radiology* 14: 30-7
Lacerda L, Bianco A, Prato M, Kostarelos K (2006) Carbon nanotubes as nanomedicines: from toxicology to pharmacology. *Advanced drug delivery reviews* 58: 1460-1470
Laffin B, Tang DG (2010) An old player on a new playground: bmi-1 as a regulator of prostate stem cells. *Cell Stem Cell* 7: 639-640
Lai CP, Mardini O, Ericsson M, Prabhakar S, Maguire CA, Chen JW, Tannous BA, Breakefield XO (2014) Dynamic biodistribution of extracellular vesicles in vivo using a multimodal imaging reporter. *ACS Nano* 8: 483-94
Larson SM, Morris M, Gunther I, Beattie B, Humm JL, Akhurst TA, Finn RD, Erdi Y, Pentlow K, Dyke J, Squire O, Bornmann W, McCarthy T, Welch M, Scher H (2004) Tumor localization of 16beta-18F-fluoro-5alpha-dihydrotestosterone versus 18F-FDG in patients with progressive, metastatic prostate cancer. *Journal of nuclear medicine : official publication, Society of Nuclear Medicine* 45: 366-73
Lee DS (2016) Radio-nanomedicine: In vivo use of tracer radioisotope-labeled. *Nanomedicine: Nanotechnology, Biology and Medicine* 12: 450
Lee DS, Im HJ, Lee YS (2015) Radionanomedicine: widened perspectives of molecular theragnosis. *Nanomedicine* 11: 795-810
Lee N, Choi SH, Hyeon T (2013) Nano-sized CT contrast agents. *Advanced materials (Deerfield Beach, Fla)* 25: 2641-60
Lee YK, Jeong JM, Hoigebazar L, Yang BY, Lee YS, Lee BC, Youn H, Lee DS, Chung JK, Lee MC (2012) Nanoparticles modified by encapsulation of ligands with a long alkyl chain to affect multispecific and multimodal imaging. *Journal of nuclear medicine : official publication, Society of Nuclear Medicine* 53: 1462-70
Lerner MB, D'Souza J, Pazina T, Dailey J, Goldsmith BR, Robinson MK, Johnson AT (2012) Hybrids of a genetically engineered antibody and a carbon nanotube transistor for detection of prostate cancer biomarkers. *ACS Nano* 6: 5143-9
Leung K (2004a) Quantum dot 800-prostate-specific membrane antigen antibody J591. In *Molecular Imaging and Contrast Agent Database (MICAD)*, Bethesda (MD): National Center for Biotechnology Information (US)
Leung K (2004b) Quantum dot-prostate-specific membrane antigen antibody J591. In *Molecular Imaging and Contrast Agent Database (MICAD)*, Bethesda (MD): National Center for Biotechnology Information (US)
Li C, Curreli M, Lin H, Lei B, Ishikawa FN, Datar R, Cote RJ, Thompson ME, Zhou C (2005) Complementary detection of prostate-specific antigen using In2O3 nanowires and carbon nanotubes. *Journal of the American Chemical Society* 127: 12484-5
Li H, Chen X, Calhoun-Davis T, Claypool K, Tang DG (2008) PC3 human prostate carcinoma cell holoclones contain self-renewing tumor-initiating cells. *Cancer research* 68: 1820-1825
Li X, Li W, Yang Q, Gong X, Guo W, Dong C, Liu J, Xuan L, Chang J (2014) Rapid and quantitative detection of prostate specific antigen with a quantum dot nanobeads-based immunochromatography test strip. *ACS applied materials & interfaces* 6: 6406-14
Lim JC, Cho EH, Kim JJ, Choi SM, Lee S, Nam SS, Park UJ, Park SH (2015a) Biological evaluation of (177)Lu-labeled DOTA-Ala(SO3H)-Aminooctanoyl-Gln-Trp-Ala-Val-N methyl Gly-His-Statine-Leu-NH2 for gastrin-releasing peptide receptor-positive prostate tumor targeting. *Nuclear medicine and biology* 42: 131-6
Lim JC, Cho EH, Kim JJ, Choi SM, Lee SY, Nam SS, Park UJ, Park SH (2015b) Preclinical pharmacokinetic, biodistribution, imaging and therapeutic efficacy of (177)Lu-Labeled glycated bombesin analogue for gastrin-releasing peptide receptor-positive prostate tumor targeting. *Nuclear medicine and biology* 42: 234-41

Lin Z, Liu Z, Zhang H, Su X (2015) Near-infrared fluorescence probe for the determination of acid phosphatase and imaging of prostate cancer cells. *The Analyst* 140: 1629-36
Lin Z, Ma Q, Fei X, Zhang H, Su X (2014b) A novel aptamer functionalized CuInS2 quantum dots probe for daunorubicin sensing and near infrared imaging of prostate cancer cells. *Analytica chimica acta* 818: 54-60
Liu CM, Hsieh CL, Shen CN, Lin CC, Shigemura K, Sung SY (2016) Exosomes from the tumor microenvironment as reciprocal regulators that enhance prostate cancer progression. *International journal of urology : official journal of the Japanese Urological Association*
Liu J, Lau SK, Varma VA, Moffitt RA, Caldwell M, Liu T, Young AN, Petros JA, Osunkoya AO, Krogstad T (2010) Molecular mapping of tumor heterogeneity on clinical tissue specimens with multiplexed quantum dots. *ACS nano* 4: 2755-2765
Liu TW, MacDonald TD, Jin CS, Gold JM, Bristow RG, Wilson BC, Zheng G (2013) Inherently Multimodal Nanoparticle-Driven Tracking and Real-Time Delineation of Orthotopic Prostate Tumors and Micrometastases. *ACS Nano* 7: 4221-4232
Liu Y, Sozontov E, Safronov V, Gutman G, Strumban E, Jiang Q, Li S (2010) 3D polymer gel dosimetry and Geant4 Monte Carlo characterization of novel needle based X-ray source. In Journal of Physics: Conference Series, p 012069. IOP Publishing
Liu Z, Yan Y, Liu S, Wang F, Chen X (2009) 18F, 64Cu, and 68Ga labeled RGD-bombesin heterodimeric peptides for PET imaging of breast cancer. *Bioconjugate chemistry* 20: 1016-1025
Lo S-T, Kumar A, Hsieh J-T, Sun X (2013) Dendrimer Nanoscaffolds for Potential Theranostics of Prostate Cancer with a Focus on Radiochemistry. *Molecular Pharmaceutics* 10: 793-812
Loureiro A, G Azoia N, C Gomes A, Cavaco-Paulo A (2016) Albumin-based nanodevices as drug carriers. *Current pharmaceutical design* 22: 1371-1390
Lovell JF, Jin CS, Huynh E, Jin H, Kim C, Rubinstein JL, Chan WCW, Cao W, Wang LV, Zheng G (2011) Porphysome nanovesicles generated by porphyrin bilayers for use as multimodal biophotonic contrast agents. *Nat Mater* 10: 324-332
Lu W, Singh AK, Khan SA, Senapati D, Yu H, Ray PC (2010) Gold Nano-Popcorn-Based Targeted Diagnosis, Nanotherapy Treatment, and In Situ Monitoring of Photothermal Therapy Response of Prostate Cancer Cells Using Surface-Enhanced Raman Spectroscopy. *Journal of the American Chemical Society* 132: 18103-18114
Lutje S, Heskamp S, Cornelissen AS, Poeppel TD, van den Broek SA, Rosenbaum-Krumme S, Bockisch A, Gotthardt M, Rijpkema M, Boerman OC (2015) PSMA Ligands for Radionuclide Imaging and Therapy of Prostate Cancer: Clinical Status. *Theranostics* 5: 1388-401
Malic L, Sandros MG, Tabrizian M (2011) Designed biointerface using near-infrared quantum dots for ultrasensitive surface plasmon resonance imaging biosensors. *Analytical chemistry* 83: 5222-9
Marchesan S, Kostarelos K, Bianco A, Prato M (2015) The winding road for carbon nanotubes in nanomedicine. *Materials Today* 18: 12-19
Mayles P, Nahum A, Rosenwald J-C (2007) *Handbook of radiotherapy physics: theory and practice*. CRC Press,
Meidanchi A, Akhavan O, Khoei S, Shokri AA, Hajikarimi Z, Khansari N (2015a) ZnFe2O4 nanoparticles as radiosensitizers in radiotherapy of human prostate cancer cells. *Materials science & engineering C, Materials for biological applications* 46: 394-9
Meidanchi A, Akhavan O, Khoei S, Shokri AA, Hajikarimi Z, Khansari N (2015b) ZnFe2O4 nanoparticles as radiosensitizers in radiotherapy of human prostate cancer cells. *Materials Science and Engineering: C* 46: 394-399
Mendoza-Sanchez AN, Ferro-Flores G, Ocampo-Garcia BE, Morales-Avila E, de MRF, De Leon-Rodriguez LM, Santos-Cuevas CL, Medina LA, Rojas-Calderon EL, Camacho-Lopez MA (2010) Lys3-bombesin conjugated to 99mTc-labelled gold nanoparticles for in vivo gastrin releasing peptide-receptor imaging. *Journal of biomedical nanotechnology* 6: 375-84

Merseburger AS, Hupe MC (2016) An Update on Triptorelin: Current Thinking on Androgen Deprivation Therapy for Prostate Cancer. *Advances in therapy* 33: 1072-93
Minner S, Wittmer C, Graefen M, Salomon G, Steuber T, Haese A, Huland H, Bokemeyer C, Yekebas E, Dierlamm J (2011) High level PSMA expression is associated with early PSA recurrence in surgically treated prostate cancer. *The Prostate* 71: 281-288
Mitani T, Harada N, Tanimori S, NAkANO Y, Inui H, Yamaji R (2014) Resveratrol Inhibits Hypoxia-Inducible Factor-1α-Mediated Androgen Receptor Signaling and Represses Tumor Progression in Castration-Resistant Prostate Cancer. *Journal of nutritional science and vitaminology* 60: 276-282
Mitani T, Yamaji R, Higashimura Y, Harada N, Nakano Y, Inui H (2011) Hypoxia enhances transcriptional activity of androgen receptor through hypoxia-inducible factor-1α in a low androgen environment. *The Journal of steroid biochemistry and molecular biology* 123: 58-64
Moon S-H, Yang BY, Kim YJ, Hong MK, Lee Y-S, Lee DS, Chung J-K, Jeong JM Development of a complementary PET/MR dual-modal imaging probe for targeting prostate-specific membrane antigen (PSMA). *Nanomedicine: Nanotechnology, Biology and Medicine*
Moon S-H, Yang BY, Kim YJ, Hong MK, Lee Y-S, Lee DS, Chung J-K, Jeong JM (2016) Development of a complementary PET/MR dual-modal imaging probe for targeting prostate-specific membrane antigen (PSMA). *Nanomedicine: Nanotechnology, Biology and Medicine* 12: 871-879
Morigi JJ, Stricker PD, van Leeuwen PJ, Tang R, Ho B, Nguyen Q, Hruby G, Fogarty G, Jagavkar R, Kneebone A (2015) Prospective comparison of 18F-fluoromethylcholine versus 68Ga-PSMA PET/CT in prostate cancer patients who have rising PSA after curative treatment and Are being considered for targeted therapy. *Journal of Nuclear Medicine* 56: 1185-1190
Morishita M, Takahashi Y, Nishikawa M, Sano K, Kato K, Yamashita T, Imai T, Saji H, Takakura Y (2015) Quantitative analysis of tissue distribution of the B16BL6-derived exosomes using a streptavidin-lactadherin fusion protein and iodine-125-labeled biotin derivative after intravenous injection in mice. *Journal of pharmaceutical sciences* 104: 705-13
Morris WJ, Tyldesley S, Pai HH, Halperin R, McKenzie MR, Duncan G, Morton G, Murray N, Hamm J (2015) ASCENDE-RT*: A multicenter, randomized trial of dose-escalated external beam radiation therapy (EBRT-B) versus low-dose-rate brachytherapy (LDR-B) for men with unfavorable-risk localized prostate cancer. In ASCO Annual Meeting Proceedings, p 3.
Muthu MS, Wilson B (2010) Multifunctional radionanomedicine: a novel nanoplatform for cancer imaging and therapy. *Nanomedicine (London, England)* 5: 169-71
Newland B, Thomas L, Zheng Y, Steinhart M, Werner C, Wang W (2016) Preparation, loading, and cytotoxicity analysis of polymer nanotubes from an ethylene glycol dimethacrylate homopolymer in comparison to multi-walled carbon nanotubes. *Journal of interdisciplinary nanomedicine* 1: 9-18
Ngwa W, Korideck H, Kassis AI, Kumar R, Sridhar S, Makrigiorgos GM, Cormack RA (2013) In vitro radiosensitization by gold nanoparticles during continuous low dose rate gamma irradiation with I-125 brachytherapy seeds. *Nanomedicine : nanotechnology, biology, and medicine* 9: 25-27
Nicolae AM, Venugopal N, Ravi A (2016) Trends in targeted prostate brachytherapy: from multiparametric MRI to nanomolecular radiosensitizers. *Cancer Nanotechnology* 7: 6
Nikolopoulou A, Amor-Coarasa A, Wuestemann T, Matei I, Hoshino A, DiMagno S, Vallabhajosula S, Peinado H, Lyden D, Babich J (2016) Tumor exosomes as molecular probes to detect breast cancer pre-metastatic niches: radiolabeling with I-131 and tissue uptake studies in "naïve" nude mice. *Journal of Nuclear Medicine* 57: 524-524
Oh E, Liu R, Nel A, Gemill KB, Bilal M, Cohen Y, Medintz IL (2016) Meta-analysis of cellular toxicity for cadmium-containing quantum dots. *Nat Nano* 11: 479-486

Okuno J, Maehashi K, Kerman K, Takamura Y, Matsumoto K, Tamiya E (2007) Label-free immunosensor for prostate-specific antigen based on single-walled carbon nanotube array-modified microelectrodes. *Biosensors & bioelectronics* 22: 2377-81
Pablico-Lansigan MH, Hickling WJ, Japp EA, Rodriguez OC, Ghosh A, Albanese C, Nishida M, Van Keuren E, Fricke S, Dollahon N, Stoll SL (2013) Magnetic nanobeads as potential contrast agents for magnetic resonance imaging. *ACS Nano* 7: 9040-8
Panini NV, Messina GA, Salinas E, Fernandez H, Raba J (2008) Integrated microfluidic systems with an immunosensor modified with carbon nanotubes for detection of prostate specific antigen (PSA) in human serum samples. *Biosensors & bioelectronics* 23: 1145-51
Park W, Cho S, Huang X, Larson AC, Kim DH (2016) Branched Gold Nanoparticle Coating of Clostridium novyi-NT Spores for CT-Guided Intratumoral Injection. *Small*
Patra S, Roy E, Madhuri R, Sharma PK (2015) Nano-iniferter based imprinted sensor for ultra trace level detection of prostate-specific antigen in both men and women. *Biosensors & bioelectronics* 66: 1-10
Patrawala L, Calhoun-Davis T, Schneider-Broussard R, Tang DG (2007) Hierarchical organization of prostate cancer cells in xenograft tumors: the CD44+ α2β1+ cell population is enriched in tumor-initiating cells. *Cancer research* 67: 6796-6805
Pei H, Zhu S, Yang M, Kong R, Zheng Y, Qu F (2015) Graphene oxide quantum dots@silver core-shell nanocrystals as turn-on fluorescent nanoprobe for ultrasensitive detection of prostate specific antigen. *Biosensors & bioelectronics* 74: 909-14
Peinado H, Alečković M, Lavotshkin S, Matei I, Costa-Silva B, Moreno-Bueno G, Hergueta-Redondo M, Williams C, García-Santos G, Ghajar CM (2012) Melanoma exosomes educate bone marrow progenitor cells toward a pro-metastatic phenotype through MET. *Nature medicine* 18: 883-891
Perner S, Cronauer MV, Schrader AJ, Klocker H, Culig Z, Baniahmad A (2015) Adaptive responses of androgen receptor signaling in castration-resistant prostate cancer. *Oncotarget* 6: 35542-55
Popovtzer R, Agrawal A, Kotov NA, Popovtzer A, Balter J, Carey TE, Kopelman R (2008) Targeted Gold Nanoparticles enable Molecular CT Imaging of Cancer. *Nano letters* 8: 4593-4596
Pratt EC, Shaffer TM, Grimm J (2016) Nanoparticles and radiotracers: advances toward radionanomedicine. *Wiley interdisciplinary reviews Nanomedicine and nanobiotechnology*
Pressly ED, Pierce RA, Connal LA, Hawker CJ, Liu Y (2013) Nanoparticle PET/CT imaging of natriuretic peptide clearance receptor in prostate cancer. *Bioconjugate chemistry* 24: 196-204
Qin J, Liu X, Laffin B, Chen X, Choy G, Jeter CR, Calhoun-Davis T, Li H, Palapattu GS, Pang S (2012) The PSA–/lo prostate cancer cell population harbors self-renewing long-term tumor-propagating cells that resist castration. *Cell stem cell* 10: 556-569
Quail DF, Joyce JA (2013) Microenvironmental regulation of tumor progression and metastasis. *Nature medicine* 19: 1423-1437
Rahman WN, Bishara N, Ackerly T, He CF, Jackson P, Wong C, Davidson R, Geso M (2009) Enhancement of radiation effects by gold nanoparticles for superficial radiation therapy. *Nanomedicine: Nanotechnology, Biology and Medicine* 5: 136-142
Rahman WN, Corde S, Yagi N, Aziz SAA, Annabell N, Geso M (2014) Optimal energy for cell radiosensitivity enhancement by gold nanoparticles using synchrotron-based monoenergetic photon beams. *International journal of nanomedicine* 9: 2459
Rauschenberger L, Staar D, Thom K, Scharf C, Venz S, Homuth G, Schlüter R, Brandenburg LO, Ziegler P, Zimmermann U (2016) Exosomal particles secreted by prostate cancer cells are potent mRNA and protein vehicles for the interference of tumor and tumor environment. *The Prostate* 76: 409-424

Roa W, Zhang X, Guo L, Shaw A, Hu X, Xiong Y, Gulavita S, Patel S, Sun X, Chen J (2009a) Gold nanoparticle sensitize radiotherapy of prostate cancer cells by regulation of the cell cycle. *Nanotechnology* 20: 375101
Roa W, Zhang X, Guo L, Shaw A, Hu X, Xiong Y, Gulavita S, Patel S, Sun X, Chen J, Moore R, Xing JZ (2009b) Gold nanoparticle sensitize radiotherapy of prostate cancer cells by regulation of the cell cycle. *Nanotechnology* 20: 375101
Rodrigues BV, Leite NC, Cavalcanti B, da Silva NS, Marciano FR, Corat EJ, Webster TJ, Lobo AO (2016) Graphene oxide/multi-walled carbon nanotubes as nanofeatured scaffolds for the assisted deposition of nanohydroxyapatite: characterization and biological evaluation. *International journal of nanomedicine* 11: 2569-85
Roivainen A, Kahkonen E, Luoto P, Borkowski S, Hofmann B, Jambor I, Lehtio K, Rantala T, Rottmann A, Sipila H, Sparks R, Suilamo S, Tolvanen T, Valencia R, Minn H (2013) Plasma pharmacokinetics, whole-body distribution, metabolism, and radiation dosimetry of 68Ga bombesin antagonist BAY 86-7548 in healthy men. *Journal of nuclear medicine : official publication, Society of Nuclear Medicine* 54: 867-72
Roma-Rodrigues C, Fernandes AR, Baptista PV (2014) Exosome in tumour microenvironment: overview of the crosstalk between normal and cancer cells. *BioMed research international* 2014
Ruan Y, Yu W, Cheng F, Zhang X, Rao T, Xia Y, Larre S (2011) Comparison of quantum-dots- and fluorescein-isothiocyanate-based technology for detecting prostate-specific antigen expression in human prostate cancer. *IET nanobiotechnology / IET* 5: 47
Rybalov M, Ananias HJ, Hoving HD, van der Poel HG, Rosati S, de Jong IJ (2014) PSMA, EpCAM, VEGF and GRPR as imaging targets in locally recurrent prostate cancer after radiotherapy. *International journal of molecular sciences* 15: 6046-6061
Saad F, Fizazi K (2015) Androgen Deprivation Therapy and Secondary Hormone Therapy in the Management of Hormone-sensitive and Castration-resistant Prostate Cancer. *Urology* 86: 852-61
Safronov V, Sozontov E, Polikarpov M (2015) Magnetite nanoparticles for nonradionuclide brachytherapy. *Journal of applied crystallography* 48: 690-692
Saha GB (2012) *Physics and radiobiology of nuclear medicine*. Springer Science & Business Media,
Salata OV (2004) Applications of nanoparticles in biology and medicine. *Journal of nanobiotechnology* 2: 1
Salimi A, Kavosi B, Fathi F, Hallaj R (2013) Highly sensitive immunosensing of prostate-specific antigen based on ionic liquid-carbon nanotubes modified electrode: application as cancer biomarker for prostate biopsies. *Biosensors & bioelectronics* 42: 439-46
Sanfilippo NJ, Cooper BT (2014) Hypofractionated radiation therapy for prostate cancer: biologic and technical considerations. *American journal of clinical and experimental urology* 2: 286
Sanvicens N, Marco MP (2008) Multifunctional nanoparticles–properties and prospects for their use in human medicine. *Trends in biotechnology* 26: 425-433
Satpati D, Satpati A, Pamale Y, Kumar C, Sharma R, Sarma HD, Banerjee S (2016) 177 Lu-labeled carbon nanospheres: a new entry in the field of targeted radionanomedicine. *RSC Advances* 6: 50761-50769
Scaffidi JP, Gregas MK, Lauly B, Zhang Y, Vo-Dinh T (2011) Activity of psoralen-functionalized nanoscintillators against cancer cells upon X-ray excitation. *ACS Nano* 5: 4679-87
Schaue D, McBride WH (2015) Opportunities and challenges of radiotherapy for treating cancer. *Nature Reviews Clinical Oncology* 12: 527-540
Schaufele F, Carbonell X, Guerbadot M, Borngraeber S, Chapman MS, Ma AAK, Miner JN, Diamond MI (2005) The structural basis of androgen receptor activation: intramolecular and intermolecular amino–carboxy interactions. *Proceedings of the National Academy of Sciences of the United States of America* 102: 9802-9807

Scher HI, Beer TM, Higano CS, Anand A, Taplin M-E, Efstathiou E, Rathkopf D, Shelkey J, Evan YY, Alumkal J (2010) Antitumour activity of MDV3100 in castration-resistant prostate cancer: a phase 1–2 study. *The Lancet* 375: 1437-1446
Schröder FH, Hugosson J, Roobol MJ, Tammela TL, Ciatto S, Nelen V, Kwiatkowski M, Lujan M, Lilja H, Zappa M (2012) Prostate-cancer mortality at 11 years of follow-up. *New England Journal of Medicine* 366: 981-990
Scopinaro F, De Vincentis G, Varvarigou AD, Laurenti C, Iori F, Remediani S, Chiarini S, Stella S (2003) 99mTc-bombesin detects prostate cancer and invasion of pelvic lymph nodes. *Eur J Nucl Med Mol Imaging* 30: 1378-82
Shah M, Da Silva R, Gravekamp C, Libutti SK, Abraham T, Dadachova E (2015) Targeted radionuclide therapies for pancreatic cancer. *Cancer gene therapy* 22: 375-9
Shah RB, Mehra R, Chinnaiyan AM, Shen R, Ghosh D, Zhou M, MacVicar GR, Varambally S, Harwood J, Bismar TA (2004) Androgen-independent prostate cancer is a heterogeneous group of diseases lessons from a rapid autopsy program. *Cancer research* 64: 9209-9216
Sharifi N, Gulley JL, Dahut WL (2005) Androgen deprivation therapy for prostate cancer. *Jama* 294: 238-244
Sharma A, Hong S, Singh R, Jang J (2015) Single-walled carbon nanotube based transparent immunosensor for detection of a prostate cancer biomarker osteopontin. *Analytica chimica acta* 869: 68-73
Sharma A, Kakkar A (2015) Designing Dendrimer and Miktoarm Polymer Based Multi-Tasking Nanocarriers for Efficient Medical Therapy. *Molecules (Basel, Switzerland)* 20: 16987-7015
Sharma PA, Maheshwari R, Tekade M, Tekade RK (2015) Nanomaterial Based Approaches for the Diagnosis and Therapy of Cardiovascular Diseases. *Curr Pharm Des* 21: 4465-78
Shukla R, Chanda N, Zambre A, Upendran A, Katti K, Kulkarni RR, Nune SK, Casteel SW, Smith CJ, Vimal J (2012) Laminin receptor specific therapeutic gold nanoparticles (198AuNP-EGCg) show efficacy in treating prostate cancer. *Proceedings of the National Academy of Sciences* 109: 12426-12431
Siegel RL, Miller KD, Jemal A (2015) Cancer statistics, 2015. *CA: a cancer journal for clinicians* 65: 5-29
Silva PM, Lima AL, Silva BV, Coelho LC, Dutra RF, Correia MT (2016) Cratylia mollis lectin nanoelectrode for differential diagnostic of prostate cancer and benign prostatic hyperplasia based on label-free detection. *Biosensors & bioelectronics* 85: 171-7
Singh BR, Singh BN, Khan W, Singh HB, Naqvi AH (2012) ROS-mediated apoptotic cell death in prostate cancer LNCaP cells induced by biosurfactant stabilized CdS quantum dots. *Biomaterials* 33: 5753-67
Sinha N, Cifter G, Sajo E, Kumar R, Sridhar S, Nguyen PL, Cormack RA, Makrigiorgos GM, Ngwa W (2015) Brachytherapy Application With In Situ Dose Painting Administered by Gold Nanoparticle Eluters. *International Journal of Radiation Oncology*Biology*Physics* 91: 385-392
Sitharaman B (2016) *Nanobiomaterials handbook*. CRC Press,
Sk UH, Kojima C (2015) Dendrimers for theranostic applications. *Biomolecular concepts* 6: 205-17
Smith CL, Ackerly T, Best SP, Gagliardi F, Kie K, Little PJ, McCorkell G, Sale CA, Tsunei Y, Tominaga T, Volaric SS, Geso M (2015) Determination of dose enhancement caused by gold-nanoparticles irradiated with proton, X-rays (kV and MV) and electron beams, using alanine/EPR dosimeters. *Radiation Measurements* 82: 122-128
Soo Lee D (2016) Radionanomedicine. *European Journal of Nanomedicine* 8: 69-69
Srivastava A, Babu A, Filant J, Moxley KM, Ruskin R, Dhanasekaran D, Sood AK, McMeekin S, Ramesh R (2016) Exploitation of Exosomes as Nanocarriers for Gene-, Chemo-, and Immune-Therapy of Cancer. *Journal of biomedical nanotechnology* 12: 1159-73

Steichen SD, Caldorera-Moore M, Peppas NA (2013) A review of current nanoparticle and targeting moieties for the delivery of cancer therapeutics. *European journal of pharmaceutical sciences* 48: 416-427
Sterzing F, Kratochwil C, Fiedler H, Katayama S, Habl G, Kopka K, Afshar-Oromieh A, Debus J, Haberkorn U, Giesel FL (2016) (68)Ga-PSMA-11 PET/CT: a new technique with high potential for the radiotherapeutic management of prostate cancer patients. *Eur J Nucl Med Mol Imaging* 43: 34-41
Suburu J, Chen YQ (2012) Lipids and prostate cancer. *Prostaglandins & Other Lipid Mediators* 98: 1-10
Suchorska WM, Lach MS (2016) The role of exosomes in tumor progression and metastasis (Review). *Oncology reports* 35: 1237-1244
Sultana S, Khan MR, Kumar M, Kumar S, Ali M (2013) Nanoparticles-mediated drug delivery approaches for cancer targeting: a review. *Journal of drug targeting* 21: 107-125
Sun G, Xu J, Hagooly A, Rossin R, Li Z, Moore DA, Hawker CJ, Welch MJ, Wooley KL (2007) Strategies for optimized radiolabeling of nanoparticles for in vivo PET imaging. *Advanced Materials* 19: 3157-3162
Sun M, Hoffman D, Sundaresan G, Yang L, Lamichhane N, Zweit J (2012) Synthesis and characterization of intrinsically radiolabeled quantum dots for bimodal detection. *Am J Nucl Med Mol Imaging* 2: 122-135
Szabo Z, Mena E, Rowe SP, Plyku D, Nidal R, Eisenberger MA, Antonarakis ES, Fan H, Dannals RF, Chen Y, Mease RC, Vranesic M, Bhatnagar A, Sgouros G, Cho SY, Pomper MG (2015) Initial Evaluation of [(18)F]DCFPyL for Prostate-Specific Membrane Antigen (PSMA)-Targeted PET Imaging of Prostate Cancer. *Molecular imaging and biology : MIB : the official publication of the Academy of Molecular Imaging* 17: 565-74
Taylor LG, Canfield SE, Du XL (2009) Review of major adverse effects of androgen-deprivation therapy in men with prostate cancer. *Cancer* 115: 2388-2399
Thind A, Wilson C (2016) Exosomal miRNAs as cancer biomarkers and therapeutic targets. *Journal of extracellular vesicles* 5: 31292
Thorek DLJ, Ulmert D, Diop N-FM, Lupu ME, Doran MG, Huang R, Abou DS, Larson SM, Grimm J (2014) Non-invasive mapping of deep-tissue lymph nodes in live animals using a multimodal PET/MRI nanoparticle. *Nature communications* 5: 3097-3097
Tian CY, Zhao WW, Wang J, Xu JJ, Chen HY (2012) Amplified quenching of electrochemiluminescence from CdS sensitized TiO2 nanotubes by CdTe-carbon nanotube composite for detection of prostate protein antigen in serum. *The Analyst* 137: 3070-5
Tian T, Zhu YL, Hu FH, Wang YY, Huang NP, Xiao ZD (2013) Dynamics of exosome internalization and trafficking. *Journal of cellular physiology* 228: 1487-95
Ting G, Chang C-H, Wang H-E, Lee T-W (2010) Nanotargeted radionuclides for cancer nuclear imaging and internal radiotherapy. *BioMed Research International* 2010
Tran HV, Piro B, Reisberg S, Tran LD, Duc HT, Pham MC (2013) Label-free and reagentless electrochemical detection of microRNAs using a conducting polymer nanostructured by carbon nanotubes: application to prostate cancer biomarker miR-141. *Biosensors & bioelectronics* 49: 164-9
Tselis N, Tunn UW, Chatzikonstantinou G, Milickovic N, Baltas D, Ratka M, Zamboglou N (2013) High dose rate brachytherapy as monotherapy for localised prostate cancer: a hypofractionated two-implant approach in 351 consecutive patients. *Radiation oncology (London, England)* 8: 115
Valic MS, Zheng G (2016) Rethinking translational nanomedicine: insights from the 'bottom-up' design of the Porphysome for guiding the clinical development of imageable nanomaterials. *Current opinion in chemical biology* 33: 126-134

Vargas H, Grimm J, F. Donati O, Sala E, Hricak H (2015) Molecular imaging of prostate cancer: translating molecular biology approaches into the clinical realm. *Eur Radiol* 25: 1294-1302
Vargas HA, Wassberg C, Fox JJ, Wibmer A, Goldman DA, Kuk D, Gonen M, Larson SM, Morris MJ, Scher HI, Hricak H (2014) Bone Metastases in Castration-Resistant Prostate Cancer: Associations between Morphologic CT Patterns, Glycolytic Activity, and Androgen Receptor Expression on PET and Overall Survival. *Radiology* 271: 220-229
Wadosky KM, Koochekpour S (2016) Molecular mechanisms underlying resistance to androgen deprivation therapy in prostate cancer. *Oncotarget*
Wailes EM, Levi-Polyachenko NH (2016) Multi-walled nanotubes for cellular reprogramming of cancer. *Nanomedicine* 12: 955-63
Walker KA, Morgan C, Doak SH, Dunstan PR (2012) Quantum dots for multiplexed detection and characterisation of prostate cancer cells using a scanning near-field optical microscope. *PloS one* 7: e31592
Wang J, Sefah K, Altman MB, Chen T, You M, Zhao Z, Huang CZ, Tan W (2013) Aptamer-conjugated nanorods for targeted photothermal therapy of prostate cancer stem cells. *Chemistry, an Asian journal* 8: 2417-22
Wang L, Zhang M, Tan K, Guo Y, Tong H, Fan X, Fang K, Li R (2014) Preparation of nanobubbles carrying androgen receptor siRNA and their inhibitory effects on androgen-independent prostate cancer when combined with ultrasonic irradiation. *PloS one* 9: e96586
Wang X, Yang L, Chen ZG, Shin DM (2008) Application of nanotechnology in cancer therapy and imaging. *CA: a cancer journal for clinicians* 58: 97-110
Washington CM, Leaver DT (2015) *Principles and practice of radiation therapy*. Elsevier Health Sciences,
Weineisen M, Schottelius M, Simecek J, Baum RP, Yildiz A, Beykan S, Kulkarni HR, Lassmann M, Klette I, Eiber M (2015) 68Ga-and 177Lu-labeled PSMA I&T: optimization of a PSMA-targeted theranostic concept and first proof-of-concept human studies. *Journal of Nuclear Medicine* 56: 1169-1176
Wendler F, Favicchio R, Simon T, Alifrangis C, Stebbing J, Giamas G (2016) Extracellular vesicles swarm the cancer microenvironment: from tumor-stroma communication to drug intervention. *Oncogene*
Wilbur DS, Chyan M-K, Hamlin D, Balkin E (2012) In vivo comparison of two anti-PSMA mAb Fab' conjugates containing branched-chain PEG derivatives with Fab' and F(ab')2. *J NUCL MED MEETING ABSTRACTS* 53: 1545-
Wolfe T, Chatterjee D, Lee J, Grant JD, Bhattarai S, Tailor R, Goodrich G, Nicolucci P, Krishnan S (2015) Targeted gold nanoparticles enhance sensitization of prostate tumors to megavoltage radiation therapy in vivo. *Nanomedicine: Nanotechnology, Biology and Medicine* 11: 1277-1283
Wong YNS, Ferraldeschi R, Attard G, de Bono J (2014) Evolution of androgen receptor targeted therapy for advanced prostate cancer. *Nat Rev Clin Oncol* 11: 365-376
Wu D, Liu Y, Wang Y, Hu L, Ma H, Wang G, Wei Q (2016) Label-free Electrochemiluminescent Immunosensor for Detection of Prostate Specific Antigen based on Aminated Graphene Quantum Dots and Carboxyl Graphene Quantum Dots. *Scientific reports* 6: 20511
Xie J, Liu G, Eden HS, Ai H, Chen X (2011) Surface-engineered magnetic nanoparticle platforms for cancer imaging and therapy. *Accounts of chemical research* 44: 883-92
Yaghini E, Seifalian AM, MacRobert AJ (2009) Quantum dots and their potential biomedical applications in photosensitization for photodynamic therapy.
Yang BY, Moon SH, Seelam SR, Jeon MJ, Lee YS, Lee DS, Chung JK, Kim YI, Jeong JM (2015) Development of a multimodal imaging probe by encapsulating iron oxide nanoparticles with functionalized amphiphiles for lymph node imaging. *Nanomedicine (London, England)* 10: 1899-910

Yang H Targeted nanosystems: Advances in targeted dendrimers for cancer therapy. *Nanomedicine: Nanotechnology, Biology and Medicine* 12: 309-316
Yang H (2016) Targeted nanosystems: Advances in targeted dendrimers for cancer therapy. *Nanomedicine* 12: 309-16
Yang J, Xie S-X, Huang Y, Ling M, Liu J, Ran Y, Wang Y, Thrasher JB, Berkland C, Li B (2012) Prostate-targeted biodegradable nanoparticles loaded with androgen receptor silencing constructs eradicate xenograft tumors in mice. *Nanomedicine* 7: 1297-1309
Yang L, Sundaresan G, Sun M, Jose P, Hoffman D, McDonagh PR, Lamichhane N, Cutler CS, Perez JM, Zweit J (2013) Intrinsically radiolabeled multifunctional cerium oxide nanoparticles for in vivo studies. *Journal of Materials Chemistry B* 1: 1421-1431
Yao H, Qiu H, Shao Z, Wang G, Wang J, Yao Y, Xin Y, Zhou M, Wang AZ, Zhang L Nanoparticle formulation of small DNA molecules, Dbait, improves the sensitivity of hormone-independent prostate cancer to radiotherapy. *Nanomedicine: Nanotechnology, Biology and Medicine* 12: 2261-2271
Yeh CY, Hsiao JK, Wang YP, Lan CH, Wu HC (2016) Peptide-conjugated nanoparticles for targeted imaging and therapy of prostate cancer. *Biomaterials* 99: 1-15
YeoHeung Y, Zhongyun D, Vesselin NS, Mark JS (2007) Electrochemical impedance measurement of prostate cancer cells using carbon nanotube array electrodes in a microfluidic channel. *Nanotechnology* 18: 465505
You JY, Lee HJ, Hwang SI, Bae YJ, Kim H, Hong H, Choe G (2015) Value of T1/T2-weighted magnetic resonance imaging registration to reduce the postbiopsy hemorrhage effect for prostate cancer localization. *Prostate international* 3: 80-6
Yuan J, You Y, Lu X, Muzik O, Oupicky D, Peng F (2006) Synthesis and characterization of nano-sized Poly(APMA)-DOTA-Copper conjugate for radionuclide cancer therapy: Assessment of stability and distribution in vivo by microPET imaging. *Journal of Nuclear Medicine* 47: 419P
Zejnullahu K, Arevalo MG, Ryan CJ, Aggarwal R (2016) Approaches to minimize castration in the treatment of advanced prostate cancer. *Urologic oncology* 34: 368-74
Zhang W, Hubbard A, Brunhoeber P, Wang Y, Tang L (2013) Automated multiplexing quantum dots in situ hybridization assay for simultaneous detection of ERG and PTEN gene status in prostate cancer. *The Journal of molecular diagnostics : JMD* 15: 754-64
Zhang W, Meng Y, Liu N, Wen X-F, Yang T (2015) Insights into chemoresistance of prostate cancer. *International journal of biological sciences* 11: 1160
Zhang X, Pei Z, Chen J, Ji C, Xu J, Zhang X, Wang J (2016) Exosomes for Immunoregulation and Therapeutic Intervention in Cancer. *Journal of Cancer* 7: 1081-7
Zhang X, Xing JZ, Chen J, Ko L, Amanie J, Gulavita S, Pervez N, Yee D, Moore R, Roa W (2008) Enhanced radiation sensitivity in prostate cancer by gold-nanoparticles. *Clinical and investigative medicine Medecine clinique et experimentale* 31: E160-7
Zhang Y, Dai W, Liu F, Li L, Li M, Ge S, Yan M, Yu J (2013) Ultrasensitive electrochemiluminescent immunosensor based on dual signal amplification strategy of gold nanoparticles-dotted graphene composites and CdTe quantum dots coated silica nanoparticles. *Analytical and bioanalytical chemistry* 405: 4921-9
Zhao S, Wang W, Huang Y, Fu Y, Cheng Y (2016) Paclitaxel loaded human serum albumin nanoparticles stabilized with intermolecular disulfide bonds. *Nanomedicine: Nanotechnology, Biology and Medicine* 12: 533-534
Zukotynski K, Jadvar H, Capala J, Fahey F (2016) Targeted Radionuclide Therapy: Practical Applications and Future Prospects. *Biomarkers in Cancer* 8: 35-38

CHAPTER 5 : GENERAL DISCUSSION AND FUTURE DIRECTIONS

5.1 PSMA-SUPPRESSION IN NEPC

Mannweiler *et al*. reported that a direct correlation between histological parameters and PSMA could not be established; specifically in AdPC patients with distant metastasis *(Mannweiler, Amersdorfer et al., 2009)*. In this study, we report the possibility of PSMA suppression in high grades of CRPC. We further show that expression of the PSMA gene, *FOLH1*, inversely correlates with markers of NE differentiation. This data supports previous clinical reports showing a suppression of PSMA-targeted nuclear scans for NEPC patients *(Chakraborty et al., 2015, Tosoian et al., 2017a, Usmani et al., 2017)*. This mounts the possibility that portions of AdPC patients undergoing ARPI will transdifferentiate to NEPC and will subsequently fail to adequately uptake PSMA-targeted radiopharmaceuticals.

In vitro modeling of NE-differentiation of PC as a result of hormonal therapy by CSS-FBS treatment of LNCaP cell line has been extensively studied *(Nouri, Caradec et al., 2017, Sang, Hulsurkar et al., 2016, Zhang, Zheng et al., 2018)*. Mechanistically, Zang *et al*. *(Zhang, Kondrikov et al., 2003)* demonstrated CSS-FBS treatment activates MEK-ERK pathway and inhibition of MEK prevents NE-differentiation under CSS-FBS. Also, their work and many other studies demonstrated the *in vitro* nerite formation in LNCaP cell line could be associated with the expression of NSE as a NE-marker. Chang *et al*. *(Chang, Wang et al., 2014)* quantified the formed neurite lengths and displayed neurite lengths are proportional with the protein levels of AR. Or work demonstrated the suppression of PSMA in this previously proposed *in vitro* model of NEPC.

Clinical reports show the possibility of a false-positive uptake of PSMA-targeted radioligand after ARPI *(Hope, Truillet et al., 2017)* and a false-negative uptake of this

radioligand in NEPC *(Chakraborty et al., 2015, Tosoian et al., 2017a, Usmani et al., 2017)*. We previously reviewed the available preclinical evidence justifying molecular backgrounds of a false-positive uptake of PSMA-targeted radioligand after ARPI *(Bakht, Oh et al., 2017b)*. However, there is a lack of preclinical evidence for the reported false-negative uptake of PSMA-targeted radioligand. The observed significant suppression of *FOLH1* expression in PDX models shown in this work are the first preclinical evidence validating false-negative uptake of PSMA-targeted radioligand in NEPC. The suggested second model of alteration of PSMA on Figure 2-12E best describes the progression of AdPC patients undergoing ARPI whom end up with NEPC.

There is literature to support that SSTR-targeted radioligands such as ^{68}Ga-DOTATOC or ^{68}Ga-DOTATATE could be valuable alternatives for PSMA-negative and non-hormone naïve patients. Usmani et al. compared ^{68}Ga-PSMA versus ^{68}Ga-DOTA NOC PET-CT in a 62-year old NEPC patient and reported that the NEPC tumor and its metastatic lesions have avid uptake of ^{68}Ga-DOTA NOC while the PSMA uptake was faint and inconclusive *(Usmani et al., 2017)*. Additionally, in a study on 12 patients with CRPC, ^{68}Ga-DOTA-TATE PET/CT is suggested for NEPC imaging and early detection of metastatic lymph node and blastic or lytic bone lesions *(Gofrit et al., 2017, Sheikhbahaei et al., 2017)*. In this study, we report an overexpression of *SSTR2* in NEPC that could potentially lead to overexpression of SSTR2 at the protein level and positivity in the uptake of SSTR-radioligand. Interestingly, Morichetti et al. reported a strong specific staining for SSTR2 in 20 cases of NEPC *(Morichetti, Mazzucchelli et al., 2010)*. We speculate that SSTR-radioligand might be a feasible tool to delineate PSMA-negative NEPC from the normal tissue while PSMA-negative NEPC is not detectable by PSA measurements or by

PSMA radiotracers. Future work to explore the role of SSTR2-targeted radionuclide therapy for the detection and/or management of NEPC is of high priority.

Two possible scenarios for a patient with a suppressed PSMA radio-ligand uptake after ARPI are illustrated on Figure 5-1. In an ideal condition, the PSMA radio-ligand should be able to delineate AdPC tumor and all metastatic lesions (Figure 5-1A); consequently, after therapy faint or a no PSMA radio-ligand uptake should be observed since ARPI suppresses the malignancy (Figure 5-1B). However, as a second possible scenario, we might face a high-grade NEPC with suppressed PSMA expression level (Figure 5-1C). In this case, SSTR2 radio-ligand might be able to delineate NEPC tumor and its metastatic lesions.

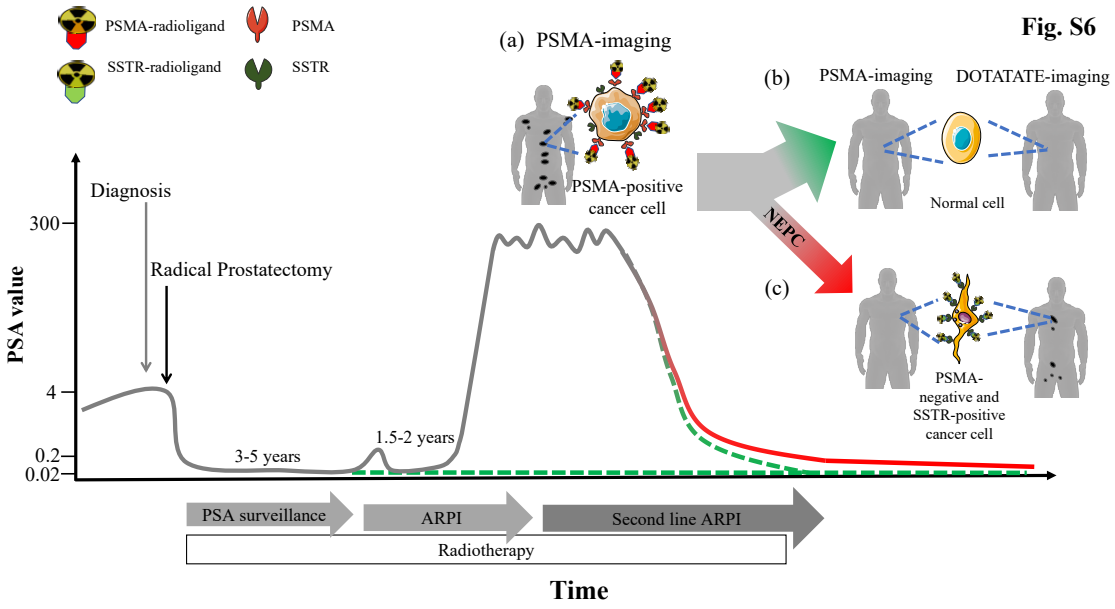

Figure 5-1 A schematic of two possible scenarios for a patient with a suppressed PSMA radio-ligand uptake after ARPI.

(a) Delineation tumor and metastatic lesions by PSMA radio-ligand before ARPI. (b) Ideal response to therapy and disappearance of the malignancy (High uptake of PSMA-radioligand and no/low DOTATATE-radioligand uptake). (c) Development of NECP with a suppressed PSMA expression level (No/low PSMA-radioligand uptake and high uptake for DOTATATE-radioligand). Some elements of this figure were produced using Servier Medical Art image bank (www.servier.com).

5.2 FDG-PET FOR NEPC SCREENING

The isoforms of GLUTs are structurally and functionally related proteins with different affinities to glucose. They are expressed in different cells based on the metabolic necessity for glucose uptake *(Qian, Wang et al., 2014)*. The elevation of glycolysis in NEPC has been previously reported *(Choi, Ettinger et al., 2018, Li, Cohen et al., 2016a)*. Despite overall contribution of GLUT in glucose metabolism, GLUT and HK family members could be associated with FDG uptake *(Avril, 2004, Yang et al., 2019)*. Like glucose, FDG is phosphorylated by HKs while their products, glucose-6-phosphate and FDG-6-phosphate, could have different levels of inhibition on HKs depending on their structure *(McKerrecher & Waring, 2013)*. Figure 5-2 represents structural domains of the

isoforms of human HK proteins *(Roberts & Miyamoto, 2015)*. Glucokinase lacks the N-terminus domain and cannot be inhibited by either glucose-6-phosphate or FDG-6-phosphate.

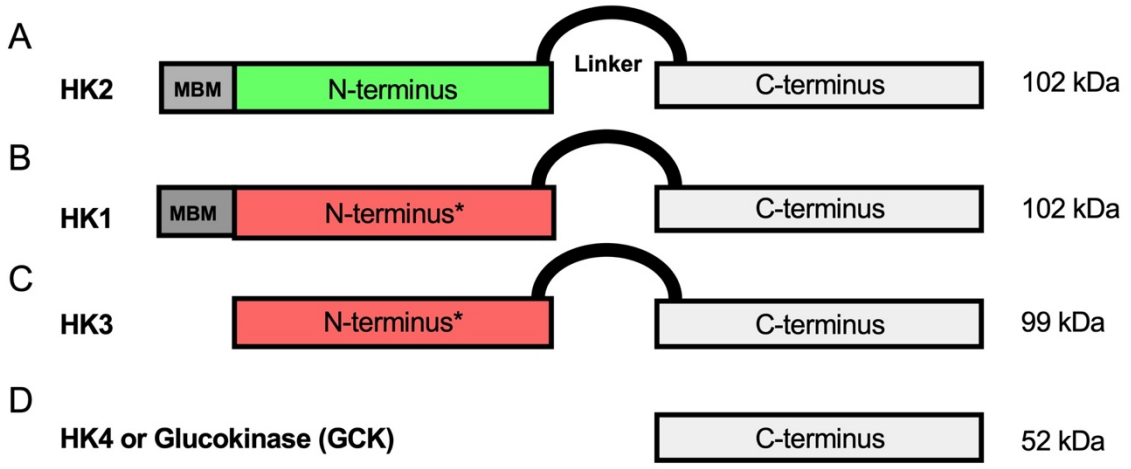

Figure 5-2 (A-D) Schematic of the structural domains of the isoforms of human HK proteins including HK1, HK2, HK3 and HK4 or glucokinase (GCK).

HK1, 2 and 3 are around 100 kDa while glucokinase is about 50 kDa. N-terminus and C-terminus domains have functional catalytic activity in HK2 while N-terminus domains in HK1 and 3 are non-functional. Mitochondrial binding motif (MBF) at the N-terminal domain can be seen only in HK2 and 1. *: non-functional domain. Adopted and modified with permission *(Roberts & Miyamoto, 2015)*.

GLUT11 is considered a high affinity glucose transporter and could be capable in elevation of glucose uptake while it is overexpressed *(Qian et al., 2014)*. McBrayer *et al*. *(McBrayer, Cheng et al., 2012)* evaluated the association of GLUT11 expression and FDG uptake in multiple myeloma. We have observed a significant elevation of GLUT11 expression in both NEPC and NELPC. Similarly, GLUT7 and 8 have high affinity to glucose *(Gonzalez-Menendez, Hevia et al., 2018)* and we observe their upregulation in samples with NEGS. Contrary to HK1-3, glucokinase which is known as a glucose sensor in pancreatic beta-cells, is not inhibited by its product glucose-6-phosphate but remains active while glucose is abundant *(McKerrecher & Waring, 2013, Roberts & Miyamoto, 2015)*. We can speculate that the apparent elevation of glucose uptake in NEPC or NELPC could be due to elevation of the expression of the aforementioned high affinity of GLUTs

(Figure 5-3). While our study provides functional support for this conclusion, it is also important to remember the complexity associated with a focus on gene expression of this vast family of glucose transport regulators. Avril's commentary *(Avril, 2004)* elaborates on the complex number of molecular, cellular, tissue and organ related variables regulating the resulting ^{18}F-FDG signal, all of which may provide inconsistencies between GLUT expression and the resulting ^{18}F-FDG signal.

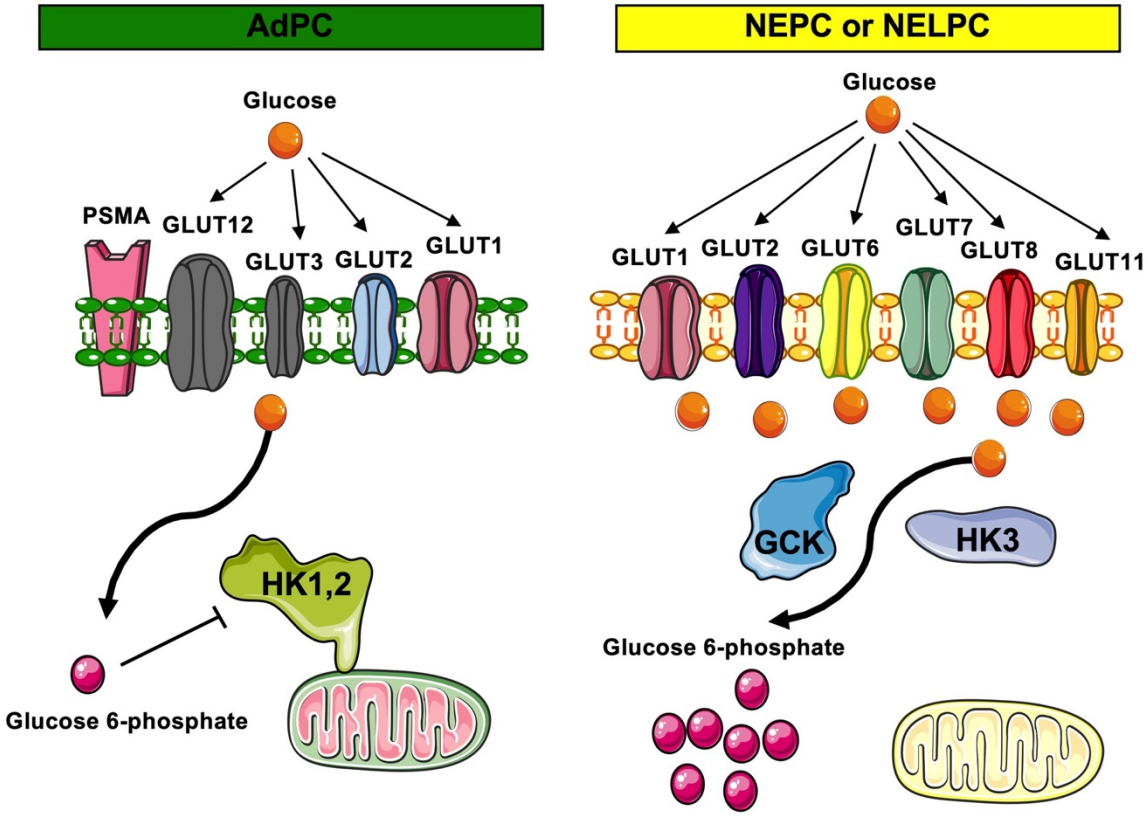

Figure 5-3 The differential expression of GLUT and HK genes favor higher glucose uptake in NEPC / NELPC in comparison with AdPC. Schematic shows the expression of high affinity GLUT genes found to be elevated in NEPC and NELPC and it could result in increased transport of glucose to the cytoplasm.
Drastic elevation of glucose sensor GCK in NEPC and NELPC is also demonstrated in this work. Some elements of this figure were produced using Servier Medical Art image bank (www.servier.com). GCK = Glucokinase

GLUT1 is a high affinity and basal glucose transporter expressed ubiquitously in human tissues. In hormone sensitive PC, GLUT1 gene expression is positively correlated with androgen

levels *(Vaz, Marques et al., 2016)*. Our work implies that GLUT1 expression has limited prognostic potential since it cannot estimate development or existence of low-AR phenotypes such as NEPC or DNPC phenotype. GLUT12 has been recently introduced as a downstream target of AR and its expression is tightly regulated by androgens *(White, Tsouko et al., 2018)*. Our data demonstrated the *SLC2A12* suppression is also a highly associated with development of PSMA-low and NE-high gene signature in mCRPC. This work shows *GCK*-enhanced expression and *SLC2A12* suppression at expression level correlate with the suppression in expression of PSMA, higher GS and shorter time to biochemical recurrence in NELPC.

Hope *et al*. *(Hope et al., 2019)* represented the detection rate of ^{68}Ga-PSMA-11 was estimated 0.94 for high- prostate-specific antigen (PSA) patients while this rate falls to 0.63 for low-PSA patients. Parida *at al*. *(Parida et al., 2018)* reported a NEPC patient with a low PSMA-radioligand uptake and a high FDG uptake. The identified low-PSA subclass of patients by Thang *et al*. *(Thang et al., 2018)* has similar imaging outcomes. The identification of this PSMA-low or discordant FDG-avid should be a high priory due to the apparent association with development of NEPC or DNPC.

5.3 ZEBRAFISH PC MODEL

For pre-clinical studies, the use of FDG-imaging in mice xenografts can be limited by several factors such as operating cost and short half-life of the radioactive substance and nonradioactive glucose probes, which are of particular interest *(Cheng et al., 2006)*. Also, the engraftment of tumors in mice can be challenging to establish and are time-consuming. This work demonstrates the feasibility of non-radioactive imaging of glucose uptake in PC xenografts using a zebrafish model as a rapid and cost-effective model.

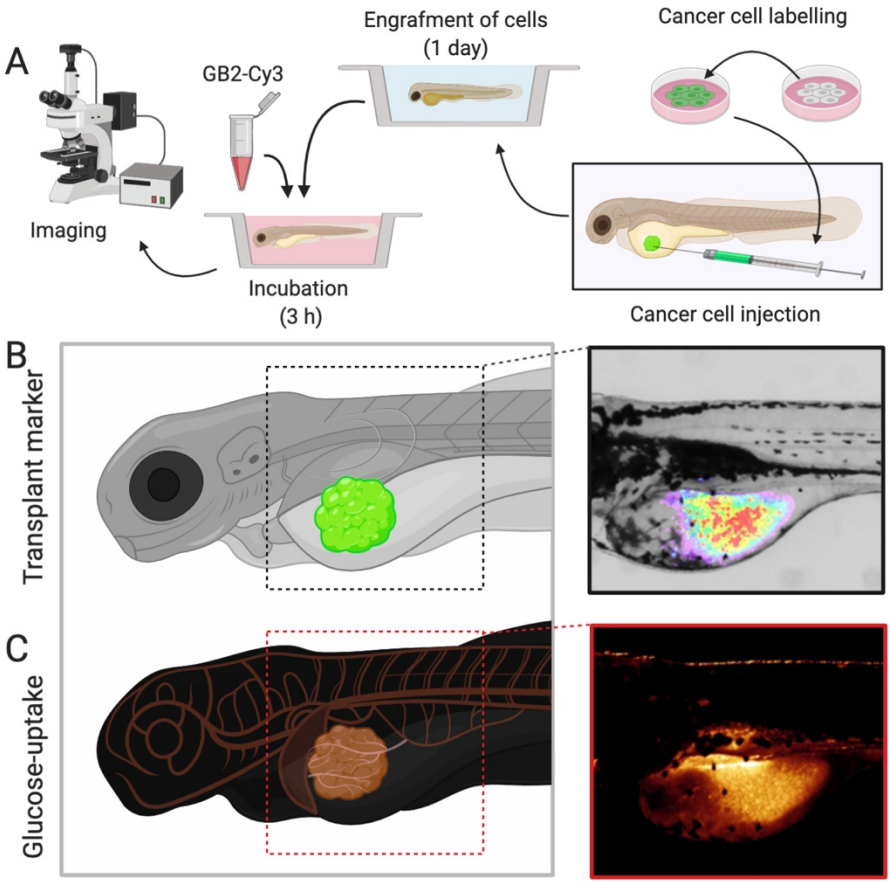

Figure 5-4 Embryo zebrafish model for non-radioactive in vivo imaging of glucose uptake.
(A) An schematic of the required steps for measurement of glucose uptake in engrafted cells. (B-C) The schematics and reprehensive images of zebrafish model of LNCaP.

5.4 FINAL CONCLUSIONS

We investigated whether the expression levels of glucose uptake-associated genes are correlated with development of NEGS and/or suppression of the PSMA gene. Data mining approaches, cell lines, mouse and zebrafish PDX models were used to demonstrate that GLUT and HK expression, specially *GCK* and *SCL2A12*, are associated with NEGS, PSMA-suppression and higher glucose uptake. This study supports the use of FDG-PET for imaging of low-PSMA PC tumors with NEGS.

5.5 REFERENCE

Avril N (2004) GLUT1 Expression in Tissue and 18F-FDG Uptake. *J Nucl Med* 45: 930-932

Bakht MK, Oh SW, Youn H, Cheon GJ, Kwak C, Kang KW (2017b) Influence of androgen deprivation therapy on the uptake of PSMA-targeted agents: emerging opportunities and challenges. *Nucl Med Mol Imaging (2010)* 51: 202-211

Chakraborty PS, Tripathi M, Agarwal KK, Kumar R, Vijay MK, Bal C (2015) Metastatic poorly differentiated prostatic carcinoma with neuroendocrine differentiation: negative on 68Ga-PSMA PET/CT. *Clinical nuclear medicine* 40: e163-166

Chang P-C, Wang T-Y, Chang Y-T, Chu C-Y, Lee C-L, Hsu H-W, Zhou T-A, Wu Z, Kim RH, Desai SJ, Liu S, Kung H-J (2014) Autophagy Pathway Is Required for IL-6 Induced Neuroendocrine Differentiation and Chemoresistance of Prostate Cancer LNCaP Cells. *PLOS ONE* 9: e88556

Cheng Z, Levi J, Xiong Z, Gheysens O, Keren S, Chen X, Gambhir SS (2006) Near-infrared fluorescent deoxyglucose analogue for tumor optical imaging in cell culture and living mice. *Bioconjugate chemistry* 17: 662-669

Choi SYC, Ettinger SL, Lin D, Xue H, Ci X, Nabavi N, Bell RH, Mo F, Gout PW, Fleshner NE (2018) Targeting MCT 4 to reduce lactic acid secretion and glycolysis for treatment of neuroendocrine prostate cancer. *Cancer Med*

Gofrit ON, Frank S, Meirovitz A, Nechushtan H, Orevi M (2017) PET/CT With 68Ga-DOTA-TATE for Diagnosis of Neuroendocrine: Differentiation in Patients With Castrate-Resistant Prostate Cancer. *Clinical nuclear medicine* 42: 1-6

Gonzalez-Menendez P, Hevia D, Mayo JC, Sainz RM (2018) The dark side of glucose transporters in prostate cancer: Are they a new feature to characterize carcinomas? *International journal of cancer* 142: 2414-2424

Hope TA, Goodman JZ, Allen IE, Calais J, Fendler WP, Carroll PR (2019) Meta-analysis of 68Ga-PSMA-11 PET accuracy for the detection of prostate cancer validated by histopathology. *J Nucl Med* 60: 786-793

Hope TA, Truillet C, Ehman EC, Afshar-Oromieh A, Aggarwal R, Ryan CJ, Carroll PR, Small EJ, Evans MJ (2017) 68Ga-PSMA-11 PET Imaging of Response to Androgen Receptor Inhibition: First Human Experience. *Journal of Nuclear Medicine* 58: 81-84

Li W, Cohen A, Sun Y, Squires J, Braas D, Graeber TG, Du L, Li G, Li Z, Xu X, Chen X, Huang J (2016a) The role of CD44 in glucose metabolism in prostatic small cell neuroendocrine carcinoma. *Mol Cancer Res* 14: 344-353

Mannweiler S, Amersdorfer P, Trajanoski S, Terrett JA, King D, Mehes G (2009) Heterogeneity of prostate-specific membrane antigen (PSMA) expression in prostate carcinoma with distant metastasis. *Pathol Oncol Res* 15: 167-72

McBrayer SK, Cheng JC, Singhal S, Krett NL, Rosen ST, Shanmugam M (2012) Multiple myeloma exhibits novel dependence on GLUT4, GLUT8, and GLUT11: implications for glucose transporter-directed therapy. *Blood* 119: 4686-4697

McKerrecher D, Waring MJ (2013) Chapter One - Property-Based Design in the Optimisation of Benzamide Glucokinase Activators: From Hit to Clinic. In *Prog Med Chem*, Lawton G, Witty DR (eds) pp 1-43. Elsevier

Morichetti D, Mazzucchelli R, Santinelli A, Stramazzotti D, Lopez-Beltran A, Scarpelli M, Bono A, Cheng L, Montironi R (2010) Immunohistochemical expression and localization of somatostatin receptor subtypes in prostate cancer with neuroendocrine differentiation. *International journal of immunopathology and pharmacology* 23: 511-522

Nouri M, Caradec J, Anne Lubik A, Li N, Hollier BG, Takhar M, Altimirano-Dimas M, Chen M, Roshan-Moniri M, Butler M, Lehman M, Bishop J, Truong S, Huang S-C, Cochrane D, Cox M, Collins C, Gleave M, Erho N, Alshalafa M et al. (2017) Therapy-induced developmental reprogramming of prostate cancer cells and acquired therapy resistance. *Oncotarget* 8

Parida GK, Tripathy S, Datta Gupta S, Singhal A, Kumar R, Bal C, Shamim SA (2018) Adenocarcinoma Prostate With Neuroendocrine Differentiation: Potential Utility of 18F-FDG PET/CT and 68Ga-DOTANOC PET/CT Over 68Ga-PSMA PET/CT. *Clinical nuclear medicine* 43: 248-249

Qian Y, Wang X, Chen X (2014) Inhibitors of glucose transport and glycolysis as novel anticancer therapeutics. *World J Transl Med* 3: 37-57

Roberts DJ, Miyamoto S (2015) Hexokinase II integrates energy metabolism and cellular protection: Akting on mitochondria and TORCing to autophagy. *Cell death and differentiation* 22: 364

Sang M, Hulsurkar M, Zhang X, Song H, Zheng D, Zhang Y, Li M, Xu J, Zhang S, Ittmann M (2016) GRK3 is a direct target of CREB activation and regulates neuroendocrine differentiation of prostate cancer cells. *Oncotarget* 7: 45171

Sheikhbahaei S, Afshar-Oromieh A, Eiber M, Solnes LB, Javadi MS, Ross AE, Pienta KJ, Allaf ME, Haberkorn U, Pomper MG, Gorin MA, Rowe SP (2017) Pearls and pitfalls in clinical interpretation of prostate-specific membrane antigen (PSMA)-targeted PET imaging. *European journal of nuclear medicine and molecular imaging* 44: 2117-2136

Thang SP, Violet J, Sandhu S, Iravani A, Akhurst T, Kong G, Ravi Kumar A, Murphy DG, Williams SG, Hicks RJ, Hofman MS (2018) Poor outcomes for patients with metastatic castration-resistant prostate cancer with low prostate-specific membrane antigen (PSMA) expression deemed ineligible for 177Lu-labelled PSMA radioligand therapy. *Eur Urol Oncol* in press

Tosoian JJ, Gorin MA, Rowe SP, Andreas D, Szabo Z, Pienta KJ, Pomper MG, Lotan TL, Ross AE (2017a) Correlation of PSMA-Targeted (18)F-DCFPyL PET/CT Findings With Immunohistochemical and Genomic Data in a Patient With Metastatic Neuroendocrine Prostate Cancer. *Clinical genitourinary cancer* 15: e65-e68

Usmani S, Ahmed N, Marafi F, Rasheed R, Amanguno HG, Al Kandari F (2017) Molecular Imaging in Neuroendocrine Differentiation of Prostate Cancer: 68Ga-PSMA Versus 68Ga-DOTA NOC PET-CT. *Clinical nuclear medicine* 42: 410-413

Vaz CV, Marques R, Alves MG, Oliveira PF, Cavaco JE, Maia CJ, Socorro S (2016) Androgens enhance the glycolytic metabolism and lactate export in prostate cancer cells by modulating the expression of GLUT1, GLUT3, PFK, LDH and MCT4 genes. *J Cancer Res Clin Oncol* 142: 5-16

White MA, Tsouko E, Lin C, Rajapakshe K, Spencer JM, Wilkenfeld SR, Vakili SS, Pulliam TL, Awad D, Nikolos F, Katreddy RR, Kaipparettu BA, Sreekumar A, Zhang X, Cheung E, Coarfa C, Frigo DE (2018) GLUT12 promotes prostate cancer cell growth and is regulated by androgens and CaMKK2 signaling. *Endocr Relat Cancer* 25: 453-469

Yang H, Zhong JT, Zhou SH, Han HM (2019) Roles of GLUT-1 and HK-II expression in the biological behavior of head and neck cancer. *Oncotarget* 10: 3066-3083

Zhang XQ, Kondrikov D, Yuan TC, Lin FF, Hansen J, Lin MF (2003) Receptor protein tyrosine phosphatase alpha signaling is involved in androgen depletion-induced neuroendocrine differentiation of androgen-sensitive LNCaP human prostate cancer cells. *Oncogene* 22: 6704-16

Zhang Y, Zheng D, Zhou T, Song H, Hulsurkar M, Su N, Liu Y, Wang Z, Shao L, Ittmann M, Gleave M, Han H, Xu F, Liao W, Wang H, Li W (2018) Androgen deprivation promotes neuroendocrine differentiation and angiogenesis through CREB-EZH2-TSP1 pathway in prostate cancers. *Nat Commun* 9: 4080-4080

APPENDICES

Appendix A

GB2-Cy3 Glucose Bioprobe Synthesis

Solvents were purchased from Caledon Laboratories (Caledon, Ontario), Sigma-Aldrich (Oakville, Ontario), or VWR Canada (Mississauga, Ontario). Other chemicals were purchased from Sigma-Aldrich, AK Scientific, Oakwood Chemicals, Alfa Aesar, or Acros Chemicals and were used without further purification unless otherwise noted. Anhydrous toluene, tetrahydrofuran (THF), diethyl ether, and *N*,*N*-dimethylformamide (DMF) were obtained from an Innovative Technology (Newburyport, United States) solvent purification system based on aluminum oxide columns. CH_2Cl_2, and acetonitrile were freshly distilled from CaH_2 prior to use. Purified water was obtained from a Millipore deionization system. All heated reactions were conducted using oil baths on IKA RET Basic stir plates equipped with a P1000 temperature probe. Thin layer chromatography was performed using EMD aluminum-backed silica 60 F254-coated plates and visualized using either UV-light (254 nm), $KMnO_4$, vanillin, Hanessian's stain, or Dragendorff's stain. Preparative TLC was done using glass-backed silica plates (Silicycle) of either 250, 500, 1000, or 2000 μm thickness depending on application. Column chromatography was carried out using standard flash technique with silica (Silicycle Siliaflash-P60, 230–400 mesh) under compressed air pressure. Standard workup procedure for all reactions undergoing an aqueous wash involved back extraction of every aqueous phase, drying of the combined organic phases with anhydrous magnesium sulfate, filtration either using vacuum and a sintered-glass frit or through a glass-wool plug using gravity, and concentration under reduced pressure on a rotary evaporator (Buchi or Synthware). ^1H Nuclear magnetic

resonance (NMR) spectra were obtained at 300 or 500 MHz, and ^{13}C NMR spectra were obtained at 75 or 125 MHz on Bruker instruments. NMR chemical shifts (δ) are reported in ppm and are calibrated against residual solvent signals of $CHCl_3$ (δ 7.26), DMSO-d_5 (δ 2.50) or methanol-d_3 (δ 3.31). HRMS analyses were conducted on a Waters XEVO G2-XS TOF instrument with an ASAP probe in CI mode.

Compound (100): (2-bromoethyl)-D-glucoside

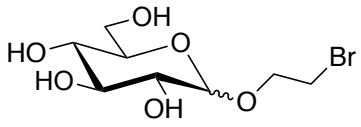

To a solution of glucose (5 g, 27.75 mmol) in 2-bromoethanol (30 mL, 0.417 mol) was added Dowex 50WX8-400 hydrogen form ion-exchange resin (5 g; the resin was washed with MeOH before use) and the reaction mixture was refluxed at 70 °C for 16 h and the reaction completion was monitored by TLC (2:1, ethyl acetate: hexanes). The reaction mixture was filtered to remove the resin, poured into methanol (10 mL) and dried ($MgSO_4$). The resulting solution was filtered and concentrated under reduced pressure. After purification of the glycosylated compound by silica gel flash column chromatography (1:1, ethyl acetate: hexanes), the desired compound was obtained as a mixture of α and β anomers (6.24 g. 78% yield). The analytical data were consistent with the literature values *(Lee et al., 2011)*.

Compound (101): (2-Bromoethyl)-2,3,4,6-tetra-*O*-benzoyl-α-D-glucoside

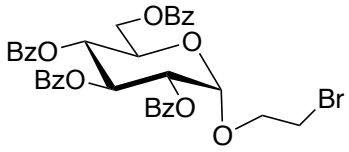

Compound 100 (1.89 g, 6.58 mmol) was dissolved in a mixture of pyridine (40 mL) and 4-DMAP (81 mg, 0.66 mmol) at 0 °C. Benzoyl chloride (6.1 mL, 53 mmol) was then added dropwise and the resulting mixture was allowed to warm to room temperature with stirring for 16 h. The mixture was quenched by the addition of methanol (10 mL) and subsequently extracted with ethyl acetate (3 × 20 mL); the combined organic extracts were washed with 1 M HCl (2 × 10 mL), saturated sodium bicarbonate (1 × 10 mL), and brine (1 × 10 mL). The organic layer was dried ($MgSO_4$), filtered and the solvent removed under reduced pressure. The resulting oil was purified using silica-gel chromatography (3:1 hexanes/ethyl acetate) to give **compound 101** (3.4 g, 74% yield). The analytical data were consistent with the literature values *(Lee et al., 2011)*.

Compound (102): [2-(*N*-Boc-piperazynoethyl)]-2,3,4,6-tetra-*O*-benzoyl-α-D-glucoside

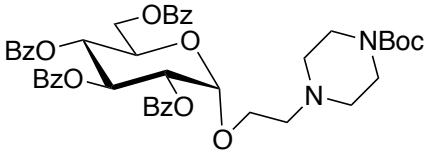

To a solution of **Compound 101** (1 g, 1.42 mmol) in 15 mL anhydrous DMF was added *N*-Boc-piperazine (529 mg, 2.84 mmol), potassium iodide (426 mg, 2.84 mmol) and Et_3N (593 μL, 4.26 mmol), and the resultant mixture was stirred at 80 °C for 10 h. After the reaction was complete, as monitored by TLC, the solution was diluted with water (10 mL),

extracted with ethyl acetate (3 × 20mL) and the combined organic layers washed with brine (1 × 20 mL). The organic layer was dried ($MgSO_4$) and concentrated under reduced pressure. The desired product was purified by silica-gel chromatography (95:3:2, $CHCl_3$: EtOH: Et_3N) to furnish a light yellow crystalline powder (680 mg, 59% yield). The analytical data was consistent with the literature values *(Lee et al., 2011)*.

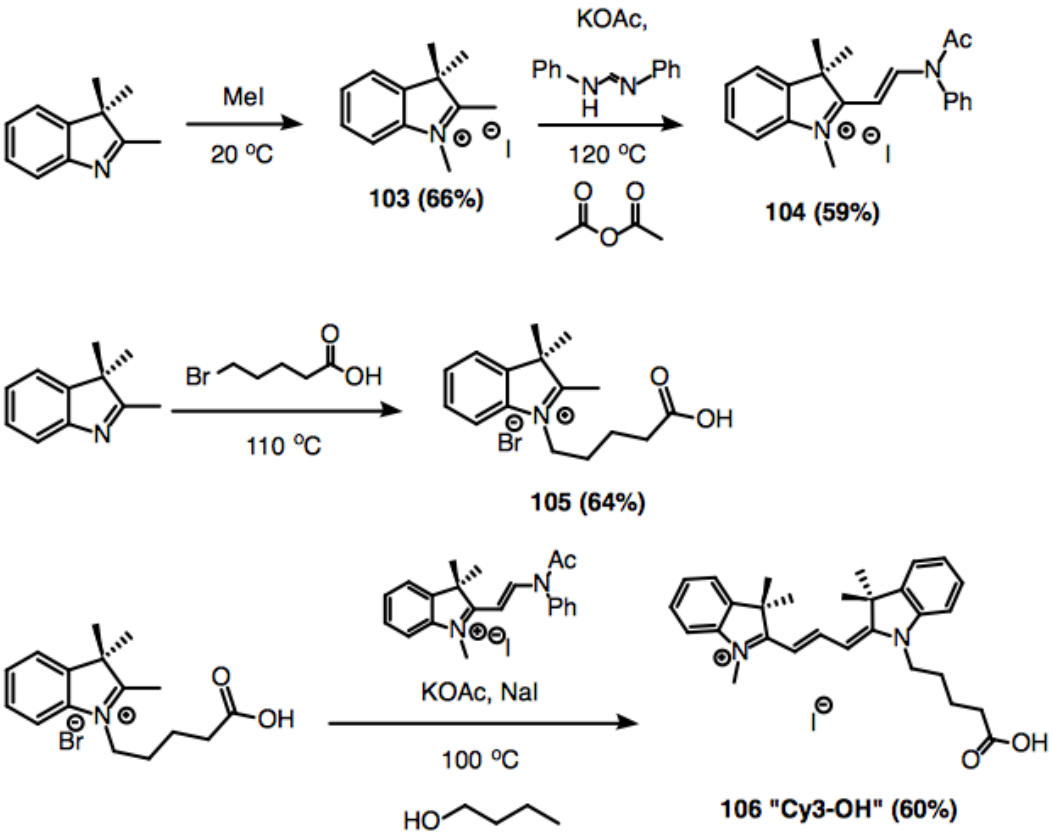

Scheme S1. Overview of the synthesis of the conjugatable dye Cy3-OH.

Compound (103): 1,2,3,3-tetramethyl-3*H*-indolium iodide

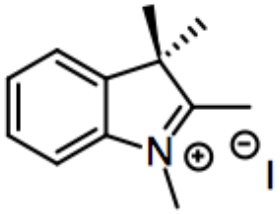

To a 0.3 M solution of 2,3,3-trimethylindolenine (5 mL, 31.15 mmol) in MeCN (104 mL), was added iodomethane (2.23 mL, 37.38 mmol) and the reaction was stirred at room temperature for 16 h, resulting in a pale pink precipitate. The precipitate was filtered and rinsed with Et_2O (3 × 10 mL) to afford compound **103** (5.1 g, 54% yield). The analytical data were consistent with the literature.

Compound (104): (*E*)-1,3,3-trimethyl-2-(2-(*N*-phenylacetamido)vinyl)-3*H*-indolium iodide

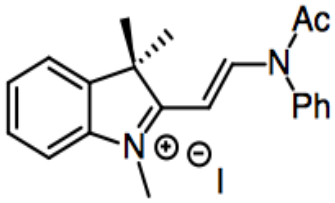

As per reference *(Korbel et al., 2001)*: To 1,2,3,3-tetramethyl-3*H*-indolium iodide, **103**, (3 g, 9.96 mmol), *N*,*N*′-diphenylformamidine (2.44 g, 12.45 mmol), and potassium acetate (98 mg, 0.996 mmol) was added 22.5 mL acetic anhydride and the mixture was heated for 5 h at 120 °C. The reaction was then allowed to cool to room temperature and the red precipitate was collected by filtration. The precipitate was washed repeatedly with Et_2O until the filtrate was colorless providing compound **104** (2.7 g, 59%). $R_f = 0.81$ (DCM : MeOH = 4 : 1). The ^{1}H NMR was consistent with the literature: ^{1}H-NMR (500 MHz, $CDCl_3$, 23 °C) δ 9.19-9.16 (d, *J* = 14.2 Hz, 1H); 3.86 (s, 3H); 2.11 (s, 3H); 1.83 (s, 6H) ppm *(Korbel et al., 2001)*.

Compound (105): 1-(4-Carboxybutyl)-2,3,3-trimethyl-3*H*-indolium bromide

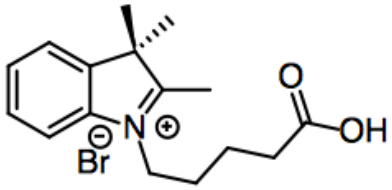

As per reference *(Korbel et al., 2001)*: To 5-bromovaleric acid (4.74 g, 26.17 mmol) was added 2,3,3-trimethylindolenine (4 mL, 24.92 mmol) and the neat reaction was stirred for 20 h at 110 °C. The reaction completion was determined when the solution had become a dark red solid and would no longer stir. The crude solid was ground up with a pestle and mortar to create a fine powder. The powder was placed on top of a filter paper in a Buchner funnel and was rinsed with boiling EtOAc (6 × 30 mL), boiling acetone (2 × 30 mL), and boiling acetone (2 × 90 mL) to yield compound **105** (5.43 g, 64%) as an off-white, pink powder. R_f = 0.12 (DCM/MeOH = 3:1). The ^{1}H NMR was consistent with the literature: ^{1}H NMR (500 MHz, CD_3OD + 1 drop D_2O, 23 °C) 7.90-7.87 (m, 1H); 7.78-7.75 (m, 1H); 7.67-7.63 (m, 2H); 4.56-4.52 (t, *J* = 7.7 Hz, 2H); 2.44-2.40 (t, *J* = 7.0 Hz, 2H); 2.04-1.96 (m, 2H); 1.80-1.72 (m, 2H); 1.61 (s, 6H) ppm *(Korbel et al., 2001)*.

Compound (106): 1-[(4″-(1″-Carboxybutyl))]-1′,3,3,3′,3′-pentamethyl-indocarbocyanine iodide, "Cy3-OH," *(Korbel et al., 2001)*

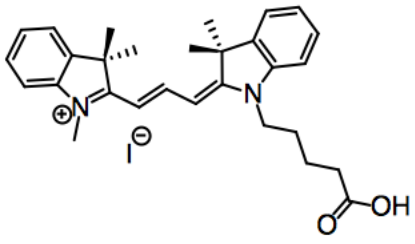

As per reference *(Korbel et al., 2001)*: To a flame-dried flask containing **104** (0.73 g, 1.59 mmol), **105** (0.54 g, 1.59 mmol), and potassium acetate (0.156 g, 1.905 mmol) was added anhydrous 1-butanol under a nitrogen atmosphere *(Korbel et al., 2001)*. The solution was stirred at 100 °C for 1.5 h. NaI

(4.58 g, 30.53 mmol) was then added to the flask and the reaction was stirred at 100 °C for a further 1 h. The reaction was cooled to room temperature and a precipitate formed overnight. The precipitate was filtered using a Buchner funnel and then rinsed repeatedly using Et_2O until the filtrate was colorless. The precipitate was collected and dissolved in DCM to give a dark purple solution. The crude mixture was purified by silica-gel flash column chromatography using a gradient elution starting at 9:1 DCM/MeOH (v/v) to 4:1 DCM/MeOH (v/v) to give the title compound **106** (543 mg, 60% yield). R_f = 0.66 (4:1 DCM/MeOH). λ_{max} 546 nm.[27] The ^{1}H NMR was consistent with the literature ^{1}H NMR (500 MHz, $CDCl_3$, 23 °C) δ 8.34-8.27 (dd, *J* = 14, 13 Hz, 1H); 7.35-7.29 (m, 4H); 7.22-7.16 (m, 2H); 7.11-7.07 (m, 2H); 6.78 (dd, *J* = 14 Hz, J = 14 Hz, 2H); 4.13 (bt, 2H); 3.71 (s, 3H); 2.47 (bt, 2H); 1.85 (m, 4H); 1.65 (s, 6H).

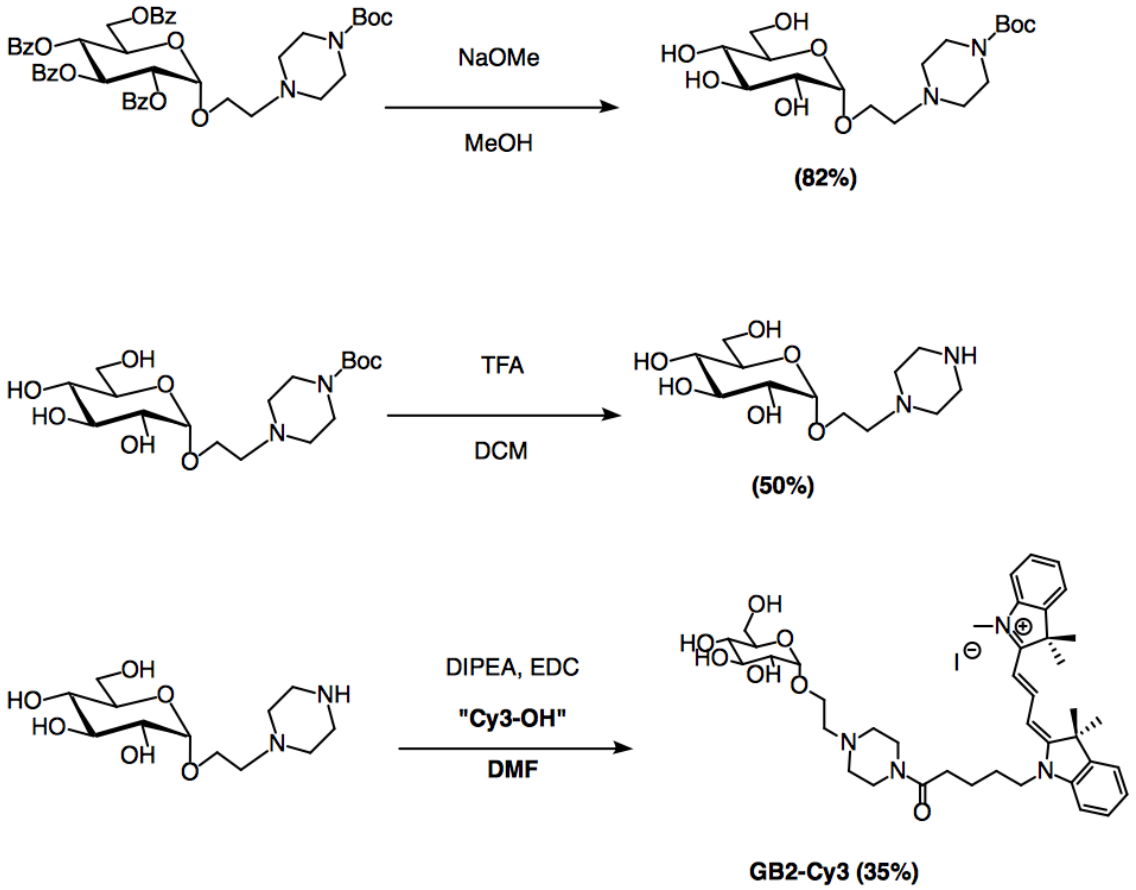

Scheme S2. Synthetic strategy for the preparation of GB2-Cy3

Compound (107): *Tert*-butyl-4-(2-(((2*S*,3*R*,4*S*,5*S*,6*R*)-3,4,5-trihydroxy-6-(hydroxymethyl)tetrahydro-2*H*-pyran-2-yl)oxy)ethyl)piperazine-1-carboxylate

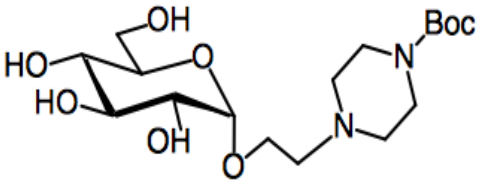

As per reference *(Park et al., 2007)*: To a solution of **104** (66.4 mg, 0.0821 mmol) in MeOH (3.3 mL) was added MeONa (~0.5 M in MeOH, 1.22 mL, 0.611 mmol) and the reaction completion was determined by TLC (100% MeOH). After the reaction was complete, the mixture was neutralized with Dowex 50WX8-400 hydrogen form ion-exchange resin (1

scoop the size of a pea), and then concentrated under reduced pressure. The residue was dissolved in a minimal amount of MeOH and the methyl benzoate ester was removed using a silica plug (25 mL SiO_2) washed with three 25 mL portions of Et_2O. Between each Et_2O portion, the filtrate was monitored by TLC to ensure only the methyl benzoate was being eluted (R_f = 0.9 to 1.0, 100% Et_2O). Unlike reference *(Park et al., 2007)*, the compound was isolated. The desired compound, **107,** was then eluted using MeOH (25 mL) and the solvent removed under reduced pressure (26.4 mg, 82% yield). The ^1H NMR was consistent with the expected spectrum *(Park et al., 2007)*.

Compound (108): (2*R*,3*S*,4*S*,5*R*,6*S*)-2-(hydroxymethyl)-6-(2-(piperazin-1-yl)ethoxy)tetrahydro-2*H*-pyran-3,4,5-triol *(Park et al., 2007)*.

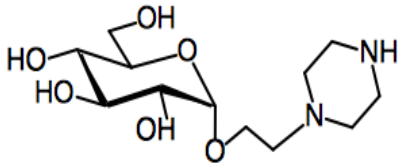

As per reference *(Park et al., 2007)*: 1:1 Trifluoroacetic acid (5.5 mL, excess) in DCM (5.5 mL) was added to compound **107** (50 mg, 0.1274 mmol) for 1 h followed by evaporation and purging with nitrogen. Unlike reference *(Park et al., 2007)*, the compound was isolated. The resulting residue was washed with toluene (3 × 5 mL) and decanted to remove any residual TFA. Any residual toluene was removed under reduced pressure to give compound **108** (18.6 mg, 50% yield). The ^1H NMR was consistent with the expected spectrum *(Park et al., 2007)*.

Compound (109): GB2-Cy3

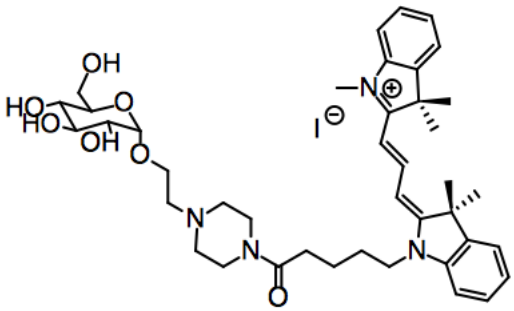

As per reference *(Lee et al., 2011)* with modifications: Compound **108** (20 mg, 0.0684 mmol) in DMF (300 µL) was slightly basified with DIPEA (20 µL) and Cy3-OH (**106**) (30.3 mg, 0.0684 mmol) and EDC (7 mg, 0.046 mmol) added as a solution in DMF (50 µL). The reaction mixture was stirred at room temperature for 2 h and the reaction was monitored by TLC. The resulting solution was purified by prep high performance liquid chromatography (HPLC) and the elution protocol is as listed: 1) 95% eluent A and 5% eluent B for 5 min, 2) linear gradient to 60% eluent A (40% B) over 4 min, 3) linear gradient to 50% eluent A (50% B) over 10 min, 4) linear gradient to 5% eluent A (95% B) over 10 min, 5) linear gradient to 0% eluent A (100% B) over 5 min, 6) constant flow with 0% eluent A (100% B) for 10 min, and 7) linear gradient to 95% eluent A (5% B) over 10 min for regeneration and washing of the column. Retention time = 12 min, scanning for a λ_{max} 546 nm to give **GB2-Cy3 (109)** (17 mg, 35% yield). The ^{1}H NMR was consistent with the literature: ^{1}H NMR (500 MHz, CD_3OD) δ 8.55 (t, *J* = 13.5 Hz, 1H), 7.54 (d, *J* = 7.5 Hz, 2H), 7.47–7.30 (m, 6H), 6.45 (dd, *J* = 13.4, 9.0 Hz, 2H), 4.20–4.17 (m, 2H), 4.08–4.05 (m, 1H), 3.83–3.80 (m, 3H), 3.67 (s, 3H) 3.63–3.42 (m, 12H), 2.57–2.54 (m, 2H), 1.97–1.79 (m, 6H), 1.78 (s, 6H), 1.77 (s, 6H) ppm *(Lee et al., 2011)*.

NMR spectrum of compound 101-106 are presented on Supplemental Figs. 16-22. HPLC spectrum of GB2-Cy3 is illustrated onAppendix Figure 1 to Appendix Figure 8.

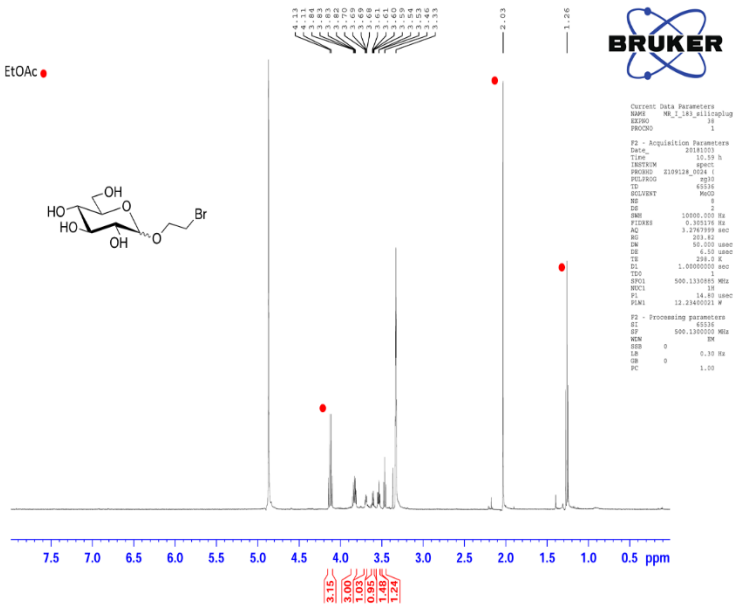

Appendix Figure 1 ^{1}H NMR spectrum of functionalized glucose (compound 100) with a minimum of 85% α-anomer.

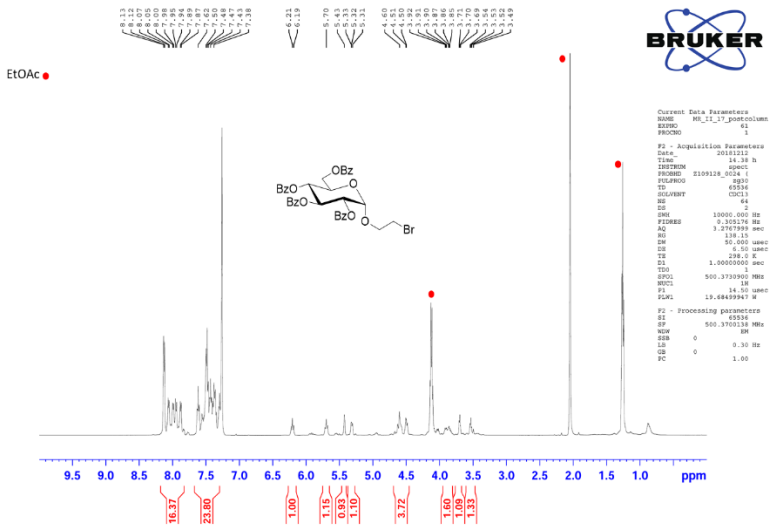

Appendix Figure 2 ^{1}H NMR spectrum of protected functionalized glucose (compound 101).

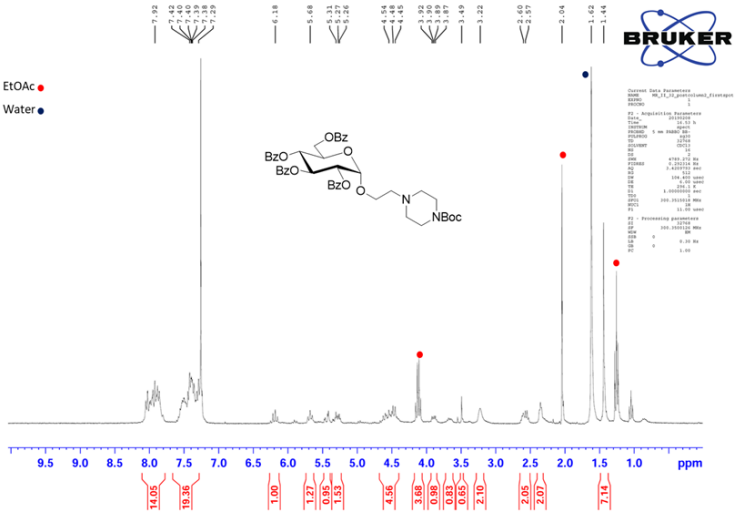

Appendix Figure 3 ^{1}H NMR spectrum of piperazine-functionalized glucose (compound 102).

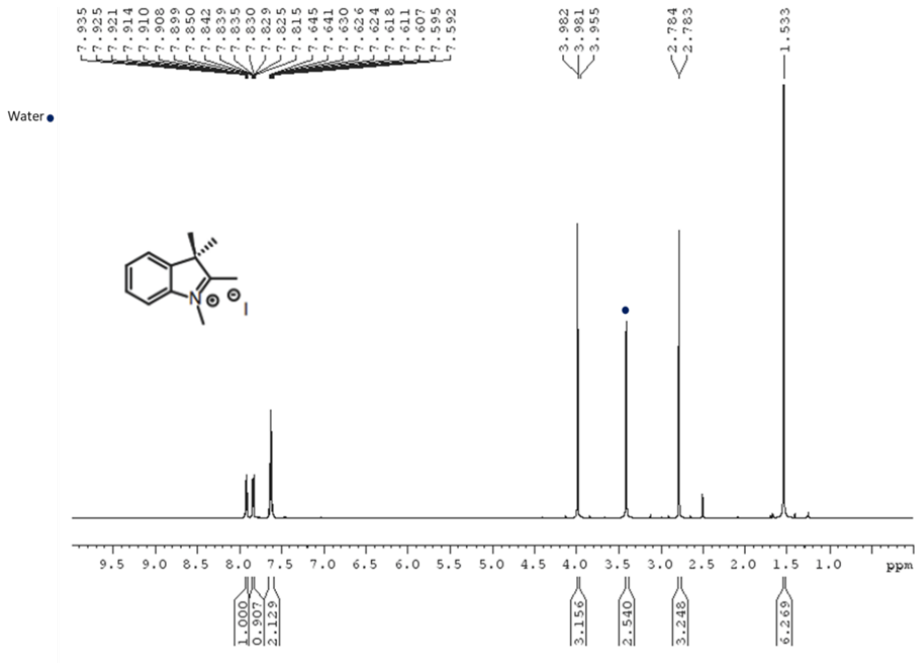

Appendix Figure 4 ^{1}H NMR spectrum of indolium salt (compound 103).

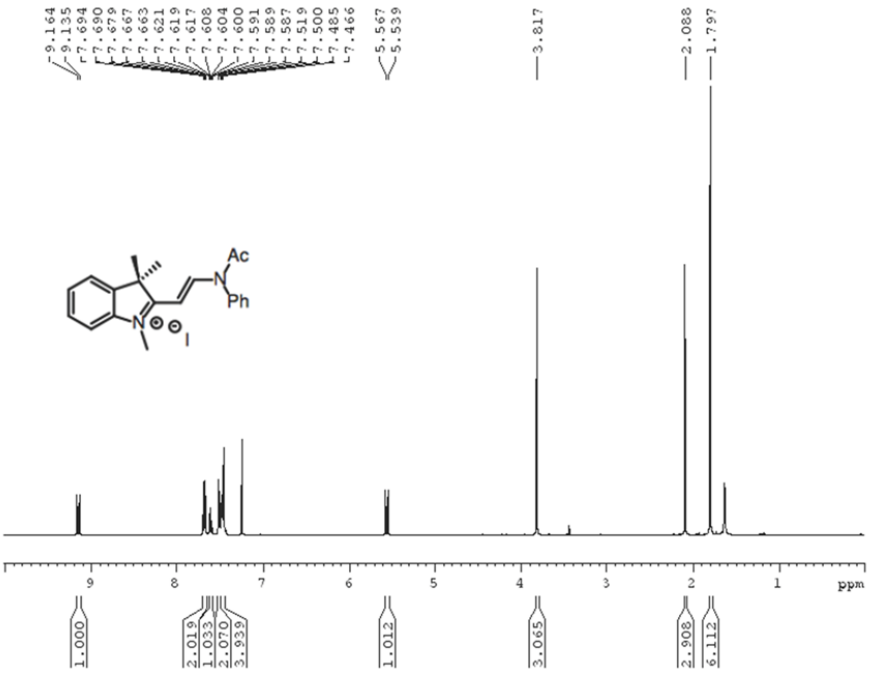

Appendix Figure 5 ^{1}H NMR spectrum of acetamide-functionalized indolium salt (compound 104).

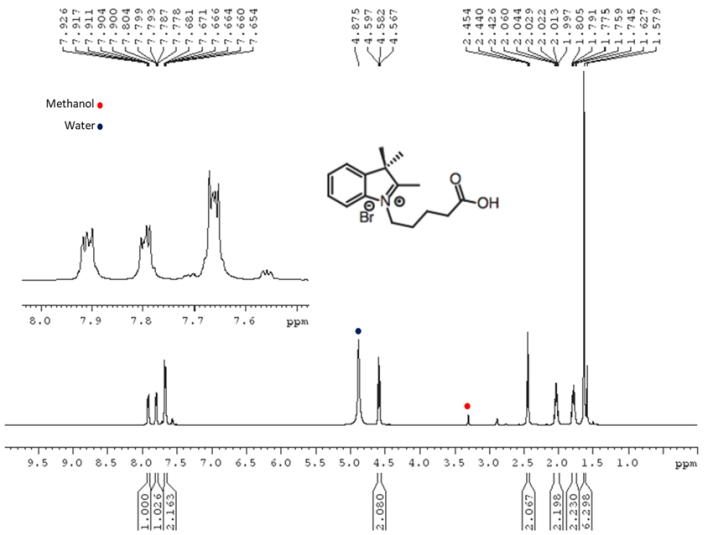

Appendix Figure 6 ^{1}H NMR spectrum of carboxylate-functionalized indolium salt (compound 105).

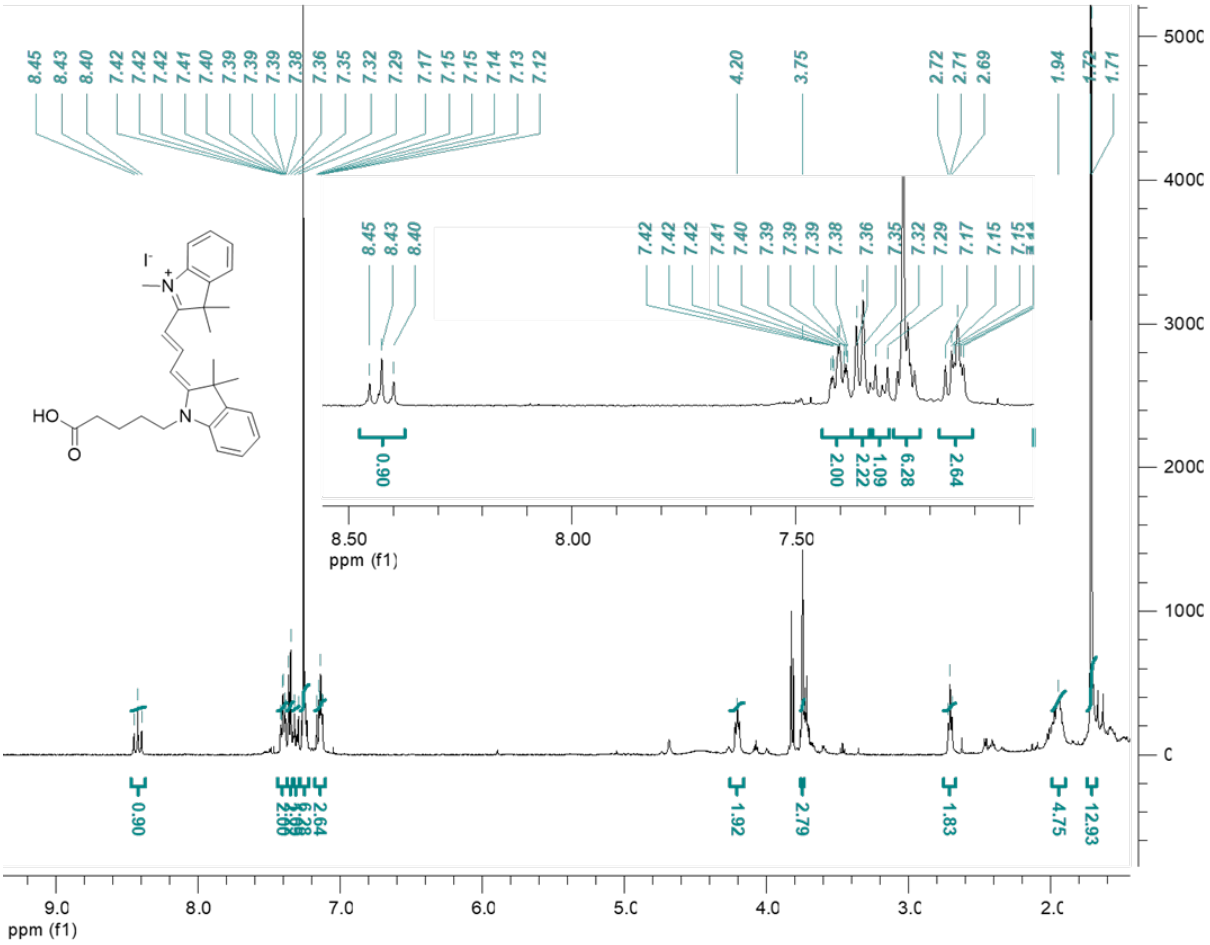

Appendix Figure 7 ^{1}H NMR spectrum of dye Cy3 (compound 106).

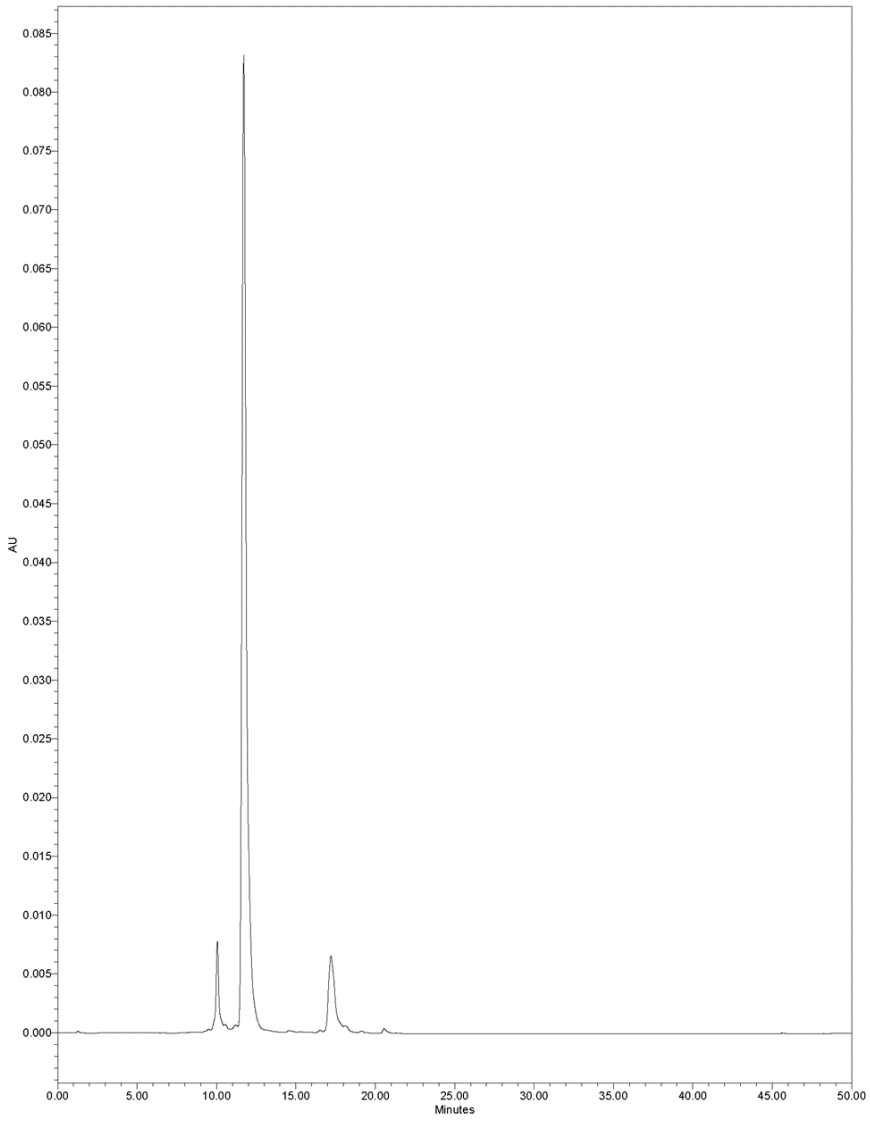

Appendix Figure 8 HPLC spectrum of GB2-Cy3 (compound 106) at 546 nm. HPLC = High performance liquid chromatography.

Reference for Appendix A

Korbel GA, Lalic G, Shair MD (2001) Reaction microarrays: a method for rapidly determining the enantiomeric excess of thousands of samples. *Journal of the American Chemical Society* 123: 361-362

Lee HY, Lee JJ, Park J, Park SB (2011) Development of fluorescent glucose bioprobes and their application on real-time and quantitative monitoring of glucose uptake in living cells. *Chemistry* 17: 143-150

Park J, Lee HY, Cho MH, Park SB (2007) Development of a cy3-labeled glucose bioprobe and its application in bioimaging and screening for anticancer agents. *Angewandte Chemie (International ed in English)* 46: 2018-22

VITA AUCTORIS

NAME:	Mohamadreza Khosravi Bakht (1984-2014) Martin K. Bakht (2014-Present)
PLACE OF BIRTH:	Tehran, Iran
YEAR OF BIRTH:	1984
EDUCATION:	Danesh Tehranpars High School, Tehran Iran, 2004
	Tehran Science and Research IA University, B.Sc., Tehran, Iran, 2009
	Tehran Science and Research IA University, M.Sc., Tehran, Iran, 2012
	Seoul National University College of Medicine, South Korea, 2016
	University of Windsor, Ph.D., Windsor, Ontario, Canada, 2019